Rainfall Dynamics and Change in East Africa



JAMES A. KING

LINACRE COLLEGE

A thesis submitted for the degree of *Doctor of Philosophy*

School of Geography and the Environment

University of Oxford

Hilary Term 2021

In memory of Matt Greenwood

If you have built castles in the air, your work need not be lost; that is where they should be. Now put the foundations under them.

Henry David Thoreau

Car le parfum de mon songe inouï,

Splendeur du ciel tropical,

M'a trop bien ébloui pour les temps à venir.

Léopold Sédar Senghor

And the sound of rain in the season of rain

Rumbles like thunder and why this should be

Is something only the rain can explain.

Gaarriye

1. Abstract

East Africa is vulnerable to changes in rainfall because of its reliance on agriculture, which supports livelihoods and drives economic development, combined with reduced adaptive capacity. Historical rainfall conditions have included an overall drying trend in the March to May season, called the long rains, as well as extreme flooding events. However, the mechanisms controlling rainfall variability in East Africa are not yet fully understood, and global climate models do not have adequate representation of present-day conditions. The models on average underestimate rainfall totals during the long rains and overestimate them during the short rains of October to November. Future projections from these models are also uncertain; the models disagree on the sign and the magnitude of changes, and the ensemble mean rainfall increase in the long rains is in opposition to recent observed drying. It is therefore difficult to plan for climate change adaptation, as neither a wetter nor a drier future can be confidently predicted. To address these issues, this thesis investigates the physical processes that affect East African rainfall on different spatial scales, and their representation in global climate models. The Indian Ocean Walker Circulation (IOWC) is an important large-scale feature which drives descending air over East Africa, and the strength of this descent is negatively correlated with rainfall totals in both rainy seasons (r = -0.57 - -0.85, p<0.05). It is also a source of model rainfall biases, as models with more (less) intense Walker Circulations produce less (more) rainfall over Kenya (r ~ 0.8, p<0.05). The Turkana Low-Level Jet (LLJ) is a meso-scale feature which affects regional rainfall through a variety of mechanisms. Its strength is negatively correlated with rainfall in Kenya, but positively correlated with rainfall in the continental interior (r = ± 0.6, p<0.1). Correlations between the LLJ strength and the large-scale zonal pressure gradient

imply a link between the IOWC and the LLJ (r =± 0.5, p<0.1) The LLJ may be decreasing in strength on decadal timescales (-0.4 - -0.8 ms $^{-1}$ decade^{-1}, p<0.05), consistent with observed climate change, but reanalysis representations of its variability and annual cycle differ. It is not adequately simulated in models as a result of simplified topography representation, and thus further contributes to the uncertainty in projections; given that the IOWC is also constrained by topography, this is suggested as a key focus for future model development. Future projections of increasing rainfall over Kenya are associated with increasing ascent over East Africa (r ~-0.8, p<0.05) and enhanced easterly winds over the Indian Ocean (r~-0.5, p<0.05), reflecting a weakening of the IOWC. Using an assessment of the ability of models to represent the IOWC to constrain future projections, it is found that models with more realistic regional dynamics only feature significant increasing rainfall trends in April, November, and December. It is therefore concluded that the ensemble mean rainfall increase across the long rains may not be plausible, that the long rains may contract in future, and that rainfall increases in the short rains are more likely.

2. Table of Contents

1. Abstract 5

3. Acknowledgements 13

4. List of Tables 16

5. List of Figures 18

6. Introduction 27

6.1. Background and Motivation 27

6.2. Aims and Objectives 37

7. Outline of Current Knowledge 40

7.1. East African Rainfall Climatology 40

7.2. East African Rainfall Variability 44

7.3. The Indian Ocean Walker Circulation 55

7.4. The Turkana Low-Level Jet 60

7.5. CMIP5 Model Performance in East Africa 62

8. Summary of Aims and Objectives for Each Chapter 71

8.1. Chapter 11 71

8.2. Chapter 12 71

8.3. Chapter 13 71

9. Notes on Thesis Format 72

9.1. Chapters Published – Authorship Declaration 73

9.2. Chapters Submitted – Authorship Declaration 74

10. Data and Methods 75

10.1. Introduction 75

10.2. Observations 76

10.2.1. Precipitation 76

10.2.2. Station Data 78

10.3. Reanalyses 80

10.4. CMIP5 Models 83

10.5. Statistical Methods Used 86

10.5.1. Correlation Analysis 86

10.5.2. Root Mean Square Error 87

10.5.3. Trend Analysis 88

10.5.3.1. Linear Regression 88

10.5.3.2. Mann-Kendall Test 89

10.5.4. Composite Analysis 90

11. Paper 1 – Representation of the Indian Ocean Walker Circulation in Climate Models and Links to Kenyan Rainfall 92

11.1. Abstract 93

11.2. Introduction 94

11.3. Data 99

11.4. Observations and Reanalysis 106

11.5. CMIP5 Models 116

11.5.1. Zonal Overturning Circulations 116

11.5.2. Wet Versus Dry Models 140

11.6. Summary and Conclusion 144

11.6.1. Summary of Walker Circulation Impacts on Kenyan Rainfall 144

11.6.2. Implications for Future Model Projections 146

11.7. Acknowledgements 149

12. Paper 2 – Variability of the Turkana Low-Level Jet in Reanalysis and Models: Implications for Rainfall 151

12.1. Abstract 152

12.2. Introduction 153

12.3. Data and Methods 160

12.4. Results 162

12.4.1. Turkana LLJ Climatology 162

12.4.1.1. Long-Term Means 162

12.4.1.2. Annual Cycle 164

12.4.1.3. Wind-Rainfall Covariability 173

12.4.2. Trends 176

12.4.2.1. LLJ Strength 176

12.4.2.2. Mechanisms 178

12.4.3. CMIP5 Models 182

12.4.3.1. Topography 183

12.4.3.2. Annual Cycle 184

12.4.3.3. Sensitivity to Topography 186

12.4.3.4. Wind-Rainfall Covariability 189

12.5. Discussion....190
12.5.1. Climatology of the Turkana LLJ....190
12.5.2. CMIP5 Performance and Implications for Projections....191
12.5.3. Long-Term Trends in the Turkana LLJ....192
12.6. Conclusion....198
12.7. Acknowledgements....201
13. Paper 3 - Future Changes in the Indian Ocean Walker Circulation and links to Kenyan Rainfall....203
13.1. Abstract....204
13.2. Introduction....205
13.3. Data....211
13.3.1. Observations and Reanalysis....211
13.3.2. CMIP5 Models....212
13.4. Results....213
13.4.1. Projections....213
13.4.1.1. Projected Changes in East African Rainfall....213
13.4.1.2. Projected Changes in Vertical Velocity (Omega)....216
13.4.1.3. Projected Changes in Zonal Winds....219
13.4.1.4. Projected Circulation Changes....222
13.4.2. Links Between Historical Biases and Future Projections of IOWC Variables 225
13.4.2.1. Rainfall Change....225

13.4.2.2. Rainfall vs. Omega 227

13.4.2.3. Rainfall vs Zonal Wind 230

13.4.2.4. Wet/Dry Future Composite Streamplots 232

13.5. Composite Projections 234

13.5.1. Composite Trends 235

13.5.2. Composite Trend Maps 237

13.6. Discussion 241

13.7. Conclusions 246

13.8. Acknowledgements 248

14. Conclusions 249

14.1. Relationships Between Key Atmospheric Processes and East African Rainfall 251

14.1.1. The Indian Ocean Walker Circulation 251

14.1.2. The Turkana Low-Level Jet 253

14.2. Representation of Key Atmospheric Processes in CMIP5 Models, and Links to Simulated Rainfall Variability 255

14.2.1. The Indian Ocean Walker Circulation 256

14.2.2. The Turkana Low-Level Jet 259

14.3. Projections of East African Rainfall 260

14.3.1. Links to Historical Model Biases 261

14.3.2. Plausible and Implausible Futures 264

14.4. Suggestions for Future Research 269

14.4.1. Foci for Model Development 269

14.4.2. Definition of the IOWC 272

14.4.3. The Future of the Turkana LLJ 274

14.4.4. Additional Outstanding Issues in East African Rainfall Research 277

14.5. Implications for Policy 278

15. Bibliography 281

3. Acknowledgements

This DPhil project was funded by the Natural Environment Research Council (NERC) through the Doctoral Training Partnership in Environmental Research (DTP). I am grateful to NERC for their investment in me, without which none of this work would have been possible. NERC also enabled me to travel to Germany, Ghana, and Yorkshire for training courses and summer schools, and to the United States, Austria, and Birmingham for academic conferences. As well as teaching me important skills, these trips introduced me to new ideas and ways of thinking.

Writing a DPhil thesis is sometimes a solitary task. However, it is also a chance to recognise that the finished product is the outcome of decades of learning from many teachers, colleagues and friends, whose contributions I am glad to record here. I acknowledge how lucky I have been to have had such support, and this DPhil stands as a monument to everyone who helped me get to where I am today. There is not space to thank everyone, which is itself a privilege.

My interest in becoming a climate scientist can be traced back to my time at the Burgate School in Fordingbridge, where a number of excellent teachers introduced me to the wonders of physics, chemistry, geography, and how to connect them all. Jim Champion, Andy Tapping, Kim Miles, and Richard Hollowbread deserve particular credit. David Pover insisted that I apply to Oxford despite woeful module results, and Kevin Rowett and Nina Lister taught me how to win an argument.

As an undergraduate at St Edmund Hall, the outstanding tuition of Rob Whittaker and Lorraine Wild helped me to realise that I enjoyed physical geography so much, I needed to work out how someone was going to pay me to do it. A conversation with Callum Munday proved pivotal, and my future supervisors Richard Washington and

Sebastian Engelstaedter encouraged and supported me during the application process.

Working in the studious, collaborative, and caffeine-fuelled atmosphere of the Climate Lab was a highlight of my time at Oxford. My work benefitted greatly from conversations with the talented scientists who worked there, all of whom have presumably now heard enough about the Turkana Jet. Thanks to Thomas Caton Harrison, David Crowhurst, Lisa Thalheimer, Callum Munday, Amy Creese, Josie Mahony, Ruksana Haque Rimi, Boipelo Tshwene-Mauchaza, Emma Howard, Neil Hart, Karsten Haustein, Rachel James, Richard Jones, Tom Webb, Marcia Zilli, Neven Fučkar, Richard Millar, David Karoly, and Myles Allen. Ellen Dyer and Dave MacLeod deserve special mention for their invaluable advice; I also thank Chris Reason for taking the time to examine the thesis alongside Ellen Dyer. Beyond Oxford, the thesis benefitted greatly from conversations with Edward Vizy, Kerry Cook, Sharon Nicholson, Peer Nowack, Caroline Wainwright, Giresse Kuete, Thierry Taguela, Oscar Lino, and Andreas Fink. Thanks to Lorenzo Tomassini for organising Africa PEG/MAC, and to David Rowell for his 2015 paper that first got me interested in East African climate as a research topic. David Ford, Alex Black, and Pete Archer saved me from IT hell on countless occasions.

Thanks also go to my colleagues at St Catherine's College – Kaja Fenn, Alex Money, Fiona McConnell, Rob Dunford, Hibba Mazhary, Liam Saddington, Janet Banfield, and Richard Bailey – and to my students there. It is a unique and special place to teach climate science, and I look forward to continuing my association with the College.

I count myself very lucky to have so many supportive friends in Oxford and beyond who have helped throughout the DPhil, often in ways they might not have realised.

My thanks to Liv, Amber, Roberta, Emma (for making me shut up and write), Josh, Liv O, TJ, Alex B, Viraj, Anna, Amelia, Shannon, and Aurélien (for living with me), Laura, Louis, Freddie (and all the OUMDC team), Elisa, Sophie, Becca M, Karen, Helena, Dan, Karl, Abbie, Joe, James, Konstantin, Derek, Kento, Britt, Alex S, Becca H, Becca D, the DTP squash collective, Lissy, Saskia, Lara, Lucia, Cami, Poppy, Owen, Gerardo, Cara, Cristiana, Alice, Salam, Eboni, George, Mala, Josie, Simphiwe, Simona, Nick, and many more. The staff and fellows of Linacre College, led by Nick Brown, gave me somewhere to belong. Clare Parody and Jeremy Paxman gave me slightly more than 15 minutes of fame.

My parents, grandparents, and my brother Martin have supported and encouraged me to aim high for 25 or so years. They have heard more about African climate and the inner workings of academia than they could ever have wanted. Ramzi and Amanda looked after me during the final stages, for which I am tremendously grateful.

I would like to give particular thanks to my supervisors, Richard Washington and Sebastian Engelstaedter. Their teaching inspired me to apply for a DPhil in African climate in the first place, and their patience, wisdom, and insight guided me through the project.

Finally, and most of all, to Naomi, for the best 3-and-a-half years imaginable. The thesis, and the man who wrote it, wouldn't be the same without you.

4. List of Tables

Table 10.1 - Details of reanalysis products used in this thesis.....82

Table 11.1 - CMIP5 models used in this study. Expansions of acronyms are available online at http://www.ametsoc.org/PubsAcronymList. Asterisks denote models used in AMIP ensemble, which are used in chapter 11 only. 101

Table 11.2 - Pearson product moment correlation coefficients between CHIRPS v2.0 rainfall and MERRA-2 400 hPa omega, averaged over Kenya (N = 24, R_{crit} = 0.388) 111

Table 11.3 - Proportion of ascending versus descending air in the region 0°–200°E, 5°N–5°S, between the surface and 200 hPa. 123

Table 12.1 - Turkana jet core wind trends and significance values for MERRA-2, ERA5, and JRA55. Trends are computed by taking the monthly average zonal wind (U) and wind speed (WS) at the jet core at 850hPa defined in Figure 12.1. Trends are denoted by the slope of the linear regression equation. Diacritical marks denote $p < 0.05$ as follows: * = significant trend in linear regression. † = significant trend with Mann-Kendall test. Note that u wind is negative, so a positive slope means a decrease in u wind. Units are m s^{-1} decade $^{-1}$.....177

Table 13.1 - Slopes of the linear regression of Kenyan rainfall for each rainy season month, 2020 to 2100, under the RCP8.5 scenario. Light green (red) shading indicates significance of positive (negative) trends at $p<0.1$ and darker green (red) shading at $p<0.05$. Units are mm day^{-1} $decade^{-1}$. 214

Table 13.2 - Pearson product moment correlation coefficients between CMIP5 model rainfall averaged over Kenya in historical coupled (1975-2005) and RCP8.5 (2070-2100) runs of the CMIP5 models listed in Table 11.1. 226

Table 13.3 - Pearson product moment correlation coefficients between CMIP5 model 400 hPa omega averaged over Kenya in historical coupled (1975-2005) and RCP8.5 (2070-2100) runs of the CMIP5 models listed in Table 11.1. B. Pearson product moment correlation coefficients between model rainfall change and 400 hPa omega change over Kenya, 2070-2100 minus 1975-2005. 227

Table 13.4 - A: Pearson product moment correlation coefficients between CMIP5 model 850 hPa zonal wind averaged over the central equatorial Indian Ocean in historical coupled (1975-2005) and RCP8.5 (2070-2100) runs of the CMIP5 models listed in Table 11.1. B. Pearson product moment correlation coefficients between model rainfall change and 850 hPa zonal wind change over the central equatorial Indian Ocean, 2070-2100 minus 1975-2005. 230

Table 13.5 - CMIP5 models used to produce 'good' and 'bad' composites of future rainfall following the procedure outlined in section 3.3. 235

5. List of Figures

Figure 7.1 – political and relief map of East Africa. DJ = Djibouti, RW = Rwanda, BU = Burundi. LT = Lake Turkana, LV = Lake Victoria (Nam Lolwe), LTN = Lake Tanganyika. Elevation data from GTOPO30. The red arrow indicates the mean location of the Turkana LLJ at 850hPa. 41

Figure 10.1 – density of raingauges contributing to CHIRPSv2.0 in 1988 (a), 1998 (b), and 2008 (c), per 0.05° grid box. 78

Figure 11.1 - CHIRPS v2.0 rainfall climatology for East Africa averaged for each month in the period 1981–2010. The black box shows the area over which Kenya rainfall is averaged. 107

Figure 11.2 - MERRA-2 omega at 400 hPa for each rainy season month, averaged over 1980–2008. The black box indicates the area used for averaging fields over Kenya, and the green box indicates that used for averaging fields over the Eastern Indian Ocean. 109

Figure 11.3 - MERRA-2 velocity potential (filled contours) and divergent wind vectors (arrows) at 200 hPa for each rainy season month, averaged over 1980–2008 109

Figure 11.4 - Longitude-height plots of MERRA-2 reanalysis climatology for MAM (top row) and OND (bottom row), 1980–2008, 15°E–130°E, averaged over 5°N–5°S. Shading is vertical velocity ($Pa \cdot s^{-1}$) with red indicating negative (upward) motion and blue indicating positive (downward) motion. Streamlines are the resultant vectors of u and $w \times 10^4$. The black line indicates the 400 hPa level. The green line indicates the box used for averaging over the ascending limb of the Walker circulation. 110

Figure 11.5 - Pearson product moment correlation coefficient between CHIRPS v2.0 rainfall averaged over Kenya and MERRA-2 400 hPa omega for 1980–2008. Hatching indicates significance at $p < 0.1$. 113

Figure 11.6 - 400 hPa omega averaged between 5°N–5°S, extending from 15°E–130°E, for March (top) and November (bottom). Each coloured line is a CMIP5 model from Table 11.1 averaged over 1975–2005 in historical coupled mode. The thick black line is the MERRA-2 reanalysis averaged over 1980–2008. Note different scales.....114

Figure 11.7 - As Figure 11.4, but for March (top) and November (bottom) in the CMIP5 ensemble (Table 11.1). Models are arranged in rows from driest over Kenya in the given month at the top left, to wettest at the bottom right. MERRA-2 data is included at the bottom left for reference. 120

Figure 11.8 - As Figure 11.7, but for the AMIP models in Table 11.1. 122

Figure 11.9 - As Figure 11.4, but for the Congo Basin (10°–30°E, 5°N–5°S) in March (top) and November (bottom).....126

Figure 11.10 - As Figure 11.4, but for model biases relative to MERRA-2 data. 129

Figure 11.11- Pearson product moment correlation coefficients between CMIP5 model rainfall averaged over Kenya and model 400 hPa omega for March (upper) and November (lower), 1975–2005. Hatching indicates significance at $p < 0.1$. Models are arranged in rows from driest over Kenya in the given month at the top left, to wettest at the bottom right. 130

Figure 11.12 - Differences between CMIP and AMIP models (CMIP minus AMIP) for March (top) and November (bottom), 1975–2008. 133

Figure 11.13 - CMIP5 model precipitation biases over Kenya for each rainy season month relative to CHIRPSv2.0, 1975–2005. 134

Figure 11.14 - CMIP5 model 400 hPa omega biases over Kenya for each rainy season month relative to MERRA-2 reanalysis, 1980–2005. 135

Figure 11.15 - CMIP5 model 850 hPa zonal wind biases over the equatorial Indian Ocean (50°E–100°E, 5°N–5°S) for each rainy season month relative to MERRA-2 reanalysis, 1980–2005. 136

Figure 11.16 - Relationship between model biases (left column) and model RMSE (right column) in rainfall and 400 hPa omega over Kenya for CMIP5 March (top row) and CMIP5 November (bottom row). Note different scales.....138

Figure 11.17 - Relationship between model biases in rainfall and 400 hPa omega over Kenya for March (left) and November (right) in AMIP models. Note different scales.....139

Figure 11.18 - As Figure 11.4, but for composite averages of the wettest four CMIP5 models in each month (top); the driest four models (middle); and the wet composites minus the dry composites (bottom).....142

Figure 11.19 - Differences between the wettest CMIP and AMIP models for the rainy season months (top) and between the driest CMIP and AMIP models (bottom).....143

Figure 12.1 - topography of the Greater Horn of Africa region from the GTOPO30 dataset at 3 arc minute resolution. The purple, blue, orange, and red boxes indicate the jet core, Western Indian Ocean, Turkana Jet entrance, and Turkana jet exit regions respectively. The black line indicates the cross-section used for vertical profiles of the Turkana Jet core. The red arrow indicates the mean direction of the LLJ.....154

Figure 12.2– Long-term mean wind speed at the cross-section through the jet core shown in Figure 12.1, for MERRA-2 (a) and ERA5 (b). Transect is between 4°S 31°E and 4°N 40°E. Data averaged from 1981-2016.....162

Figure 12.3 - as Fig. 12.2, but for wind speed at 850hPa/hybrid level 12. Red box is as per Fig. 12.1; blue box was used to test for sensitivity of results to area averaging (no significant differences were found between the boxes used).....164

Figure 12.4 - seasonal cycle of jet core zonal wind at 850hPa from reanalysis datasets plus the ensemble mean of the 25 CMIP5 models listed in Table 2. The blue shaded area indicates ±1 standard deviation of the CMIP5 ensemble mean.....165

Figure 12.5 - Comparison of underlying topography of the Turkana Channel from GTOPO30, ERA5, MERRA-2, and JRA55.....167

Figure 12.6 - Differences in near-surface temperature for each month in reanalysis between the jet entrance box and the jet exit box (A) and between the Western Indian Ocean box and the jet exit box (B; for 900hPa geopotential height (C and D); and for 850hPa vertical velocity (omega; E and F) 168

Figure 12.7 - seasonal cycles of near-surface temperature from reanalysis data at Wajir (a), Marsabit (b), and Lodwar (c) stations, compared to station observations. 171

Figure 12.8 - Pearson product moment correlation coefficients between reanalysis jet core zonal wind timeseries and MSLP data from 1981-2016 for MERRA-2 (a), ERA5 (b), and JRA55 (c). Shading indicates areas where the correlation is significant at the 95% confidence level. 172

Figure 12.9 - Pearson product moment correlation coefficients between reanalysis jet core zonal wind timeseries and CHIRPSv2.0 rainfall data from 1981-2016 for MERRA-2 (a), ERA5 (b), and JRA55 (c). Shading indicates significance at the 95% confidence level. 176

Figure 12.10 - composite differences (2010-2016 minus 1981-1987) for 900hPa geopotential height for MERRA-2 (a), ERA5 (b), and JRA55 (c). Green and blue boxes denote jet entrance and exit regions respectively. 179

Figure 12.11– linear trend of mean sea level pressure (MSLP) for MAM and OND in MERRA-2 (a), ERA5 (b), and JRA55 (c), over the period 1981-2016. Stippling indicates regions where trends are significant at 95% confidence.....181

Figure 12.12 - model topography over the East African domain for CMCC-CM (A), CCSM4 (B), BNU-ESM (C), and FGOALS-g2 (D). 184

Figure 12.13- annual cycle of zonal wind at jet core for CMIP5 models listed in Table 11.1. 186

Figure 12.14 - 850hPa wind speed, averaged over 1975-2005, for historical coupled runs of CMCC-CM (A), CCSM4 (B), BNU-ESM (C), and FGOALS-g2 (D). The red box indicates the area used for calculating the jet core wind speed. 187

Figure 12.15 - as Figure 12.14 but for a cross-section through the Turkana Channel as per Figure 12.1. 188

Figure 12.16 - As Figure 12.9 but for CMCC-CM (A), CCSM4 (B), BNU-ESM (C), and FGOALS-g2 (D) over 1975-2005. 190

Figure 13.1 - linear regression of composite averages in 400hPa vertical velocity for March (left), April (middle), and May (right), 2020-2100, under the RCP8.5 scenario. Stippling denotes areas where the trend significance $p<0.05$. For each month, the top 5 models with strongest drying/weakest wetting (top row) and strongest wetting (bottom row) are averaged to form a composite. 216

Figure 13.2 - as Figure 13.1, but for October (left), November (middle), and December (right). 218

Figure 13.3 - linear regression trends in 850hPa zonal wind for March (left), April (middle), and May (right), 2020-2100, under the RCP8.5 scenario. Stippling denotes areas where $p<0.05$. For each month, the top 5 models with strongest drying/weakest wetting (top row) and strongest wetting (bottom row) are averaged to form a composite. 219

Figure 13.4 - as Figure 13.3, but for October (left), November (centre), and December (right). 222

Figure 13.5 - Longitude-height plots of the circulation over the equatorial Indian Ocean, 15˚E-130˚E, averaged over 5˚N-5˚S, for March (left), April (middle), and May (right). Shading is vertical velocity (ω) (Pa s-1) with red indicating negative (upward) motion blue indicating positive (downward) motion. Streamlines are the resultant vectors of u and ω x 10^4. For each month, the means for 1975-2005 (historical coupled runs) are subtracted from the means for 2070-2100 (RCP8.5). For each month, the top 5 models with strongest drying/weakest wetting (top row) and strongest wetting (bottom row) are averaged to form a composite. 223

Figure 13.6 - as Figure 13.5, but for October (left), November (middle), and December (right). 225

Figure 13.7 - Wet minus dry model composites of 400hPa omega, averaged over 2070-2100 under the RCP8.5 scenario.....229

Figure 13.8 - Wet minus dry model composites of 850hPa zonal wind, averaged over 2070-2100 under the RCP8.5 scenario.....231

Figure 13.9 - Wet minus dry model composites of the circulation over the equatorial Indian Ocean , averaged over 2070-2100 under the RCP8.5 scenario. Shading is

vertical velocity (ω) (Pa s^{-1}) with red indicating negative (upward) motion and blue indicating positive (downward) motion. Streamlines are the resultant vectors of u and ω x 10^4. 233

Figure 13.10 - Rainfall projections over Kenya from the 'good' (blue) and 'bad' (red) model composites shown in Table 6 for MAM, over 2020-2100 under RCP8.5. The dotted line is a linear regression model fitted to each composite time series. 235

Figure 13.11 – as Figure 13.10 but for OND. 236

Figure 13.12 - linear regression trends of precipitation over East Africa for the 'good' composites listed in Table 13.5, 2020-2100, RCP8.5. Hatching indicates significance at $p<0.1$.....238

Figure 13.13 - as Figure 13.12, but for the 'bad' composites listed in Table 13.5. ...239

Figure 14.1 – mean 1981-2005 rainfall over Kenya across the rainy season months. Blue = CHIRPSv2.0. Red = CMIP5 ensemble mean. Green – ensemble range (wettest minus driest model). 257

6. Introduction

6.1. Background and Motivation

Anthropogenic climate change is the most significant challenge facing humanity in the 21st century (Ripple et al. 2020). As of November 2020, the monthly average CO_2 recorded at the Mauna Loa observatory in Hawaii was 412.89 ppm (NOAA, 2020), and the average surface concentration in the calendar year 2019 was 409.8 ±1 ppm. Atmospheric CO_2 levels are higher than at any point in the last 800,000 years (Blunden and Arndt 2020) and the radiative forcing impacts resulting from an enhanced greenhouse effect are affecting the climate on scales from the global to the regional. The radiative impacts of greenhouse gas (GHG) emissions are determined by their cumulative concentrations in the atmosphere, rather than the rate at which they are emitted (Allen et al. 2009). Therefore, the resulting climate change will continue until net global emissions reach zero (Forster et al. 2020), and afterwards due to the presence of lagged effects in the Earth system (e.g. Brown et al. 2019) and heat storage in the oceans (e.g. Dias et al. 2020). Despite international efforts to ratify climate policy, global emissions continue to rise (Jackson et al. 2019). It is therefore an urgent task for the scientific community to improve our understanding of climate change processes and impacts, both to guide adaptation and provide firm evidence for the necessity of mitigation.

While the impacts of climate change are experienced globally, responses and the need for adaptation are often local. Combinations of physical and socioeconomic factors make East Africa especially vulnerable to climate variability and change, particularly in terms of rainfall (Thomas et al. 2020). The region is highly dependent

on agriculture for both subsistence farming and the export of cash crops which contribute to its economic development. For example, around 75% of the working population of Kenya, Somalia, and Ethiopia are employed in small-scale farming (Salami et al. 2010). Export crops such as coffee and tea are among the largest sources of foreign currency in Kenya and Ethiopia. Furthermore, the region's electricity supply, which has been vital for Kenya's emergence as a technology hub for Africa (Easterling 2014), has been enhanced in recent years by the development of hydroelectricity (Kaunda et al. 2012) and wind power generation; the Lake Turkana Wind Power project, in northwestern Kenya, is currently the largest wind power project in Africa (Cormack and Kurewa 2018). The East African economy is therefore closely linked to climatic variability, with reliable rainfall and low-level wind acting as key influences on livelihoods and economic productivity. The mean annual rainfall varies widely across the region as a result of the strong influence of lakes and the complex local topography (Hession and Moore 2011); although it exceeds 1200 mm year $^{-1}$ in the Ethiopian Highlands and around Lake Victoria (Nicholson 2017), arid regions of Somalia and northern Kenya can receive as little as 200 mm year $^{-1}$. In much of the region, annual rainfall totals are low with strong seasonal dependence. Combined with low adaptive capacity as a result of , among other factors, economic 'underdevelopment' stemming from the legacies of colonialism (Fahnbulleh 2007, Alemazung 2010); complex water governance systems that adversely affect small scale farmers (Schreiner and van Koppen 2020); limited access to flood and drought warnings (Opiyo et al. 2014); and a close relationship between water security, gender, and social capital in farming communities (Balfour et al. 2020), this results in a high degree of vulnerability to perturbations from the mean climatic state. Rainfall-related hazards are projected to scale with climate change on both global and regional scales (Papalexiou and Montanari 2019), and East Africa has suffered

from a number of recent extreme rainfall events. Drought conditions have prevailed over the last few decades (Nicholson 2015), with severely decreased seasonal rainfall totals in 1983-1984 (Devereux 2000), 2010-2011 (Lyon 2014), and 2015 (Philip et al. 2017) resulting in food shortages for millions of people across Kenya, Ethiopia, and Somalia. The 2010-2011 droughts were made more damaging by the subsequent floods in late 2011 (Nicholson 2016a), while there have also been severe floods in Kenya in 1997-1998 (Nicholson 2017) and 2019-2020 (Wainwright et al. 2020). Changing patterns of rainfall over East Africa have been linked to anthropogenic climate change via a number of different mechanisms and investigatory approaches (e.g. Williams and Funk 2011, Lott et al. 2013, Rowell et al. 2015, Hoell et al. 2017, Giannini et al. 2018, Han et al. 2019, Marthews et al. 2019). The disproportionate impacts of climate change in Africa relative to the Global North raise issues of climate justice, given that the continent contributes fewer greenhouse gas emissions than any other (Fields 2005). Scientific understanding of the African climate lags behind that of other regions of the world, as contemporary climate research is computationally intensive and requires resources unavailable to many researchers within Africa; historically, it has also not been a priority for climate research undertaken elsewhere (James et al. 2018). Climate researchers in the Global North should therefore pursue efforts toward addressing knowledge gaps in the climate of Africa while engaging in knowledge exchange and meaningful collaboration with researchers on the continent (Washington et al. 2006, James et al. 2018, North et al. 2020). For example, projects with African institutions as equal partners, and programmes which allow African researchers to benefit from the resources and funding available at institutions in the global North, should be prioritised (Cundill et al. 2019). So-called 'helicopter science' (e.g. Minasny et al. 2020, Olufadewa et al. 2020) should be avoided in research into African climate, in order that any scientific

advances made have the potential to make a genuine difference to climate change adaptation.

Climate models are the sole experimental tools available for studying the climate system, and are therefore central to any investigation into the response of East African rainfall to anthropogenic forcing in both the present and the future. While advances in our understanding of climate processes can be derived from idealised model experiments, and targeted investigations on specific areas are done using regional climate models (RCMs), the most important such models are the general circulation models (GCMs) developed by modelling organisations worldwide as part of the World Climate Research Programme's (WCRP) Coupled Model Intercomparison Project (CMIP). Data from CMIP models are publicly available, and form the basis of much research into climate impacts, as well as informing the assessment reports of the Intergovernmental Panel on Climate Change (IPCC). This thesis focuses on the 5th generation of CMIP models (CMIP5; Taylor et al. 2012), although its conclusions and recommendations are also applicable to future model generations. It should also be noted that similar intercomparison projects have been undertaken for RCMs, including the CORDEX-Africa project (Hewitson et al. 2012). However, RCMs are always to some extent reliant on GCMs for boundary conditions when run into the future, and therefore an assessment of GCM performance is a prerequisite for the use of RCMs (Giorgi et al. 2009).

The consensus approach used in the IPCC reports can be summarised as 'one model, one vote' (Knutti 2010). This means that each model in the ensemble is assumed to be an equally representative simulation of Earth's climate, and consequently that projections from different models have equal value; future changes in climate variables are deemed 'robust' when models agree, and projections are based on the

ensemble mean of all available models. Detailed investigation of model performance reveals that, for Africa generally and East Africa specifically, this approach may be of limited value. GCMs have global strengths but regional weaknesses, and no climate model has been developed on the African continent (James et al. 2018); model performance over Africa is generally low relative to other parts of the world (Zebaze et al. 2019). In East Africa, models have substantial rainfall biases in simulations of the present-day climate which result in an annual cycle which is the reverse of what is observed (Tierney et al. 2015), with poor overall performance relative to observations and significant variation between models (Ongoma et al. 2019). While models agree on warming, the sign of future rainfall projections over Africa varies considerably, leading in many regions to small ensemble mean changes which conceal large changes of opposing signs in different models (Washington et al. 2013, Collins et al. 2013, Hoell et al. 2017). In East Africa specifically, the CMIP5 ensemble mean projects a wet signal for the 21st century during the March-April-May rainy season, in direct opposition to observed trends (Rowell et al. 2015). This phenomenon, termed the 'East African Climate Paradox', has motivated closer scrutiny of simulations of East African rainfall; a growing literature to which this thesis contributes. On a shorter-term basis, seasonal forecasting of East African rainfall, which is vital for agriculture planning, remains challenging owing to a limited understanding of regional climate dynamics (MacLeod 2018, 2019; Walker et al. 2019).

In the absence of physically plausible ensemble means, a more sophisticated approach to developing projections is required. This thesis adopts a process-based climate model evaluation methodology, in which the physical processes controlling East African rainfall variability and change are investigated and CMIP5 models'

ability to simulate them interrogated. It is not sufficient to assume models with accurate rainfall output statistics over Africa are reliable, given that these can be produced by unrealistic atmospheric dynamics within models (James et al. 2015). Models that are unable to accurately simulate the mean state of climate will not produce plausible projections, as these will be derived from forcings applied to an erroneous set of baseline conditions. A process-based approach can provide constraints on models, enabling assessment of plausible future changes, and has been applied successfully for other areas of Africa (James et al. 2015, Creese and Washington 2016, 2018; Munday and Washington 2017, 2018, 2019). Over East Africa, models' rainfall biases are well documented (Tierney et al. 2015), but the reasons behind these biases are not well understood; similarly, approaches to constraining future projections using methodologies developed for better-understood regions of the world have yielded mixed results (Rowell et al. 2016). Consequently, future rainfall projections are not well constrained (Rowell et al. 2015, Nicholson 2017).

The climate of East Africa is complex, with the mechanisms that control rainfall acting on multiple spatial and temporal scales (Nicholson 2017). In identifying the 'climate paradox', Rowell et al. (2015) called for more detailed investigation into these mechanisms and their representation in climate models. Issues of scale are particularly important in global climate models, since their strengths lie in simulating features of the general circulation on a global scale rather than the regional and local scale processes that determine East African rainfall. Interannual variability of rainfall is affected by perturbations to the mean state or background circulation. Similarly, climate change may either be a perturbation to the mean state or a modification of the mean state itself. Therefore, investigations into climate

model performance must determine how well this mean state is simulated (James et al. 2018). East Africa is notable for its relative aridity compared to other regions of the tropics; the area lacks extensive rainforests and is not a hotspot for deep convection (Liu and Zipser 2005), meaning model rainfall biases cannot be fully attributed to the local impact of parameterised convection schemes. In a recent review of the controls on East African rainfall, Nicholson (2017) identified a number of key factors affecting the East African rainy seasons, with interactions between remote forcings, regional circulations, and local geographic factors. East African rainfall is affected by sea surface temperatures (SSTs) in the Pacific and Indian Oceans (Black 2005). The former exerts its influence via the El Niño Southern Oscillation (ENSO), which exhibits teleconnections to East Africa (Hoell et al. 2017), while the influence of the latter is expressed through the Indian Ocean Dipole (IOD), which is also a key driver of rainfall variability (Black 2005). Both ENSO and the IOD are SST patterns which affect East African rainfall variability via shifts in the Walker Circulation (Mutai et al. 2012), a series of zonal overturning cells in the tropics (Bjerknes 1969). Climatologically, East Africa's relative aridity is related to its position underlying the descending limb of the Indian Ocean branch of the Walker Circulation during rainy season months (Mutai et al 2012, Nicholson 2017, Zhao and Cook 2021). The Indian Ocean Walker Circulation (IOWC) thus constitutes a crucial component of the mean state of the regional circulation proximate to East Africa, and factors affecting rainfall variability are expressed through perturbations to the zonal overturning circulation (Vellinga and Milton 2019). Therefore, plausible simulation of the IOWC is of paramount importance in climate models. While individual aspects of the IOWC have been examined in the CMIP5 ensemble (Hirons and Turner 2018), these have not been combined to examine how models' rainfall biases are affected by their representation of the IOWC as system containing zonal and vertical

components, nor has this analysis been extended to future projections. This thesis aims to address these knowledge gaps.

The complex topography of East Africa is both a key influence on rainfall variability and a challenge for CMIP5 models because of their coarse resolution. An important example of this is the Turkana Low-Level Jet (LLJ; Kinuthia and Asnani 1982). The jet is forced by the local topography as the prevailing flow moves through the Turkana Channel in northwestern Kenya (Indeje et al. 2001). The jet is present throughout the year (Nicholson 2016b), and its divergent flow is a contributing factor to regional aridity along with the IOWC (Kinuthia 1992); it also has wider influences on rainfall in East and central Africa through a variety of mechanisms (Lin 2009, Viste and Sorteberg 2013, Hartman 2018, Vizy and Cook 2019, Munday et al. 2020). Nicholson (2017) identifies the jet as a process linking the regional circulation to broader-scale remote forcing, making it a key feature of the East African hydroclimate, but its annual cycle, interannual variability, and the mechanisms which control its variability are not yet fully understood (Hartman 2018). In particular, it is not clear how the jet relates to the wider circulation affecting East Africa, or to rainfall during the rainy seasons. Furthermore, while inaccurate simulation of the jet has been proposed as a source of uncertainty in seasonal forecasting models over East Africa (MacLeod 2019), no study has addressed its representation in CMIP5 models. Improved projections of East African rainfall will require a better understanding of the dynamics of the LLJ, as well as how well it is represented in current model generations. This thesis therefore identifies the Turkana LLJ as a second key focus for investigating rainfall processes and modelling in East Africa.

The importance of spatial scale in understanding the dynamics of the tropical circulation, and by extension the ability of climate models to represent those dynamics, further motivates the focus of this thesis on the IOWC and the Turkana LLJ. The former represents a control on East African rainfall which is part of the global-scale tropical circulation. The latter is a key feature of the mesoscale flow, which may act to modulate the effects on rainfall of the synoptic-scale fluctuations in zonal pressure gradients (themselves influenced by the IOWC) on the smaller spatial scales which are relevant to climate change adaptation and policy. Interactions between features on different scales produce the observed East African rainfall climatology, and models must therefore be able to represent multi-scalar interactions in order to accurately simulate it.

From a dynamics perspective, scale effects in the tropics are important because of the reduced impact of rotation on the tropical circulation. This is expressed mathematically via the meridional gradient in the Coriolis parameter (i.e. the Rossby parameter, β), which decreases to zero at the equator. The result, as demonstrated by Webster (1983), is that quantitative differences exist between the spatial scale of circulation features in the tropical relative to the midlatitudes. Synoptic scale variations in pressure and temperature in the tropics are an order of magnitude smaller at the equator than in the midlatitudes, because the lack of rotation enables the tropical atmosphere to adjust more rapidly to the existence of horizontal pressure gradients. Surface heating produces vertical, rather than horizontal, temperature advection, as a result. Mathematical descriptions of tropical convection cannot be balanced with respect to the flow field without inclusion of mesoscale processes, such as localised vertical motion aggregated at the planetary scale to produce the ascending limb of the Hadley Circulation. Perturbations from the mean state of the

tropical atmosphere consequently arise from interactions between synoptic, mesoscale, and planetary scale features (Webster 1983).

Multiple interacting scales of organisation are therefore evident in the East African troposphere (Hession and Moore 2011). For example, the Turkana LLJ, which is forced by topography, is an important mesoscale feature which affects rainfall through a combination of processes (Nicholson 2016b). The jet itself is affected by the synoptic situation, such as the presence of ridging off the coast of Kenya (Vizy and Cook 2019) and the Somali Jet (Hartman 2018). On planetary scales, the IOWC controls the upper-level descent which acts to cap deep convection over East Africa, and determines the strength and direction of the low-level zonal winds over the Indian Ocean which transport moisture to East Africa and produce rainfall through moisture flux convergence. This flow is modulated in turn by the Turkana LLJ (Viste and Sorteberg 2013). This thesis focuses on the IOWC and Turkana LLJ as key features of the planetary-scale and meso-scale circulations, which are at opposite ends of the length scale of features affecting East African rainfall, because of the importance of both scales. It further investigates interactions between the two systems, as these multi-scalar interactions are crucial for understanding East African rainfall (Hession and Moore 2011) but are not well represented in CMIP5 models (Munday and Washington 2018).

This thesis aims to address the uncertainty surrounding rainfall projections in this region by investigating how two under-investigated drivers of regional hydroclimatic variability – the Indian Ocean Walker Circulation and the Turkana Low-Level Jet - affect East African rainfall, and how well they are represented in CMIP5 models. By applying a process-based methodology, it aims both to improve our understanding of

East African climate, and to provide a basis for refining current and future generations of climate model projections.

6.2. Aims and Objectives

The overarching aim of this thesis is to assess the ability of climate models to simulate and project rainfall over East Africa. The thesis focuses on CMIP5 models for several reasons. CMIP5 is the most widely used set of models for making climate projections. Although the subsequent CMIP6 generation was beginning to be released at the time this thesis was submitted (January 2021), only a few models were available, whereas the CMIP5 ensemble provides ~ 40 fully coupled models, enabling a larger sample covering a broad spectrum of model resolution and quality. Models participating in CMIP5 follow a common set of experimental guidelines prescribed by the WCRP. This means that all models use the same forcings and provide the same diagnostic and prognostic variables, enabling direct intercomparison between them. Therefore, by performing the same analyses on different models, it will be possible to identify how key processes influence East African rainfall across the ensemble. Comparison with observations and reanalysis enables assessment of the models' reliability. The overarching aim can therefore be broken down into the following objectives:

- To understand the relationship between the IOWC and East African rainfall in the observed climate
- To assess the representation of this relationship in CMIP5 historical coupled runs

- To understand how the representation of the IOWC is related to the spread of CMIP5 model rainfall biases
- To determine the annual cycle and interannual variability of the Turkana LLJ in reanalysis data
- To investigate the multi-scalar interactions between the wider regional climate and the Turkana LLJ
- To investigate the representation of the Turkana LLJ in CMIP5 historical coupled runs, and how this is related to representation of topography and resolution
- To evaluate if and how future East African rainfall projections from CMIP5 models are affected by biases in their simulations of the present-day mean state
- To propose future rainfall scenarios for East Africa based on model plausibility

Process-based model evaluation can also be used to constrain projections where there is a substantial spread among the members of a large ensemble. In addition, it follows from the previous points that this approach can identify specific foci for future model development which can improve representation of East African rainfall. Scientific research is a continuous process, and it is to be expected that completed research projects will raise further research questions. Therefore, the thesis also aims:

- To identify foci for improving representation of East African rainfall in future generations of climate models

- To suggest future directions for research into East African rainfall and climate model evaluation

Finally, when studying complex systems such as the climate, the scientist must be open to unexpected findings. In the course of investigating the annual cycle and interannual variability of the Turkana LLJ (chapter 12), a putative slowing trend was found in the jet core which required further investigation. This became an additional objective:

- To understand the variability of the Turkana LLJ under recent climate change

The next chapter provides an overview of the literature on East African hydroclimate and the factors affecting it, the two main climatic features investigated in this thesis (the Indian Ocean Walker Circulation and the Turkana low-level jet), and the ability of CMIP5 models to represent the region's climate.

7. Outline of Current Knowledge

7.1. East African Rainfall Climatology

For the purposes of this thesis, East Africa is defined primarily as the area including the 'Greater Horn of Africa' countries of Kenya, Ethiopia, and Somalia, as well as parts of Djibouti, Eritrea, Uganda, and South Sudan. Different definitions of 'East Africa' are rife in the literature (Nicholson 2017); although the thesis does assess model rainfall simulation in other areas, it primarily focuses on Kenya due to its location at the core of the bimodal rainfall region (Dunning et al. 2016). Furthermore, Nicholson (2017) demonstrates that Kenya is highly representative of the wider bimodal rainfall region in East Africa, with correlations between annual rainfall in Kenya and the region as a whole of 0.82-0.90 over the period 1922-2012. Kenya is also interesting scientifically for its complex climate featuring multiple interacting rainfall drivers on varying spatiotemporal scales (Nicholson 2017) which in part derives from its position on the equator with a seasonal monsoon running parallel to the coast. This makes the East African climate, and Kenya specifically, a challenge for GCMs. Kenya also has a relatively dense network of reporting meteorological stations relative to other East African bimodal rainfall regions, despite a decline in the density of reporting stations which is a common issue in tropical Africa (Washington et al. 2006, 2013; Maidment et al. 2015, James et al. 2018). The density of reporting stations used in the Climate Hazards Group Infrared Precipitation with Stations version 2 dataset (CHIRPSv2.0; Funk et al. 2015), which is used extensively in this thesis, is shown in Fig. 10.1.

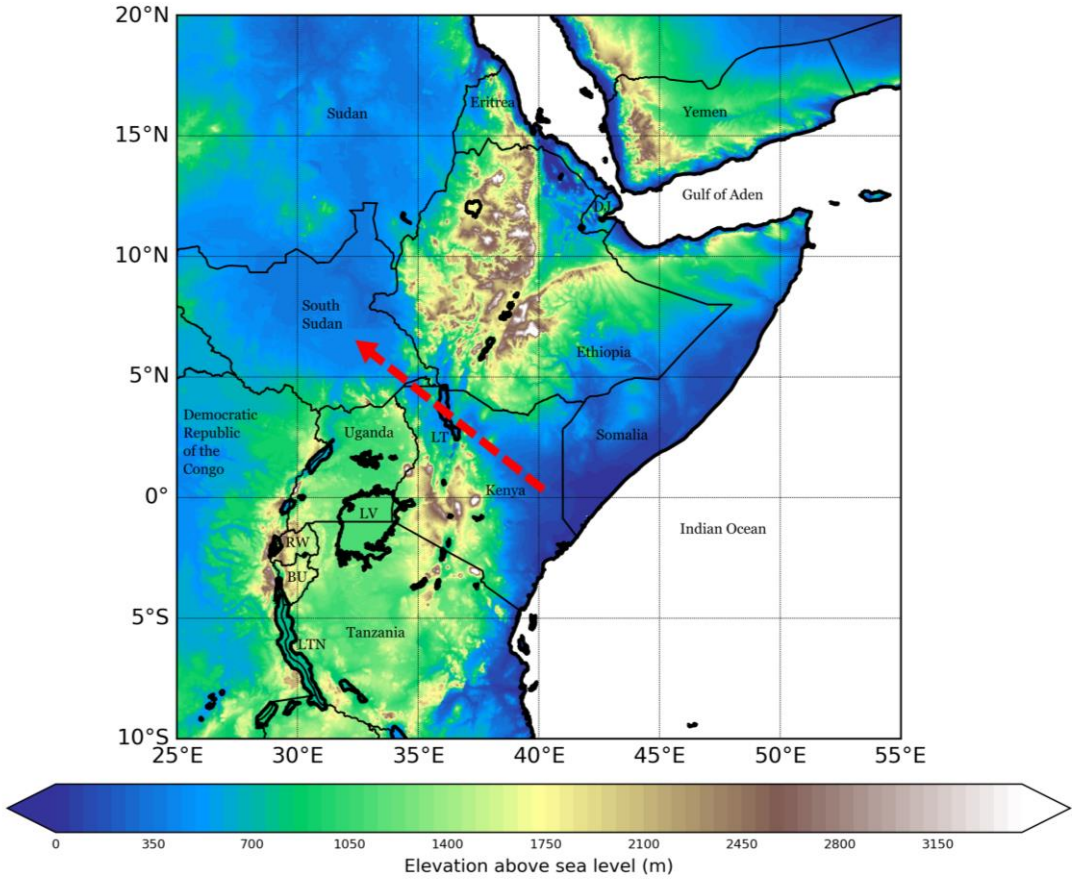


Figure 7.1 – political and relief map of East Africa. DJ = Djibouti, RW = Rwanda, BU = Burundi. LT = Lake Turkana, LV = Lake Victoria (Nam Lolwe), LTN = Lake Tanganyika. Elevation data from GTOPO30. The red arrow indicates the mean location of the Turkana LLJ at 850hPa.

The region is notable for a high degree of topographic complexity (Slingo et al. 2005, Naiman et al. 2017), and consequently there are significant variations in rainfall amount and seasonality over relatively small spatial scales across the East African domain (Hession and Moore 2011). The East African Highlands are oriented on a north-south axis through the region, bisected by the Turkana Channel, with additional lower relief in coastal areas and in the Rift Valley. Although there are areas of relatively high annual rainfall due to orographic forcing at greater elevations, much of East Africa is dry with an annual rainfall of between 800mm and 1200mm (Nicholson 2017). The relative aridity of the region is unusual because of its location

on the western coast of an equatorial ocean with warm coastal SSTs, where tropical rainforests are generally found elsewhere in the world (such as in Indonesia or Brazil) . This, combined with other atypical features such as a monsoon flow that runs parallel to the coast rather than perpendicular, led Trewartha (1961) to term East Africa a 'problem climate'; that is, a region where complex multi-scalar interacting factors result in a climatology which is difficult to understand from a dynamics perspective, and, consequently, difficult to simulate in a climate model (Nicholson 2017).

For much of the area, the predominant rainfall climatology is bimodal. The main rainy seasons are generally referred to as the 'long rains' (March-April-May) and the 'short rains' (October-November-December). The highland regions of Ethiopia differ from most of Kenya, Somalia, and Djibouti in experiencing more of a unimodal climatology, with peak rainfall occurring in June-July-August-September, known locally as 'Kiremt' (Diro et al. 2010). The 'long rains' are generally viewed as more important in the bimodal rainfall region, as they provide the majority of the annual rainfall and coincide with the growth seasons of key crops (Camberlin et al. 2009).

In a broad sense, these rainy seasons can be seen as resulting from the seasonal migration of the intertropical convergence zone (ITCZ) into the summer hemisphere (Hills 1978), although the complexities of local rainfall dynamics limit the explanatory power of the ITCZ in accounting for rainfall patterns and changes (Nicholson 2017). For instance, the region experiences moisture advection from both the Congo Basin and Gulf of Guinea to the West (Giannini et al. 2018), and the Indian Ocean to the East (Viste and Sorteberg 2013). Westerly flow from the eastern equatorial Atlantic is also a source of moisture flux into East Africa (Kijazi and Reason 2012), with anomalous westerlies implicated in increased rainfall in southern

Tanzania (Kijazi and Reason 2009). Low-level flows of moist air into the region from the west are blocked by the highland areas; while the amount of moisture advection from the east is modulated by sea-surface temperatures and the low-level wind field over the Indian Ocean (Williams et al. 2012). In particular, the local topography acts to channel the Indian monsoon flow such that it acts parallel to the coast, moving northeasterly from November to March and southwesterly from May to October, with the dry seasons of July-August-September and December-January-February coinciding with the peak strength of this monsoon as moisture advection from the Indian Ocean is blocked and SSTs reduced in the west of the basin. The monsoon flow is thus focussed into the so-called Somali Jet, which is typically found at a height of between 1200-2100m (Findlater 1969), or 850hPa (Boos and Emanuel 2009); roughly the same height as much of the East African highlands (Fig. 7.1). The peak phase of the southwesterly monsoon (July/August) is associated with strong rainfall in the eastern Sahel, with similar circulation anomalies enhancing both rainfall over India and regions of East Africa that have a summer rainfall peak such as northern Ethiopia (Bhatt 1989). These include low pressure, cool SST anomalies, and enhanced cloud cover over the northern Indian Ocean (Bhatt 1989). Conversely, the northeasterly monsoon flow in OND coincides with enhanced rainfall in the bimodal region of East Africa, and is associated with positive Indian Ocean Dipole SST anomalies (Kripalani and Kumar 2004).

In a model sensitivity experiment with the East African highlands removed, Slingo et al. (2005) found a significant weakening of the Asian monsoon system – the changes in Indian Ocean surface heat flux brought about by this would radically alter the rainfall climatology across Africa. The topography also acts to form a low-level jet (LLJ) in the Turkana channel (Kinuthia 1992), which is a persistent feature

throughout the year in spite of the reversal of the prevailing low-level flow (Nicholson 2016b). The jet creates low-level divergence and convergence patterns which influence local rainfall (Hartman 2018). On a larger scale, the region is affected by the Walker circulation. This is a zonal overturning cell, which is affected by sea surface temperature (SST) in both the Pacific and Indian Oceans (Williams and Funk 2011); climatologically, East Africa sits under a descending limb of the circulation, which is characterised by upper-tropospheric easterly winds and a surface return flow of westerlies over the equatorial Indian Ocean (Nicholson 2017). Weak westerlies are associated with flooding – in 1997 the flow actually became easterly (Birkett et al. 1999), and a switch between easterlies and westerlies can explain the rapid change from floods in 2010 to drought in 2011 (Nicholson 2016a). Interestingly, topography also has a role in the maintenance of this circulation; Naiman et al. (2017) performed a similar experiment to Slingo et al. (2005) but on a global scale, and found that orography constrains the IOWC such that its strength was reduced by 45% when mountains were removed. Segele et al. (2015) identified key circulation features of wet and dry wet seasons, with wet seasons generally including a strong monsoon trough over the Indian Ocean, an intense Mascarene high (east of Madagascar), a strong Somali Jet, enhanced moisture flux, and a steep vertical decline in moist static energy (and vice versa for dry seasons).

7.2. East African Rainfall Variability

Rainfall in East Africa is strongly affected by sea surface temperature, both locally in the Indian Ocean, and remotely from the Pacific Ocean (Ogallo 1989, Black 2005). These teleconnections are modulated via adjustments to the mean state of the

tropical circulation, which is a coupled ocean-atmosphere system (Vellinga and Milton 2019). The interactions between the Indian and Pacific SSTs are complex, and modes of variability on different timescales in both oceans interact to influence East African rainfall variability, although the proximity of the Indian Ocean means it is active as an influence on rainfall all year round (Ogallo 1989). An important interannual signal is the so-called Indian Ocean Dipole (IOD), which in its positive phase is characterised by warm SST anomalies off the East African coast in the western Indian Ocean and cool anomalies in the eastern Indian Ocean, and vice versa in its negative phase, with phases defined by the zonal SST anomaly difference between the west (50° E–70° E, 10° S–10° N) and east (90° E–110° E, 10° S–0°S) of the ocean basin (Saji et al. 1999). Black (2005) showed that East African rainfall in SON has a stronger dependence on the strength of the dipole than on SST anomalies in either the western or eastern Indian Ocean, and further that the anomalous low-level zonal wind field which develops during a positive IOD event as a result of the SST gradient is associated with increased rainfall over East Africa, as a result of anomalously high moisture flux convergence into the region. As a coupled ocean-atmosphere mode of internal variability, the IOD is strongly influenced by positive Bjerknes feedback processes which mean that small changes in the zonal SST gradient can generate large SST dipoles as pressure-driven zonal winds enhance the gradient through upwelling of cooler water when the surface waters are affected by wind stress (Ng et al. 2018). Moving from interannual to multidecadal timescales, Indian Ocean SST seems to be the primary driver of East African rainfall variability; reconstructions of local rainfall and SST using proxy archives show that wetter periods in East Africa coincide with cooler SSTs in the eastern Indian Ocean over the last millennium (Tierney et al. 2015), analogous to a positive IOD.

The Pacific Ocean also exhibits a teleconnection to East African rainfall which affects interannual variability, through the El Niño Southern Oscillation. Broadly speaking, the El Niño (positive) phase of ENSO is associated with wetter conditions and the La Niña (negative phase) with drier conditions. In terms of atmospheric dynamics, ENSO affects East African rainfall by similar mechanisms to the IOD; that is, modification of the Walker circulation (Reason et al. 2000). During La Niña, warm SST anomalies intensify in the western equatorial Pacific, enhancing ascent/convergence in the eastern Indian Ocean and descent/divergence over East Africa. El Niño is associated with low-level easterly anomalies over the Indian Ocean, advecting moisture into East Africa, while the anomalies are westerly in La Niña (Reason et al. 2000, Schreck and Semazzi 2004). Reason et al. (2000) noted complex interactions between winds and Indian Ocean SST during ENSO events, with characteristic shifts in the Walker Circulation associated with a north-south SST dipole in the western Indian Ocean. The timing of ENSO events mean that they have a greater influence on the short rains; Nicholson and Kim (1997) pointed out that ENSO indices change sign during MAM, making an ENSO signal in the long rains season hard to detect. Ogallo (1988) demonstrated that the strongest correlation between the Southern Oscillation Index and East African rainfall was in OND, but that there were significant lagged correlations during the JJAS dry season. As well as rainfall intensity, there is a suggested link between rainy season duration and ENSO. Both duration and intensity contribute to the success of a rainy season, and Dunning et al. (2016) found that the short rains ended 7 days later in El Niño years and 5 days earlier in La Niña years.

However, not all extreme wet or dry rainy seasons in East African can be attributed to ENSO (Ogallo 1988). The ENSO link appears to be stronger for wet years than dry

years; Nicholson (2015) found that ENSO was extremely positive in 15 out of 19 wet years, but extremely negative in just 10 out of 23 dry years. This seemingly weaker impact of La Niña could arise through variability in ENSO itself – Johnson (2013) identified 4 distinct varieties of La Niña, of which only 2 were found to lead to dryer conditions in East Africa (Hoell et al. 2014). Nicholson's (2015) results also point to non-linear interactions between Pacific and Indian Ocean SSTs, given that both oceans are known to affect East African rainfall. For instance, Lanckriet et al. (2015) showed in a multivariate regression model that northern Ethiopian rainfall is significantly affected by ENSO and the IOD, and that the relative impacts of each contribute to drought and famine. Chambers et al. (1999) found that anomalous warming in the western Indian Ocean frequently coincides with El Niño events , although it is possible to have an IOD event in the absence of ENSO (Ham et al. 2017), and IOD events tend to evolve as a separate mode of variability once they have begun (Chakravorty et al. 2014b). A positive IOD at the same time as a positive ENSO enhances the easterly winds across the equatorial Indian Ocean (which are associated with greater East African rainfall) to a greater extent than would be seen if either oscillation were operating in isolation (Chakravorty et al. 2014b). On the other hand, Ummenhofer et al. (2009) found that extreme rainfall over East Africa during the short rains was predominantly controlled by warm SST anomalies in the western equatorial Indian Ocean rather than the SST gradient *per se*.

The mechanism by which ENSO and the IOD are linked is still a topic of active research. Recent work suggests that, rather than ENSO forcing the IOD, the opposite may be true; a negative IOD in autumn may favour an El Niño (and a positive IOD may favour La Niña) approximately 15 months afterwards (Wieners et al. 2017). Meanwhile, Vigaud et al. (2017) suggested mechanisms by which Pacific SST may

affect the long rains, which are not strongly linked to ENSO – identifying recurring convection regimes associated with wet and dry conditions, they find teleconnection mechanisms which are dynamically similar to those associated with ENSO. Wetter long rains occur when there are cooler SSTs in the western Pacific warm pool, and dry conditions when those SSTs are warmer, with the signal modulated by the Indian Ocean. Liebmann et al. (2014) found that SSTs could explain around 40% of the variance in the long rains in a model ensemble. The literature in recent years has found SST impacts on East African rainfall variability to be much more complex and non-linear than the initial quasi-dipolar ENSO/IOD signals might have suggested (Liebmann et al. 2014) – different factors operate on different timescales and interact with each other. In order to better understand the links between East African rainfall and the broader tropical climate, the thesis argues that a renewed focus on the Walker Circulation is important given the key role played by zonal SST gradients, zonal winds, and vertical velocity in East African climate. Further, the complex multi-scalar interactions between different climatic processes require further attention. In this thesis, the Turkana low-level jet is proposed as a key feature of the East African climate which links the broader-scale Walker circulation to local-scale rainfall variability in East Africa.

In terms of intraseasonal variability, recent work has suggested a link to the Madden-Julian Oscillation (MJO) (Nicholson 2017). This system, which has a characteristic 30-60 day timescale, is considered the primary mode of tropical rainfall variability over these timescales (Madden and Julian 1994). The MJO has a convective core which moves eastwards across the Indian and Pacific Oceans – the air in front of the core tends to be anomalously moist, and the air behind it to be dry. The tropospheric heating resulting from this convection generates dry westerly Kelvin waves and

easterly Rossby waves (Zaitchik 2017), which link the MJO to African rainfall. For the long rains, wet conditions tend to be found in the coastal areas of East Africa in the first phase of the MJO cycle and in the inland highlands during the second phase (Hogan et al. 2015); in the former phase, deep convection is suppressed over Africa and low-level moisture advection from the Indian Ocean is dominant, generating stratiform rainfall. In the latter, MJO activity is associated with convection over central Africa and westerly moisture advection (Nicholson 2017). The MJO also exerts an influence over the interannual variability of the long rains, explaining 44% of the variability across the region, though its influence was found not to be as significant in the coastal regions (Pohl and Camberlin 2006) and strongest at the end of the long rains in May (Berhane and Zaitchik 2014). For the short rains, the link with the MJO is strongest at the beginning of the season (October/November) (Berhane and Zaitchik 2014). This interannual link is also spatially differentiated; in the highlands, the MJO exerts its influence via modification of the low-level southeasterly winds, while in the coastal lowlands, the MJO convective core suppresses rainfall when located in the western Pacific, via enhancement of the Walker circulation (Zaitchik 2017). The MJO is a perturbation to the mean state of the tropical circulation (Vellinga and Milton 2019), meaning a realistic representation of the latter is necessary for any climate model simulation of the former.

East Africa's recent climatic history has been dominated by a number of severe drought events, for example in 1983-84, 2010-11, and 2015-2017. These extreme events are embedded within a general decline in rainfall in the region, predominantly in the long rains (Rowell et al. 2015). The dearth of high-quality rainfall observations in the region mean that the exact magnitude of the decline in the long rains depends

on the dataset used, as is often the case in the tropics (Washington et al. 2013, Gehne et al. 2016). Assessing a variety of gauge-based and satellite rainfall products, Maidment et al. (2015) found that the magnitude of the trend varied from -14mm yr^{-1} to -65mm yr^{-1} per decade over the period 1983-2010. Hoell et al. (2017) found a statistically significant drying trend for the long rains between 1979 and 2013 which was over 1 standard deviation greater than the mean trends over the period 1901-2013, calculated using a sliding 35-year window, leading them to term the current drying as the 'most extreme and prolonged dry period of the instrumental record' (Hoell et al. 2017, p1939). A precipitation decline of -0.4mm $month^{-1}$ $year^{-1}$ was found for southwestern Ethiopia for the period 1948-2006 (Jury and Funk 2013). In contrast to this, the short rains have shown a weak upward trend in precipitation, though the significance of this trend is limited by a low signal-to-noise ratio in with respect to interannual variability (Liebmann et al. 2014). The increase has not compensated for the decline in the long rains, and the large year-on-year fluctuations can exacerbate the impacts of the MAM drying (Rowell et al. 2015). While it is important to take into account the effects of breakpoint selection when considering reported trends (Lewandowsky et al. 2015) there is evidence to suggest a more rapid decline in the long rains post 1998/99 – mean MAM precipitation in the period 1999-2009 was over 15% less than in 1979-1998 (Lyon and DeWitt 2012), a trend associated with increased drought frequency during MAM after 1998 (Lyon 2014). Wainwright et al. (2019) indicated that the long rains decline can be attributed to a contraction of the season rather than a reduction in rainfall intensity, lending further importance to the suggestion of Nicholson (2017) that analyses of rainfall change and variability should consider individual months within rainy seasons, rather than aggregating months into a seasonal mean that obscures differences in atmospheric dynamics between them.

Theories attempting to explain this drying signal have generally focussed on SSTs (Nicholson 2017), with work also being done by the event attribution community to investigate the role of anthropogenic climate change on drought events. Less attention has been given to the potential impact of aerosols, though this may also be important. The relative role of Indian vs Pacific Ocean SSTs in driving East African drying remains somewhat contentious, with one issue being the 'warm pool' region of the western Pacific which can arguably extend into the Indian Ocean. The weakening or enhancement of the Walker circulation provides a dynamic lens for understanding how SSTs can remotely affect East African rainfall; while ENSO provides much of the interannual variability in the Walker circulation, it is however difficult to argue that ENSO could be driving a multidecadal trend of Walker circulation intensification (L'Heureux et al. 2013). Lyon and DeWitt (2012) argued that the abrupt decline in the long rains post-1998-99 was driven by contemporaneous changes in the tropical Pacific, which are independent of ENSO – they used model runs forced by Pacific SSTs which were able to reproduce East African drying. This argument was further developed by Lyon (2014), who found that tropical Pacific and Indian Ocean SST anomalies had a stronger impact in the short rains, but that the long rains decline was primarily driven by natural multidecadal variability in the Pacific, and by Lyon et al. (2014), who argued that the MAM Pacific SST trend when ENSO is removed resembles the Pacific Decadal Oscillation (the leading mode of SST variability in the northern Pacific – Newman et al. 2016). Lyon et al. (2014) found that an atmosphere-only model captured many features of the observed precipitation signal when forced by Pacific SST only. Hoell et al. (2014) noted that the specific spatial expression of La Niña events post-1995 would have a greater impact on East African drying than those pre-1995, and linked this to the shift in Pacific SSTs reported by Lyon and DeWitt (2012), although their study used coarse-resolution reanalysis data

which is limited for analysis of Walker circulation moisture flux, and the relationship between these La Niñas and MAM rainfall is unclear. For the Ethiopian summer rains, composite analysis yielded a strong influence of SSTs in the Pacific and Gulf of Guinea depending on what region of Ethiopia was studied (Diro et al. 2010); 6 discrete rainfall regions were identified, highlighting the regional complexity of these teleconnections.

The Indian Ocean is also of great importance in driving the proximate Walker Circulation. There were severe floods in 1997-98 in East Africa which coincided with a strong El Niño event, but Latif et al. (1999) found that ENSO did not directly drive these floods, but rather that the primary link was to warmer SST in the western Indian Ocean. Jury and Funk (2013) linked drying trends over Ethiopia to the same cause, with increased oceanic precipitation in the western Indian Ocean associated with warming and consequent tropospheric subsidence over East Africa. Similarly, Williams and Funk (2011) identified that warming in the Indian Ocean over the last 60 years has been 2-3 times more rapid than the tropical Pacific, and that this warming is robustly linked to increased subsidence over East Africa and drying in MAM. Indian Ocean SST also seems to drive local rainfall variability on longer timescales up to centennial and beyond, again through modification of the Walker circulation (Tierney et al. 2015).Nevertheless, Indian Ocean SST variability could itself been driven by the Pacific, as Chakravorty et al. (2014a) argued that Indian Ocean SST underwent a shift making it more sensitive to Pacific SST after 1970 – around the start point of the long rains decline. Williams et al. (2012) also pointed to a shift towards increasing sensitivity of rainfall to Indian Ocean SST post-1980, whereas before this time summer rainfall was more strongly linked to the surface pressure gradient between East Africa and the Congo Basin/Gulf of Guinea. On the

other hand, Ham et al. (2017) found a weakening correlation between ENSO and the IOD after 1999, dynamically linked to changes in the spatial patterns of ENSO suppressing an IOD response. More recent work has added additional complexity to the current state of knowledge surrounding the drivers of East African rainfall, highlighting the need for an assessment of how well models are able to represent regional dynamics. For example, Liu et al. (2020) argue that the IOD does not exert a strong influence on the short rains, instead identifying three sub-regions of the Indian Ocean that influence East African rainfall via the propagation of Kelvin and Rossby waves manifesting as wind convergence anomalies. Similarly, Zhang et al. (2020) have proposed the existence of an 'Indian Ocean Tripole', but the sub-regions in their study are not co-located with those of Liu et al. (2020).

In view of the debate over whether the Indian or Pacific SSTs are more important, a more tenable approach would seem to be that a combination of both can act, with one or the other more important in a certain year given their quasi-independent modes of variability and the key roles played by the Walker Circulation and moisture fluxes which can originate from different regions. For example, Lanckriet et al. (2015) found significant links between ENSO, the IOD, and the Indian Monsoons on northern Ethiopian rainfall; synergistic interactions between all three were a strong cause of droughts in 1983-5. Using cluster analysis, Vigaud et al. (2017) analysed recurring convection regimes and found that wet regimes are associated with cooler western Pacific and warmer central Pacific SST, with opposite SST patterns during dry regimes. The occurrence of dry regimes has increased and wet regimes decreased since 1999, supporting Lyon and DeWitt's (2012) findings of a precipitation shift, but non-linearities in the relationship between Pacific SST and rainfall regimes suggest that the Pacific signal is locally modulated through the Indian Ocean.

Which ocean basin is more important has implications for the attribution of recent drying. The rapid warming of the Indian Ocean and western Pacific over recent decades shows a fingerprint of anthropogenic climate change, whereas an explanation for drying based on decadal oscillations in the central Pacific would ascribe the warming to natural variability (Hoell et al. 2017). That study found that East African long rains drying occurred in model experiments when the natural and anthropogenic SST signals were combined to a greater extent that when these signals were run in isolation, suggesting an anthropogenic component, but this finding was limited by model variation (see section 2.4). Attribution studies of individual events have also been inconclusive; for the 2011 drought, which featured the failure of consecutive short and long rains, Lott et al. (2013) found no anthropogenic influence on the short rains failure (which was attributed to ENSO) but that the long rains failure was made more likely by global warming – this influence, however, was dependent on the exact spatial expression of the SST warming. For the 2015 Ethiopian drought, Philip et al. (2017) were unable to make a link to anthropogenic climate change, but ENSO correlations were detected. The effect of anthropogenic warming on ENSO itself remains an open question; while studies have found increases in the frequency of extreme La Niña events (Cai et al. 2015) and extreme El Niños (Wang et al. 2017) in future projections, the reliability of this is difficult to ascertain given model SST biases.

The effect of aerosols on East African climate is not well understood (Rowell et al. 2015). It has been shown that anthropogenic aerosol emissions influenced droughts in West Africa through weakening of the monsoon system there (Ackerley et al. 2011). Aerosols also impact the Asian Monsoon system, by weakening land-ocean temperature contrasts and modifying local clouds such that atmospheric stability is

increased and convection reduced, leading to drying in south Asia (Li et al. 2016), but this monsoon is most active during dry seasons in East Africa. Rowell et al. (2015) noted that uncertainties in model responses to aerosols limit understanding of their impacts on East African rainfall, although projections from Scannell et al. (2019) suggest that plausible declines in future anthropogenic aerosol emissions could result in a reduced short rains duration. Overall, the literature demonstrates that the Walker Circulation is a key mechanism by which SST variability is translated to East African rainfall variability.

7.3. The Indian Ocean Walker Circulation

The Indian Ocean Walker Circulation (IOWC) is a mean state zonal overturning cell located over the equatorial Indian Ocean. It is part of the global Walker Circulation (Bjerknes 1969), a series of coupled ocean-atmosphere equatorial cells that, together with the meridional Hadley Circulation, are key drivers of climate variability in the tropics (Tanaka et al. 2004). In the Pacific, the Walker Circulation is associated with the El Niño Southern Oscillation, with the location of the core ascending regions determined by warm SST anomalies and enhanced by zonal surface wind feedback (Bjerknes feedback; Tompkins 2001); associations between warm SST and ascent in the troposphere are also found in the Indian Ocean Walker Circulation (Williams and Funk 2011). El Niño events are associated with reduced summer monsoon rainfall in India as the ascending phase of the Walker Circulation shifts towards the tropical Indian Ocean and enhances descent over India, thus disrupting the southwesterly monsoon flow (Krishnamurthy and Goswami 2000). ENSO variability is conventionally measured using the Southern Oscillation Index (SOI; Walker and

Bliss 1932), which is the surface pressure difference between stations at Tahiti (17.55° S, 149.617° W) and Darwin (12.4°S, 130.867° W). Additional attempts to define the atmospheric component of the Walker Circulation have used mid-tropospheric vertical velocity fields (Wang 2002) or vertical mass flux (Schwendike et al. 2014); combinations of wind, divergence, and vertical velocity fields (e.g. Hastenrath et al. 2002); and deviations from the zonal mean velocity potential field at 200hPa (Tanaka et al. 2004). Defining the atmospheric component of the circulation is challenging mathematically (S. Zhao, personal communication) because of its seasonal nature (Hastenrath et al. 2002), and combination of vertical and zonal components with measurements varying over several orders of magnitude. Ascending, descending, and zonal components should therefore all be considered when investigating the atmospheric Walker circulation (Li et al. 2015). Because of its association with ENSO, the majority of definitions of the circulation are focused on the Pacific cell. However, an overturning cell over the Indian Ocean has been identified (Hastenrath et al. 2011). This primarily consists of ascending air over the Maritime Continent between 90° E and 120° E, a zone of very warm SST and tropical rainforest ecosystems associated with deep convection driven by strong latent heat release (Liu and Zipser 2005); easterly flow at around 200 hPa; subsidence over the western Indian Ocean and East Africa, below which topography and lakes force a characteristic zone of low-level ascent (Nicholson 2017); and a near-surface return flow at around 850 hPa (Hastenrath et al. 2007, Hirons and Turner 2018). This return flow is strongly correlated to OND rainfall in East Africa, with stronger westerlies associated with drier short rains and vice versa for weaker westerlies (Hastenrath et al. 2010, Mutai et al. 2012). Over Tanzania, heavy rainfall that led to flooding during the short rains of 2006 was associated with warming over the western Indian Ocean leading to uplift, moisture flux convergence, and enhanced

easterly flow associated with Walker Circulation shifts (Kijazi and Reason 2009). The association between vertical motion over the Indian Ocean basin and East African rainfall in the long rains months implies a link between basin-wide overturning and East African rainfall in MAM as well (Vigaud et al. 2017), although the circulation is less evident in these months by some definitions (Hastenrath et al. 2011). For example, wet MAM seasons in Tanzania were found to be associated with enhanced moisture flux from both the Indian Ocean and the Congo basin, while dry seasons were associated with anomalous westerly flow over the Indian Ocean (Kijazi and Reason 2012) – these low-level winds are part of the IOWC (Nicholson 2017). The circulation is closely coupled to the zonal SST gradient between the western and eastern Indian Ocean, which has been argued to drive the large-scale Walker Circulation response which in turn affects East African rainfall (Ummenhofer et al. 2009). In particular, the anomalous zonal SST gradient pattern known as the Indian Ocean Dipole (IOD) is important, with positive IOD conditions (warming in the western Indian Ocean and cooling in the east) resulting in a weakened overturning and consequently more rain over East Africa as the descending limb has less power to cap the development of convection (Black 2005, Behera et al. 2005). The IOD, ENSO, and the Walker Circulation are interconnected in ways that have yet to be fully understood, but the association between ENSO phases and East African rainfall suggests the IOWC 'transmits' the ENSO signal to East Africa (Lyon 2014, Hoell et al. 2014, Vigaud et al. 2017). Although ENSO is not active during the long rains, MAM rainfall has been found to exhibit sensitivity to SST gradients in the western Pacific, with resultant atmospheric dynamics analogous to the ENSO influence on zonal overturning (Liebmann et al. 2014).

The IOWC exerts a strong influence on East African rainfall. It follows that variability and trends in the IOWC are important for understanding observation of East African rainfall (Nicholson et al. 2017). However, the lack of an agreed-upon definition of the global Walker Circulation, let alone the IOWC, means that published studies vary in their approach to trend analysis, and consequently to the sign and magnitude of the trends themselves (Chung et al. 2019). L'Heureux et al. (2013), analysing sea level pressure (SLP) differences between Indonesia and the Eastern Pacific, found a significant increase in the strength of the Pacific component of the Walker Circulation from 1950-2011 on 20-40 year timescales, associated with both the increased global mean surface temperature and the trend towards La Niña-like conditions in the Pacific post-1995 (Hoell et al. 2014). McGregor et al. (2014) used a more comprehensive approach incorporating analysis of vertical velocity and zonal winds. They found a strengthening of the Walker Circulation on a global scale between 1992 and 2011 and attributed this to shifts in the locations of convergence/divergence as a result of Atlantic warming, although their study used a single reanalysis dataset (ERA-Interim) and a single model, and there was a small margin between descending IOWC air and Congo Basin ascent, complicating the interpretation of results from the perspective of East African rainfall. Nicholson (2015) found an intensification of the IOWC during the short rains between 1948 and 2012. Idealised aquaplanet simulations by Li et al. (2015) support the hypothesis that a strengthened Walker Circulation is a physically plausible outcome of increasing global SST, but such simulations are of limited value in understanding rainfall change over land. On the other hand, Tanaka et al. (2004), with a method based on 200hPa velocity potential in the NCEP/NCAR reanalysis, found a weakening trend in the global Walker Circulation in the late 20th century. Power and Kociuba (2011), using a method based on analysis of SLP gradients using different

areas for spatial averaging, argued that the circulation has weakened across the Indo-Pacific region in the late 20th and early 21st centuries. More recently, Dhame et al. (2020) have used atmosphere-only GCM experiments to argue that a reorganisation, rather than a straightforward strengthening or weakening, of the IOWC in response to Indian Ocean SST changes can explain observed trends in the short rains – however, only a single CMIP5 GCM was used (see section 7.5). A clear issue here is the selection of time periods over which trends are computed, as L'Heureux et al. (2013) explicitly demonstrate. Similarly, Nicholson (2015) has noted that the strength of the teleconnection between ENSO and East African rainfall, modulated via the IOWC, has varied throughout the 20th century. Chung et al. (2019) attempt to reconcile differing published trends, suggesting that the strengthening of the Pacific circulations derived from reanalyses is greater than that derived from satellites. Chung et al. (2019) conclude that the strong interannual variability of the Walker Circulation can explain many of the differences between studies as a result of timescale selection.

In reconciling observed (or reanalysis) changes in the Walker Circulation with actual East African rainfall trends, Nicholson (2015, 2017) makes the important suggestion that the IOWC interacts over East Africa with other Walker Circulations. This can be interpreted as the outcome of relative changes in the strength of the IOWC versus the Atlantic Walker Circulation (Liebmann 2014, McGregor et al. 2014), which is supported by the strong correlation obtained by Walker et al. (2020) between zonal winds in central Africa and East African rainfall. A key aim of chapter 11 is to determine the dynamic nature of the relationship between the IOWC and East African rainfall in both the real atmosphere and CMIP5 simulations, but a focus on

other Walker Circulations is encouraged as a focus for future research (see chapter 14).

7.4. The Turkana Low-Level Jet

The Turkana LLJ is a significant feature of the East African climate. The Turkana Channel separates the East African Highlands to the south from the Ethiopian Highlands to the North. The channel itself is oriented on a southeast-to-northwest axis, and is approximately 700km long, with sides around 1000km in height. The LLJ is an annually persistent southeasterly wind at roughly 850 hPa which blows through the channel. A more extensive description of the regional topography and jet characteristics is provided in section 12.2.

The jet has a variety of impacts on East African rainfall. Its divergent flow and annual persistence results in dry conditions in the Turkana Channel (annual rainfall ~186 mm) which are unusual for land areas on the equator (Kinuthia and Asnani 1982, Nicholson 2016b). However, the flow itself is humid, and acts as a major source of moisture flux from the warm equatorial Indian Ocean into inland areas of East and Central Africa, including key agricultural regions of Ethiopia (Viste and Sorteberg 2013); easterly LLJs, including the Turkana LLJ, are vital sources of water vapour into tropical Africa (Munday et al. 2020). The LLJ may also have impacts on triggering convective rainfall both locally, as a result of turbulence at the jet's margins and associated small-scale overturning (Hartman 2018, O. Lino, personal communication), and further inland, as a result of convergence at the jet exit associated with rainfall over South Sudan (Vizy and Cook 2019). Further afield, the interactions of the jet with the wider circulation over central tropical Africa have

been suggested to drive the formation of mesoscale convective systems, which are important rainfall-producing features in central and West Africa (Kinuthia 1992, Lin 2009).

Despite its acknowledged influence on regional hydroclimate (Kinuthia 1992, Nicholson 2016b, Vizy and Cook 2019), there are a number of open questions regarding the drivers and variability of the jet. It is generally acknowledged that the LLJ is topographically forced as a result of the Bernoulli effect, as the low-level flow is forced through the gap between mountain ranges (Indeje et al. 2001, Vizy and Cook 2019). High-resolution model experiments have demonstrated that the instantaneous jet velocity is determined by the relief of the channel (Indeje et al. 2001). However, the jet is always southeasterly regardless of the prevailing wind conditions (Nicholson 2016b), which at this location are dominated by the seasonal reversal of the Somali Jet. The interactions between this larger-scale flow and the Turkana LLJ have yet to be conclusively determined. Indeje et al. (2001) suggest the contribution to the LLJ strength from the Somali Jet was equal to that of local topography and surface heating. Hartman (2018) suggested that the jet is driven by temperature gradients, with advection of cooler air from the Somali jet between April and October enhancing the jet strength, but this mechanism does not reflect the only published annual cycle of the jet, using ERA-Interim reanalysis, which suggests a jet minimum during boreal summer (Nicholson 2016b). Vizy and Cook (2019) find a link between synoptic high pressure over the western equatorial Indian Ocean and LLJ strength, which implies a link between the jet and the wider tropical circulation, but this too has not been investigated. The lack of continuous observational data of the jet means that analyses of its behaviour rely on reanalysis datasets which produce different jet mean states (Vizy and Cook 2019) for reasons that have only partially

been accounted for. The annual cycle of the jet remains largely uninvestigated, as does its interannual variability and representation in climate models beyond those specifically set up to investigate it as experimental tools (Indeje et al. 2001); it has been suggested that the limited ability of seasonal forecasting models to simulate the LLJ is a contributing factor to their poor performance in forecasting the long rains in particular (MacLeod 2019). Improving our understanding of the Turkana LLJ is therefore important for understanding East African rainfall. Specifically, understanding the annual cycle and interannual variability of the jet and its links to the winder circulation will enable better projections to be made of how the jet may plausibly change in future, and how this will affect East African rainfall. Further, analysis of how well the jet is simulated by CMIP5 models can provide a constraint on their performance and a means to assess the plausibility of future projections of East African rainfall. Given the jet's importance for the region's rainfall climatology, an understanding of how it may be affected by climate change is needed.

7.5. CMIP5 Model Performance in East Africa

The African continent is increasingly recognised as a priority for climate model improvement, given its importance for global climate and the comparative lack of attention it has received from the climate science community (James et al. 2018). Assessment of model performance over East Africa has revealed that models tend to have global strengths but regional weaknesses. This was highlighted by Rowell et al. (2015) who identified the 'East African Climate Paradox': in contrast to recent drying, CMIP5 coupled models under the high RCP8.5 scenario generally project wetting in the immediate future, which also holds for the lower RCP4.5 scenario (Ongoma et al. 2017). This problem has provided impetus for increasing process-

based analysis of model performance over East Africa; that is, analysis that moves beyond assessing models' ability to reproduce mean statistics which takes model dynamics into account (James et al. 2015). CMIP5 model representations of basic climate processes over East Africa are limited (Ongoma et al. 2019), with large SST biases in relevant ocean basins (Cai and Cowan 2012, Yang et al. 2014), limited representation of SST-rainfall teleconnections (Rowell 2013), and simplified topography which limits the representation of important small-scale features (Woodhams et al. 2018, Munday et al. 2020). CMIP5 coupled models have poor representation of the annual cycle of rainfall, generally underestimating the long rains and overestimating the short rains (Tierney et al. 2015); they tend to show the short rains as the main rainy season across much of East Africa when the opposite is true (Yang et al. 2015).

These errors are often attributed to biases in model SSTs, which tend to be too warm in the southern hemisphere and too cool in the north (Wang et al. 2014). This biases the ITCZ position and its interaction with the Asian monsoon, which is important for rainy season onset (Black 2005). These biases robustly continue into future projections; Li et al. (2016) showed that many models projected a positive IOD-like pattern into the future which would result in a wetter East Africa, but that this signal is largely an artefact of model errors in simulating present-day climate. Similarly, Zhang et al. (2017) showed that the atmosphere-only version of the ACCESS1-3 model gives different precipitation changes when forced by different models' SST projections; these bias-derived differences explained 20-25% of the precipitation changes over the Indian and Pacific Oceans, indicating a strong dependence on model SST in future precipitation changes. This is important because GCMs are biased towards a positive IOD phase, which is associated with higher rainfall totals in

East Africa during the short rains; this model bias has persisted through model generations from CMIP3 to CMIP5, and is associated with thermocline-SST feedback and unrealistically strong mean state easterly winds over the Indian Ocean (Cai and Cowan 2013). The coupled nature of the Walker Circulation means that determining whether SST biases or atmospheric biases are responsible for mean state errors is a complex problem (Cai and Cowan 2013), and there has not been a comprehensive investigation to date of the interaction between the atmospheric dynamics associated with these SST patterns and East African rainfall. Additionally, the extent to which model rainfall biases are purely due to SST, as opposed to other underlying causes related to the modelling of atmospheric dynamics, has not been investigated. No study has specifically investigated the representation of the IOWC or the Turkana LLJ in coupled models. An ability to simulate these mean state characteristics is crucial for making reliable future projections, especially given that the key drivers of East African rainfall variability, from ENSO and the IOD to the MJO, act through perturbations to this mean state (Vellinga and Milton 2019), and specifically to the IOWC.

Coupled models have characteristic biases in their representations of relevant atmospheric dynamics; James et al. (2017) showed that HADGEM3-GC2 had low-level westerlies of the wrong sign over the Indian Ocean, indicating a severely problematic representation of the Walker circulation. This was subsequently found to be the case in a number of CMIP5 models by Hirons and Turner (2018). James et al. (2017) recommend further assessment of model circulations over the Indian Ocean as a means of better understanding the 'Climate Paradox'. Rowell et al. (2015) drew attention to the projections of increasing MAM rainfall in CMIP5. More detail was provided by Ongoma et al. (2017), who found that rainfall increased in both MAM

and OND in CMIP5 projections for both RCP8.5 and RCP4.5, with a greater increase in the short rains and over central Kenya and Lake Victoria – a finding which also led the authors to call for more research into model performance over East Africa. Giannini et al. (2018) posit that these future wetting signals derive from a weakening of the zonal overturning circulation which enhances moisture advection from the Congo Basin into East Africa. This suggests that model biases in East African rainfall have a basis in model dynamics, and cannot be explained purely with respect to the convective parameterisation schemes which generate model rainfall, despite improvements in the simulation of extreme rainfall and small-scale circulations such as sea breezes when high-resolution models with explicit convection such as CP4-Africa (Stratton et al. 2018) have been used (Finney et al. 2020). Regional climate models (RCMs) also exhibit significant biases, with East African rainfall variability generally less well simulated than elsewhere on the continent (Kim et al. 2014). Recent regional model intercomparison studies undertaken as part of the Coordinated Regional Climate Downscaling Experiment in Africa (CORDEX-Africa; Nikulin et al. 2012) indicate an increase in mean daily short rains precipitation, as in CMIP5, but a decrease in mean daily long rains precipitation; however, the relative performance of CORDEX-Africa RCMs was found to be heterogeneous depending on domain, variable, and process under investigation (Ogega et al. 2020). In any case, East African rainfall is determined by the interaction of large-scale structures with local topography. RCM projections in such circumstances are therefore limited by the performance of the driving GCM (McSweeney et al. 2015), since synoptic-scale errors in the GCM propagate into the RCM as boundary conditions (Addor et al. 2016). Given the known limitations of GCMs in this region, a renewed focus on their dynamic performance is advocated.

The complex topography of East Africa is an important factor in regional rainfall characteristics, from constraining the monsoon flow into South Asia (Slingo et al. 2005) and the IOWC itself (Naiman et al. 2017) to triggering orographic rainfall (Hession and Moore 2011) and driving the Turkana LLJ (Hartman 2018). It follows that the comparatively low spatial resolution of CMIP5 GCMs limits their ability to simulate regional hydroclimate. This is one area where higher-resolution modelling can add value (Indeje et al. 2001, Finney et al. 2020). Within the CMIP5 ensemble, model resolution varies, as does the representation of topography. Munday and Washington (2018) found that model topography was important in explaining CMIP5 model rainfall biases over southern Africa, where the relief is also complex. In particular, whether a model was wet or dry was related to its representation of topography in areas where moist low-level flow from the Indian Ocean is advected over land. Similar processes are at work in East Africa, particularly with respect to the Turkana LLJ (MacLeod 2019). This thesis therefore considers model topography over East Africa to be an important consideration in assessing the reliability of projections; this is addressed through the lens of the Turkana LLJ in chapter 12.

There has not been a detailed investigation into how CMIP5 models represent the IOWC. Some recent studies have addressed the question of how well models can represent the circulation globally. Kociuba and Power (2015) find that CMIP5 models are unable to reproduce observed changes in the zonal surface pressure gradient in the Pacific associated with the Walker Circulation. Model experiments by McGregor et al (2014) using a single CMIP5 CGM (CAM4) indicate that the model is better able to reproduce the mean state of the Pacific WC than the IOWC, when forced with observed SST values. Dhame et al. (2020) also undertook a sensitivity experiment using a single GCM, finding that the IOWC affects East African rainfall,

but the model used was unable to capture the observed long rains decline. Chung et al. (2019) argue that the strong internal variability component of the Pacific WC trend from 1979-2014 means that the CMIP5 ensemble mean WC is not reliable, but that some individual ensemble members are able to reproduce the observed changes. It follows from this that model processes must be investigated in detail when considering the plausibility of projections of climate variables which are affected by the Walker Circulation.

In this thesis, a process-based approach to evaluating climate models is adopted. This is in agreement with Emanuel's (2020) argument that conclusions about the inner workings of the climate system should not be drawn from simulations in the absence of a solid understanding of the physical behaviour of those systems which is derived from theory and observation. Considering a model to be realistic if it can reproduce publicly available rainfall measurements, when it may in fact have been calibrated against those same measurements (Oreskes et al. 1994) is therefore insufficient (Emanuel 2020). Conventional methods to quantify model rainfall performance based on comparison with observations are limited over East Africa, owing to an incomplete understanding of regional climate dynamics, and a limited observational network (Fig. 10.1). Although gridded rainfall datasets are available which perform well relative to point observations in East Africa (Gebrechorkos et al. 2017, Kimani et al. 2017), our understanding of model rainfall biases is limited by the observations available. This is particularly the case for smaller scales of analysis, but also applies on country-wide scales in East Africa; there are no currently active raingauges in Somalia contributing to CHIRPS (fig. 10.1) or GPCP datasets (James et al. 2018). Furthermore, some rainfall datasets exhibit large biases relative to observations in East Africa. Kimani et al, (2017) found that errors in the GPCP and

PERSIANN-CDR datasets in April varied from +50 mm month^{-1} to -100 mm month^{-1} over central Kenya. Gebrechorkos et al. (2017) found that the ARC2, a product developed specifically for Africa, underestimated total rainfall at stations in Kenya, Ethiopia, and Tanzania by 30%. The biases were attributed to the inability of some rainfall datasets to capture different rainfall regimes, and in particular to GPCP's sensitivity to raingauge density which is low in East Africa (Kimani et al. 2017). Gridded datasets are also sensitive to spatial resolution, with higher-resolution datasets such as CHIRPS outperforming lower-resolution datasets as a result of the region's complex topography affecting rainfall on smaller scales which are eliminated by regridding to a lower spatial resolution (Gebrechorkos et al. 2017). Aggregating rainfall trends on coarse scales may also result in a loss of detail; for example, despite the general trend for decreasing precipitation during the long rains, high-resolution datasets suggest modest rainfall increases in western Ethiopia and Kenya which are obscured when lower-resolution interpolation is used (Gebrechorkos et al. 2019). Therefore, approaches common in climate model evaluation, such as the application of skill scores based on observational comparisons, are insufficient in East Africa because the observations themselves are not necessarily reliable. Rowell et al. (2016) demonstrate that a skill-score based approach for constraining model ensembles is not adequate because there is a strong dependence of the resulting constrained ensemble on the specific metrics selected. Consequently, a subset of models selected based on accurate reproduction of rainfall statistics in one part of Africa may contain entirely different models to one selected based on accurate reproduction of rainfall elsewhere. Models with accurate reproduction of surface temperature are not necessarily those with accurate rainfall. A further issue with this 'performance-based' approach is that is that describing model biases relative to observations does not provide information about how those biases are linked to mechanisms of future

change in the models; which, after all, is the primary task of evaluating a climate model (Baumberger et al. 2017), especially in East Africa where mechanisms of future change are uncertain (Rowell et al. 2015). The approach does not enable model developers to identify model processes or parameterisations which require improvement or modification, nor does it follow that a model with an ability to reproduce climate observations is doing so as the result of accurate physical processes; in tropical Africa, the opposite has been shown to be the case (James et al. 2015). Projections made using a model which can reproduce observed rainfall measurements cannot be assumed, a priori, to be plausible responses of the climate system to increased radiative forcing. It is therefore argued that this approach is not by itself sufficient for assessment of model performance over Africa, and its use to determine the likelihood of projected tropical climate change outcomes in IPCC reports is potentially problematic (Flato et al. 2013).

A process-based approach to model evaluation is therefore required, which takes into account the atmospheric dynamics within models which may explain their differences in terms of output statistics. This has been highlighted as a necessary approach in the African climate literature (Washington et al. 2006, Rowell et al. 2015, 2016, James et al. 2018), and follows from the limitations of the performance-based metrics described above, combined with the existence of well-known model rainfall biases for which there is not yet a clear physical explanation based on atmospheric dynamics (Tierney et al. 2015, Rowell et al. 2015). This approach has yielded significant advances in our understandings of regional rainfall projections in West Africa (James et al. 2015), southern Africa (Munday and Washington 2017), and central Africa (Creese and Washington 2016). In the literature reviewed above, the IOWC and the Turkana LLJ emerge as key influences on East African rainfall, but

these have yet to be extensively investigated in CMIP5 models, nor linked to the models' rainfall biases. This thesis contributes by providing an explanation of model diversity through representation of the IOWC, and by determining whether or not CMIP5 models can represent the Turkana LLJ and its links to rainfall. Recent work on process-based metrics has identified key variables (or indices of variables) which can be used to constrain models over East Africa. For example, McSweeney et al. (2015) demonstrate an approach based on systematic application of expert judgement to climate model simulations, identifying simulations of large-scale climate features as 'implausible' or 'biased' relative to reanalysis, with the aim of selecting the optimum GCM for downscaling experiments over Africa and other regions. Dyer and Washington (2020) evaluate the key processes acting during the long rains in ERA-Interim reanalysis to determine a set of diagnostics to evaluate model simulation of the East African long rains. These studies are important sources of information for climate change adaptation planning in East Africa. It is clear that a focus on interacting processes across spatial scales is key to explaining model behaviour and understanding future change in East Africa (Rowell et al. 2015, Vellinga and Milton 2019). This thesis contributes by providing a detailed evaluation of model representations of IOWC-rainfall connections as a source of East African rainfall biases, as well as consideration of the Turkana LLJ as a limiting factor in the ability of coarse-scale GCMs to accurately simulate East African rainfall. This emerging literature can guide downscaling, hydrological modelling, and impact planning, as well as model development.

8. Summary of Aims and Objectives for Each Chapter

The aims and objectives (research questions) for each chapter are included within the chapters themselves, but are also provided here for reference.

8.1. Chapter 11

- What is the relationship between the reanalysis vertical components of the Indian Ocean Walker circulation and observed Kenyan rainfall?
- How is this relationship represented in CMIP5 models?
- How are the CMIP5 rainfall biases in the East African region associated with their simulations of the Walker circulation?

8.2. Chapter 12

- What is the climatology of the Turkana LLJ in MERRA-2, ERA5, and JRA55, and how does it interact with regional rainfall?
- How has the Turkana LLJ changed over recent decades (1981-2016) and what might account for these changes?
- How is the Turkana LLJ and its links to rainfall represented in CMIP5 models, and how does model topography affect this representation?

8.3. Chapter 13

- What are the projected changes in rainfall over Kenya in CMIP5 models up to 2100?
- What are the projected changes in omega and zonal wind associated with the IOWC?

- Do future projections reflect historical model biases?

9. Notes on Thesis Format

This thesis follows the paper-based route as laid out in the examination requirements for the DPhil in Geography and the Environment at the University of Oxford. The thesis consists of three scientific papers with a framing document consisting of an introduction, literature review, and conclusion. For all three papers, I was the lead author; my supervisors and colleagues are credited in the published and submitted versions as co-authors. Sections 9.1 and 9.2 include authorship statements for each paper.

Previous versions of various sections of the thesis have been presented at a number of conferences, including several meetings of the UK Met Office African Meteorology and Climate Working Group ('Africa MAC') in various locations; the European Geosciences Union (EGU) General Assembly in Vienna; the Centennial Meeting of the American Meteorological Society (AMS) in Boston, Massachusetts; the Royal Meteorological Society Student and Early Career Scientists' Annual Conference in Birmingham; the GCRF African SWIFT International Summer School on the Tropical Meteorology of West and East Africa in Kumasi; the GOTHAM/PIK Summer School on Teleconnections in the Climate System in Potsdam; and the NERC DTP Wessex Conference in Bristol. My thanks to all who make these events possible, whether in person or remotely. Meeting fellow researchers from around the world to discuss climate science has been a highlight of my time as a DPhil candidate, and helped me find my place in a welcoming global community of scholars.

The graphically intensive nature of this work means that some figures are not best represented on an A4 page. Full high-resolution image files of all figures in the thesis are provided separately in the 'Additional Materials' section of the Research Theses Digital Submission platform, for the reference of examiners.

9.1. Chapters Published – Authorship Declaration

Chapter 11 is published in the *International Journal of Climatology* as follows:

Representation of the Indian Ocean Walker Circulation in Climate Models and Links to Kenyan Rainfall

James A. King[1], Richard Washington[1], and Sebastian Engelstaedter[1]

[1]School of Geography and the Environment, University of Oxford.

Received 12.12.2019, Accepted 16.6.2020, Published 6.7.2020

Int. J. Climatol, https://doi.org/10.1002/joc.6714

I devised and designed the research, carried out the analysis, and wrote the paper. As my supervisors, Richard Washington and Sebastian Engelstaedter assisted with the development of the methodology, discussed the interpretation of results, and provided comments on the manuscript during the preparation and revision of the paper.

Chapter 12 is published in the *Journal of Geophysical Research: Atmospheres* as follows:

Variability of the Turkana Low-Level Jet in Reanalysis and Models: Implications for Rainfall

James A. King[1], Sebastian Engelstaedter[1], Richard Washington[1], and Callum Munday[1]

[1]School of Geography and the Environment, University of Oxford

Received 22.10.2020, Accepted 19.4.2021, published (preliminary version) 23.4.2021

J. Geophys. Res. Atmos., https://doi.org/10.1029/2020JD034154

I devised and designed the research, carried out the analysis, and wrote the paper. Sebastian Engelstaedter made Figure 12.4 and contributed linear regression analysis of the Turkana LLJ which forms part of Table 4. Richard Washington and Sebastian Engelstaedter assisted with the development of the methodology, discussed the interpretation of results, and provided comments on the manuscript during the preparation of the paper. Callum Munday contributed discussions on the framing of the paper and provided comments on the manuscript during the submission process.

9.2. Chapters Submitted – Authorship Declaration

Chapter 13 is currently (27th[th] April 2021) undergoing peer review at the *Journal of Geophysical Research: Atmospheres* as follows:

Future Changes in the Indian Ocean Walker Circulation and links to East African Rainfall

James A. King[1] and Richard Washington[1]

[1]School of Geography and the Environment, University of Oxford, Oxford, UK

Received 14.1.2021

I devised and designed the research, carried out the analysis, and wrote the paper.

10. Data and Methods

10.1. Introduction

The process-based climate model evaluation methodology used in this thesis requires both climate model data, and observed and observationally-derived data products to provide benchmarks against which to assess the models. The model data used are from the Coupled Model Intercomparison Project Phase 5 (CMIP5; Taylor et al. 2012), which reflected the state-of-the art in GCM simulation during the time when the majority of the analysis was undertaken. Output from these models provides the basis for projections of future climate provided by the IPCC, and thus guides international climate policy; evaluation of the plausibility of the model output is therefore important to ensure climate policy is guided by the best possible science. To evaluate the model output data, reanalysis, gridded rainfall and temperature datasets are used, as well as measurements from weather stations (though quality control issues in raw station data mean direct observations are only used as supplementary data sources, and post-processed data incorporated into gridded datasets are used preferentially – see section 10.2.2). Chapters 11, 12, and 13 each provide more detailed overviews of the observational and observationally-derived datasets used to answer specific research questions. There are a number of datasets available to the climate scientist for investigating key variables such as rainfall and temperature. Subjective decisions on which to use must therefore be made. In each chapter, these decisions are justified based on published evaluations of datasets for

the variables in question. Dataset selection was also determined to some extent by data availability, for example for particular model variables. This section gives an overview of the datasets used, as well as the statistical approaches applied.

10.2. Observations

10.2.1. Precipitation

This thesis is primarily concerned with evaluating model rainfall. While the CMIP5 model precipitation field includes snow and hail, most precipitation during the East African wet seasons falls as liquid rain (with the exception of snowfall over the highest mountains, such as Kilimanjaro and Mt Kenya (Chan et al. 2008)). Measuring rainfall is a non-trivial task, with observations having a degree of dependence on the type of raingauge used to make the measurements (Haselow et al. 2019) and the use of manual versus automatic observations (Valík et al. 2020). Datasets can also differ depending on the methodology employed to derive information about rainfall from remote sensing platforms such as satellites (Gehne et al. 2016). In general, it is advantageous to combine point measurements of rainfall from stations with remotely sensed data to reduce the influence of interpolation techniques on the rainfall amount (Awange et al. 2015). This does still require a network of well-maintained and regularly reporting raingauges however. This is a particular problem in tropical Africa, where the number of reporting stations, which was already low when compared to the global North, has been steadily decreasing since the late 1980s owing to a variety of factors including conflict and privatisation (Washington et al. 2006, 2013). Figure 10.1 indicates the geographical distribution

of reporting raingauges in the East African domain over time. While the density of raingauges in central Ethiopia has remained more or less constant, there are fewer reporting raingauges in Kenya in 2008 compared to 1988, and there have been no reporting raingauges in Somalia since the 1990s. The clustering of raingauges in East Africa shown in Figure 10.1 indicates that the density of raingauges is much greater around major cities such as Addis Ababa, while there may not be any reporting raingauges in rural areas where the impact of rainfall change on agriculture may be more significant. One reason for the focus on Kenya in this thesis is the more even geographical distribution of raingauges across recent decades, when compared to Ethiopia and Somalia (Figure 10.1).

There are a number of gridded rainfall products available based on ground observations, such as CRU (Harris et al. 2015) and GHCN (Menne et al. 2012), and combining gauge and satellite data, such as TAMSAT (Tarnavsky et al. 2014) and GPCP (Huffman et al. 2009). Although these datasets facilitate direct comparison with climate models, they do not generally rely on different raingauge networks, especially in regions such as East Africa where data are sparse (Kimani et al. 2017). Therefore, the differences between products relate to the statistical approaches used to fill the gaps between observations, and/or their resolution, especially in regions of complex topography (Dinku et al. 2018). In this thesis, the reference dataset used for rainfall is the Climate Hazards Group Infrared Precipitation with Stations version 2.0 (CHIRPSv2.0; Funk et al. 2015). Developed specifically for drought monitoring requirements in the tropics, this dataset combines quality-controlled observations of rainfall from stations with satellite-based estimates using a cold cloud duration retrieval algorithm (Funk et al. 2015). As detailed in chapters 11 and 12, this dataset has been extensively validated over East Africa by researchers independent of its

development team, and has been consistently found to be the best-performing gridded rainfall product with respect to point data from observational campaigns and weather stations (e.g. Kimani et al. 2017, Gebrechorkos et al. 2017). The dataset outperforms TAMSAT and ARC2 on the monthly timescales which the thesis focuses on (Dinku et al. 2018). Its high spatial (0.05°) and temporal (up to 1 day) resolution make it ideal for investigating rainfall variability and change in areas of complex topography such as East Africa, while its use of satellite data to cover areas with sparse gauge coverage reduces the interpolation-dependence of more strongly rain gauge-based products.

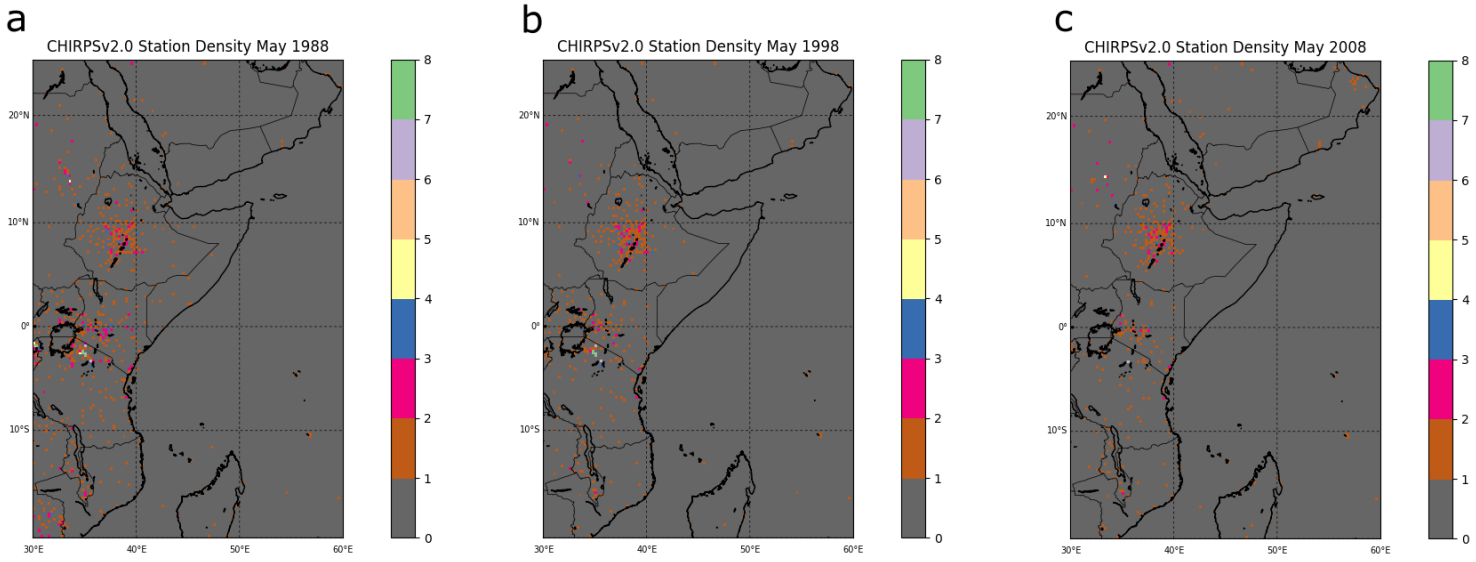


Figure 10.1 – density of raingauges contributing to CHIRPSv2.0 in 1988 (a), 1998 (b), and 2008 (c), per 0.05° grid box.

10.2.2. Station Data

The smaller spatial scale of the analysis in chapter 12 (on the Turkana LLJ) enables the use of direct observations of the atmosphere from meteorological stations. Data

were obtained from the Global Weather Observation Data section of the UK Met Office Integrated Data Archive System (MIDAS; Met Office 2012), which provides a global dataset of weather observations at 3-hourly intervals, for three stations in the Turkana Channel area (see section 12.3). Quality control flags are provided for each station (methodology outlined at http://cedadocs.ceda.ac.uk/1488/7/MIDAS_User_Guide_for_UK_Land_Observations_Version20200921.pdf). It is important to note, however, that MIDAS data quality conventions are only monitored within the UK, and that station data from stations in rural Kenya may not be as rigorously quality-controlled. For the station data used in chapter 12, quality control codes are non-zero for occasional periods, often lasting several weeks, of the observations at each of the three stations used. For example, during July and August 1985, a quality control flag is applied for wind speed observations at Lodwar station. This indicates that full quality control has not been applied for these periods. While the influence of these flags on data averaged over multiple decades is not likely to be substantial (T. Caton Harrison, personal communication), it nonetheless means that these values, while the only available direct measurements in the region, should not be viewed with the same level of confidence as station data from the UK network. It is also not methodologically advisable to compare climate model simulations to point-scale observational data, as interpolation of gridded data to a single longitude/latitude grid reference gives different results depending on the resolution of the input (Hofstra et al. 2010). The observations of surface winds are also not directly comparable to the 850hPa winds being analysed in chapter 12. Therefore, station data do not constitute the primary source of data for model assessment in this thesis. It has been noted that the sparsity and temporal and qualitative inconsistency of meteorological observations in tropical Africa is a limiting factor on our understanding of regional climate processes and

trends (Washington et al. 2006, 2013; Maidment et al. 2015, James et al. 2018). Sections 12.5 and 14.4 discuss in more detail the need for observational constraints on the Turkana LLJ and provide suggestions for future research.

10.3. Reanalyses

In the absence of direct observations of key aspects of the atmospheric circulation, in particular the vertical velocity and oceanic wind fields used in this thesis to derive information about the IOWC, it is necessary to use reanalysis data as a proxy for such observations. Reanalysis datasets are used to initialise numerical weather prediction (NWP) models, and are also commonly used as reference datasets in climate science for fields where there are either no direct observations, or where observations are of low quality (Parker 2016). Reanalysis projects assimilate meteorological observations to generate a 'best estimate' of the state of the atmosphere at a specific time (the 'analysis'), which is then used to initiate a weather forecast. The assimilation scheme which generates the analysis fields is continuously developed and improved (e.g. Hersbach et al. 2020), and the analysis fields are re-generated over a period of several decades using a fixed NWP scheme (the 're-analysis').

Observations are assimilated and in some cases directly incorporated into reanalysis datasets (such as precipitation in MERRA-2; Gelaro et al. 2017). However, dynamical fields in the datasets are determined in part by NWP models (such as the IFS system in ERA5; Hersbach et al. 2020). Therefore, reanalyses should not be considered observations; rather, they can be understood as model simulations of recent climate which are constrained by and incorporate observations (Parker 2016). Reanalyses are subject to uncertainty from many of the same sources as GCMs, for

example in the use of parameterisations for convection and cloud development, which is particularly important over tropical Africa; Wright and Fueglistaler (2013) showed that different parameterisations used resulted in significant differences between reanalyses in the representation of tropical convection, and further that moisture is not conserved in reanalyses. For features such as the Turkana LLJ which are constrained by topography, representation in reanalyses can be affected by spatial resolution (Vizy and Cook 2019). Additionally, evaluation of reanalysis data against satellite scatterometer measurements of surface wind has revealed some differences between datasets over the Indian Ocean, for example in representation of the annual cycle of the Somali Jet between the QuickSCAT satellite dataset and the previous-generation NCEP and ERA-Interim reanalyses (Collins et al. 2012); the NCEP product also underestimates surface wind magnitude and intraseasonal variability over the Indian Ocean compared to QuickSCAT (Goswami and Sengupta 2003). The current generation ECMWF reanalysis, ERA5, shows improved performance relative to ERA-Interim in terms of surface wind biases when assessed against the ASCAT satellite product, though some biases remain over the tropical Indian Ocean with excessively strong winds in the eastern tropical Indian Ocean and excessively weak winds in the west, which could affect its representation of the Walker circulation through the effect of surface winds on SST through Bjerknes feedback (Belmonte Rivas and Stoffelen 2019). However, Luo et al. (2020) find that MERRA-2 (see below) and ERA-Interim perform well with respect to ship-based SST measurements in the Atlantic, with biases on the order of ~0.1K, concluding that the SSTs in these reanalyses are most likely reliable. ERA5 shows higher SST biases against the same benchmark but these are still small (on the order of ~0.2K) (Luo and Minnett 2020). While scatterometer winds are measured at the surface, which means that direct evaluation of model winds at 850hPa is not possible using them,

the analyses of Goswami and Sengupta (2003), Collins et al. (2012) and Belmonte Rivas and Stoffelen (2019) demonstrate that reanalysis winds do not represent an ideal observational benchmark and instead are used here out of necessity for direct comparison to model wind data above the surface (Parker 2016).

Reanalysis products are more model-dependent in sparsely instrumented regions such as East Africa, and for variables for which there is no consistent observational network, such as for wind over the oceans and upper tropospheric variables. Three reanalysis datasets are used in this thesis: the Modern-Era Retrospective Analysis for Research and Applications (MERRA-2) reanalysis (Gelaro et al. 2017); the European Centre for Medium-Range Weather Forecasts Reanalysis 5 (ERA5; Hersbach et al. 2020); and the Japanese 55-year Reanalysis Project (JRA-55; Kobayashi et al. 2015). The key features of these datasets are listed in Table 10.1.

Table 10.1 - Details of reanalysis products used in this thesis.

Product	**Institution**	**Spatial Resolution**	**Temporal Resolution**	**Time Period**	**Assimilation Scheme**
MERRA-2	NASA (USA)	0.625˚ x 0.5˚	3 hrs	1980-present	3D-VAR
ERA5	ECMWF (UK/EU)	0.2815˚ x 0.2815˚	1 hr	1950-present	4D-VAR ensemble
JRA-55	JMA (Japan)	0.5625˚ x 0.5625˚	3 hrs	1958-present	4D-VAR

How the datasets are used in each chapter depends on the research questions being asked. For chapter 11, preliminary analysis did not reveal substantial differences between reanalysis datasets in terms of their representation of the IOWC

overturning, in line with recent studies on dynamic and thermodynamic performance of reanalyses which indicate a good level of coherence between different products (Wang et al. 2019, Pokhrel et al. 2020). The chapter was further informed by Hua et al. (2019), who compared reanalysis winds over tropical Africa with quality-controlled radiosonde observations and found MERRA-2 to be the best performing. Since these winds are part of the regional-scale circulation investigated in the thesis, chapter 11 (and by extension chapter 13) use MERRA-2 as a reference dataset. Chapter 12 is concerned with the variability of the Turkana LLJ, a feature which is represented differently in various reanalyses (Vizy and Cook 2019). As the research questions for the chapter involve analysing the plausibility of trends in the jet strength, all three reanalyses are investigated in detail.

10.4. CMIP5 Models

The CMIP5 ensemble (Taylor et al. 2012) provides a standardised set of GCM model experiments. As part of the intercomparison project, over 20 modelling centres from around the world provide ~40 coupled models which are run using prescribed forcings in a standardised set of experiments. As well as coupled ocean-atmosphere GCMs, the ensemble also includes Earth System Models (ESMs). These simulate interactive carbon cycles, vegetation functional types, and atmospheric chemistry (e.g. reactive species in the troposphere), and the feedback between these systems and the Earth's radiative balance. The spatial resolution and complexity of CMIP5 models is generally increased relative to the previous CMIP3 generation, but is not standardised; differences in model resolution and model construction provide a quantifiable envelope of uncertainty (Hawkins and Sutton 2011) within which

differences in model behaviour can be investigated and accounted for in terms of differing levels of performance.

Within the range of prescribed forcing experiments that make up the CMIP5 dataset, this thesis uses two main scenarios. The historical coupled simulations represent the recent past (generally from 1850-2005), and as such provide the benchmark for comparison with observations and reanalysis. These model runs are forced with standardised estimates of greenhouse gas concentrations, sulphate aerosols, solar input, and volcanic eruptions. Integration lengths for the historical experiment vary, but data are generally available for the entire 20th century and the first decade of the 21st. For consistency, the period 1975-2005 is used to represent the recent climate, noting the need to balance out observational data availability with the need for timeseries of sufficient length to avoid the spurious identification of trends (≥30 years where possible; Lewandowsky et al. 2015, Mudelsee et al. 2019). Where other time periods are used, this is as a result of data availability of rainfall or reanalysis datasets at the time of writing (as detailed in chapters 11, 12, and 13).

The future change scenarios in CMIP5 are based on the concept of representative concentration pathways (RCPs; van Vuuren et al. 2011), whereby the name of the scenario refers to the radiative forcing of the atmosphere (in W m^{-2}) relative to pre-industrial levels. By framing the scenario around a physical quantity, this aims to avoid an overly prescriptive approach to socio-economic change – the projection of which is not physically based – but which can be reconciled with a range of possible future trajectories of global economic behaviour (van Vuuren and Carter 2014). This thesis uses the RCP8.5 scenario, which corresponds to a radiative forcing level of 8.5 W m^{-2} in 2100, which is equivalent to a GHG concentration of ~1370 ppm CO_2 equivalent (van Vuuren et al. 2011). This scenario was selected for two main reasons.

From a scientific point of view, selecting a high radiative forcing increase should result in stronger change mechanisms in the models, thereby reducing the signal-to-noise ratio and enabling clearer identification of change mechanisms for process-based evaluation. From a socioeconomic and political perspective, RCP8.5 includes a range of plausible futures in which global GHG emissions continue to increase, as a result of modest increases in technology efficiency and income growth combined with limited international success in reducing emissions (Riahi et al. 2011); a situation reflective of ongoing emissions increases (Jackson et al. 2019) and inaction on emissions reduction on the part of corporations (Finke et al. 2016, Ganguly et al. 2018) and governments (Luderer et al. 2013, Copland 2020, McLaren and Markusson 2020).

The ensemble of models selected is detailed in Table 11.1. The models were selected based on the availability of key variables in both historical coupled and RCP8.5 experiments. Additionally, the atmosphere-only historical runs (AMIP) are used to assess the impact of sea surface temperature (SST) biases in chapter 11; where an AMIP version of a model was not available, a comparable model from the same modelling centre was selected. For consistency, the first ensemble member (R1I1P1) for each model was used, and ensembles and composites were calculated after first having interpolated models onto a common 360 x 180 grid. CMIP5 models are not completely independent of one another, as commonalities in fundamental code, parameterisations, and other aspects of model architecture can be shared between modelling centres (Knutti et al. 2013). Consequently, within the constraints imposed by data availability, a wide range of models from different centres have been chosen, and differences between the models accounted for in terms of their dynamics using both rigorous statistics and examination of model processes.

10.5. Statistical Methods Used

The thesis uses common statistical methods to assess relationships between variables and potential trends in the datasets. It is important to acknowledge the limitations of classical statistics when applying them to climate data. A principal issue is that the extremely high number of data points in gridded data risks the spurious attribution of statistical significance, which some have argued invalidates their usage (e.g. Ambaum 2010). This thesis does not take such a strong position against significance testing, but rather acknowledges that any use of indicators such as *p* values should not alone provide a means to a conclusion. Therefore, the statistical analyses are combined with composite analysis techniques and detailed examination of model dynamic fields to ensure any conclusions drawn have a firm physical basis (Chai and Draxler 2014). Where statistical methods are applied to relatively small sample sizes, such as the trend analyses in chapter 12, the issue of potentially spurious results is related to the interpretation of significance rather than the inevitability of significant results in very large samples. To improve rigour, multiple methods of trend analysis are applied and interpretation is guided by consideration of the physical plausibility of statistically significant trends.

10.5.1. Correlation Analysis

Firm conclusions about cause and effect in complex systems such as the atmosphere cannot be drawn through covariability analysis alone, but this method does enable the identification of relationships between variables which provide suggestions for further investigation into the possibility of an underlying dynamical link, or an

influence exerted by a third variable (Sanderson and Knutti 2012). Covariability between variables in phase space is assessed using x/y scatter plots. For spatial data, the Pearson product moment correlation coefficient is used. This test assesses the relationship between two variables by dividing their covariance (the sum of the differences between data points and the sample mean) by the total variance (as represented by the sum of the sample standard deviations). The test statistic *r* is thus given by

$$r_{x,y} = \frac{\sum(x-\bar{x})(y-\bar{y})}{\sqrt{\sum(x-\bar{x})^2 \sum(y-\bar{y})^2}} \quad (10.1)$$

For gridded data, Pearson's *r* is calculated for each grid point (x,y) at each time step and the results are plotted as a map. The goodness of fit is measured by the square of the *r* value. The statistical significance of *r* is then assessed using *p* values derived from the two-tailed Student's t-distribution at confidence intervals of 90% or 95%. An *r* value closer to ±1 indicates a high degree of covariability, and a *p* value closer to 0 suggests a low probability that the covariance is attributable to random change (i.e. a high probability that a null hypothesis of no meaningful relationship between the variables can be rejected).

10.5.2. Root Mean Square Error

The root mean square error (RMSE) is a standard metric of error commonly used in climate science to measure the performance of a model relative to observations (Chai and Draxler 2014). It is used here to provide a metric for model performance in

interrelated dynamic fields, in order to build up a statistical picture of the model's ability to realistically simulate the East African climate. The RMSE value is given by

$$RMSE = \sqrt{\frac{\sum_{t=1}^{T}(x_{1,t}-x_{2,t})^2}{T}} \quad (10.2)$$

for equal-length sets of model values $x_{1,t}$ and observations $x_{2,t}$. The smaller the RMSE value, the closer the model timeseries is to the observed or observationally-derived timeseries. The square term in equation 10.2 removes directionality from the measurement of model error, which is a limitation when model biases can either be positive or negative within the same ensemble (as is the case with the variables under consideration in this thesis). Therefore, the RMSE is not used in isolation, but rather is combined with measures of model bias to ensure that models with 100% biases (for example, when the mean state equatorial zonal winds over the Indian Ocean are in the wrong direction) are not considered 'realistic' based on low RMSE values.

10.5.3. Trend Analysis

Two standard methods of analysing trends are used in the thesis. The primary method used is linear regression, but the Mann-Kendall test is also employed for additional trend verification where a non-parametric test is applicable.

10.5.3.1. Linear Regression

Simple linear regression is a standard method for quantifying how a variable changes over time. In this thesis, linear regression is used on timeseries data in both index

(e.g. the zonal wind speed in the Turkana Channel) and grid point forms (e.g. gridded rainfall data with multiple timesteps at each grid point). For the latter, the linear regression coefficients are calculated for each grid point at each time step. A least-squares algorithm is employed to estimate the slope of the linear regression curve

$$y = mx + c + \varepsilon \quad (10.3)$$

where y is the climatic variable in question, x is time, m is the slope, c is the y-intercept, and ε is an error term, such that the residual distance $\hat{\varepsilon}$ between the curve and the pairwise values x, y is minimised. The slope then gives the rate of change of the variable over time. Significance is assessed using *p* values derived from the two-tailed Student's t-distribution at confidence intervals of 95%.

10.5.3.2. Mann-Kendall Test

Linear regression analysis requires that the trend in the data can be assumed to be linear. While this is treated as a valid assumption for the purposes of revealing underlying variability in East African climate on interannual to decadal timescales, based on the known existence and physical plausibility of linear climatic trends in the region under recent anthropogenic climate change (Hoell et al. 2017), it is useful for the purposes of rigour to apply a non-parametric test to determine the presence of a trend independent of this assumption. In climate science, the Mann-Kendall test is often used to determine whether time series data have monotonic increasing or decreasing trends (i.e. if values in the timeseries tend to be larger or smaller than the values preceding them; Bari et al. 2016). The test statistic *S* for a time series with n data points is given by

$$S = \sum_{i=1}^{n-1} \sum_{j=i+1}^{n} sign\,(x_j - x_i) \quad (10.4)$$

where x_j and x_i are the values of the time series and j > i. If $S > 0$, the values in the time series tend to increase with time, and they tend to decrease with time if $S < 0$. The significance can then be determined using *p* values. The slope of the Mann-Kendall trend is estimated using the Theil-Sen slope estimator. This is computed by taking the median of the set of points x_i, y_i (where y contains timeseries data, x is the time coordinates thereof, and j > i) as follows

$$Slope = median\left\{\frac{y_j - y_i}{x_j - x_i}\right\} \quad (10.5)$$

A line can then be fitted to the data by using the median as m in equation 10.3, with the y-intercept c set as the median of the values $y_i - mx_i$. This method is based on that of Gogic and Trajkovic (2013).

10.5.4. Composite Analysis

Composite analysis is a tool used in climate science to determine the circulation characteristics particular to a given set of conditions, for example comparing drought and flood conditions. This can then be used to derive physical hypotheses to explain the salient climate processes (Boschat et al. 2016, Howard and Washington 2018, Vizy and Cook 2019). It follows that the approach can also be used in process-based climate model evaluation to identify common signals in the circulation in models

with biases in a particular direction, for example wet versus dry models (Creese et al. 2019). By comparison between composites and reanalysis, and between past and future composites, process-based constraints on model projections can be developed (Creese et al. 2019). Composites are constructed by taking the arithmetic mean of model values x_1, ..., x_n at each grid box i, j, after first interpolating the model data onto a common grid. The averaging is as in Munday and Washington (2019), as follows

$$\frac{x_{1,i,j}+x_{2,i,j}+\cdots x_{n,i,j}}{n} \quad (10.6)$$

Composite differences (e.g. wet composite minus dry composite) are used to further elucidate the circulation differences between subsets of models. Where this approach is used, the criteria for selecting which models are included in the composite mean are explained in the chapter in question.

11. Paper 1 – Representation of the Indian Ocean Walker Circulation in Climate Models and Links to Kenyan Rainfall

11.1. Abstract

Reliable climate change projections over East Africa are vital because of regional vulnerability to precipitation changes. However, global climate models from Coupled Model Intercomparison Project Phase 5 (CMIP5) display significant biases in their representation of key East African rainfall seasons, which call into question the reliability of projected climate change. We investigate the links between models' representation of rainfall over Kenya during the Long and Short Rains and the proximate Walker Circulation. There is a strong correlation in the Short Rains between model biases in Kenyan rainfall and in the mid-to-upper tropospheric vertical velocity associated with this circulation. The overturning Indian Ocean Walker cell at the equator is absent in 5/25 models during the Short Rains – these models exhibit wet biases. In the Long Rains, dry biased models overestimate the strength of the descending limb of the circulation over East Africa. Omega biases over the Congo Basin are linked to broader Walker Circulation biases. During the Long Rains, models overestimate equatorial descent more generally across the Western Hemisphere tropics (0°E-200°E). A significant correlation is obtained across the model ensemble between model rainfall over Kenya and Western Hemisphere equatorial ascent during November. Atmosphere-only models display some improvements over coupled models, but biases of a similar magnitude remain. We therefore propose Indian Ocean Walker Circulation errors as a key source of bias in CMIP5 East African rainfall. The results add to recent work on CMIP5 biases in this region, demonstrating that the Indian Ocean Walker Circulation should be a focus for future model improvement and a consideration when assessing the reliability of climate projections over East Africa. Further work is needed on the causes of Walker Circulation biases (in particular the role of SST), and on

understanding the impact of Walker Circulation biases on modelled tropical rainfall elsewhere in the world.

11.2. Introduction

Climate models are our primary tool for projecting the global climate system's response to warming brought about by anthropogenic greenhouse gas emissions. They are used to formulate policy on scales from the global to the local, but often exhibit substantial biases in vital output fields such as precipitation (Li and Xie 2014, James et al. 2015, Rowell et al. 2015, Tierney et al. 2015, Ongoma et al. 2017, James et al. 2018). In some regions of the world, models display sizeable systematic biases relative to observations – errors which, having a shared direction, may be indicative of a common underlying dynamical problem (Sanderson and Knutti 2012). It is therefore important to understand the underlying physical processes operating within models with respect to biases, so that these biases can be both foci for targeted model improvement (James et al. 2015, Collins et al. 2018, James et al. 2018) and can be taken into account when assessing the reliability of projections derived from a specific model or model ensemble (McSweeney et al. 2015). Global climate models are run at spatial resolutions that make it difficult to replicate the complexity of the circulation responsible for specific characteristics of regional circulations. The approach whereby climate model performance is evaluated based on dynamical processes is therefore of particular use in climate projections on smaller spatial scales useful to policy-makers (Collins et al. 2018), and is more revealing than simply relying on a comparison between model output and a reference dataset (James et al. 2015), especially in regions such as the tropics where observational data may be

sparse or of poor quality (Washington et al., 2013, Gebrechorkos et al. 2018). Therefore, studying model dynamics in such regions can have useful impacts on both the modelling and climate adaptation communities.

Models participating in the Coupled Model Intercomparison Project Phase 5 (CMIP5; Taylor et al. 2012) exhibit systematic biases in their representation of historical rainfall over East Africa (Yang et al. 2014, Tierney et al. 2015). The models tend to underestimate rainfall in the Long Rains season (March-April-May), some by over half, and to overestimate it in the Short Rains season (October-November-December), some by over 100%. In historical coupled simulations, the magnitude of the model ensemble range (i.e. the difference between the wettest and driest models) is greater than the observed monthly mean rainfall in all rainy season months other than April (Tierney et al. 2015).

An understanding of model rainfall biases is crucial to climate change adaptation planning in East Africa (Collier et al. 2008, Shongwe et al. 2011, Uhe et al. 2018). Around 75% of the working population are involved in rain-fed agriculture (Lyon 2014), and hydroelectricity provides the majority of the region's energy; rainfall is thus closely linked to development (Funk et al. 2008, Borgomeo et al. 2018). East Africa has recently experienced a series of severe droughts, for example in 1983-84 and 2010-11 (Lyon 2014), with drought conditions prevailing since around 2008 (Nicholson 2016a). Around 17.5 million people are at risk from food shortages in Ethiopia, Somalia, and Kenya (Williams and Funk 2011) and links have been suggested between drought and conflict in Somalia (Thalheimer and Webersik 2020). Uncertain rainfall projections raise significant dilemmas (Washington et al. 2006, Giannini et al. 2018). For instance, should countries invest in more irrigation infrastructure and hydroelectric power, given projected rainfall increases (Kaunda et

al. 2012)? Or, rather, should they focus on reducing the impacts of drought events, given the climatic trends of the last 30-40 years? A first step towards addressing these questions is an understanding of the causes behind models' rainfall biases. Elsewhere in Africa, model rainfall bias has been shown to condition the nature of projected climate change (Munday and Washington, 2019).

The seasonal cycle of rainfall in East Africa is associated with the northward/southward movement of the tropical rain belt, although the complexity of the local topography and rainfall dynamics limits the explanatory power of this feature (Nicholson 2018). Important fundamental influences on East African rainfall include moisture flux from the Indian Ocean (Viste and Sorteberg 2013, Yang et al. 2015b), moist static energy profiles (Yang et al. 2015b), and topography (Slingo et al. 2005, Hession and Moore 2011, Naiman et al. 2017). Dynamically the rainfall is modulated on intraseasonal to interannual timescales by the Madden-Julian Oscillation (Berhane and Zaitchik 2014, Zaitchik 2017), Indian Ocean SST, and the Quasi-Biennial Oscillation (Vellinga and Milton 2018). The understudied low-level jet in the Turkana Channel may also have a role in controlling regional aridity and rainfall variability (Nicholson 2016b, Hartman 2018, MacLeod 2019).

Efforts to understand the nature of future climate change have put a premium on circulation over thermodynamics in the tropical atmosphere (Chadwick et al., 2013). On a global scale, the wider multi-cell Walker circulation is associated with the El Niño Southern Oscillation (ENSO), and while the strength of the teleconnection between East African rainfall and ENSO, primarily observed during the Short Rains, has varied throughout the observational record (Nicholson 2015), the Walker Circulation may act as a mechanism by which the ENSO signal (and Pacific SST

warming more generally) is transmitted to East Africa via modification of vertical velocity and moisture transport (Black 2005, Hoell et al. 2014, Lyon 2014).

Models tend to exhibit positive IOD biases in boreal autumn and winter (Cai and Cowan 2013), but attribution of recent East African spring drying to the IOD is limited because the IOD is generally neutral in this season. Furthermore, the tendency of models to project increasing spring rainfall under future forcing scenarios, in direct contrast to the recent observed drying trend, has been termed the 'East African Climate Paradox' (Rowell et al. 2015, Wainwright et al. 2019). While the 'paradox' refers to the Long Rains, the majority of the models' projections of wetting occur during the Short Rains in response to projected Walker Circulation weakening (Tierney et al. 2015, Kociuba and Power 2015, Endris et al. 2018). This is in opposition to recent observations, leading the models' representation of the Walker Circulation to become a significant source of uncertainty in future projections (Tierney et al. 2015, Giannini et al. 2018).

The link between the Walker Circulation and East African rainfall in observations has been well established (e.g. Black et al. 2003, Behera et al. 2005, Liebmann et al. 2014, Vigaud et al. 2017, Liebmann et al. 2017), particularly for the Short Rains where there is a strong correlation between surface equatorial westerlies and rainfall (Mutai et al. 2012). These westerlies, which form part of the overturning Walker cell in the Indian Ocean, are in turn closely correlated with the zonal SST gradient in the Indian Ocean. This is most pronounced during boreal winter when the Indian Ocean Dipole (IOD) is most active (Black 2005). The Pacific component of the Walker Circulation has been observed to be strengthening on decadal timescales since the 1950s (L'Heureux et al. 2013), coincident with a decadal drying signal over East Africa during the Long Rains (Rowell et al. 2015). A dynamic link between the two

has been suggested; SST warming in the eastern Indian Ocean (a negative IOD) has led to increased convection/precipitation in the east of the basin (Liebmann et al. 2017), resulting in easterly movement of air aloft which suppresses convection over East Africa (Williams and Funk 2011, Liebmann et al. 2017). Recent work has linked model rainfall biases in East Africa to erroneous low-level zonal winds over the equatorial Indian Ocean (Hirons and Turner 2018), which are part of the overturning circulation. The Walker Circulation has also been found to be poorly represented over Madagascar, with an overly simplified connection between Indian Ocean subsidence and Southern African convection (Munday and Washington 2018). Given that SST warming in the Indian and Pacific oceans is likely to be anthropogenic, whereas ENSO is fundamentally a natural mode of variability modified by warming, it is likely that both anthropogenic and natural forcings need to be considered to explain the recent drying trend – however, model biases frustrate such attribution (Hoell et al. 2017). In addition, work on the Walker circulation tends to focus on the zonal winds and/or the ascending component, whereas both ascending and descending components interact to produce observed rainfall (Li et al. 2015). Here, we add to this analysis by presenting an assessment of how models' circulation biases affect their rainfall biases. We aim to address the following questions:

1. What is the relationship between the reanalysis vertical components of the Indian Ocean Walker Circulation and observed Kenyan rainfall?
2. How is this relationship represented in CMIP5 models?
3. How are the CMIP5 rainfall biases in the East African region associated with their simulations of the Walker Circulation?

The layout of the rest of the paper is as follows: Section 11.3 introduces the datasets used. Section 11.4 reviews the rainfall climatology of Kenya and examines the Walker Circulation/rainfall relationship using gridded rainfall and reanalysis data. Section 11.5 analyses the representation of the Walker Circulation in CMIP5 models and its links to Kenyan rainfall. Section 11.6 summarises the paper in the context of future climate projections, and provides a conclusion.

11.3. Data

Rainfall data used in this study were obtained from version 2 of the Climate Hazards Group Infrared Precipitation with Stations dataset (CHIRPSv2.0; Funk et al. 2015). This is a high-resolution (0.05°) gridded dataset which combines observed rainfall from raingauges with remotely sensed infrared measurements of cold cloud duration. It has performed well in assessments of precipitation datasets over East Africa relative to station data, and has been suggested to be the best available satellite estimate of rainfall over eastern equatorial Africa (Kimani et al. 2017, Gebrechorkos et al. 2018). Given the lack of direct observations of the upper troposphere, reanalysis data were used as the reference climatology for the Walker Circulation. Reanalysis products differ slightly in their representations of the tropospheric circulation over equatorial Africa (Washington et al. 2013, Maidment et al. 2015). While the difficulty of obtaining direct observations of tropospheric vertical motion over the oceans precludes direct validation studies for the time being, version 2 of the Modern-Era Retrospective Analysis for Research and Applications (MERRA-2) reanalysis (Gelaro et al. 2017) has been suggested to be the most realistic of those currently available at representing tropospheric wind fields over equatorial Africa

when compared to quality-controlled observations from radiosondes (Hua et al. 2019). Given that such winds are part of the overturning cells upon which this article is focussed, MERRA-2 data has been used. ERA-Interim and NCEP2 data produced similar results (not shown).

The climate model data used are from CMIP5 (Taylor et al. 2012). A subset of 25 GCMs was selected based upon the availability of vertical velocity and wind fields from the historical coupled runs, and forcing experiments with the RCP8.5 scenario (which is the closest to observed recent CO_2 concentration increases (Sanford et al. 2014)) for use in future work (Table 11.1). The first ensemble member for each model was used over the period 1975-2005. Initial analysis using the first three ensemble members for two randomly selected models (ACCESS1-3 and MPI-ESM-LR) indicated that the results were not sensitive to the ensemble member selected – no statistically significant differences were found between the ensemble members for the correlations between monthly mean precipitation and 400hPa vertical velocity over Kenya. The individual models varied in resolution from 0.5625° to 7.84°. Consequently, where model composites were calculated, the data were first regridded onto a common 1°x1° grid using a nearest neighbour interpolation algorithm**.** A subset of 22 atmosphere-only models (AMIP) was selected from the CMIP5 ensemble, which are denoted with asterisks in Table 11.1. Analysis involving wind field computations using spherical harmonic functions (e.g. velocity potential) was performed using the Windspharm library (Dawson 2016).

Table 11.1 - CMIP5 models used in this study. Expansions of acronyms are available online at http://www.ametsoc.org/PubsAcronymList. Asterisks denote models used in AMIP ensemble, which are used in chapter 11 only.

Model Name	Modelling Group	Mean March Kenya Rainfall (mm/day)	Mean November Kenya Rainfall (mm/day)
ACCESS1-3*	Commonwealth Scientific and Industrial Research Organisation and Bureau of Meteorology (Australia)	0.72018468	5.39158201
BCC-CSM1-1-M*	Beijing Climate Centre, China Meteorological Administration	3.12062645	4.77377367
BNU-ESM*	College of Global Change and Earth System Science, Beijing Normal University	0.50848675	2.30800176

CanESM2	Canadian Centre for Modeling and Analysis	2.20307994	3.82551479
CanAM4* (atmosphere only)	Canadian Centre for Modeling and Analysis	3.519263	4.191565
CCSM4*	National Center for Atmospheric Research (USA)	1.12436569	4.88698149
CESM1-CAM5*	National Science Foundation, Department of Energy, National Center for Atmospheric Research (USA)	0.88511753	4.35356998
CMCC-CM*	Centro Euro-Mediterraneo per I Cambiamenti Climatici (Italy)	1.52150857	3.66852021
CNRM-CM5*	Centre National de Recherches	1.19458139	3.20929885

	Météorologiques (France)		
CSIRO-Mk3-6-0*	Commonwealth Scientific and Industrial Research Organisation in collaboration with the Queensland Climate Change Centre of Excellence (Australia)	1.85005295	3.11245489
EC-EARTH	EC-EARTH consortium (Europe)	1.29948533	3.00232744
FGOALS-g2*	LASG, Institute of Atmospheric Physics, Chinese Academy of Sciences; and CESS, Tsinghua University	1.54839027	4.2387495
FIO-ESM	The First Institute of Oceanography, SOA (China)	1.97875655	2.83555794
GFDL-CM3*	Geophysical Fluid Dynamics Laboratory (USA)	0.35625046	4.54361105

GISS-E2-R*	Goddard Institute for Space Studies (USA)	2.65551329	4.94359398
HadGEM2-A* (atmosphere only)	Met Office Hadley Centre (UK)	2.047307	3.890381
HadGEM2-AO	Met Office Hadley Centre (UK)	0.99927062	3.21843314
INMCM4*	Institute for Numerical Mathematics (Russia)	3.36340737	5.58793449
IPSL-CM5A-LR*	L'Institut Pierre-Simon Laplace (France)	0.67848229	1.46617961
IPSL-CM5A-MR*	L'Institut Pierre-Simon Laplace (France)	1.60588074	1.69666374
IPSL-CM5B-LR*	L'Institut Pierre-Simon Laplace (France)	0.37739533	3.11946
MIROC5*	National Institute for Environmental Studies (Japan), Atmosphere and Ocean Research	2.63725114	2.90290928

	Institute (University of Tokyo), Japan Agency for Marine-Earth Science and Technology		
MIROC-ESM-CHEM	National Institute for Environmental Studies (Japan), Atmosphere and Ocean Research Institute (University of Tokyo), Japan Agency for Marine-Earth Science and Technology	1.26737058	3.3539691
MPI-ESM-LR*	Max Planck Institute for Meteorology (Germany)	0.75810111	1.71675229
MPI-ESM-MR*	Max Planck Institute for Meteorology (Germany)	0.88501096	2.56478405
MRI-AGCM3-2H* (atmosphere only)	Meteorological Research Institute (Japan)	2.567191	3.473036

MRI-CGCM3	Meteorological Research Institute (Japan)	0.52001166	4.85260153
NorESM1-M*	Norwegian Climate Centre	1.74336731	5.244816

11.4. Observations and Reanalysis

The vertical motion associated with the Walker Circulation acts as a large-scale control on rainfall over Kenya during the short rains (Mutai et al. 2012). It has been suggested as a mechanism for recent drying trends in the long rains (Williams and Funk 2011), and many CMIP5 models exhibit mean-state biases in the low-level zonal winds which are associated with the circulation (Hirons and Turner 2018). We explore the possibility that rainfall biases in CMIP5 models are linked to the models' representation of vertical motion in both the ascending and descending limbs of the Indian Ocean Walker Circulation. Here, we briefly review the climatological Walker Circulation and its links to the observed rainfall climatology within the two main Kenyan rainy seasons.

Rainfall in the Greater Horn of Africa (GHA) region generally displays either a unimodal or bimodal regime. The Ethiopian Highlands region has a unimodal rainfall climatology with a rainy season extending from July to September (Dunning et al. 2016), although there is complex seasonality in sub-regions (Diro et al. 2011). Areas further south, including Kenya, have a bimodal rainfall climatology, with a 'Long Rains' season from March to May and a 'Short Rains' which is considered by

some to extend from October to December (Yang et al. 2015a) but by others to only include October and November (e.g. Nicholson 2017). Fig. 1 illustrates the spatial distribution of rainfall in each month of these two rainy seasons. For Kenya, rainfall maxima in excess of 250mm month^{-1} are located in the central highlands around Mt. Kenya in April and November, as well as along the eastern edge of Lake Victoria in April and along the coast in May. North-west Kenya, around Lake Turkana, is consistently dry with less than 100mm month^{-1} of rainfall in each month of the rainy seasons. Averaged across the Kenya domain (box in Fig. 11.1), the wettest Long Rains month is April (4.22 mm day^{-1}) and the wettest Short Rains month is November (3.06 mm day^{-1}).

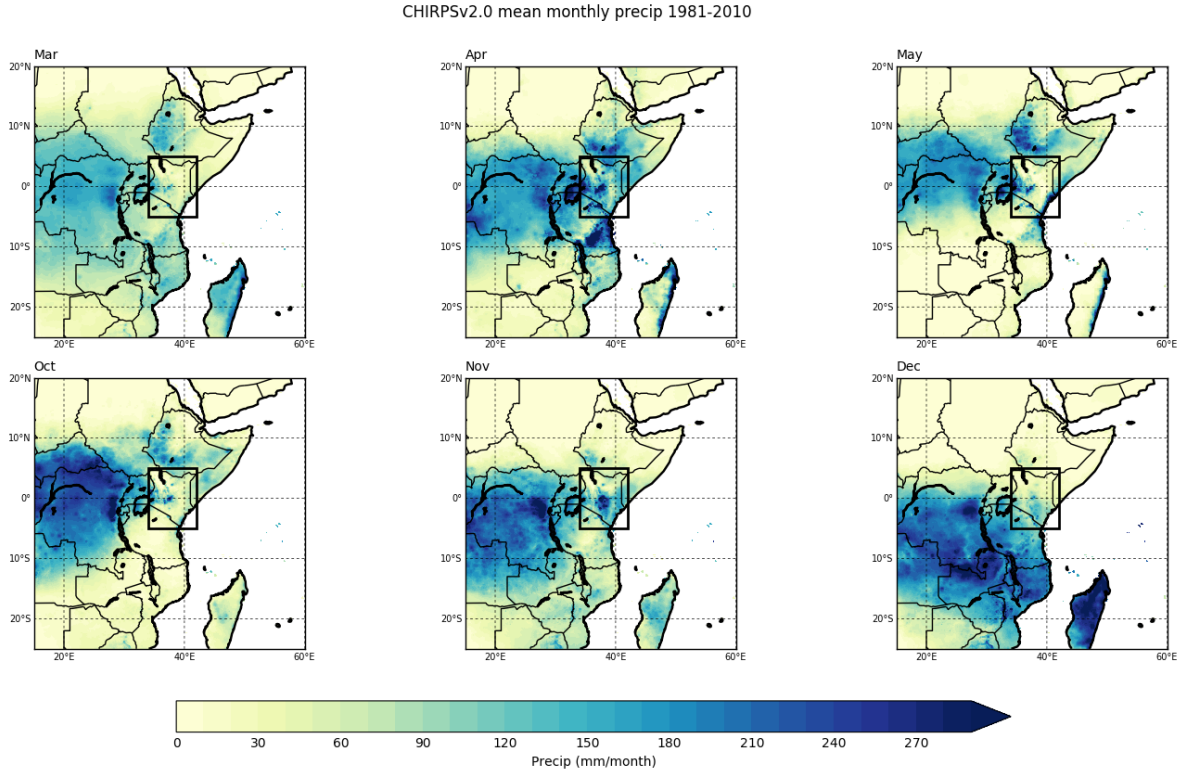


Figure 11.1 - CHIRPS v2.0 rainfall climatology for East Africa averaged for each month in the period 1981–2010. The black box shows the area over which Kenya rainfall is averaged.

The climatological structure of the vertical velocity (omega) component of the Indian Ocean Walker Circulation in MERRA2 reanalysis can be seen in Figs. 11.2, 11.3, and 11.4. The core ascending region over the Maritime Continent is strongest in April during the Long Rains (-0.065 Pa s^{-1}) and November during the Short Rains (-0.094 Pa s^{-1}) (Fig. 2). In March, the upper-tropospheric descent over Kenya is 10° more longitudinally extensive than in April and 20° more extensive than in May. The region of ascent over the Indian Ocean is more extensive in May; there are also clear differences in the strength of descent between the months. March (0.027 Pa $s^{-1)}$ and May (0.021 Pa s^{-1}) have stronger descent over Kenya than April (0.013 Pa s^{-1}). October (0.029 Pa s^{-1}) and December (0.027 Pa s^{-1}) have stronger descent than November (0.024 Pa s^{-1}) (Fig. 11.2) Months within the rainy seasons are characterised by ascending air throughout the troposphere extending westward as far as 50°E (December) from the Maritime Continent across the Equatorial Indian Ocean. We extend this analysis of vertical motion to the 200hPa velocity potential field and its associated divergent wind, which is frequently used to diagnose overturning circulations in the tropics by linking the lifting of the 200hPa geopotential to patterns of convergence and divergence in the wind field. (Tanaka et al. 2004, Schwendike et al 2014, Hart et al. 2018). Fig. 11.3 indicates that a zonal gradient in large-scale atmospheric vertical motion is present across the equatorial Indian Ocean in MAM and OND, and also indicates upper-level convergence over Kenya associated with both the Maritime Continent and Congo Basin regions of ascent.

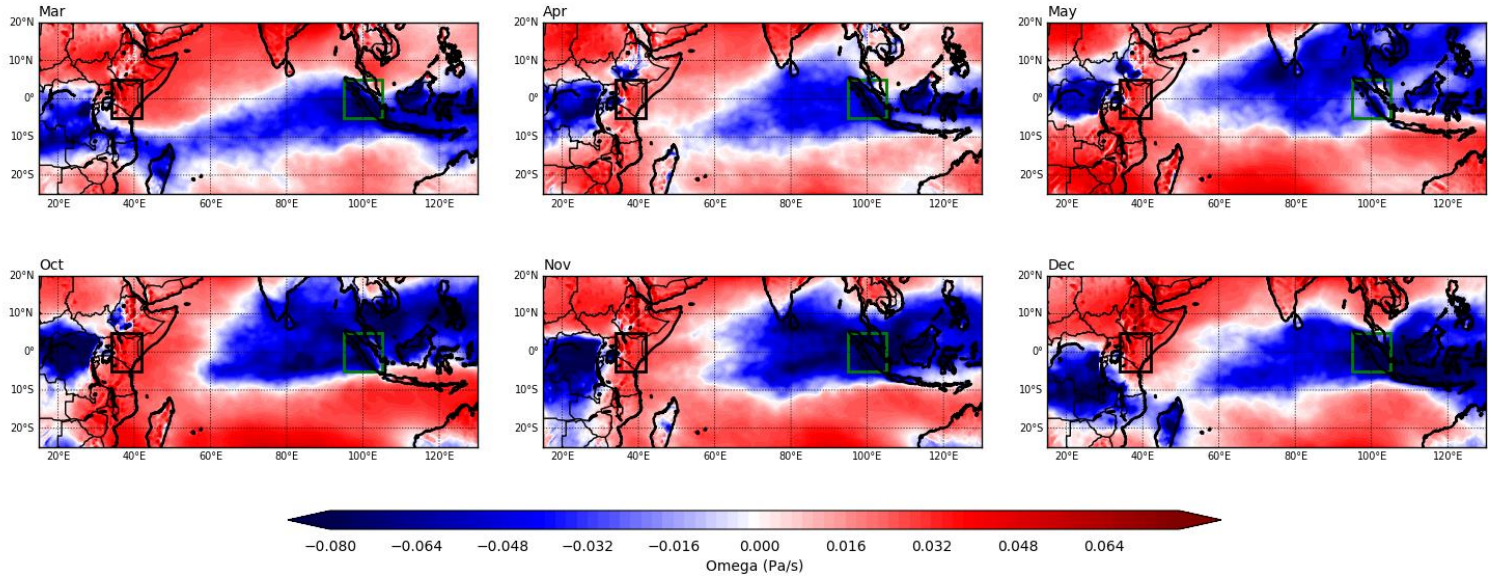


Figure 11.2 - MERRA-2 omega at 400 hPa for each rainy season month, averaged over 1980–2008. The black box indicates the area used for averaging fields over Kenya, and the green box indicates that used for averaging fields over the Eastern Indian Ocean.

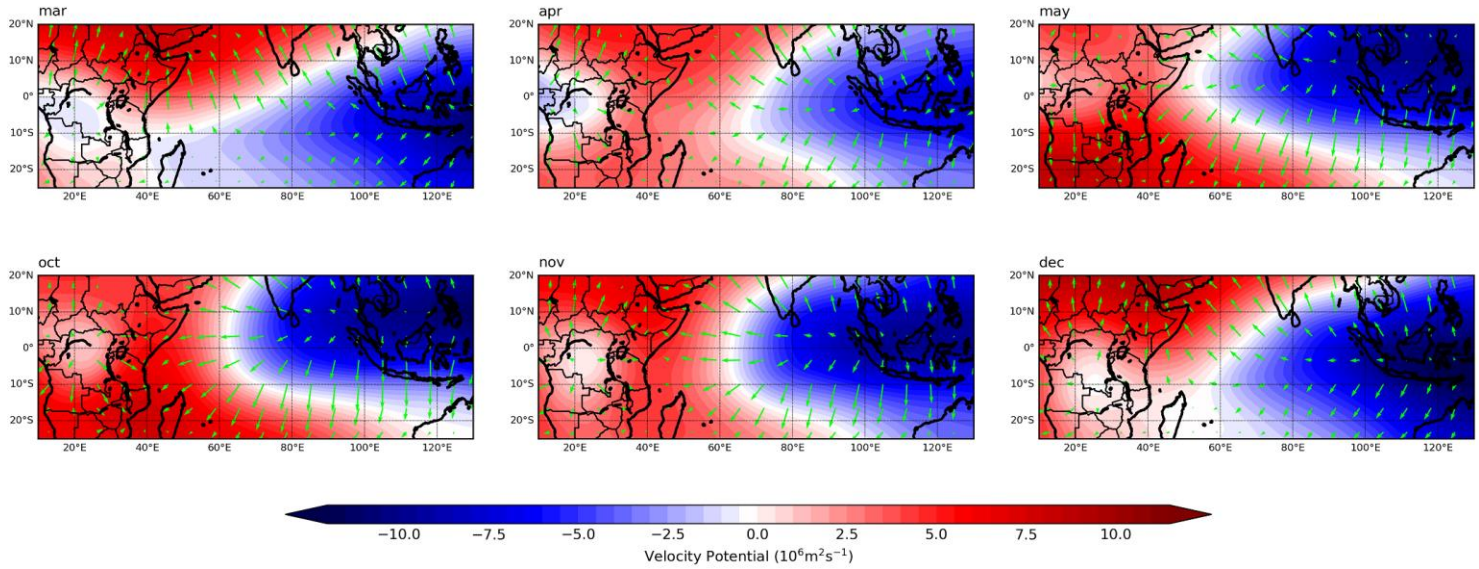


Figure 11.3 - MERRA-2 velocity potential (filled contours) and divergent wind vectors (arrows) at 200 hPa for each rainy season month, averaged over 1980–2008

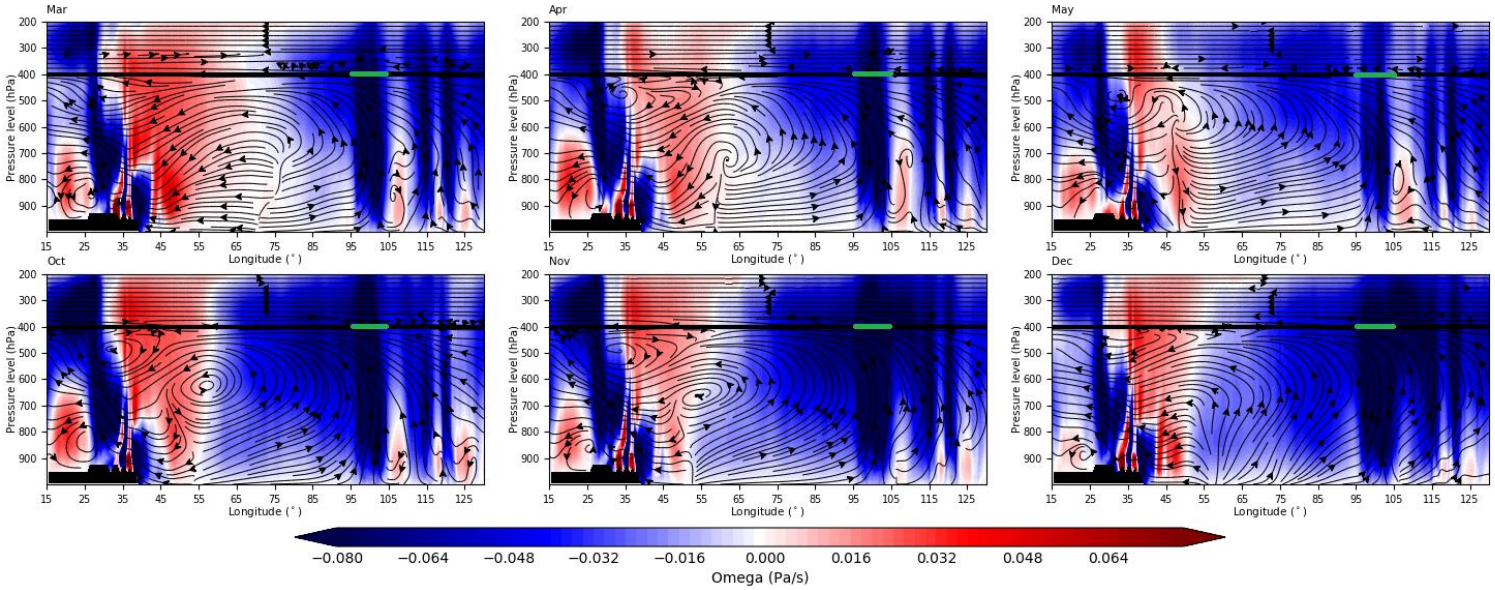


Figure 11.4 - Longitude-height plots of MERRA-2 reanalysis climatology for MAM (top row) and OND (bottom row), 1980–2008, 15°E–130°E, averaged over 5°N–5°S. Shading is vertical velocity (Pa·s^{-1}) with red indicating negative (upward) motion and blue indicating positive (downward) motion. Streamlines are the resultant vectors of u and w × 10^4. The black line indicates the 400 hPa level. The green line indicates the box used for averaging over the ascending limb of the Walker circulation.

The descending limb of the circulation overlies Kenya (34°E–42°E), extending down to around 700 hPa over the land, below which there is ascent (Figure 11.4) The effects of the region's complex topography can be seen near to the surface, with alternating bands of ascent and descent suggestive of localized overturning circulations in the East African Highlands around Lake Victoria (Figure 11.4). The strength and extent of the descending limb acts as an upper limit on deep convection over Kenya to a varying degree depending on the month. The wettest months in the two rainy seasons (April and November) correspond to the periods when descent over Kenya is weaker and ascent over the Indian Ocean is stronger. This suggests

that the Walker circulation strength could explain why April and November are the wettest months within the Kenyan rainy seasons.

The streamlines in Figure 11.4 indicate the presence of an overturning circulation which is more pronounced during the less wet short rains, particularly in October/November, but is also active during the long rains. The circulation is characterized by lower-tropospheric westerlies and mid-to-upper-tropospheric easterlies over the eastern equatorial Indian Ocean.

Statistically significant negative correlations ($p < 0.05$) were obtained between Kenya rainfall and 400 hPa omega averaged over Kenya for all rainy season months in the period 1981–2005 (Table 11.2), except October. The correlations were strongest in March during the long rains, and in November during the short rains. A significant correlation for October ($p < 0.1$) was obtained after the anomalously wet October of 1982 was removed. This suggests an important role for omega in controlling climatological rainfall over Kenya during the rainy seasons. The following analysis links this to the descending limb of the Indian Ocean Walker circulation.

Table 11.2 - Pearson product moment correlation coefficients between CHIRPS v2.0 rainfall and MERRA-2 400 hPa omega, averaged over Kenya (N = 24, R_{crit} = 0.388)

March	April	May	October	November	December
R=-0.769 *p*= 7.10E-06	*R*=-0.720 *p*= 9.37E-06	*R*=-0.573 *p*= 0.00274	*R*=-0.260 *p*=0.209	*R*=-0.847 *p*= 9.073E-08	*R*=-0.797 *p*= 1.846E-06

Figure 11.5 reveals the dominant structure of the Indian Ocean Walker circulation associated with Kenyan rainfall. There is a strong negative correlation between observed rainfall over Kenya and reanalysis omega at 400 hPa, both over the country itself and over the western Indian Ocean throughout the rainy seasons. This refers to enhanced Kenyan rainfall when the climatological descent over this region is weakened. An exception is October, where the correlation over Kenya itself is positive – this explains the lack of a significant correlation in Table 11.2 prior to the removal of data from 1982. There is a significant positive correlation in the eastern Indian Ocean which is most pronounced during the short rains; this refers to higher rainfall over Kenya when the ascending limb of the Indian Ocean Walker circulation over the western Indian Ocean is weaker. Additionally, we calculated the interannual Pearson product moment correlation coefficient (for MERRA2 monthly data) between the 400 hPa omega over Kenya and the equatorial zonal winds at 850 hPa using the box defined in Figure 6a of Hirons and Turner (2018) (50°E–100°E, 5°N–5°S). For OND, we obtained a value of $r = 0.46$, indicating a statistically significant degree of covariance ($p = 0.01$, $n = 30$); when there is more descent over Kenya, the equatorial westerlies tend to be stronger, indicating a more pronounced overturning circulation. A dynamical link is hereby demonstrated between Kenyan rainfall and both the local descent and remote ascent at 400 hPa which comprise the vertical components of the Indian Ocean Walker circulation.

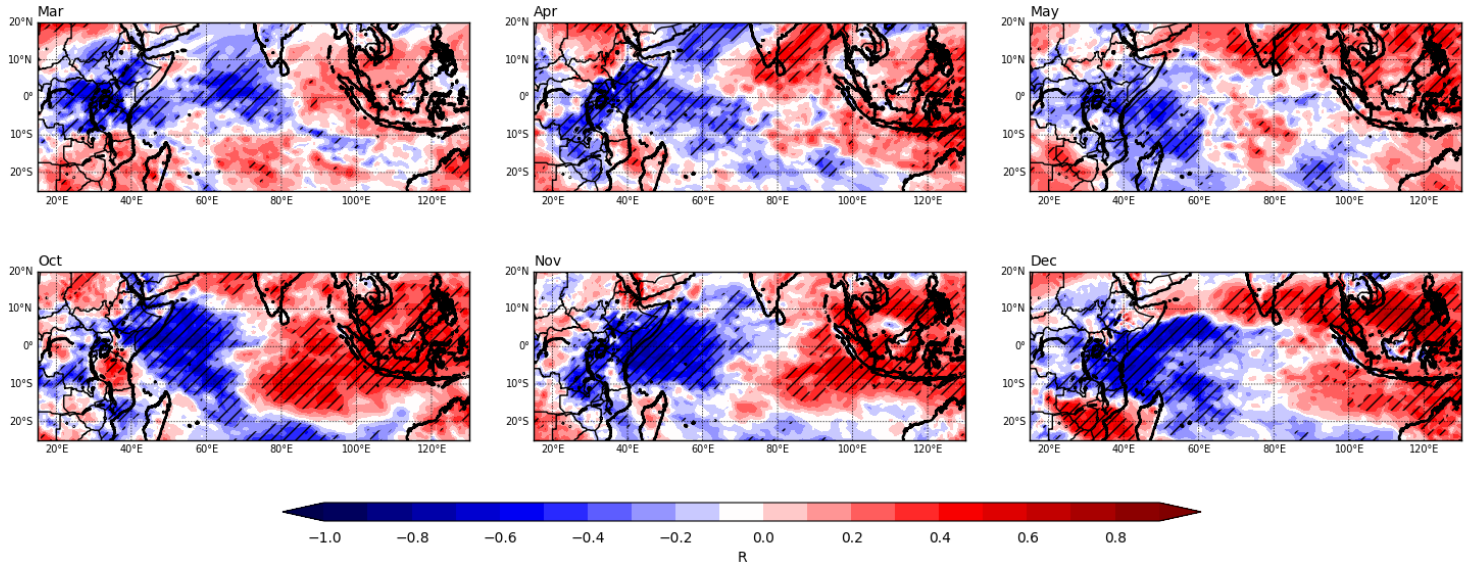


Figure 11.5 - Pearson product moment correlation coefficient between CHIRPS v2.0 rainfall averaged over Kenya and MERRA-2 400 hPa omega for 1980–2008. Hatching indicates significance at $p < 0.1$.

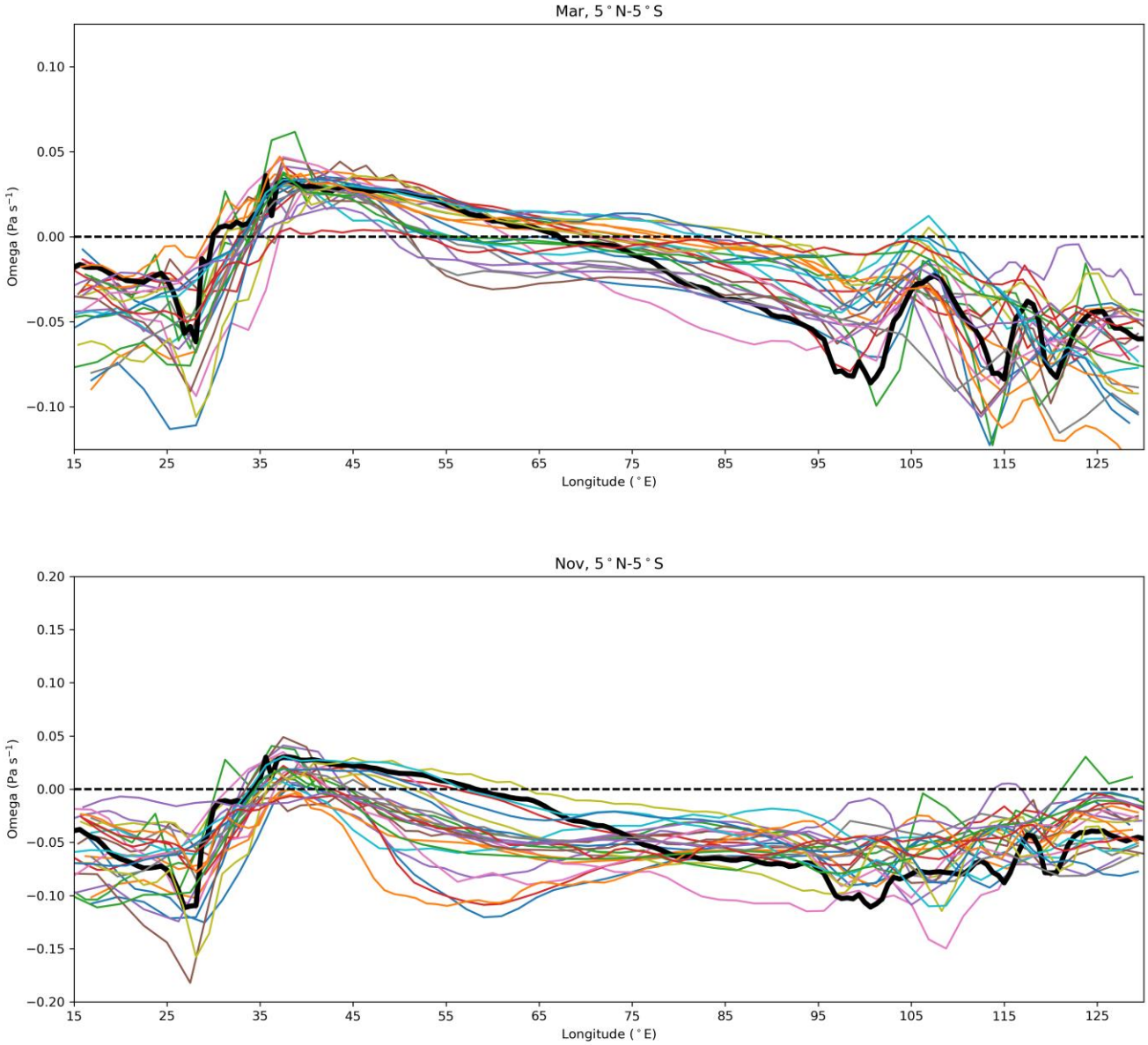


Figure 11.6 - 400 hPa omega averaged between 5°N–5°S, extending from 15°E–130°E, for March (top) and November (bottom). Each coloured line is a CMIP5 model from Table 11.1 averaged over 1975–2005 in historical coupled mode. The thick black line is the MERRA-2 reanalysis averaged over 1980–2008. Note different scales.

The differences between months demonstrate the limitations of considering each rainy season as homogeneous (Nicholson, 2017). Figures 11.2 and 11.4 show the variations in ascent and descent at the 400 hPa level, which is the core of both the ascending and descending limbs of the circulation over the Indian Ocean. The climatological descent over Kenya varies in strength between the months, and there is ascent over the Lake Victoria basin in all months (though this is most extensive in April). A more Hadley-like mode is evident in March, but other months show a clear zonal structure between the core ascending regions. There are also differences between the location of the ascending limb over the African continent in October–November versus December; this is located further to the south during December and extends across the Mozambique Channel to Madagascar (Figure 11.2). Descent at 400 hPa is a consistent feature of the omega climatology over Kenya during both the long and short rains, although there is a greater degree of overturning shown by the streamlines in October–November compared to December. These differences in structure explain why December is not considered part of the short rains by some authors (Nicholson, 2017), despite being a comparatively wet month. The discontinuity over Kenya of the band of ascending (and thus convergent) air at the equator demonstrates that the widely-held assumption of East African rainfall being primarily controlled by the seasonal migration of the zonal inter-tropical convergence zone (ITCZ) (e.g., Camberlin et al., 2009) may no longer be sufficient given more up-to-date understandings of the tropical rainbelt, which is not exactly co-located with the zone of maximum low-level convergence (Nicholson, 2018).

11.5. CMIP5 Models

11.5.1. Zonal Overturning Circulations

In our analysis of the coupled models listed in Table 11.1, we address three questions: are there quantifiable links between the biases in models' representations of Kenyan rainfall and omega over Kenya; what might the similarities be in terms of the convective structure between models that are particularly wet or dry over the country; and do the models behave differently when SST biases are controlled using AMIP runs?

We first examine the extent to which the models can reproduce the observed zonal structure of the Walker circulation with respect to vertical motion. Figure 11.6 shows the climatological omega across the equatorial Indian Ocean for March and November for the CMIP5 models in Table 11.1, along with the MERRA-2 reanalysis. The zonal structure revealed in Figure 11.6 is interesting because of the similarity between March and November, given that the canonical overturning circulation is deemed to be active primarily in OND (e.g., Hastenrath et al., 2002). Although the pattern is stronger in November, both months feature ascent over the Maritime Continent and the Congo Basin, and descent over East Africa. While there is substantial inter-model variation as suggested by previous studies on CMIP5 representation of East African climate, the models are in general agreement with the reanalysis pattern.

We examine the climatological zonal overturning circulations in the coupled historical runs of the CMIP5 models listed in Table 11.1 (Figure 11.7). We plot the climatological omega and streamlines (u, w x 10^4) for the domain 15E°–130°E, 5°N–

5°S during each month in the rainy seasons, along with biases relative to MERRA-2 (Figure 11.8). Both figures are arranged based on the climatological rainfall over Kenya, with the driest models at the top left and the wettest models at the top right. For March, the reanalysis data show a clear pattern of ascent over the Maritime Continent and descent over the Western Indian Ocean, with descent in the mid-to-upper troposphere overlying ascent over Kenya (Figure 11.4). This circulation is represented with varying degrees of accuracy in the CMIP5 ensemble. Figure 11.7 indicates that drier models tend to overstate both the longitudinal extent and the strength of the descending limb over East Africa. This is consistent with convective inhibition over East Africa and consequently a drier Kenya. For instance, the four driest models extend their descending limbs up to 20° further east than MERRA-2, and are between 4 and 6 times drier than CHIRPSv2.0 over Kenya during this month. On the other hand, the wetter models in the ensemble tend to have much larger regions of ascent extending across the Indian Ocean, weaker descent over East Africa, and in the notable case of BCC-CSM1-1-M, ascent overlying descent across the equatorial IO in a pattern scarcely reminiscent of the canonical zonal overturning circulation. A representative wet model, INMCM4 is 54.9% wetter than CHIRPSv2.0 for this month, has a descending limb which is over 3 times weaker than MERRA-2, and while the strength of its ascending limb is similar to MERRA-2, the model extends the ascent westward by around 25° of longitude. For the AMIP models (Figure 11.8), some improvements relative to the coupled models are noticeable. In March, the descending limb is more longitudinally constrained across the ensemble, with troposphere-wide descent overlying East Africa and the western Indian Ocean to around 55°E, a comparable extent to MERRA-2. Some models, such as ACCESS1-3, display less realistic motion over the Indian Ocean in AMIP mode than CMIP. Of

the four driest (wettest) models in AMIP, 2 (3) were also among the four driest (wettest) models in CMIP.

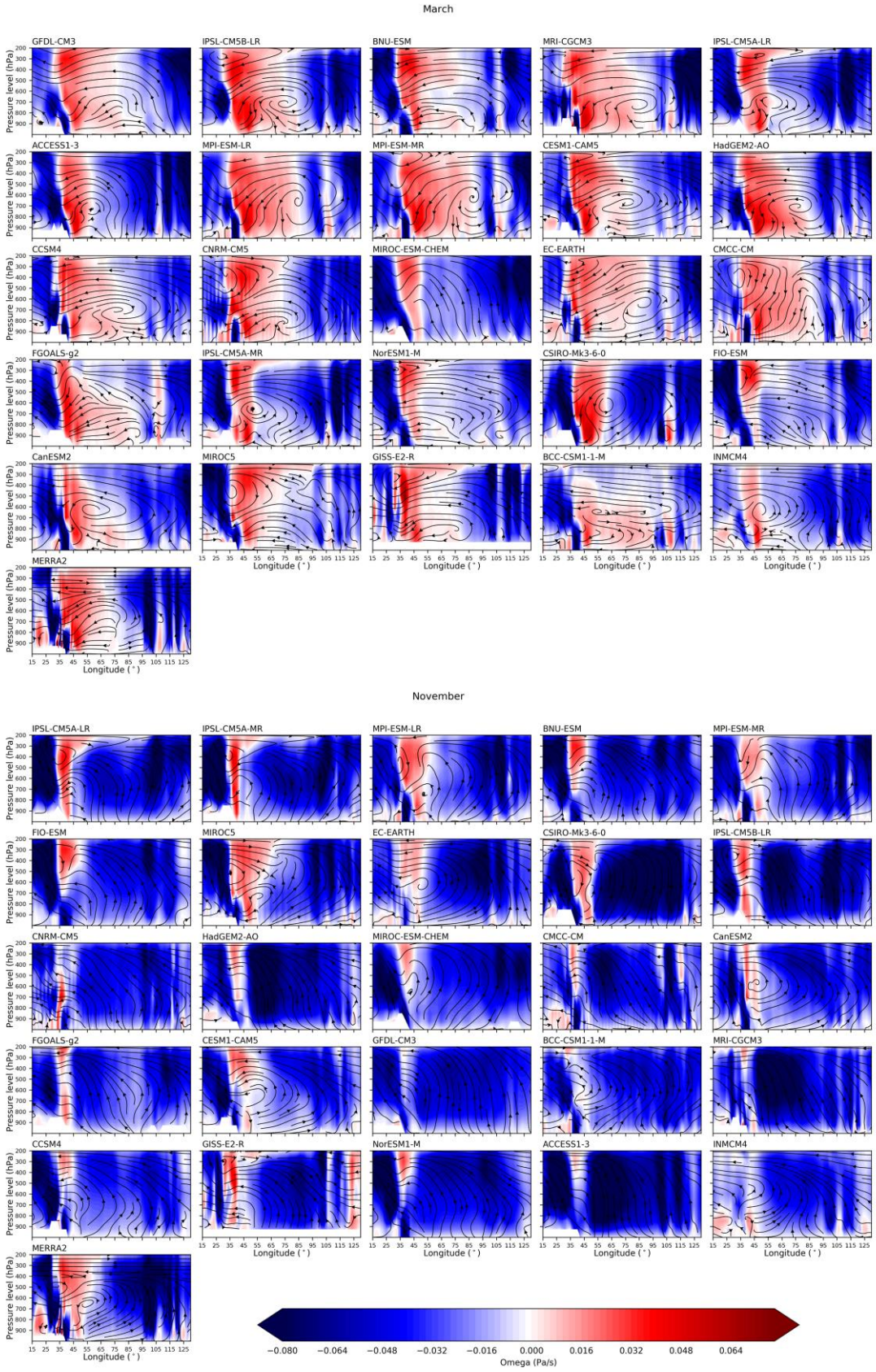

March
GFDL-CM3
IPSL-CM5B-LR
BNU-ESM
MRI-CGCM3
IPSL-CM5A-LR
ACCESS1-3
MPI-ESM-LR
MPI-ESM-MR
CESM1-CAM5
HadGEM2-AO
CCSM4
CNRM-CM5
MIROC-ESM-CHEM
EC-EARTH
CMCC-CM
FGOALS-g2
IPSL-CM5A-MR
NorESM1-M
CSIRO-Mk3-6-0
FIO-ESM
CanESM2
MIROC5
GISS-E2-R
BCC-CSM1-1-M
INMCM4
MERRA2
Pressure level (hPa)
Longitude (°)
November
IPSL-CM5A-LR
IPSL-CM5A-MR
MPI-ESM-LR
BNU-ESM
MPI-ESM-MR
FIO-ESM
MIROC5
EC-EARTH
CSIRO-Mk3-6-0
IPSL-CM5B-LR
CNRM-CM5
HadGEM2-AO
MIROC-ESM-CHEM
CMCC-CM
CanESM2
FGOALS-g2
CESM1-CAM5
GFDL-CM3
BCC-CSM1-1-M
MRI-CGCM3
CCSM4
GISS-E2-R
NorESM1-M
ACCESS1-3
INMCM4
MERRA2
−0.080 −0.064 −0.048 −0.032 −0.016 0.000 0.016 0.032 0.048 0.064
Omega (Pa/s)

Figure 11.7 - As Figure 11.4, but for March (top) and November (bottom) in the CMIP5 ensemble (Table 11.1). Models are arranged in rows from driest over Kenya in the given month at the top left, to wettest at the bottom right. MERRA-2 data is included at the bottom left for reference.

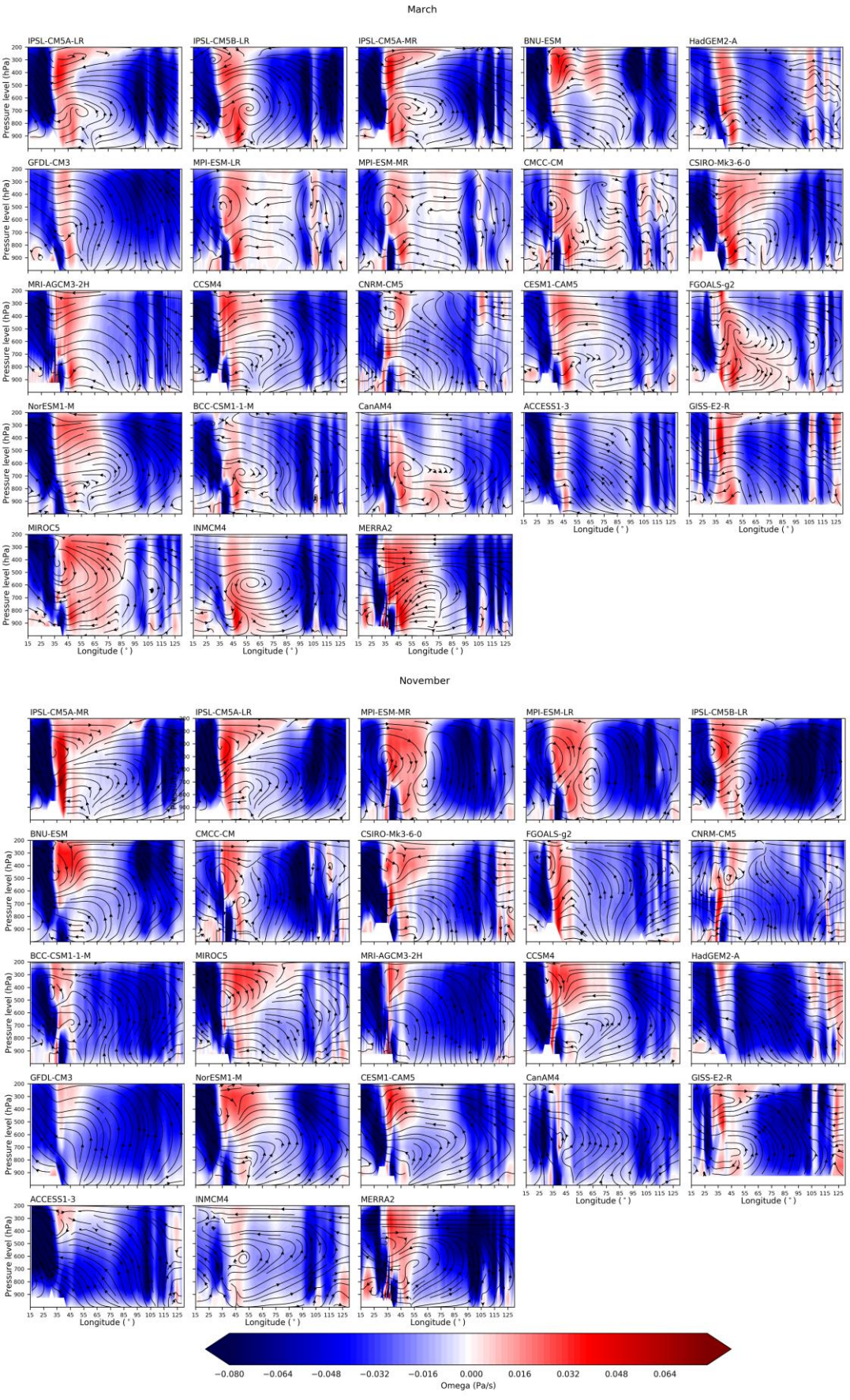

March
IPSL-CM5A-LR
IPSL-CM5B-LR
IPSL-CM5A-MR
BNU-ESM
HadGEM2-A
GFDL-CM3
MPI-ESM-LR
MPI-ESM-MR
CMCC-CM
CSIRO-Mk3-6-0
MRI-AGCM3-2H
CCSM4
CNRM-CM5
CESM1-CAM5
FGOALS-g2
NorESM1-M
BCC-CSM1-1-M
CanAM4
ACCESS1-3
GISS-E2-R
MIROC5
INMCM4
MERRA2
Pressure level (hPa)
Longitude (°)
November
IPSL-CM5A-MR
IPSL-CM5A-LR
MPI-ESM-MR
MPI-ESM-LR
IPSL-CM5B-LR
BNU-ESM
CMCC-CM
CSIRO-Mk3-6-0
FGOALS-g2
CNRM-CM5
BCC-CSM1-1-M
MIROC5
MRI-AGCM3-2H
CCSM4
HadGEM2-A
GFDL-CM3
NorESM1-M
CESM1-CAM5
CanAM4
GISS-E2-R
ACCESS1-3
INMCM4
MERRA2
−0.080 −0.064 −0.048 −0.032 −0.016 0.000 0.016 0.032 0.048 0.064
Omega (Pa/s)

Figure 11.8 - As Figure 11.7, but for the AMIP models in Table 11.1.

Simplification of model topography may also be influencing the surface patterns of omega over East Africa, with the localized overturning circulations over land largely absent, and the characteristic vertical structure of surface ascent up to 800 hPa capped by upper-level descent extending throughout the troposphere missing from a number of models. The streamlines indicate that an overturning circulation over the equatorial Indian Ocean is present in a majority of models, but its location is variable. The streamlines at the surface are also indicative of zonal wind biases in a number of models – this has been identified as a key source of model precipitation error in the short rains season by Hirons and Turner (2018), whereby the observed surface westerlies become easterly in some coupled models, leading to erroneous patterns of moisture flux. In terms of the broader zonal structure of ascent across the Walker circulation in the Western Hemisphere (averaged at the equator from 0° to 200°E), the CMIP5 ensemble mean shows more descending air than reanalysis during the dry-biased long rains months (Table 11.3), and there is also a significant correlation obtained between the proportion of Western Hemisphere ascending tropospheric air in each model and that model's rainfall over Kenya for November (R = .409, n = 25, α = .05). This implies that models have Walker circulation biases extending beyond the Indian Ocean Basin.

Table 11.3 - Proportion of ascending versus descending air in the region 0°–200°E, 5°N–5°S, between the surface and 200 hPa.

	MERRA2		CMIP5 Ensemble (n=25)	
	% Ascent	% Descent	% Ascent	% Descent
March	84.74	15.26	73.67	26.33
April	85.91	14.09	76.14	23.86
May	81.32	18.68	77.29	22.71
October	80.20	19.80	77.34	22.66
November	79.26	20.74	80.05	19.95
December	85.70	14.30	79.74	20.26

For November, the impact of the Walker circulation is clear (Figure 11.7). The CMIP5 models generally have wet biases in this month, meaning that the driest models are closest to observed rainfall amounts. These models are close to the reanalysis in terms of their Walker circulation representation, with a broad band of ascent extending throughout the troposphere east of 55°E balanced by descent over Kenya. Even in these models, the core of this descent is narrower by around 10° of longitude and in the driest models extends down to the surface over Kenya. This may lead to increased dry biases over land, and again highlights the impact of model topography on precipitation modelling in this region. The wettest models, by

contrast, either feature a greatly reduced zonal overturning circulation, or exhibit a band of ascent extending across the equatorial Indian Ocean and into East Africa in which the Walker circulation is mostly absent. In ACCESS1-3, the region of descent over Kenya found in reanalysis is absent and ascent is found instead; the model's average rainfall for Kenya in November is 5.39 mm·day^{-1} compared to 3.06 mm·day^{-1} in CHIRPSv2.0. Interestingly, the 3 IPSL models all extend the descending limb to the surface over East Africa – the two configurations of IPSL-CM5A are both substantially drier than observations in November (1.47 mm·day^{-1} for IPSL-CM5A-LR and 1.70 mm·day^{-1} for IPSL-CM5A-MR) and across OND.

In the AMIP models, some differences in the structure of the overturning circulation are observed for November (Figure 11.8). There is an increase in the longitudinal extent of the descending limb of the Walker circulation and a corresponding decrease in the extent of the ascending limb, bringing the models closer to the circulation seen in MERRA-2. Notably, the equatorial westerlies in some models (such as the three IPSL models) are better represented with respect to MERRA-2 than they are in the coupled runs. However, rainfall biases remain, in some cases of opposite signs compared to the coupled versions. For example, CSIRO-MK3-6-0 running in coupled mode has a descending limb which extends around 20° of longitude less than in MERRA-22, and a positive precipitation bias relative to CHIRPS (+0.29 mm·day^{-1}). In AMIP mode it exhibits an omega structure which is much closer to MERRA-2, but a negative precipitation bias (−0.62 mm·day^{-1}). Of the four driest (wettest) models in AMIP, 3 (3) were also among the four driest (wettest) models in CMIP.

We next considered the structure of CMIP5 vertical motion over the Congo Basin (10°E–30°E, 5°N–5°S). This is a key zone of convection driving the Walker circulation and an important moisture source for East Africa. Figure 11.9 shows a

characteristic zone of descending air overlying the Congo Basin below 700 hPa, which is present in all East African rainy season months in reanalysis. This is either underestimated or does not appear in the models. There is also disagreement on the direction of the zonal winds among the models, with some showing surface easterlies and others westerlies. Given that the moisture flux into East Africa from the Congo basin is projected to be of increasing importance in future (Giannini et al., 2018), the realism of these low-level winds warrants further study (though beyond the scope of this article). Related to this is the question of whether or not the low-level subsidence observed in MERRA-2 is realistic. Neupane (2016) did not find this feature in previous generations of reanalysis, but Kuete et al. (2019) link vertical velocity at this location to variability in the southern branch of the African Easterly Jet.

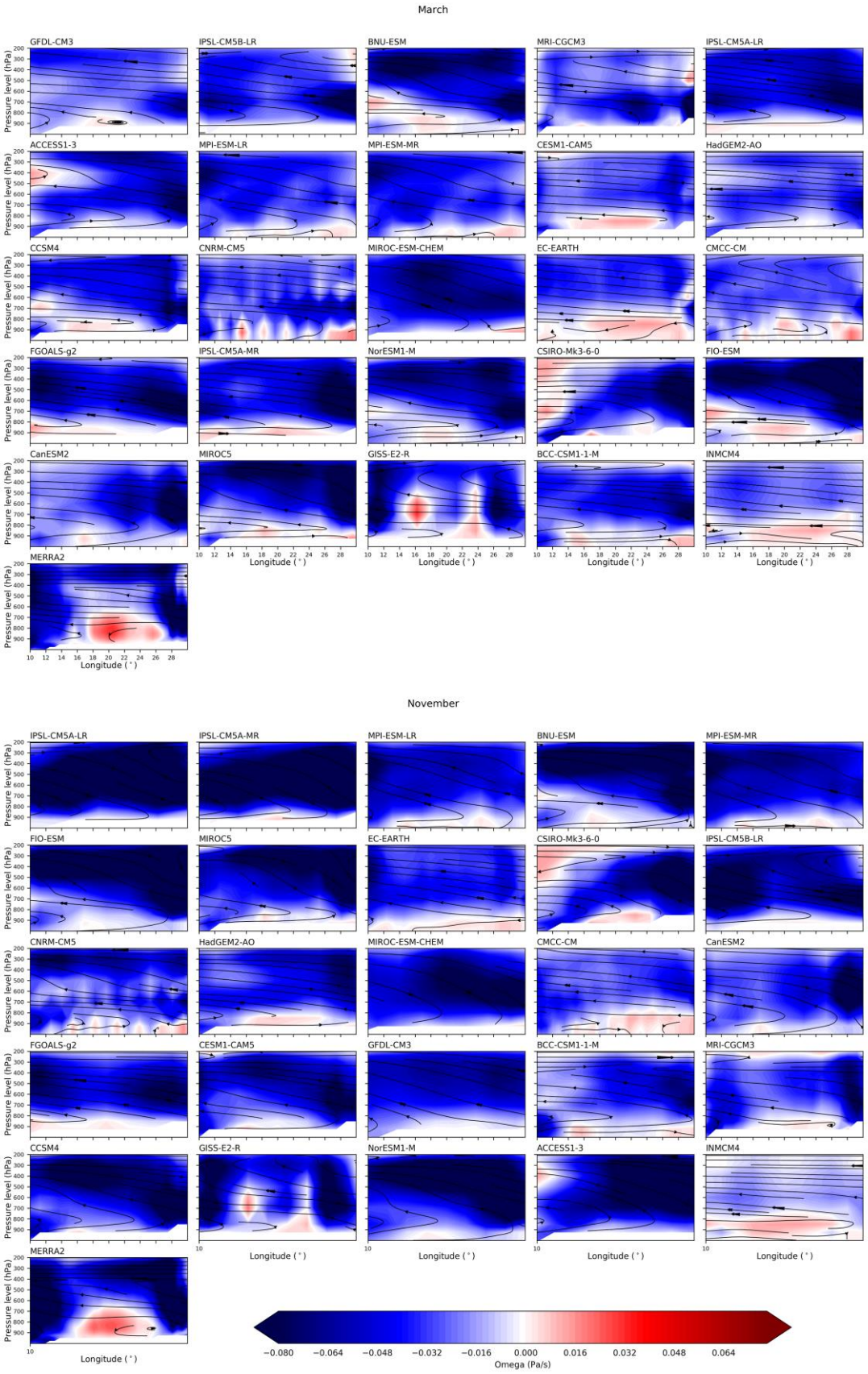


Figure 11.9 - As Figure 11.4, but for the Congo Basin (10°–30°E, 5°N–5°S) in March (top) and November (bottom).

The CMIP5 biases in the vertical structure of omega relative to MERRA2 (Figure 11.10) indicate that models generally underestimate the strength of the zonal overturning circulation in November, with positive biases in the eastern Indian Ocean and negative biases over the west showing that the climatological regions of ascent and descent are both too weak during this month. In March, dry models such as IPSL-CM5B-LR and MRI-CGCM3 are more likely to have descending biases across the Indian Ocean, inhibiting convective potential, whereas wetter models such as BCC-CSM1-1-M and INMCM4 are more likely to have ascending biases. In dry models, the orientation of the streamlines at the 300–400 hPa level in the central Indian Ocean suggests the upper-level easterlies in these models may be too strong, potentially resulting in a drying mechanism analogous to that described by Williams and Funk (2011).

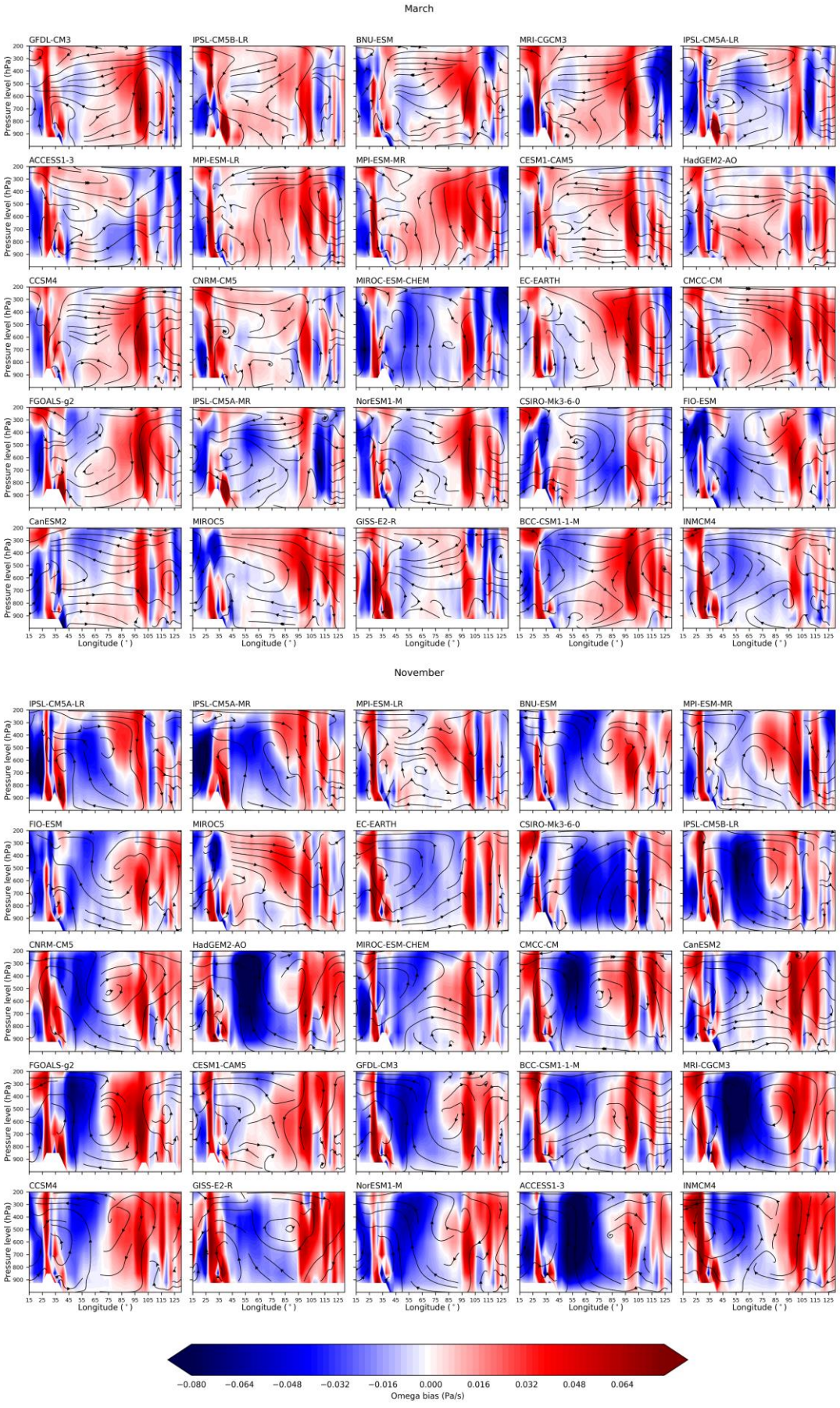

March
GFDL-CM3
IPSL-CM5B-LR
BNU-ESM
MRI-CGCM3
IPSL-CM5A-LR
ACCESS1-3
MPI-ESM-LR
MPI-ESM-MR
CESM1-CAM5
HadGEM2-AO
CCSM4
CNRM-CM5
MIROC-ESM-CHEM
EC-EARTH
CMCC-CM
FGOALS-g2
IPSL-CM5A-MR
NorESM1-M
CSIRO-Mk3-6-0
FIO-ESM
CanESM2
MIROC5
GISS-E2-R
BCC-CSM1-1-M
INMCM4
Pressure level (hPa)
Longitude (°)
November
IPSL-CM5A-LR
IPSL-CM5A-MR
MPI-ESM-LR
BNU-ESM
MPI-ESM-MR
FIO-ESM
MIROC5
EC-EARTH
CSIRO-Mk3-6-0
IPSL-CM5B-LR
CNRM-CM5
HadGEM2-AO
MIROC-ESM-CHEM
CMCC-CM
CanESM2
FGOALS-g2
CESM1-CAM5
GFDL-CM3
BCC-CSM1-1-M
MRI-CGCM3
CCSM4
GISS-E2-R
NorESM1-M
ACCESS1-3
INMCM4
Omega bias (Pa/s)

Figure 11.10 - As Figure 11.4, but for model biases relative to MERRA-2 data.

There is less differentiation between the model biases for November (Figure 11.10). The models generally have strong omega biases and ascending streamlines over the western and central Indian Ocean throughout the troposphere, indicative of excessive ascent and a weak or absent overturning circulation. The ascent over the Maritime Continent is generally too weak, suggesting that the mechanisms which cause excessive ascent over the Equatorial Indian Ocean are associated with reduced ascent in this region.

The correlations between model rainfall and 400 hPa omega (Figure 11.11) do, however, suggest that some models are able to capture the spatial structure of the link between the Walker circulation and rainfall (though these should be treated with caution given the biases in both fields). In both March and November, the negative correlation between omega over Kenya and rainfall is observed in all models apart from FGOALS-g2. However, in March models tend to include a narrower than observed band of negative omega/rainfall correlation centred on the equator, which implies a more Hadley-like circulation is acting as a control on rainfall. The existence of this negative correlation extending as far east as the Maritime continent in some of the wetter models (e.g., CanESM2 and MIROC5) supports this implication. For November, the models are less successful at simulating the large region of positive correlation associated with ascent over the Maritime Continent – this is generally less meridionally extensive than in the observations/reanalysis, and is not statistically significant in a number of models.

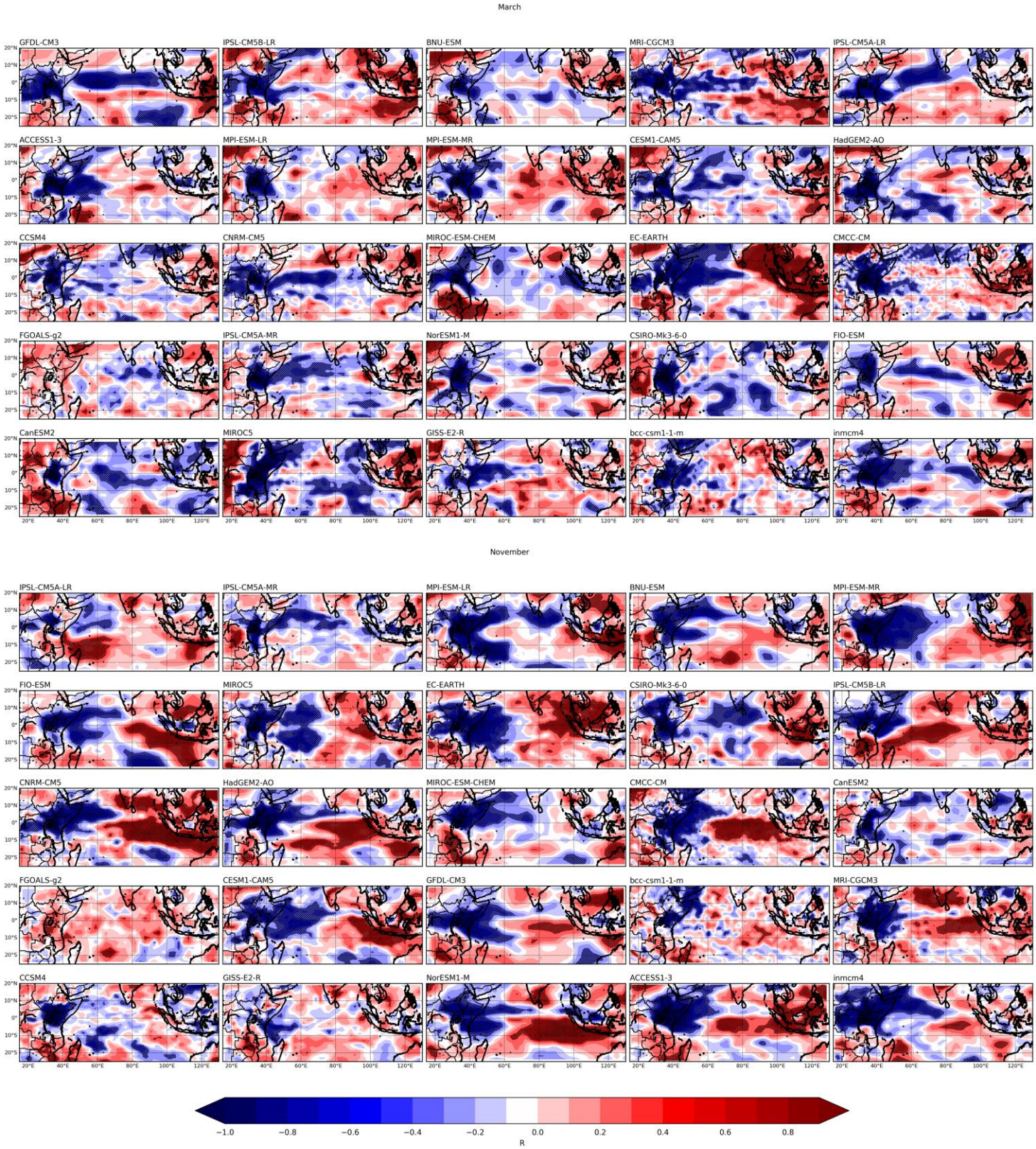


Figure 11.11- Pearson product moment correlation coefficients between CMIP5 model rainfall averaged over Kenya and model 400 hPa omega for March (upper) and November (lower), 1975–2005. Hatching indicates significance at $p < 0.1$. Models are arranged in rows from driest over Kenya in the given month at the top left, to wettest at the bottom right.

The CMIP minus AMIP differences (Figure 11.12) indicate that the strength of the overturning circulation in the coupled models differs between coupled and atmosphere-only configurations. For March, all models in the ensemble show greater descent over East Africa and the western Indian Ocean in CMIP than AMIP, and varying amounts of increased ascent over the Maritime Continent. This indicates a stronger overturning in coupled models than in atmosphere-only models. The reverse is the case for November, where the models exhibit increased ascent across the western Indian Ocean in CMIP relative to AMIP.

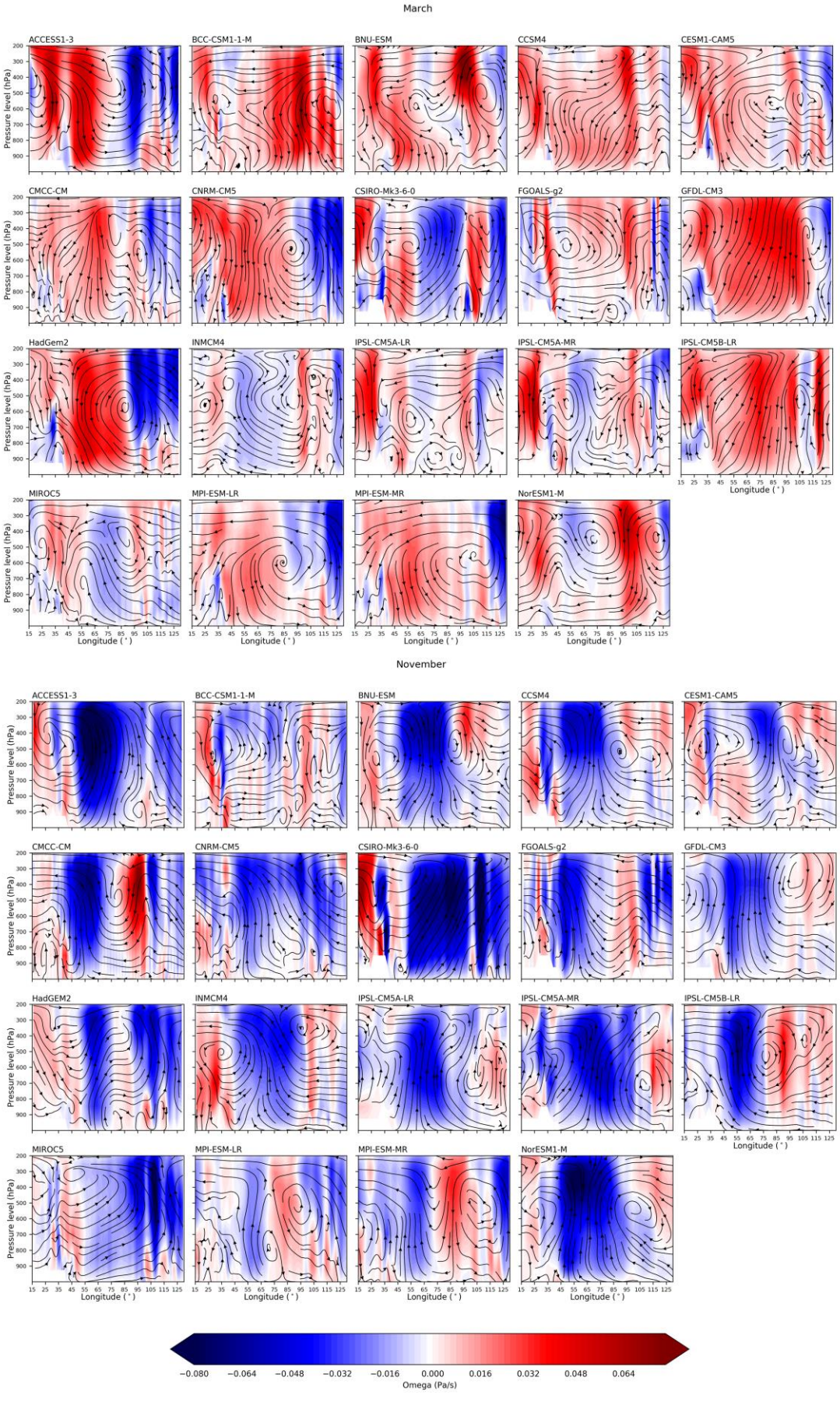

March
ACCESS1-3
BCC-CSM1-1-M
BNU-ESM
CCSM4
CESM1-CAM5
CMCC-CM
CNRM-CM5
CSIRO-Mk3-6-0
FGOALS-g2
GFDL-CM3
HadGem2
INMCM4
IPSL-CM5A-LR
IPSL-CM5A-MR
IPSL-CM5B-LR
MIROC5
MPI-ESM-LR
MPI-ESM-MR
NorESM1-M
Pressure level (hPa)
Longitude (°)
November
ACCESS1-3
BCC-CSM1-1-M
BNU-ESM
CCSM4
CESM1-CAM5
CMCC-CM
CNRM-CM5
CSIRO-Mk3-6-0
FGOALS-g2
GFDL-CM3
HadGEM2
INMCM4
IPSL-CM5A-LR
IPSL-CM5A-MR
IPSL-CM5B-LR
MIROC5
MPI-ESM-LR
MPI-ESM-MR
NorESM1-M
Pressure level (hPa)
Longitude (°)
−0.080 −0.064 −0.048 −0.032 −0.016 0.000 0.016 0.032 0.048 0.064
Omega (Pa/s)

Figure 11.12 - Differences between CMIP and AMIP models (CMIP minus AMIP) for March (top) and November (bottom), 1975–2008.

Figures 11.13, 11.14, and 11.15 summarize the biases of the CMIP5 models for each rainy season month in precipitation over Kenya (vs. CHIRPS v2.0), 400 hPa omega over Kenya (vs. MERRA-2), and 850 hPa zonal wind over the equatorial Indian Ocean (vs. MERRA-2), respectively. Figure 11.13 demonstrates the well-known precipitation biases of CMIP5 models over East Africa (e.g., Tierney et al., 2015), namely that MAM rainfall is generally underestimated while OND rainfall is generally overestimated. Figure 11.14 supports our contention that these precipitation biases can be understood on climatological timescales as a function of the models' representations of vertical motion associated with the Indian Ocean Walker circulation. In MAM, a majority of models are biased towards stronger descent over Kenya (positive omega bias), whereas in OND they are biased towards weaker descent or ascent (negative omega bias). Finally, Figure 11.15 suggests a potential link between the Indian Ocean Walker circulation and MAM rainfall biases as well as OND. As well as extending the findings of Hirons and Turner (2018) that CMIP5 model zonal winds associated with this circulation have easterly biases in OND resulting in anomalously high moisture flux into East Africa, this plot suggests that the reverse is the case in MAM where models tend towards anomalously strong westerlies. The vertical motion and zonal wind biases have a common direction with respect to East African rainfall, implying that they are part of the same overturning cell. We suggest that further analysis of these wind biases may help resolve the ambiguity in the literature on the role of the Indian Ocean Walker circulation during the long rains.

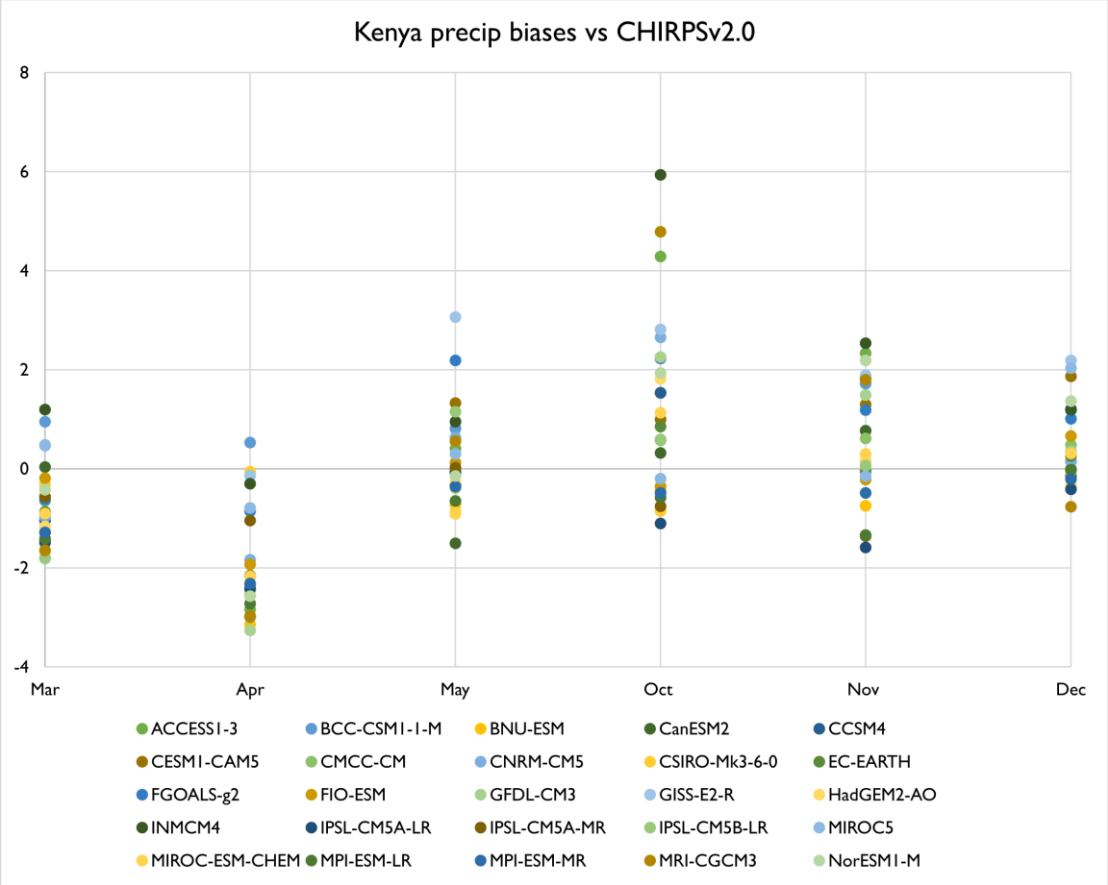


Figure 11.13 - CMIP5 model precipitation biases over Kenya for each rainy season month relative to CHIRPSv2.0, 1975–2005.



Figure 11.14 - CMIP5 model 400 hPa omega biases over Kenya for each rainy season month relative to MERRA-2 reanalysis, 1980–2005.

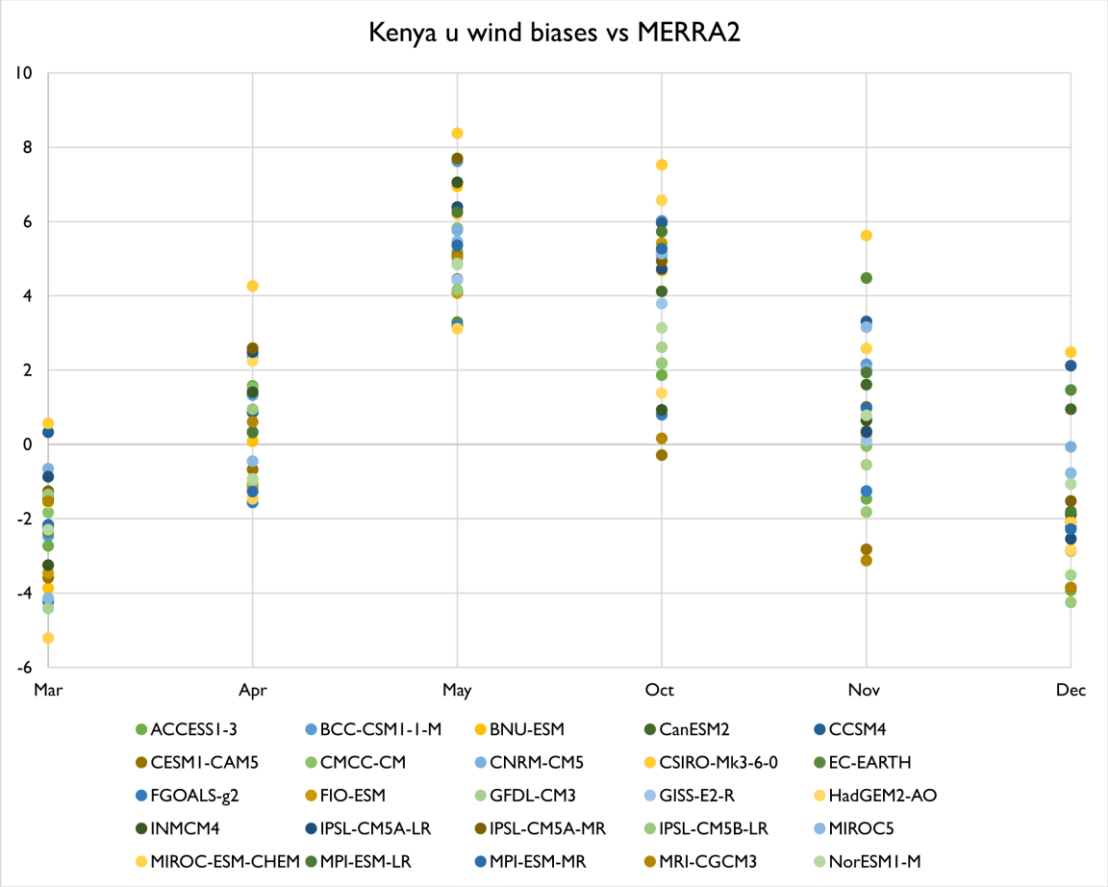


Figure 11.15 - CMIP5 model 850 hPa zonal wind biases over the equatorial Indian Ocean (50°E–100°E, 5°N–5°S) for each rainy season month relative to MERRA-2 reanalysis, 1980–2005.

We next plot the model biases in precipitation over Kenya (relative to CHIRPS v2.0) against the model biases in omega (relative to MERRA-2) for each month over the period 1981–2005. We also plot RMSE (Equation 11.1) in precipitation against RMSE in omega for the same period.

$$RMSE = \sqrt{\frac{\sum_{t=1}^{T}(x_{1,t}-x_{2,t})^2}{T}} \qquad (11.1)$$

Equation 11.1 – Root Mean Square Error (RMSE) for two timeseries $x_{1,t}$ and $x_{2,t}$, both of length T.

Figure 11.16 indicates that there is a relationship between model biases in the descending limb of the Walker circulation over Kenya and rainfall over Kenya. Models with stronger descent (positive omega bias) over Kenya are also generally drier (negative rainfall bias), dependent on the rainy season month. During the long rains, the relationship holds for March (R^2 = .243, p = .01), April (R^2 = .201, p = .02), and May (R^2 = .341, p = .002). During the short rains, there is a strong relationship in October (R^2 = .728, $p = 6 \times 10^{-8}$) and November (R^2 = .506, $p = 7 \times 10^{-5}$) but not December (R^2 = .025, p = .45). This relationship is also present in the AMIP models (Figure 11.17) in both March (R^2 = .369, p = .003) and November (R^2 = .475, p = −.0005). In AMIP, models in March tend towards wet biases, in opposition to CMIP. In November, there is an equal spread of dry and wet biased models in AMIP, whereas CMIP models tend towards wet biases.

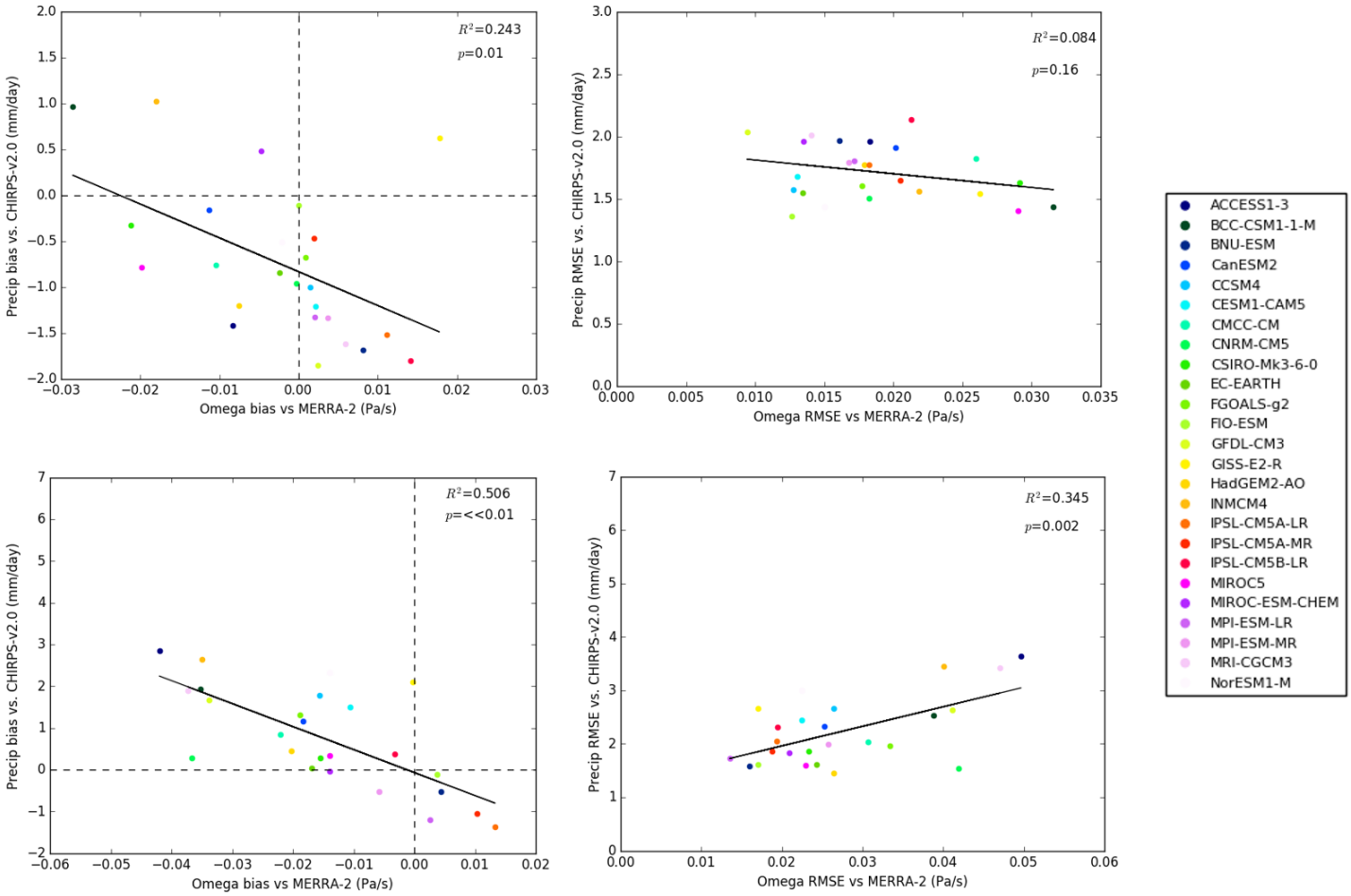


Figure 11.16 - - Relationship between model biases (left column) and model RMSE (right column) in rainfall and 400 hPa omega over Kenya for CMIP5 March (top row) and CMIP5 November (bottom row). Note different scales.

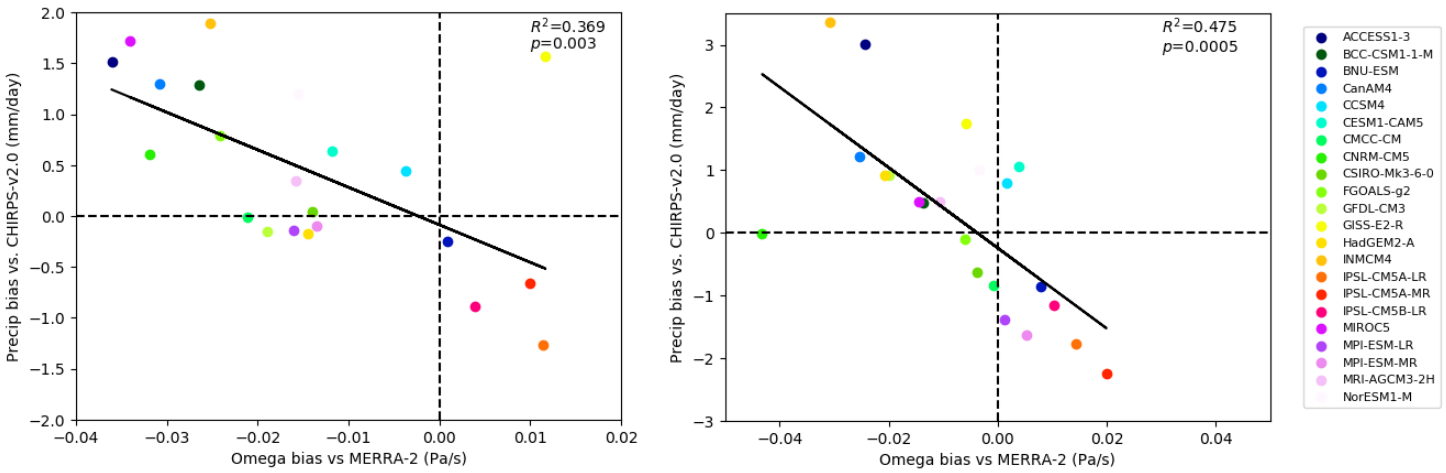


Figure 11.17 - Relationship between model biases in rainfall and 400 hPa omega over Kenya for March (left) and November (right) in AMIP models. Note different scales.

The RMSE plots in Figure 11.16 give a more general indication of the links between model biases by removing the directionality of the relationship shown in the bias plots, in order to assess whether low error in omega is associated with low error in rainfall relative to the reference datasets. In this case, the relationship is not significant in any of the long rains months, but is both significant and positive in the short rains. This indicates that models with greater biases in Kenya omega during OND also have greater biases in Kenya rainfall. In the long rains months, several models have low RMSE in precipitation but also high RMSE in omega. This suggests that although these models are successful at reproducing observed rainfall statistics, their dynamics are potentially less realistic. These models include: BCC-CSM1-1-M, GISS-E2-R, INMCM4, and MIROC5 (March); BCC-CSM1-1-M, CSIRO-Mk3-6-0, FGOALS-g2, MIROC5, and MPI-ESM-LR (April); and CNRM-CM5 and NorESM1-M (May). In the short rains months, the link between RMSE in precipitation and in omega is stronger. With the exception of CNRM-CM5 during November/December

and GFDL-CM3 in December, there are no models exhibiting low RMSE in precipitation with high RMSE in omega; rather, models tend to have correspondingly high or low error values in both variables. It is noteworthy that several of the models which have 'good' rainfall but 'bad' omega during the long rains are 'bad' in both variables during short rains months (including INMCM4 and FGOALS-g2). These models generally exhibit strong wet biases in OND. They are also among the wettest models in the ensemble for MAM, but since the ensemble as a whole is drier than observations during this season, these models return a low RMSE score. This suggests a link between the underlying model processes causing wet biases in both rainy seasons.

11.5.2. Wet Versus Dry Models

The composites of the four driest CMIP5 models in monthly averages for each rainy season month (Figure 11.18 middle panel) further suggest a role for the Walker circulation. The models are generally too dry in the long rains and too wet in the short rains, with 75% of models being too dry during MAM and 65% of models being too wet in OND. The composites show much more extensive descent and more pronounced overturning circulations over the western Indian Ocean and East Africa in March and April relative to OND. In the short rains dry model composite, the overturning circulations are weaker and shallower – though these dry models are closer to observed values of rainfall, the structures by which the rainfall is produced can thus be called into question.

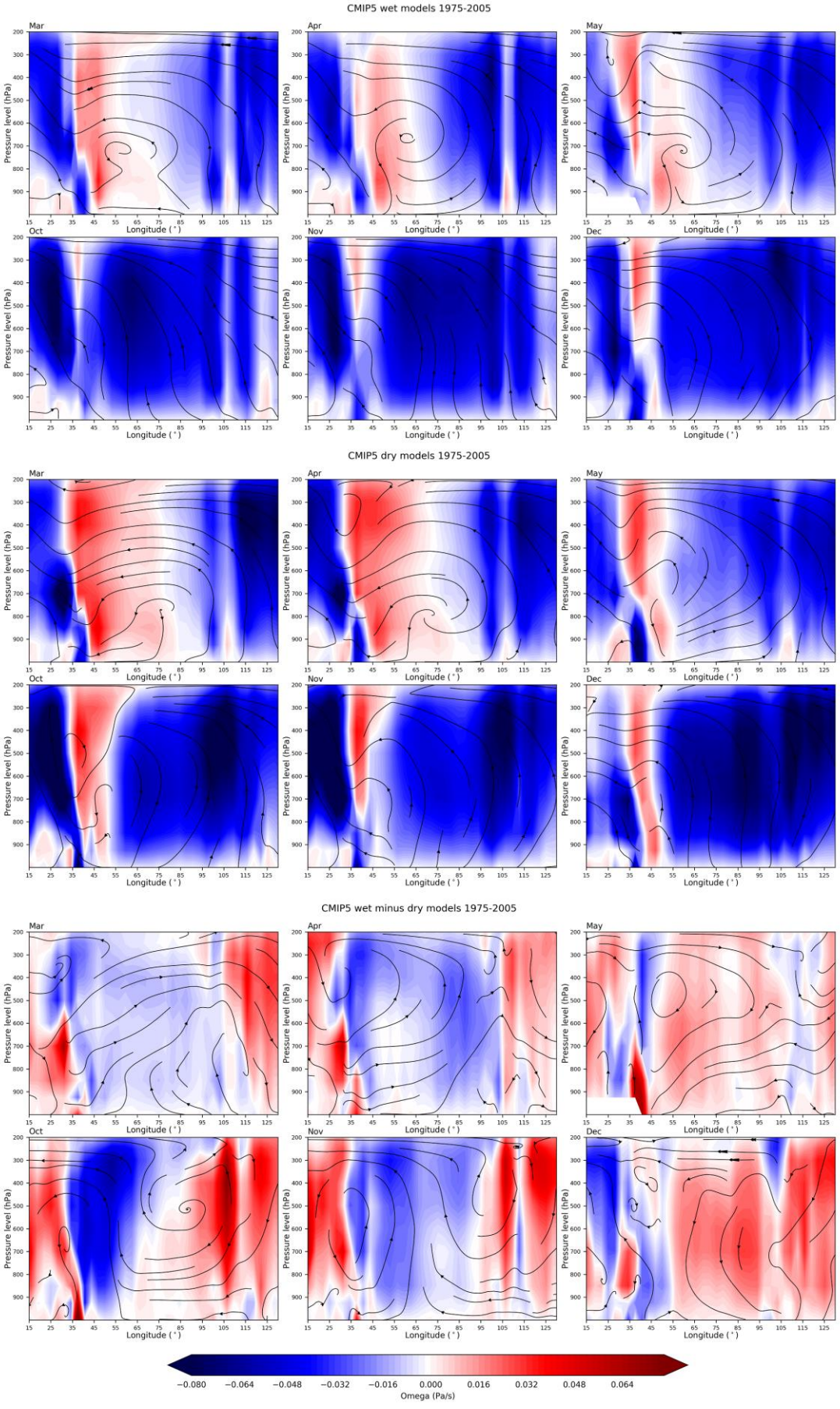

CMIP5 wet models 1975-2005
Mar
Apr
May
Oct
Nov
Dec
Pressure level (hPa)
Longitude (°)
CMIP5 dry models 1975-2005
Mar
Apr
May
Oct
Nov
Dec
Pressure level (hPa)
Longitude (°)
CMIP5 wet minus dry models 1975-2005
Mar
Apr
May
Oct
Nov
Dec
Pressure level (hPa)
Longitude (°)
−0.080
−0.064
−0.048
−0.032
−0.016
0.000
0.016
0.032
0.048
0.064
Omega (Pa/s)

Figure 11.18 - As Figure 11.4, but for composite averages of the wettest four CMIP5 models in each month (top); the driest four models (middle); and the wet composites minus the dry composites (bottom).

For the wet composites, a similar picture emerges. The wet models in MAM show markedly less descent over East Africa and less ascent over the Maritime Continent, with an additional band of ascent between 40°E–45°E (Figure 11.18, top panel). During the short rains (especially October and November), there is little evidence of an overturning circulation in the wet composites, with the easterly orientation of the streamlines at the surface indicative of zonal wind biases over the equatorial Indian Ocean. The wet minus dry composites indicate a role for the Walker circulation over the Indian Ocean, with wet models characterized by a weaker descent over East Africa, weaker ascent over the Maritime Continent, and erroneous zonal winds in the lower troposphere (Figure 11.18, bottom panel). This picture is supported by the differences between composites of the driest and wettest CMIP and AMIP models (Figure 11.19). In MAM, when CMIP5 exhibits a dry bias, the coupled model dry composites have more descent over the domain than the atmosphere-only dry composites. The reverse is true for the wet composites in OND, when CMIP wet models have increased ascent over the domain compared to AMIP.

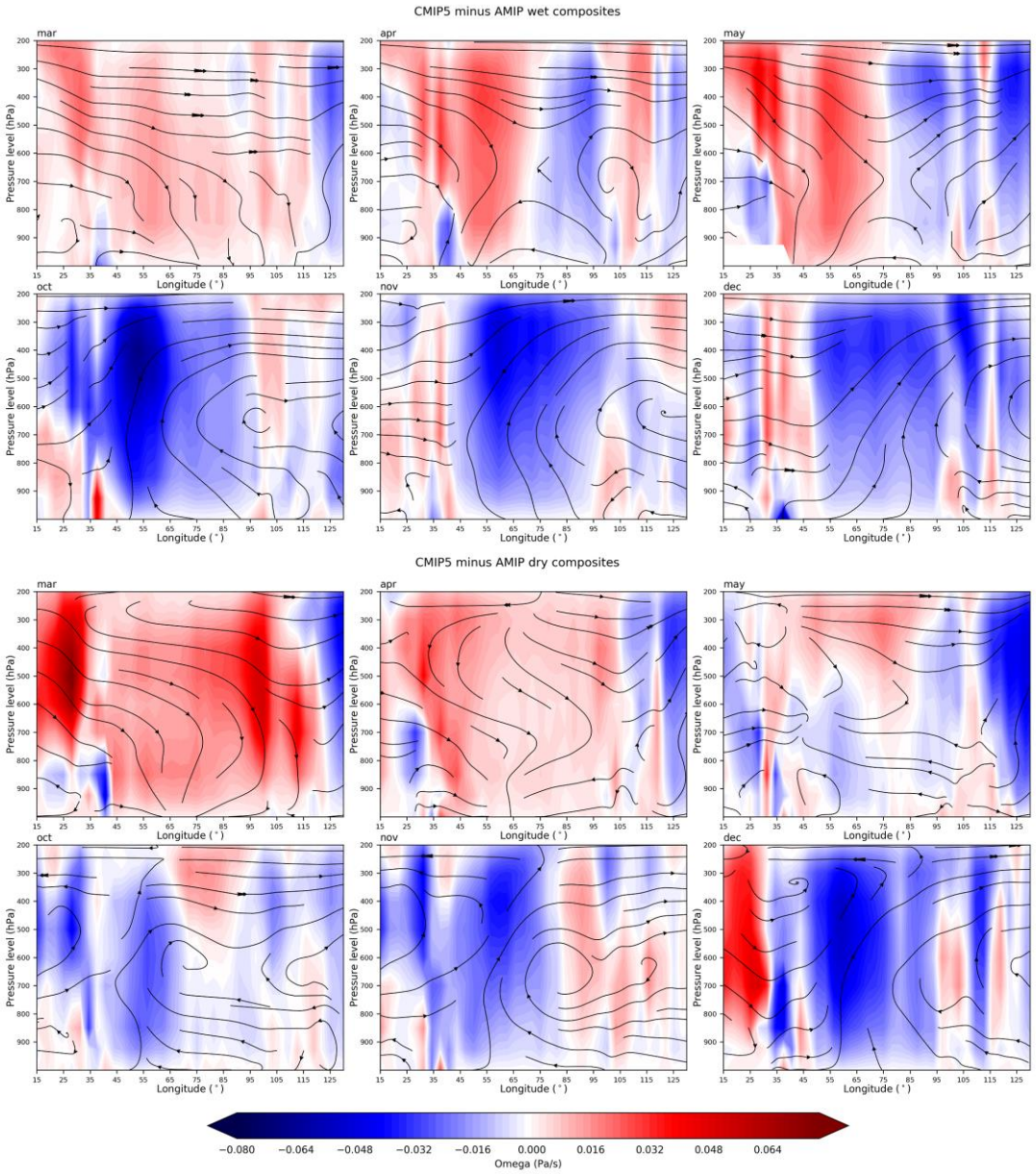


Figure 11.19 - Differences between the wettest CMIP and AMIP models for the rainy season months (top) and between the driest CMIP and AMIP models (bottom).

11.6. Summary and Conclusion

11.6.1. Summary of Walker Circulation Impacts on Kenyan Rainfall

CMIP5 models exhibit well-known biases over Kenya, and East Africa more generally. They underestimate the magnitude of rainfall during the long rains (MAM), some by over half, and overestimate rainfall during the short rains (OND), some by over 100%. There is also a general spring wetting trend in CMIP5 projections which has been questioned given the observed multi-decadal drying trend in the region. In this study, we show that the models' representations of the zonal Walker circulation over the equatorial Indian Ocean are unrealistic. Most models simulate the descending limb of the Walker cell over the western Indian Ocean and East Africa during the long rains months in a too strong and too extensive manner compared to the MERRA-2 reanalysis (Figure 11.10), inhibiting convective potential over East Africa and potentially leading to positive low-to-mid tropospheric pressure anomalies which may inhibit the advection of warm moist air from the eastern Indian Ocean. This behaviour is apparent in the dry/wet composites (Figure 11.18), in which the dry models for MAM have stronger and more extensive descent over East Africa, and a more clearly defined zonal overturning circulation, than the wet models in the same months. This picture is consistent with a dry bias over Kenya during the long rains season, although the circulation is less well defined during this season (Liebmann et al., 2017). However, Figure 11.6 indicates that the zonal structure of vertical motion over the equatorial Indian Ocean is similar in both rainy seasons, with ascent over the Maritime Continent and the Congo Basin balanced by

descent over East Africa. This descent acts to dampen deep convection over East Africa, and may contribute towards the relative aridity of Kenya compared to other regions on the equator. We encourage further research to develop a more precise definition of the seasonal cycle of the Indian Ocean Walker circulation.

During the short rains season, 19/25 models either underestimate the overturning cell or miss it out entirely (Figure 11.7). In November, four models feature a Hadley Cell-like band of almost uniform convection extending throughout the troposphere, rather than the characteristic pattern of ascent in the east and descent in the west seen in reanalysis. This broad convection over the equatorial Indian Ocean, when combined with warming SSTs in the Indian Ocean, could increase moisture availability for East African rainfall – when combined with the mean-state zonal wind biases found in coupled models by Hirons and Turner (2018), in which models produce surface easterlies rather than the observed westerlies, this would increase moisture flux into East Africa and result in a substantially wetter short rains season. Models are known to have biases in the Indian Ocean Dipole during OND (Cai and Cowan, 2013), and this has been shown to be connected to their representations of the Walker circulation (Hirons and Turner, 2018). More work is needed to further disentangle the relationship between omega, wind, and SST biases, and their respective controls on East African rainfall in CMIP5 models. Given that CMIP5 rainfall biases over the Congo Basin are associated with differences in moisture flux (Washington et al., 2013), the representations of omega and zonal wind over the region shown in Figure 11.6 warrant further investigation. Models with divergent moisture flux over the Congo Basin are dry in that region (Washington et al., 2013), but may also transport more of that moisture to East Africa. For example, the model identified by Washington et al. (2013) as the driest over the Congo in SON (CNRM-

CM5) is the fifth-wettest over East Africa in October. The location of the boundary between Congo ascending air and East African descending air may be one of the key factors determining whether a climate model, and indeed an observed rainy season, is particularly wet or dry over East Africa. On a global scale, Table 11.3 suggests that further investigation into CMIP5 equatorial vertical motion may reveal biases towards descending air in MAM, with implications for rainfall elsewhere in the Tropics.

The comparison between AMIP and CMIP models suggests that the Walker circulation biases in coupled models are at least partially attributable to the SST biases known to be an issue in CMIP5. When SST is controlled, models have less strong descent over the Western Indian Ocean during the long rains, and less strong ascent over the same region during the short rains. An improvement in the representation of equatorial westerlies over the Indian Ocean during November is a notable feature of the AMIP models (Figure 11.8). This is consistent with a correction to the positive IOD-like SST bias exhibited by CMIP5 models, though it should also be noted that AMIP models cannot represent the nature of the IOD and its associated westerlies as a coupled ocean–atmosphere system.

11.6.2. Implications for Future Model Projections

Models have biases in the mean state of the Walker circulation over the Indian Ocean, with consequent impacts on their representation of rainfall over Kenya. While this study focusses on the historical coupled simulations of CMIP5, its findings are relevant to the interpretation of these models' projections of future rainfall in the region under anthropogenic climate change (Yang et al., 2014). It is not sufficient to base assessments of the reliability of models' future rainfall projections on their

rainfall output alone (James et al., 2015). Models which have unrealistic dynamics related to a projected variable of interest in historical coupled simulations (for which they can be assessed against observations) cannot be considered reliable sources of climate projections. Conversely, those models which do have accurate dynamics can be considered more reliable in their future projections. This process-based approach to climate model evaluation is useful both for selecting projections from specific models in the absence of a physically plausible signal in the ensemble mean (Creese and Washington, 2016), and for assessing which global climate models are most suitable for use in regional downscaling experiments (McSweeney et al., 2015). While this article does not explicitly address the effect of model resolution, this might also provide some insights into the reasons behind the differences in model circulations; preliminary analysis indicated a weak but significant relationship between model resolution and the strength of ascent over the Maritime Continent in November (not shown), and this could be linked to the broader circulation. Recent experiments using a high-resolution convection-permitting regional model over East Africa have yielded improvements in the representation of rainfall in the area (Finney et al., 2019); driving such a model with more realistic large-scale flow at the boundaries of the regional simulation could lead to additional such improvements. Additionally, the strong correlations obtained between omega and rainfall in all rainy season months could benefit seasonal forecasting of rainfall in East Africa, which historically has been more difficult for the long rains owing to a lack of reliable teleconnections (MacLeod, 2018; Walker et al., 2019).

The improvements yielded by AMIP in simulating the current Walker circulation structure over the Indian Ocean suggest that coupled models may not yield reliable projections of future climate in the region. It follows that projections made by

applying a ΔSST function to observed data (i.e., adding a warming factor to provide forcing rather than simulating the ocean explicitly) may have value in this region – especially when combined with the high-resolution regional models now available such as that of Stratton et al. (2018). However, care should be taken in the interpretation of such experiments, since the IOD and ENSO are coupled ocean–atmosphere systems and future changes in their behaviour, which are unlikely to simply be a linear warming of their current states, would affect East African rainfall.

In this article, we have addressed three questions. First, we quantified the relationship between the Indian Ocean Walker circulation and Kenyan rainfall using reanalysis and gridded rainfall. Next, the representation of the zonal Walker circulation over the equatorial Indian Ocean in CMIP5 models was investigated, and found to differ substantially from the MERRA-2 reanalysis. Finally, we examined the models' Walker circulation/rainfall relationships in the context of known CMIP5 rainfall biases. These models have rainfall biases over East Africa which can be accounted for as a result of the Walker circulation biases – in particular, the wet bias during the short rains is associated with a significantly reduced overturning circulation in most models, and the dry bias during the long rains with excessive subsidence over East Africa. The mean state of the Walker circulation in the models is therefore not that which is seen in reanalysis. Consequently, projections of Kenyan rainfall made using these models are derived from forcings applied to an erroneous baseline. This means that their future projections may not be plausible. Future work will consider whether models with distinctly realistic or unrealistic Walker circulations in the historical coupled runs project distinctly different future rainfall signals. Additionally, the influence of model topography on East African rainfall requires further study, particularly with regard to low-level convection, moisture flux

(convergence), and the influence of the Turkana low-level jet. More work is needed to further disentangle the relationship between omega, wind, and SST biases, and their respective controls on East African rainfall, as well as the impact of the Walker circulation in observations and models in other parts of the Tropics.

11.7. Acknowledgements

James A. King is funded by the UK Natural Environment Research Council (NERC) through the Doctoral Training Partnership in Environmental Research (grant NE/L002621/1). This work forms part of his doctoral thesis. The CMIP5 data used in this study were downloaded from the UK Centre for Environmental Data Analysis (CEDA), (https://catalogue.ceda.ac.uk/uuid/d2d8f982d66cce55bb59fc769ca39264?jump=related-docs-anchor). CHIRPS rainfall data were downloaded from the Climate Hazards Group at the University of California, Santa Barbara. (ftp://ftp.chg.ucsb.edu/pub/org/chg/products/CHIRPS-2.0/global_monthly/netcdf/). MERRA-2 data were downloaded from the NASA Goddard Earth Sciences Data and Information Services Centre (https://disc.gsfc.nasa.gov/datasets?keywords=%22MERRA-2%22&page=1&source=Models%2FAnalyses%20MERRA-2). The authors thank Ellen Dyer, Dave MacLeod, David Crowhurst, and Callum Munday for their valuable input. The comments of two anonymous reviewers helped improve the manuscript.

This chapter has demonstrated how the Indian Ocean Walker Circulation influences East African rainfall, and how biases in IOWC simulation in CMIP5 models are dynamically linked to the biases in their simulated rainfall climatology. The next chapter concerns the Turkana LLJ, which, like the IOWC, is an important feature of the tropical circulation which affects the mean climatology and the interannual variability of East African rainfall. Following the approach used in chapter 11, its links to rainfall in reanalysis and observations are assessed, and its simulation in the CMIP5 models examined. Chapter 12 devotes more attention to the annual cycle and interannual variability of the LLJ in reanalysis because this is not currently well understood. An important additional reason for doing this is because previous work on the Turkana LLJ has devoted little attention to its interactions with the larger-scale circulation affecting East Africa. We argue that the Turkana LLJ is connected to the IOWC through its relationship to large scale zonal gradients in surface pressure. Therefore, the Turkana LLJ can be understood as an additional second-order impact of the IOWC on East African rainfall. Interactions between large-scale circulations and small-scale features which are dependent on topography are known to be a contributing factor to poor CMIP5 model performance in terms of simulating African rainfall (Munday and Washington 2018). Limited representation of the Turkana LLJ is a source of error in modelled East African rainfall (MacLeod 2019), but an understanding of its drivers can enable first-order approximations of future LLJ change, and consequent rainfall change, to be determined.

12. Paper 2 – Variability of the Turkana Low-Level Jet in Reanalysis and Models: Implications for Rainfall

12.1. Abstract

The complex topography of East Africa poses challenges for accurate modelling of regional climate. The Turkana Channel in northwestern Kenya is an important feature because of a persistent low-level jet (LLJ) which blows through it, which has complex interactions with local and regional rainfall. We establish the annual cycle and interannual variability of the LLJ in the ERA5, MERRA-2, and JRA-55 reanalyses. The jet is strongest during wet seasons in the surrounding region. Results suggest a statistically significant weakening of the LLJ over the last 30-40 years in two out of the three reanalyses. We propose an explanation based on the jet's relationship with regional warming patterns and zonal surface pressure gradients, which link the jet to larger-scale climate dynamics including the Walker Circulation. If these changes continue in future, there may be significant implications for rainfall including increases in northwest Kenya and decreases further inland. However, the global models used to produce climate projections vary in their simulations of the LLJ in part because of their representations of topography. Consequently, it is not possible to assess how future LLJ changes will affect regional climate using CMIP5 models alone. Differences between the reanalyses preclude their direct use for model evaluation. Improving the processes by which topographical observations are mapped onto model grids could lead to improvements in simulation of East African climate. A field campaign to measure the LLJ directly could resolve uncertainties in the literature, help constrain reanalyses, and determine which models have the most realistic LLJ representation.

12.2. Introduction

The Turkana Channel in northern Kenya is one of the most prominent topographic features in East Africa (Figure 12.1). It separates the East African highlands to the south and the Ethiopian highlands to the north. The channel is oriented on a SE-NW axis, and is around 700km long. Its width varies from 700km at its widest point to around 150km at its narrowest. The channel floor is between 300-600m above sea level, with hills forming the sides of the channel rising to ~≥1000m. There are a number of hills within the channel itself, notably Mount Marsabit (1531m), Mount Kulal (2293m) and the Huri Hills (1252m). The area experiences an arid hot desert climate; the regional capital, Lodwar, has a mean annual temperature of ~29°C and a mean annual rainfall of ~186mm.

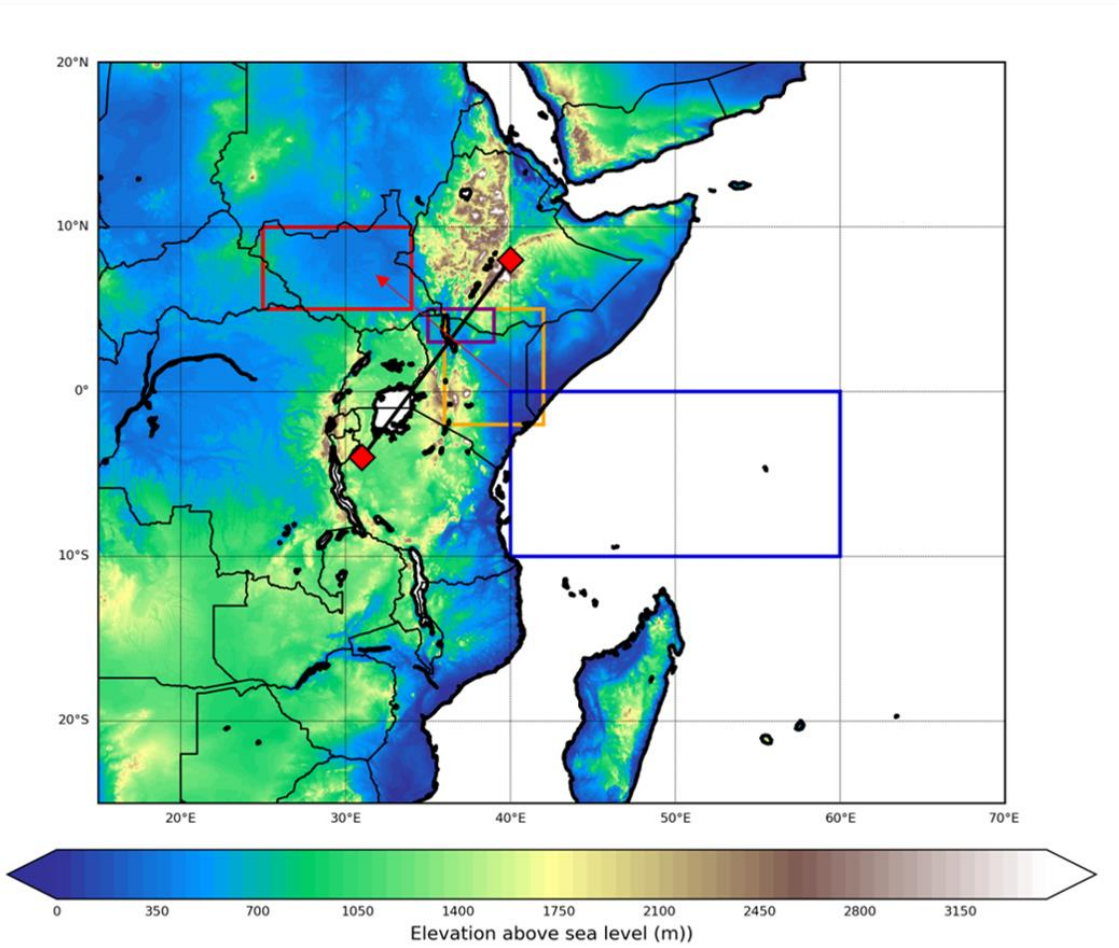


Figure 12.1 - topography of the Greater Horn of Africa region from the GTOPO30 dataset at 3 arc minute resolution. The purple, blue, orange, and red boxes indicate the jet core, Western Indian Ocean, Turkana Jet entrance, and Turkana jet exit regions respectively. The black line indicates the cross-section used for vertical profiles of the Turkana Jet core. The red arrow indicates the mean direction of the LLJ.

Aircraft pilots working in Kenya have long been aware of the existence of strong low-to-mid-tropospheric winds in this region (Kinuthia and Asnani 1982). A southeasterly low-level jet (LLJ) is present in the Turkana Channel throughout the year at an altitude of 600m, and was first described by Kinuthia and Asnani (1982) based on pilot balloon measurements. They reported mean wind speeds of around 25 m s^{-1} and peak speeds of over 50 ms^{-1} at Marsabit. More extensive pilot balloon analysis at multiple locations in the channel was conducted by Kinuthia (1992). He found that the jet was characterised by strongly divergent flow in the morning, with

higher jet speeds in the narrower parts of the channel, suggesting Bernoulli forcing of the flow. The shape of the channel results in a southeasterly jet regardless of whether the prevailing low-level winds to the southeast of the channel, dominated in this region by the seasonal reversal of the Somali Jet, are northerly or southerly (Kinuthia 1992). He reported jet maxima in the morning and at midday, although jet occurrence was possible at any time of day, and found the jet to split vertically into two distinct cores, one at 300m-2000m and another at 2000m-3100m (except at Marsabit owing to the influence of mountainous terrain there). Kinuthia's (1992) observations also indicated very high peak jet speeds of >50 m s^{-1}. It should be noted, however, that single theodolite pilot balloon observations, which assume a constant balloon ascent rate, may be biased towards high wind speeds as a result of turbulence.

Nicholson (2016) presented the first climatology of the jet using reanalysis data. She found jet maxima of ~18 m s^{-1}, much lower than Kinuthia and Asnani (1982) and Kinuthia (1992). Additionally, the reanalysis climatology suggested the jet was mainly nocturnal, with maxima at midnight or 6am in agreement with analyses of other LLJs (Allen and Washington 2013, Rife et al. 2010), but not the observations of Kinuthia (1992) who reported 9am or 12am maxima. Nicholson (2016) found the jet to be strongest in September-October-November and December-January-February, and weakest from May to August.

Indeje et al. (2001) used a regional climate model (RCM) to investigate the drivers of the Turkana LLJ. Their findings supported the Kinuthia (1992) hypothesis that the main forcing mechanism for the jet is the Bernoulli effect, with the channel dimensions controlling its velocity profile at different locations. Additionally, the magnitude of the jet core wind speed was found to be affected by the large-scale

background flow associated with the Somali Jet, but equal importance for jet formation and maintenance was given to local-scale thermal and frictional effects. Hartman (2018) argued - based on reanalysis data - that thermal forcing is of primary importance in jet formation, maintenance, and variability. He suggested that the jet strength is controlled by the temperature gradient along the Turkana Channel, finding it to be enhanced during the April to October period by the advection of cooler air from the Indian Ocean into southeastern Kenya by the Somali Jet, and reduced between November and March when the Somali Jet is reversed; in this period, the Somali Jet is less energetic (Boos and Emanuel 2009) and is advecting air from a different (continental) air mass. This implies that the jet maximum and minimum are coincident with those of the Somali Jet, in contrast to the reanalysis climatology obtained by Nicholson (2016); neither of the two published observational studies ran for long enough to produce an annual cycle. On shorter timescales, Vizy and Cook (2019) propose a connection between high pressure ridging off the Kenyan coast and strong jet events. While the jet is not a 'gap wind' *sensu* Overland and Walter (1981) because it is not at sea level, this suggests that it behaves in a similar way as the flow accelerates along a pressure gradient parallel to the channel axis with the wind field properties strongly determined by topography and the pressure field combined (Indeje et al. 2001). Gap winds of this type have been found in the tropics and subtropics, for example in the Gulfs of Papagayo (10°N) and Tehuantepec (15°N) off the west coast of Central America (Holbach and Bourassa 2014).

The influence of the jet on rainfall within the Turkana Channel itself is evident from the arid nature of the local climate. Kinuthia (1992) noted that the desert regions of northern Kenya have the same size and shape as the LLJ. This aridity results from

the highly divergent flow aloft in the channel (Kinuthia 1992), which leads to dominant downward motion (positive omega) and the consequent inhibition of convective rainfall (Indeje et al. 2001, Hartman 2018). Nicholson (2016) also ascribed the aridity of the area surrounding the Turkana Channel to the jet's divergent flow, as well as suggesting a link between the jet's diurnal cycle and rainfall (with rainfall typically occurring when the jet is weakest), although it is difficult to distinguish these effects form the diurnal cycle of convection. Vizy and Cook (2019) extend this analysis, finding strong negative correlations between reanalysis jet strength and rainfall in the channel and surrounding regions. The jet has a complex relationship to rainfall in the exit region of South Sudan, with a strong jet likely to trigger low-level convergence and convective rainfall in the early morning in the west of the country but not the east. This is due to the increased convergence in the strong jet case being offset by reduced atmospheric moisture content.

The LLJ may also have an impact on rainfall further afield. Despite the aridity of the Turkana Channel, the jet itself is a key vector for moisture flux into East Africa. Viste and Sorteberg (2013) showed that 32% of the moisture falling as rain over the Ethiopian Highlands passes through the Turkana Channel. Indeed, LLJs in Eastern Africa and southern Africa are key conduits of water vapour from the Indian Ocean to the African interior. Kinuthia (1992) suggested that the Turkana LLJ could have an impact on the African Easterly Waves (AEWs), which are responsible for much of the convective rainfall in West Africa, by imparting vorticity to the African Easterly Jet (AEJ) at the jet exit. This hypothesis is supported by Lin (2009), who demonstrated that AEWs and their associated mesoscale convective systems (MCSs) can be generated by vortex shedding associated with horizontal wind shear at the Turkana Jet exit. Furthermore, Lin (2009) suggested that this vorticity contribution

from the Turkana Jet and the Ethiopian Highlands could be a precursor to tropical cyclones and hurricanes in the Atlantic Ocean. This is comparable to the effect reported by Holbach and Bourassa (2014) in the Pacific, where topographically forced gap winds from central America contribute vorticity to cyclone formation. The jet also contributes to the local economy through the generation of electricity by the Lake Turkana Wind Power Project, one of Africa's largest wind farms.

Rainfall change and variability have substantial impacts on East African societies and economies. It is therefore important to be able to make reliable projections of how anthropogenic climate change will affect rainfall (Washington et al. 2006, Giannini et al. 2018). The ability of climate models to represent East African climate is a caveat on studies using models to understand the drivers of variability and change, and on future projections (Rowell et al. 2015, James et al. 2018, Hirpa et al. 2019). General circulation models (GCMs) participating in Coupled Model Intercomparison Project 5 (CMIP5; Taylor et al. 2012) tend to project a wetter future for East Africa (Ongoma et al. 2017, Han et al. 2019) – however, this is in opposition to the observed drying trend, a problem known as the East African climate paradox (Rowell et al. 2015). Models are also known to have substantial rainfall biases in East Africa, underestimating the magnitude of the long rains and overestimating the short rains (Tierney et al. 2015). A number of possible reasons for models' limited reliability in the region are under investigation, including biases towards a positive Indian Ocean Dipole (IOD) state (Cai and Cowan 2013), erroneous representation of zonal winds (Hirons and Turner 2018, Walker et al. 2019) and the Walker Circulation (King et al. 2020), and the impact of aerosols (Scannell et al. 2019). Differences in the background state of the circulation can determine the trajectory of model projections of East African rainfall (Cook et al. 2020). One significant source of uncertainty

arises from East Africa's highly complex topography, which has a major impact on rainfall (Hession and Moore 2011, Ogwang et al. 2014), but which CMIP5 models are unable to capture in detail owing to their resolution (James et al. 2018). Therefore, a key task for improving our understanding of East African rainfall change is to investigate the effects of topographic features (such as the Turkana LLJ) on the observed climate over the last few decades.

Given its links to rainfall, and importance for wind power, investigation of any multidecadal trends in the Turkana LLJ strength is important, with implications for future climate change impacts in East Africa. Additionally, the nature of the jet as a regional-scale topographically-forced feature with wider-scale climate impacts means it is a challenge to represent in climate models (Collins et al. 2018, James et al. 2018). The Turkana LLJ specifically has been suggested as a reason for the limited ability of seasonal forecasting models to represent interannual variability in East African rainfall (MacLeod 2019). This paper therefore presents the first analysis (to our knowledge) of the long-term behaviour of the jet, as well as its representation in CMIP5 models. We aim to address the following research questions:

1. What is the climatology of the Turkana LLJ in MERRA-2, ERA5, and JRA55, and how does it interact with regional rainfall?

2. How has the Turkana LLJ changed over recent decades (1981-2016) and what might account for these changes?

3. How is the Turkana LLJ and its links to rainfall represented in CMIP5 models, and how does model topography affect this representation?

The remainder of the paper is organised as follows. Section 12.3 introduces the datasets used and methods of analysis. Section 12.4.1 describes the climatology of the Turkana LLJ and its links to regional rainfall. Section 12.4.2 evaluates changes in the Turkana LLJ strength over the period 1981-2016, and suggests potential mechanisms for observed trends; Section 12.4.3 assesses the ability of CMIP5 models to represent the jet, its annual cycle, and its correlation with regional rainfall. Section 12.5 discusses and summarises the findings, and Section 12.6 concludes the chapter.

12.3. Data and Methods

Rainfall data used in this study were obtained from version 2 of the Climate Hazards Group Infrared Precipitation with Stations dataset (CHIRPSv2.0; Funk et al. 2015). This is a high-resolution (0.05°) gridded dataset which combines observed rainfall from raingauges with remotely sensed infrared measurements of cold cloud duration. It has performed well in assessments of precipitation datasets over East Africa relative to station data (Kimani et al. 2017, Gebrechorkos et al. 2018) especially for the monthly means used in this study (Dinku et al. 2018).

Given the lack of available climatological observations of low-to-mid tropospheric wind speed in the Turkana Channel, reanalysis data are used to assess the decadal behaviour of the Turkana LLJ. Reanalysis products differ in their representations of the tropical African troposphere (Washington et al. 2013, Maidment et al. 2015); consequently, three reanalysis data sets were used: version 2 of the Modern Era Retrospective Analysis for Research and Applications (MERRA-2; Gelaro et al. 2017); the European Centre for Medium-Range Weather Forecasts Reanalysis 5

(ERA5; Hersbach et al. 2020); and the Japanese 55-year Reanalysis Project (JRA-55; Kobayashi et al. 2015). The JRA55 data used here are on the dataset's native hybrid pressure levels rather than isobaric levels; conversions to hPa are as per Japan Meteorological Agency (2014), whereby hybrid level 12 equates to 846.96hPa. MERRA-5 and ERA5 are on isobaric levels. Details of the reanalyses used are presented in Table 10.1.

MERRA-2 has been suggested to be the most realistic reanalysis of those currently available at representing tropospheric wind fields over equatorial Africa when compared to quality-controlled radiosonde observations (Hua et al. 2019), whereas ERA5 performed best in a global-scale assessment of near-surface winds (Ramon et al. 2019).However, the latter study did not assess reanalysis performance against measurements in tropical Africa, and found little difference in seasonal mean wind performance between datasets (Ramon et al. 2019). Torralba et al. (2017) found good agreement between MERRA-2, JRA55, and ERA-Interim (the predecessor of ERA5) for both 10m and 850 hPa wind speed trends, although both reduced wind speeds over land and stronger wind speed trends were found in JRA55 relative to the other datasets. 10m surface wind and 2m air temperature observations were obtained from the UK Met Office Integrated Data Archive System (MIDAS; Met Office (2012)) for three stations located along the channel axis: Wajir (1.75°N, 40.067°E), Marsabit (2.3°N, 37.9°E), and Lodwar (3.117˚N, 35.617˚E). Topography data are obtained from the US Geological Survey GTOPO30 dataset at 3 arc minute resolution (Gesch et al. 1999).The climate model data used are from CMIP5 (Taylor et al. 2012). A subset of 25 models was selected based on wind data availability from historical coupled runs (Table 11.1.). The first ensemble member for each model was used over the period 1975-2005.

12.4. Results

12.4.1. Turkana LLJ Climatology

12.4.1.1. Long-Term Means

We first plot the long-term means of the Turkana LLJ, in MERRA-2, ERA5, and JRA55 datasets. Figure 12.2 indicates that in the MERRA-2 reanalysis, the jet is present in the long-term mean windspeed field. The jet core is between 10 and 14 m s^{-1}, with the core lying between 900 and 800 hPa. The ERA5 LLJ is also present at the same height range but with less extension. In JRA55 the jet has a weaker core speed on average than MERRA-2 or ERA5 (not shown). The JRA55 LLJ is also more vertically extensive than in MERRA-2 or ERA5, extending from hybrid level 5 (978hPa) to hybrid level 13 (818hPa) (not shown).

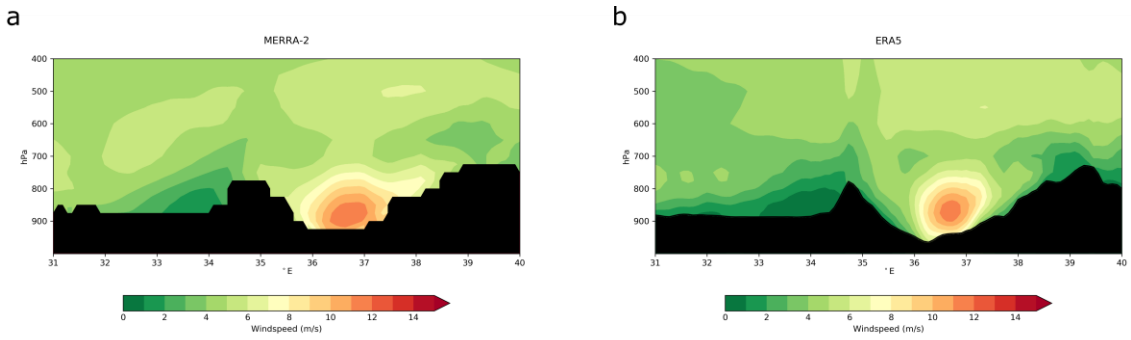


Figure 12.2– Long-term mean wind speed at the cross-section through the jet core shown in Figure 12.1, for MERRA-2 (a) and ERA5 (b). Transect is between 4°S 31°E and 4°N 40°E. Data averaged from 1981-2016.

Plotting wind vectors at 850hPa/hybrid level 12 (Figure 12.3) indicates the presence of a strong easterly flow in the Turkana Channel in the monthly averages throughout the year. It is noteworthy that the jet persists as a southeasterly flow when the prevailing wind at this height, the Somali Jet, undergoes a seasonal reversal from northerly cross-equatorial flow in boreal winter to southerly cross-equatorial flow in boreal summer associated with the Asian Monsoon (Boos and Emanuel 2009). The jet core, being between 3 and 5 degrees north of the Equator, experiences a weak Coriolis deflection. The Rossby radius of deformation, which is the length scale at which the geostrophic balance between pressure gradient forces and the Coriolis force becomes important, is given by

$$L = \frac{NH}{f} \qquad (11.1)$$

where N is the Brunt-Vaisala frequency, H the depth of the troposphere, and f the Coriolis parameter. Assuming a jet core at 4°N, with the troposphere at 18km in height, and a temperature of 25°C at 850hPa, L ~ 13000km, which is much greater than the length of the jet axis (no more than 1000km). This implies a weak effect of Coriolis on the jet. However, the Rossby number for the jet flow, assuming a constant velocity of 15 ms^{-1}, is ~2.3, suggesting a balance between inertial accelerations and Coriolis (Hartman 2018).

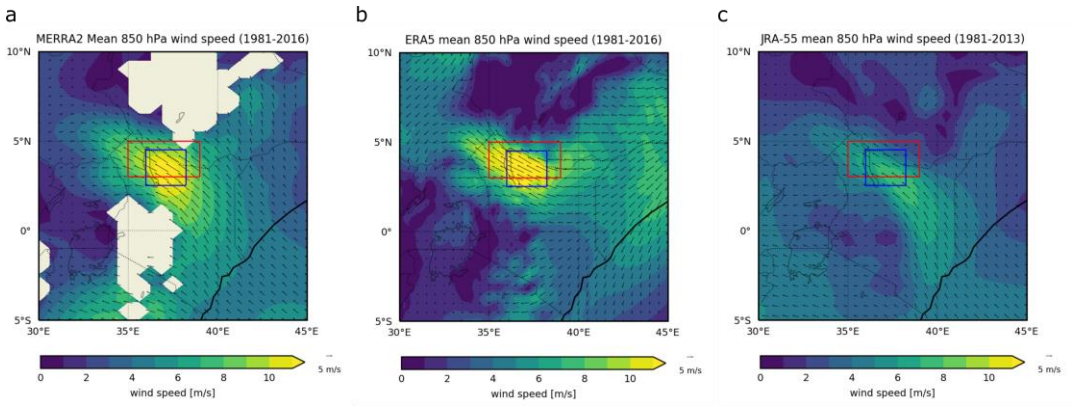


Figure 12.3 - as Fig. 12.2, but for wind speed at 850hPa/hybrid level 12. Red box is as per Fig. 12.1; blue box was used to test for sensitivity of results to area averaging (no significant differences were found between the boxes used).

The long-term means of 850hPa windspeed (Fig. 12.4), however, indicate differences between the datasets. The annual JRA55 jet is weaker than the annual means of MERRA-2 and ERA5, with an annual mean of ~8 m s^{-1} in the former dataset compared to ~12 m s^{-1} in the latter datasets. Additionally, the directionality of the wind is slightly different for each reanalysis. ERA5 shows winds entering the Turkana channel from the east/north-east whereas MERRA2 and JRA55 show winds entering from the south/south-east.

12.4.1.2. Annual Cycle

The jet is primarily a zonal wind feature, with a core centred at around 850 hPa in the reanalysis datasets. The annual cycle of zonal wind at the jet core area (850hPa, 3°N-5°N, 35°E-39°E, pink box in Figure 12.1) (Figure 12.4) for the reanalyses datasets is broadly in agreement with that obtained by Nicholson (2016) from the ERA-Interim reanalysis**.** The reanalysis LLJs exhibit a bimodal climatology with peak wind speeds in boreal spring and boreal autumn/winter. Minimum wind speeds are experienced in

July (boreal summer). While the seasonality of the jet is the same in all three reanalyses, there is variation in the jet's magnitude. MERRA-2 consistently has the strongest jet throughout the year, with average peak zonal wind speeds 2 m s^{-1} faster than ERA5 between December and March. ERA5 and MERRA-2 do have similar jet strength in May-September when the jet is weaker; therefore, the annual cycle of jet strength is more pronounced in MERRA-2 than ERA5. JRA55 has similar peak speeds to ERA5 from November to March, but much lower speeds between May and September as the jet almost disappears (~1 m s^{-1}) in July. JRA55 has the most pronounced annual cycle of all three reanalyses.

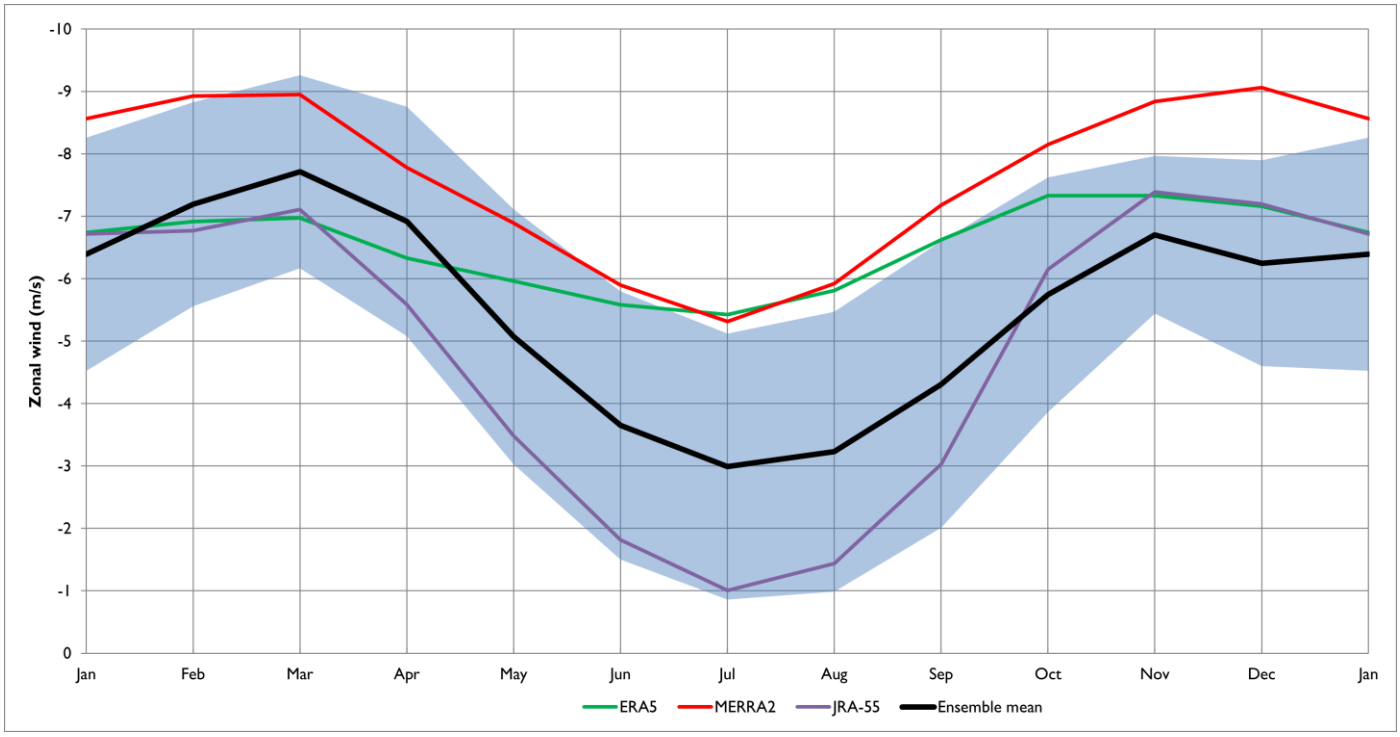


Figure 12.4 - seasonal cycle of jet core zonal wind at 850hPa from reanalysis datasets plus the ensemble mean of the 25 CMIP5 models listed in Table 2. The blue shaded area indicates ±1 standard deviation of the CMIP5 ensemble mean.

The ensemble mean CMIP5 model annual cycle is in good agreement with the reanalyses in terms of seasonality, though with a faster zonal wind in February-

March (7.8 m s^{-1}) compared to November-January (6.8 m s^{-1}) - the reanalyses do not have such a seasonal difference between zonal wind speeds. Similar results were obtained using scalar wind speed integrated in the jet core region between 800hPa and 900hPa (not shown).

Vizy and Cook (2019) also note the stronger LLJ in MERRA-2 when compared to ERA5. They ascribe this to Bernoulli forcing, noting that the underlying topography in MERRA-2 features a narrower Turkana Channel, as well as either lower or absent topography in the channel which is present in ERA5. Our analysis concurs with these findings. However, JRA55, which also has a narrower Turkana Channel than ERA5 and even less representation of within-channel topography (Fig. 12.5), has a jet which is comparable in strength to ERA5 during peak months and much weaker during boreal summer. Therefore, differences between reanalysis datasets cannot be attributed to topography alone.

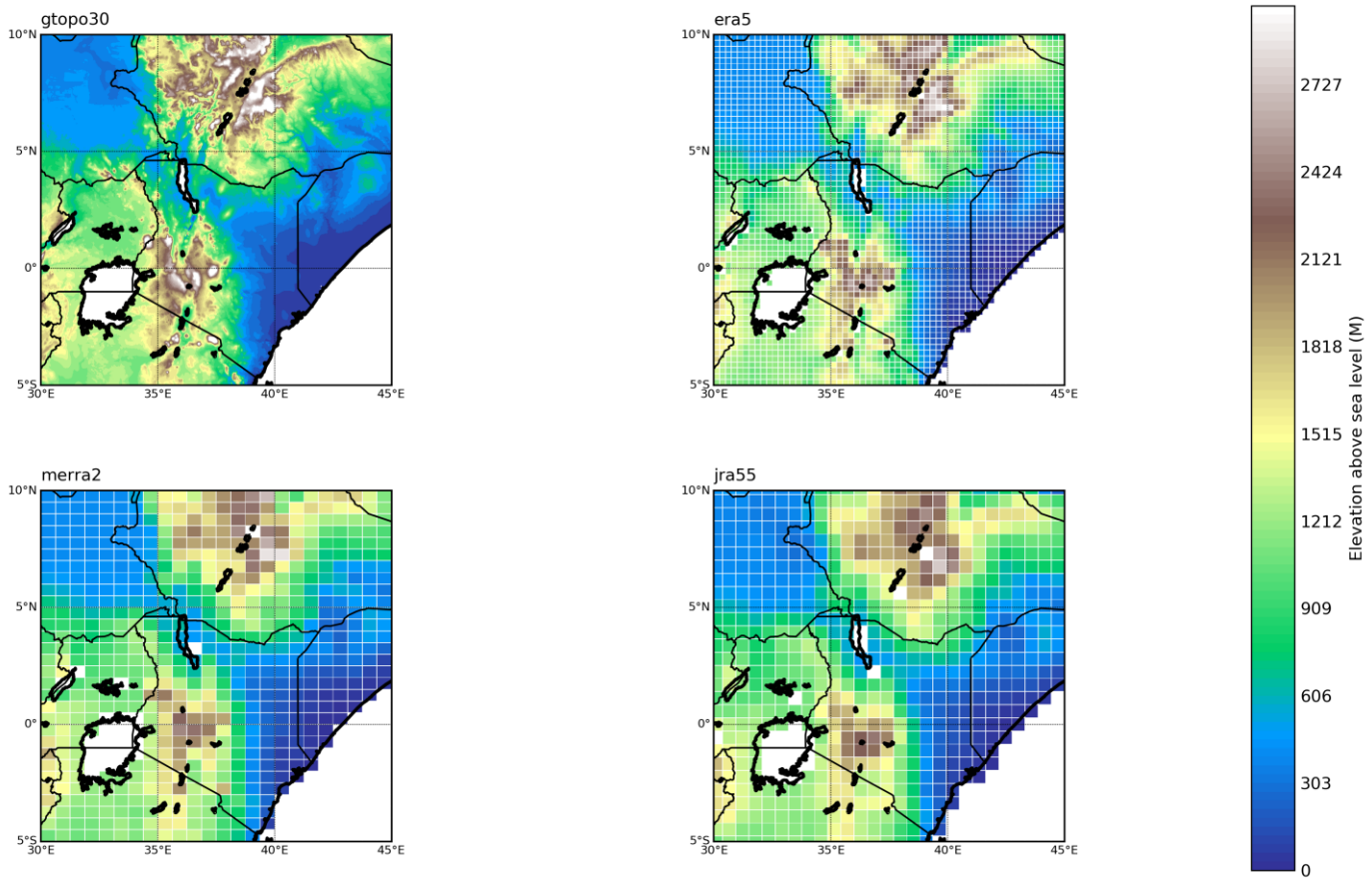


Figure 12.5 - Comparison of underlying topography of the Turkana Channel from GTOPO30, ERA5, MERRA-2, and JRA55.

We next consider the annual cycles of dynamic fields which may play a role in forcing the jet. Following Hartman (2018), we plot annual cycles of the differences between the jet exit and the jet entrance, and between the jet exit and the western equatorial Indian Ocean (WEIO) for three key fields: near-surface temperature, 900hPa geopotential height, and 850hPa vertical velocity (omega). The areas used for averaging are shown as boxes in Figure 12.1. This indicates how the strength of the gradients along the jet axis vary seasonally and between the different reanalyses.

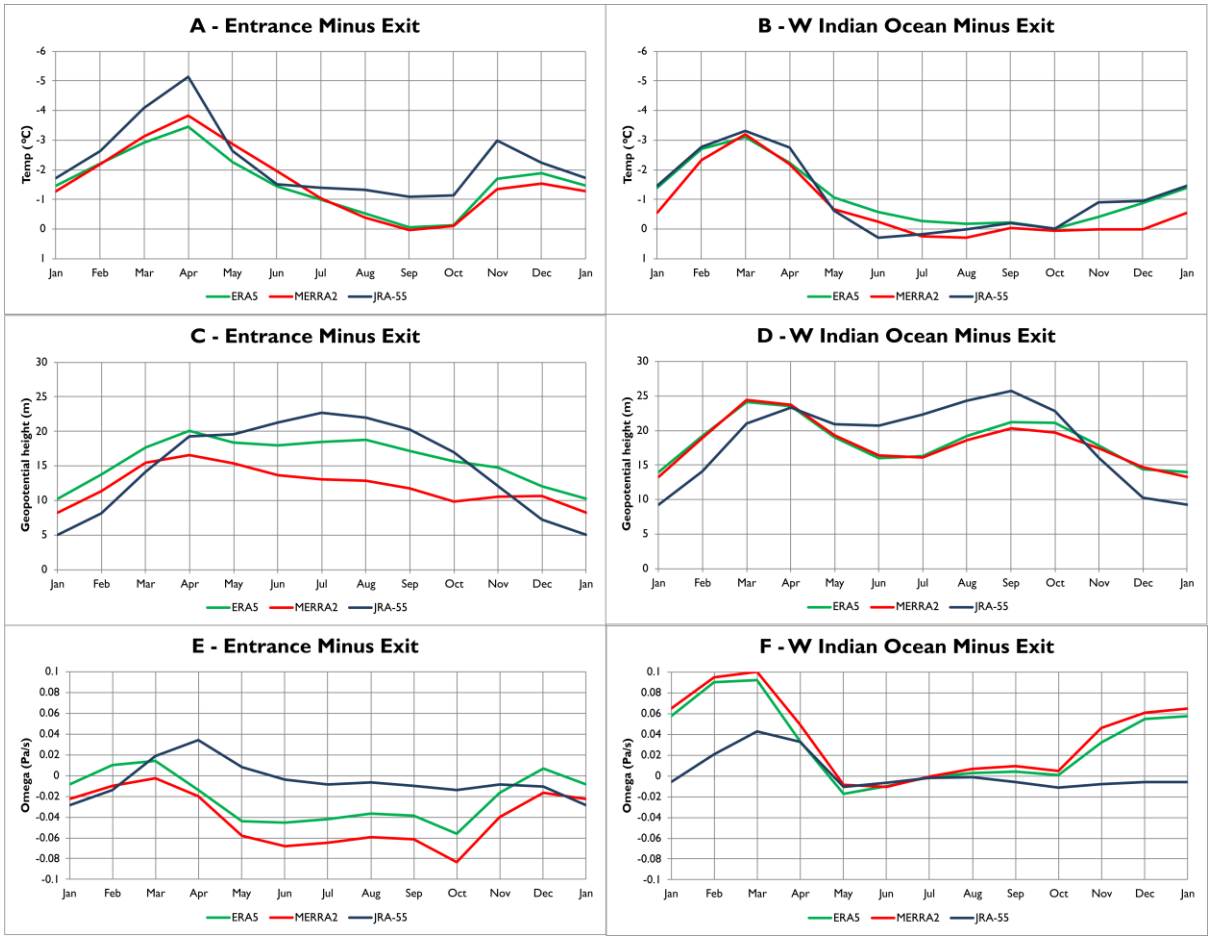


Figure 12.6 - Differences in near-surface temperature for each month in reanalysis between the jet entrance box and the jet exit box (A) and between the Western Indian Ocean box and the jet exit box (B; for 900hPa geopotential height (C and D); and for 850hPa vertical velocity (omega; E and F)

For the jet entrance, exit, and WEIO areas, the annual cycle of temperature gradients in reanalysis are in broad agreement. In all areas, temperature peaks in boreal spring and experiences a minimum in boreal summer. For the entrance zone, MERRA-2 is the hottest reanalysis apart from in May, July, and January when ERA5 is hotter by ~0.1-0.3°C; the temperatures of the 2 datasets are in general very similar. JRA55 is consistently around 1°C cooler at the entrance. At the jet exit, the annual cycle of temperature has greater amplitude, with a more pronounced peak in March for all datasets. MERRA-2 is again narrowly the hottest and JRA-55 cooler by up to 1°C, but there is closer agreement between the datasets than the exit. Peak jet

speeds coincide with higher temperatures in the channel, but boreal spring is markedly warmer than boreal autumn despite similar jet strength. The temperature gradient between the entrance and exit and between the WEIO and exit peaks in boreal spring when the jet is strong, and is lowest in boreal summer when the jet is weak (Figure 12.6 A and B). This does imply a link between the temperature gradient and the jet strength – however it does not entirely account for the annual cycle because the temperature gradients in boreal autumn are weaker than spring despite the jet having a similar magnitude. Furthermore, in all months apart from May and June, the reanalysis with the strongest along-channel temperature gradient is JRA55, which has the weakest jet of the three datasets for most of the year. The entrance minus exit gradient for JRA55 is significantly different ($p > 0.05$) from MERRA-2 and ERA5.

For 900hPa geopotential height (Zg; Figure 12.6, C and D), the gradients between the entrance/WEIO and exit also vary seasonally. For the entrance minus exit differences (Figure 12.6 C), MERRA-2 and ERA5 have a similar annual cycle with the steepest gradient in April and the shallowest in January; MERRA-2 consistently has a smaller Zg difference than ERA5, and this difference is statistically significant at $p > 0.05$. JRA55 has a stronger gradient peaking in July, which is effectively in antiphase with the annual cycle of jet zonal wind strength. For the Zg difference between the WEIO and the jet exit (Figure 12.6 D), the datasets have boreal spring and summer peaks that correspond more closely to the jet annual cycle – implying a role for ocean-land pressure gradients in the jet's climatology, although the stronger gradients in JRA55 do not translate straightforwardly into a faster jet. As the jet lies almost on the equator, with a non-negligible but small Coriolis deflection, the jet cannot be described purely as a geostrophic wind; however, neither is it straightforwardly

dependent on the pressure gradient force. Hartman (2018) suggests a balance between Coriolis, pressure, and inertial effects in the maintenance of the jet, which is supported by his calculation of the Rossby number for the jet as ~2.33 and the large Rossby deformation radius at these latitudes (see section 12.4.1.1). The Zg over the WEIO is influenced by the strength of the Somali Jet, suggesting its influence on the Turkana LLJ may be more complex than the temperature advection mechanism proposed by Hartman (2018).

The omega gradients (Figure 12.6, E and F) indicates stronger gradients in vertical motion when the jet is strong. The weaker gradients during boreal summer could be attributable to the influence of the Somali Jet, which results in suppression of the pressure gradient due to prevailing downward motion across Kenya. It is notable that in JRA55, the vertical motion averaged across the entrance region is downward in boreal summer whereas it is upward in the other 2 reanalyses. In spring and summer, JRA55 has weaker ascent in this region. This results in an omega gradient from the entrance to the exit of almost zero in boreal summer, during which the jet strength in JRA55 drops almost to zero. The differences between all three reanalyses for the WEIO minus exit difference in omega are statistically significant ($p > 0.05$). In all three variables, the reanalyses are more similar for the exit region than the entrance regions. This may reflect the greater influence of parameterisations relating to moist processes over the WEIO and/or the differences in the relative strength of the Somali Jet between the reanalyses.

Figure 12.7 compares surface temperature for the stations at Wajir (1.75°N, 40.067°E), Marsabit (2.3°N, 37.9°E), and Lodwar (3.117˚N, 35.617˚E) with the nearest reanalysis grid box. All three stations lie within the entrance or core regions of the channel. Marsabit station is located on a hill and is the highest above sea level of the stations (1345m), whereas Lodwar (515m) and Wajir (244m) are located on the channel floor.

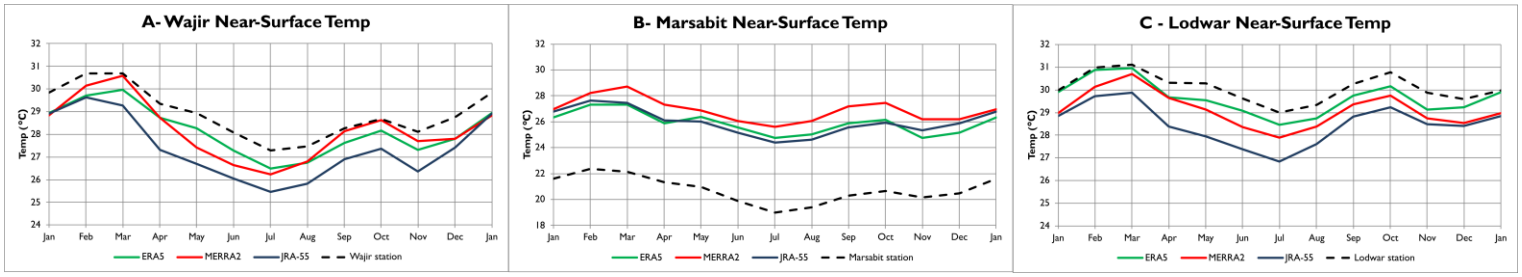


Figure 12.7 - seasonal cycles of near-surface temperature from reanalysis data at Wajir (a), Marsabit (b), and Lodwar (c) stations, compared to station observations.

Figure 12.7 indicates that the reanalysis annual cycle of temperature has a slight cool bias at Wajir and Lodwar. The strong warm bias for Marsabit can be attributed to area-averaged elevation in reanalyses which results in an overall more flattened topography. There are statistically significant differences (p <0.05) between the mean temperatures at all stations and the reanalysis temperatures interpolated to the station locations, as well as between the individual reanalyses at Lodwar (all reanalyses different from one another), Wajir (significant differences between JRA55 and the other reanalyses) and Marsabit (significant differences between MERRA-2 and the other reanalyses). Quality control issues with the station data in this area mean these observations should be interpreted with some caution; nevertheless, the reanalyses are consistent in being cooler than observations at Wajir and Lodwar, and warmer than observations at Marsabit.

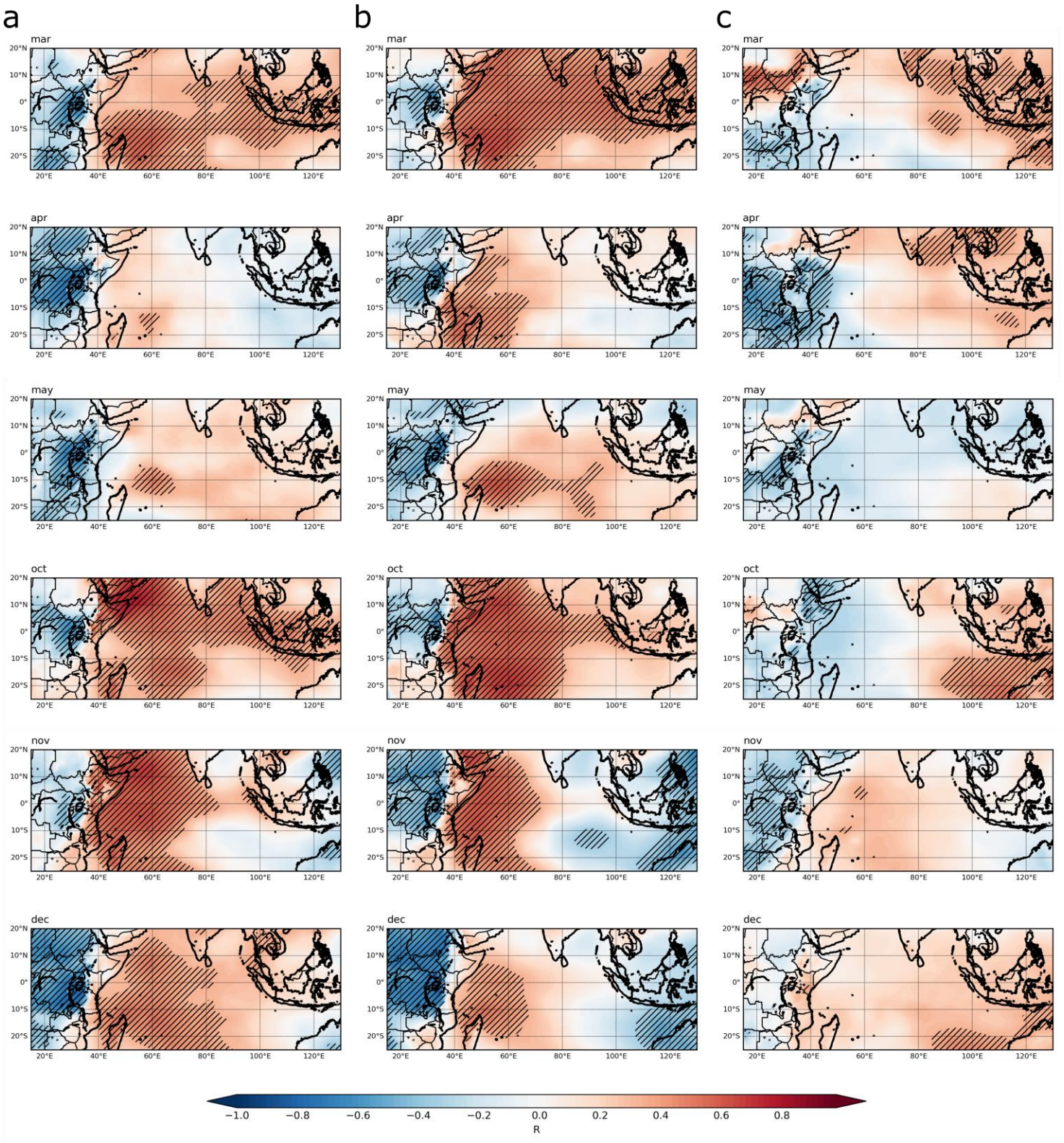


Figure 12.8 - Pearson product moment correlation coefficients between reanalysis jet core zonal wind timeseries and MSLP data from 1981-2016 for MERRA-2 (a), ERA5 (b), and JRA55 (c). Shading indicates areas where the correlation is significant at the 95% confidence level.

Vizy and Cook (2019) observe that on synoptic timescales, a strong Turkana LLJ is associated with high pressure ridging off the coast of East Africa which drives an anomalous southeasterly flow. For the purposes of our investigation into the jet's climatology, we plotted the correlation between jet core zonal wind speed and mean sea level pressure (MSLP) for each of the three reanalyses during the months of the two main East African rainy seasons (Figure 12.8). The results demonstrate that the mechanism suggested by Vizy and Cook (2019) has an analogue on climatological timescales, with jet zonal wind speed exhibiting significant correlations with MSLP along the East African Coast in all rainy season months for both MERRA-2 and ERA5. This correlation is however not evident in JRA-55 other than for November, and significant correlations of the opposite sign for the Kenya coast are obtained for April and October. Given the physical plausibility of Vizy and Cook's (2019) mechanism, this may cast doubt upon the ability of JRA-55 to represent the jet's variability.

12.4.1.3. Wind-Rainfall Covariability

This section investigates the link between the Turkana LLJ and regional rainfall. We plot the Pearson product moment correlation coefficient between the 850hPa zonal wind speed in the jet core for each reanalysis dataset and CHIRPSv2.0 rainfall for each grid point in each bimodal rainy season month over the period 1981-2016 (Figure 12.9). There are strong and significant correlations between the jet and rainfall in the surrounding area, with similar relationships obtained for each of the three reanalyses. The jet strength is negatively correlated with precipitation across

Tanzania, Kenya, and southern Ethiopia, as well as in the Turkana Channel itself, reflecting the divergent flow of the jet (Kinuthia 1992, Vizy and Cook 2019). Meanwhile, jet strength is positively correlated with rainfall in the African interior, especially across the northern part of the Congo Basin. This may be linked to the jet's suggested influence on MCS propagation via vortex shedding effects on the African Easterly Jet (Lin 2009), or on downstream convergence. In January-September, when the jet is at its weakest, higher jet strength is linked with lower rainfall in the Turkana channel and across South Sudan, central and northern Ethiopia, and eastern Sudan and Chad (not shown).

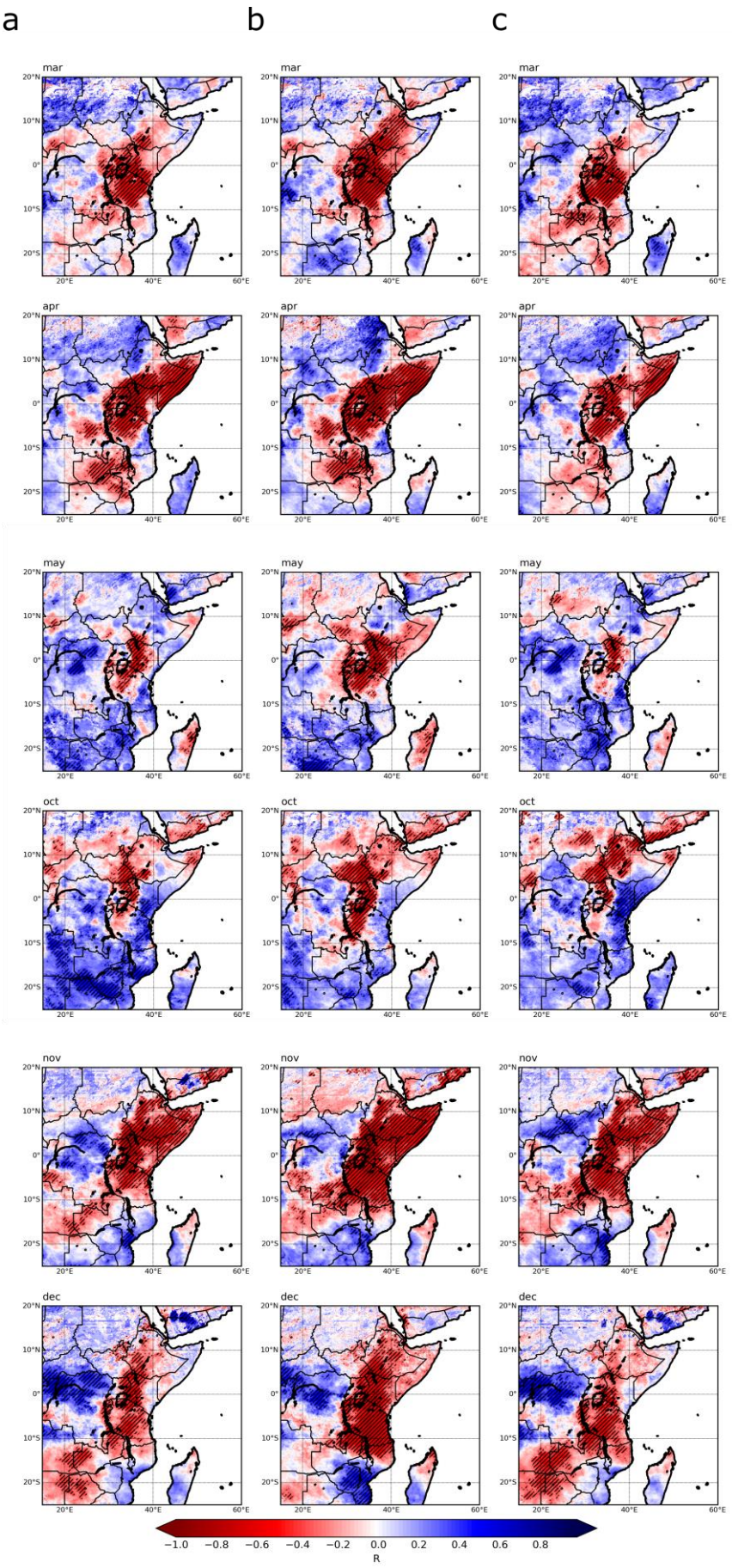

a
b
c
mar
apr
may
oct
nov
dec
20°N
10°N
0°
10°S
20°S
20°E
40°E
60°E
−1.0
−0.8
−0.6
−0.4
−0.2
0.0
0.2
0.4
0.6
0.8
R

Figure 12.9 - Pearson product moment correlation coefficients between reanalysis jet core zonal wind timeseries and CHIRPSv2.0 rainfall data from 1981-2016 for MERRA-2 (a), ERA5 (b), and JRA55 (c). Shading indicates significance at the 95% confidence level.

12.4.2. Trends

12.4.2.1. LLJ Strength

To our knowledge, no investigation has been published into the strength of the Turkana LLJ on multidecadal timescales. Here, we present such an analysis using reanalysis data (Table 12.1). Trends were computed with linear regressions of both zonal wind and wind speed based on monthly average values at the jet core for the period 1981-2016. A Mann-Kendall test with Theil-Sen slope estimation was also performed to provide an independent metric for estimating trends; the two tests were in agreement in the majority of cases for both variables, with the exceptions of April (MERRA-2 zonal wind and ERA5 windspeed trends were significant at $p<0.05$ for Mann-Kendall but not linear regression), May (MERRA-2 wind speed trend was significant for linear regression but Mann-Kendall was not), and September (MERRA-2 wind speed trend was significant for linear regression but Mann-Kendall was not). The results indicate a strong possibility that the Turkana LLJ has been weakening since 1981. For the MERRA-2 reanalysis, there are negative trends in jet core zonal wind which are statistically significant ($p<0.05$) for all months except for February and June (although there is a significant zonal wind trend in June using the Mann-Kendall test ay $p<0.1$), and wind speed trends for all months excluding February, April, and June.. For JRA55, there are significant ($p<0.05$) negative trends for January, March, May, July, and December in jet core zonal wind, and January, March, May, July, September, and December for wind speed. A significant negative

trend at $p<0.1$ is obtained for February using the Mann-Kendall test. By contrast, the only trend obtained in ERA5 was for April, where there is a significant increase in jet core zonal wind speed at the $p<0.05$ confidence level using the Mann-Kendall test. This is opposite to the trend in MERRA-2 for the same month. Although the jet is primarily a zonal wind feature, we also found significant decreases in the strength of the meridional wind component at the jet core in 7 months of the year (MERRA-2) and 8 months of the year (JRA55), with ERA5 displaying contrasting increases in meridional wind in February and April (not shown).

*Table 12.1 - Turkana jet core wind trends and significance values for MERRA-2, ERA5, and JRA55. Trends are computed by taking the monthly average zonal wind (U) and wind speed (WS) at the jet core at 850hPa defined in Figure 1. Trends are denoted by the slope of the linear regression equation. Diacritical marks denote p < 0.05 as follows: * = significant trend in linear regression. † = significant trend with Mann-Kendall test. Note that u wind is negative, so a positive slope means a decrease in u wind. Units are m s^{-1} $decade^{-1}$.*

	Jan			**Feb**			**Mar**			**Apr**			**May**			**Jun**		
	MERRA-2	ERA5	JRA-55	MERRA-2	ERA5	JRA-55	MERRA-2	ERA5	JRA-55	MERRA-2	ERA5	JRA-55	MERRA-2	ERA5	JRA-55	MERRA-2	ERA5	JRA-55
U	0.81*†	0.05	0.58*†	0.15	-0.29	0.33	0.48*†	-0.1	0.53*†	0.38†	-0.21	0.34	0.41*†	-0.01	0.42*†	0.34	0.07	0.11
WS	-0.87*†	-0.03	-0.59*†	-0.21	0.38	-0.35	-0.59*†	0.17	-0.58*†	-0.37	0.30†	-0.39	-0.31*	0.10	-0.49*†	-0.28	-0.03	-0.31
	Jul			**Aug**			**Sep**			**Oct**			**Nov**			**Dec**		
U	0.54*†	0.12	0.26	0.46*†	0.17	0.08	0.44*†	0.26	0.16	0.61*†	0.17	0.13	0.68*†	0.04	0.24	0.87*†	0.09	0.55*†
WS	-0.51*†	-0.09	-0.58*†	-0.41*†	-0.14	-0.26	-0.44*	-0.20	-0.45*†	-0.65*†	-0.15	-0.26	-0.78*†	-0.04	-0.30	-0.94*†	-0.07	0.55*†

12.4.2.2. Mechanisms

To better understand the mechanisms behind the weakening jet strength in reanalysis, as well as the differences between the datasets, we analysed changes in 900 hPa Zg. A composite difference approach was taken; for each month in reanalysis, the average conditions for 1981-1987 were subtracted from the most recent 7-year period available for each field (2010-2016).

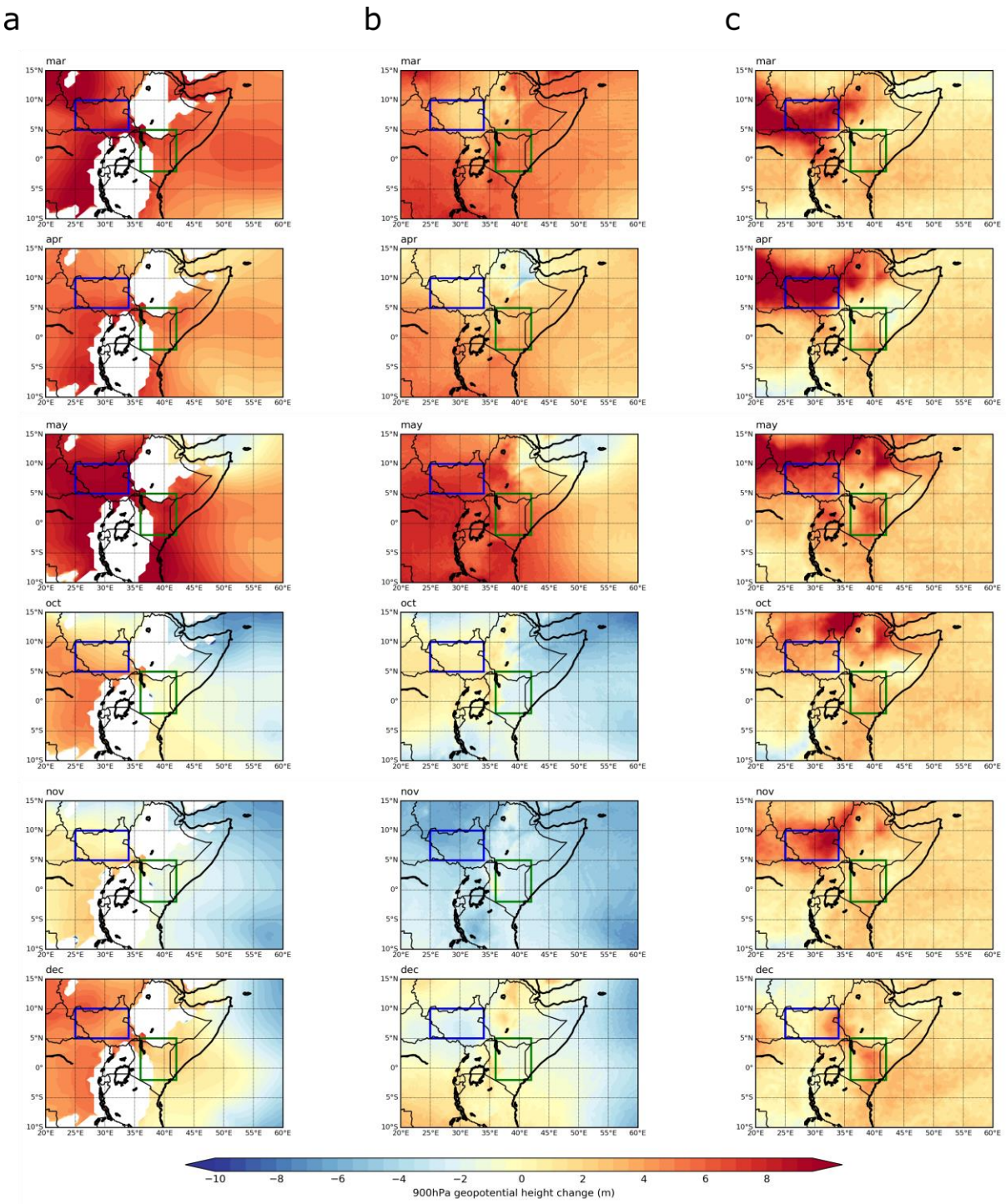


Figure 12.10 - composite differences (2010-2016 minus 1981-1987) for 900hPa geopotential height for MERRA-2 (a), ERA5 (b), and JRA55 (c). Green and blue boxes denote jet entrance and exit regions respectively.

For MERRA-2, wind trends are observed for 9 months of the year at $p<0.05$ and 11 months at $p<0.1$. In the 900 hPa Zg composite differences (Figure 10), there is a general increase in geopotential height inland in MAM and OND, with some decreases along the GHA coast and over the Indian Ocean in boreal autumn/winter. Zg increases to a greater extent in the jet exit than the jet entrance, apart from in February, when there is no significant trend in LLJ zonal wind speed (not shown). The changing gradient in geopotential height along the channel axis from the jet entrance to the jet exit, with higher Zg in the jet exit region compared to the jet entrance, is consistent with the weakening of the LLJ shown by MERRA-2 in OND. This is because an increase in the geopotential heights at the jet exit relative to the entrance is indicative of a reduction in the pressure gradient force acting along the jet axis. This effect is less noticeable in MAM for MERRA-2, potentially due to reduced influence from larger-scale tropical circulations in this season; however, increases in Zg offshore are reduced compared with inland.

In JRA55, there are significant decreases in Turkana LLJ zonal wind in 4 months of the year at $p<0.05$ and 6 months at $p<0.1$. JRA55 shows a strong increase in geopotential height at the jet exit in MAM and a reduced increase in OND. The increasing inland geopotential height is evident in several months in which JRA55 shows a decrease in jet strength (March, May, and December).

The ERA5 dataset does not have any significant changes in LLJ zonal wind at $p<0.05$, and only a single month (September) has a decreasing trend at the $p<0.1$ level.). The Zg in ERA5 shows weaker increases than MERRA-2 in MAM, and the sign of change is reversed in November and December with decreases in geopotential height inland of the Turkana Channel. In ERA5, inland decreases in Zg result in little change in the along-channel pressure gradient. By contrast, MERRA-2 and JRA55

have Zg changes that could explain the jet slowing trends as a function of a changing geopotential height gradient along the channel.

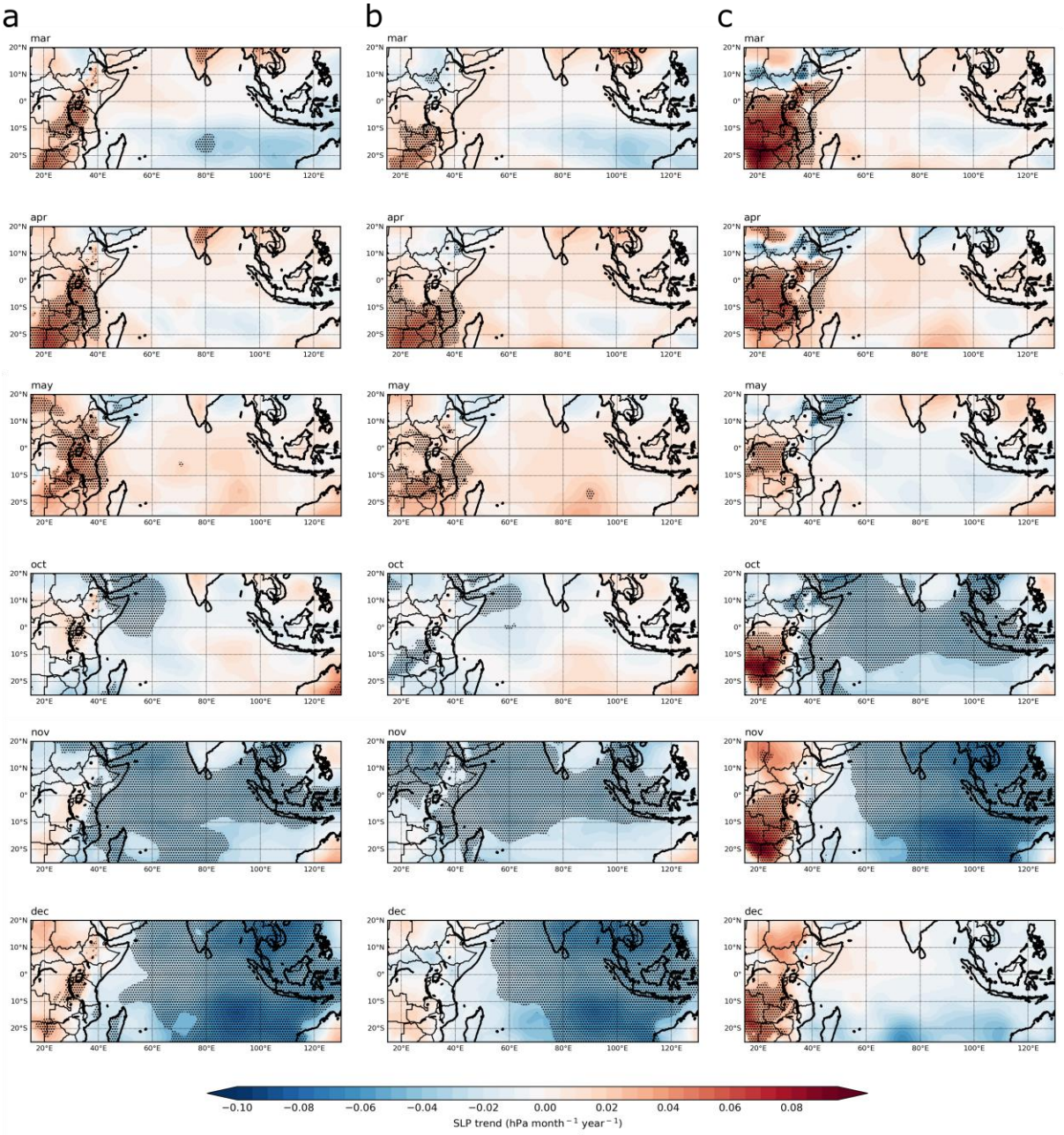


Figure 12.11– linear trend of mean sea level pressure (MSLP) for MAM and OND in MERRA-2 (a), ERA5 (b), and JRA55 (c), over the period 1981-2016. Stippling indicates regions where trends are significant at 95% confidence.

Figure 11 shows the linear trend in mean sea level pressure (MSLP) for March-April and October-December for each of the three reanalysis datasets. While there is

variation in the locations of the signals between the reanalyses, some general patterns emerge. For March, April, and May, there are statistically significant increases in MSLP over land in East Africa, on the order of 0.05 hPa month^{-1} year $^{-1}$. These are confined to the south of the Equator in ERA5, and are most intense in JRA-55, whereas the trend in MERRA-2 extends in a band extending further north into East Africa. Increasing MSLP trends inland are also seen in MERRA-2 and JRA55 in October, November, and December, though not in ERA5 which has trends of the opposite sign. Additionally, large-scale statistically significant decreases in MSLP of up to -0.1 hPa month^{-1} year $^{-1}$ are seen in the Indian Ocean during OND in MERRA-2 and ERA5, and in ON in JRA55. While we note the limitations of using pressure reduced to sea level for areas of high relief such as much of East Africa, we nevertheless consider the broad-scale nature of these changes, taken together with geopotential height, to be suggestive of potential mechanisms for the slowing trend in the reanalysis jet.

12.4.3. CMIP5 Models

The previous sections demonstrated that Turkana LLJ is a significant feature for the regional climate, and is associated with rainfall variability in the Turkana Channel and downstream in the Congo Basin. Here we assess the abilities of CMIP5 models to represent the LLJ. The models used are listed in Table 11.1. We note that, because of the close relationship between the jet and regional topography, modelling studies focussing on the jet specifically should use regional-scale climate models (RCMs) (e.g. Indeje et al. 2001). However, CMIP5 models are used in many estimates of future regional climate change, including in East Africa. Assessing how well they

reproduce a key control on regional rainfall is therefore important. In particular, higher-resolution CMIP5 models may have improved jet representation.

12.4.3.1. Topography

As discussed in section 12.4.1, good representation of regional topography is important for accurate modelling of the jet (Vizy and Cook 2019). This poses problems for GCMs in regions of complex topography, especially in Africa where inaccurate representation of topographic features can lead to large-scale model errors and biases (Munday and Washington 2018). In this section, we therefore investigate the representation of the jet in two high-resolution models (CMCC-CM and CCSM4) and two low-resolution models (BNU-ESM and FGOALS-g2). Figure 12.12 shows the substantial differences in topography between these models. CMCC-CM and CCSM4 have a channel of width ~250km at the core which is comparable to the observed topography in Figure 12.1. BNU-ESM has a much more simplified channel as a result of its lower resolution, with reduced channel depth relative to the sides. Representation of the channel is not, however, purely a function of resolution; FGOALS-g2 has the same spatial resolution as BNU-ESM but features flatter topography across the domain. The channel floor in this model is approximately 600m higher than in GTOPO30. Given the close relationship between the jet and regional topography (Indeje et al., 2001), models which do not accurately represent the topography are likely to struggle in capturing the salient features of the jet. Figure 12.12 suggests that a horizontal spacing of 1.25° or finer is required to represent the channel, and therefore the LLJ. We investigate this below.

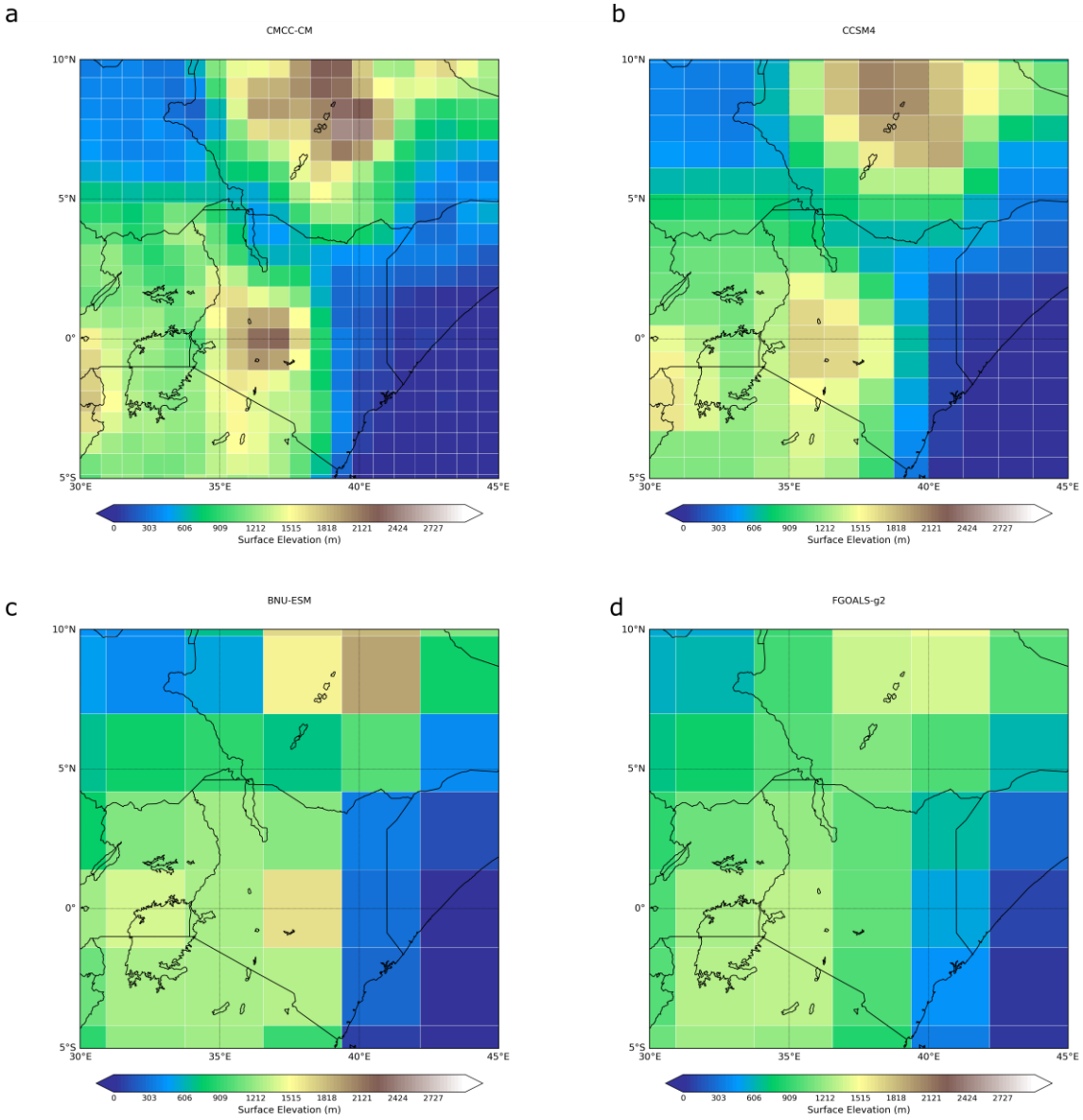


Figure 12.12 - model topography over the East African domain for CMCC-CM (A), CCSM4 (B), BNU-ESM (C), and FGOALS-g2 (D).

12.4.3.2. Annual Cycle

We plot the annual cycle of CMIP5 850 hPa zonal wind (Figure 12.13). The spread of individual model zonal winds is greater than the annual variation in the jet itself. The model annual cycle is more pronounced than the reanalyses – five models (CCSM4, EC-EARTH, BNU-ESM, MRI-CGCM3, and FIO-ESM) have stronger zonal winds

than any reanalysis in March and seven in April (the above plus NorESM1-M and ACCESS1-3), but 21 models have weaker zonal winds than MERRA-2 and ERA5 in July. Only one model, MIROC-ESM-CHEM, exceeds MERRA-2 jet speeds in November. The amplified Turkana LLJ annual cycle may result from the effects of simplified topography on the regional circulation – models with simplified representation of the East African highlands are likely to feature Somali Jets extending further inland than in observations, as these highlands are important for constraining the Somali Jet (Slingo et al. 2005). This jet peaks in boreal summer, when its flow at the latitude of the Turkana Channel is primarily meridional. Therefore, if the Somali Jet is not as well constrained by the East African Highlands in the models, it may extend inland as far as the Turkana Jet core region and produce an exaggerated reduction of the zonal wind component during boreal summer. Topography also has an important impact on constraining the Walker Circulation in which the zonal winds across the IO are embedded (Naiman et al. 2017) – given that these winds have been found to be erroneous in some CMIP5 models (Hirons and Turner 2018), models with simplified topography may also have biases in the prevailing winds into the Turkana Channel. Some outlying models in Figure 12.13 exhibit unrealistic annual cycles. For example, MRI-CGCM3 has stronger winds in boreal summer than in boreal spring or autumn/winter. In INMCM4, the sign of the zonal wind reverses in boreal summer, indicating that the wind at the jet core becomes westerly – this is not seen in reanalysis where the zonal wind is always easterly.

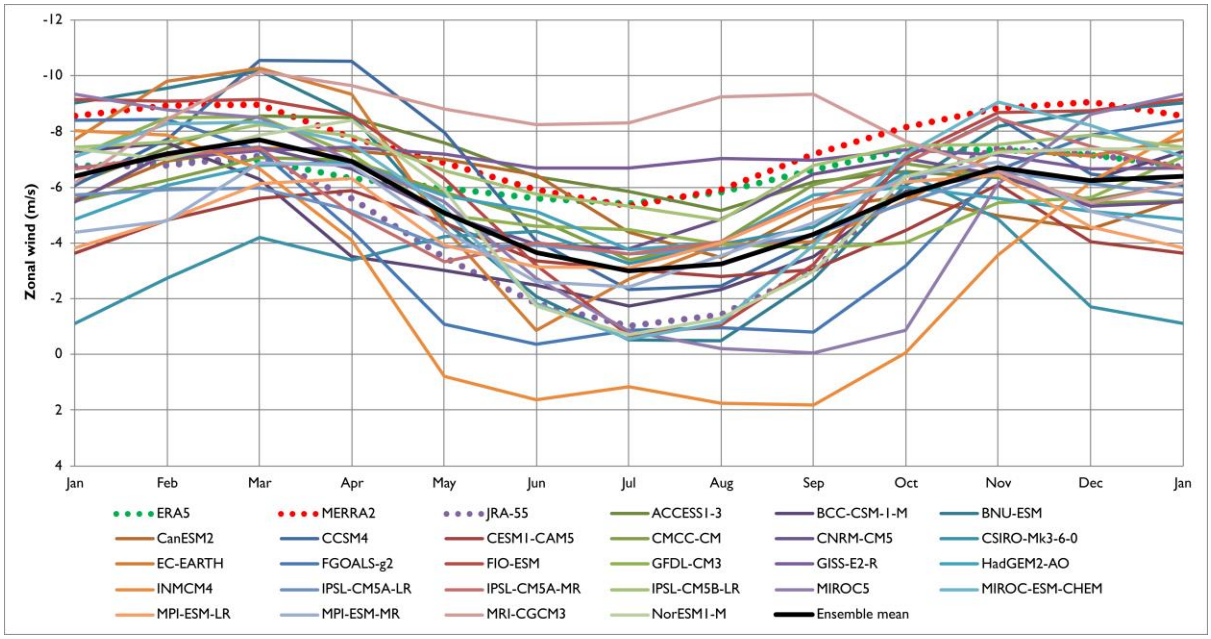


Figure 12.13- annual cycle of zonal wind at jet core for CMIP5 models listed in Table 11.1.

The reanalyses are characterised by similar peak zonal wind speeds in MAM and OND, with slightly stronger winds in OND. By contrast, 13/25 models have stronger winds in MAM.

12.4.3.3. Sensitivity to Topography

To investigate the effects of topography on CMIP5 model simulations of the LLJ, we compare the behaviour of the models in Figure 12.12.

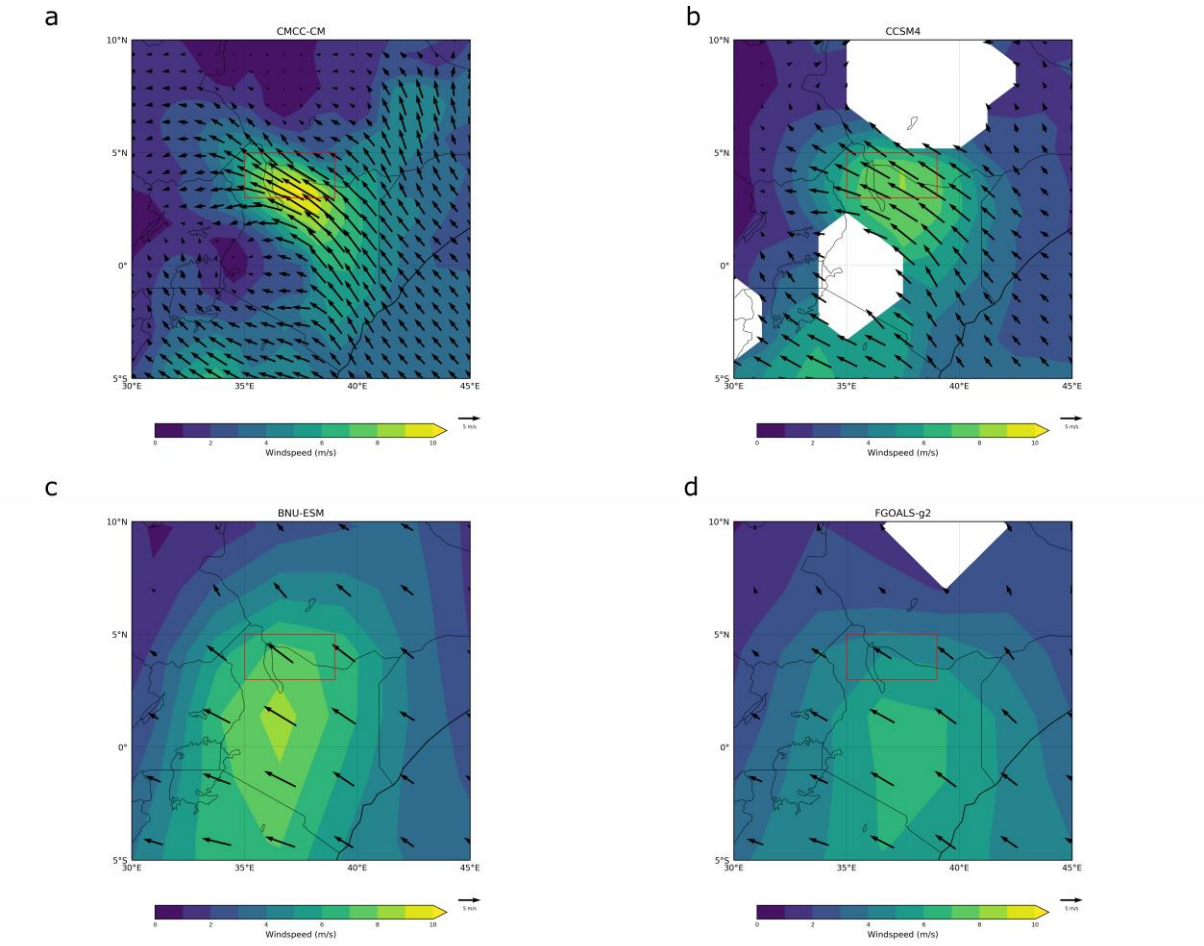


Figure 12.14 - 850hPa wind speed, averaged over 1975-2005, for historical coupled runs of CMCC-CM (A), CCSM4 (B), BNU-ESM (C), and FGOALS-g2 (D). The red box indicates the area used for calculating the jet core wind speed.

Figure 12.14 indicates substantial differences between the high and low-resolution models. In CMCC-CM and CCSM4, the jet is well-resolved within the Turkana Channel, with a clear acceleration and narrowing of the mean flow. The highest resolution model, CMCC-CM, also has the fastest mean jet speed (~11 m s^{-1}). By contrast, the jet is not evident in the low-resolution models. While BNU-ESM and FGOALS-G2 do feature stronger southeasterly winds in the vicinity of the jet entrance, the wind vectors show little evidence that a low-level jet is being formed as a result of the channeling of the mean flow by the topography. Instead, a larger-scale area of increased zonal wind is found over Kenya in the long-term average. This may reflect inland incursion of the offshore Somali Jet as a result of the simplified

representation of topography in these models, as has been suggested by sensitivity experiments (e.g. Slingo et al. 2005). The wind speeds are also lower in these models compared to CMCC-CM and CCSM4. This implies a role for resolution in determining the ability of CMIP5 models to simulate the Turkana LLJ.

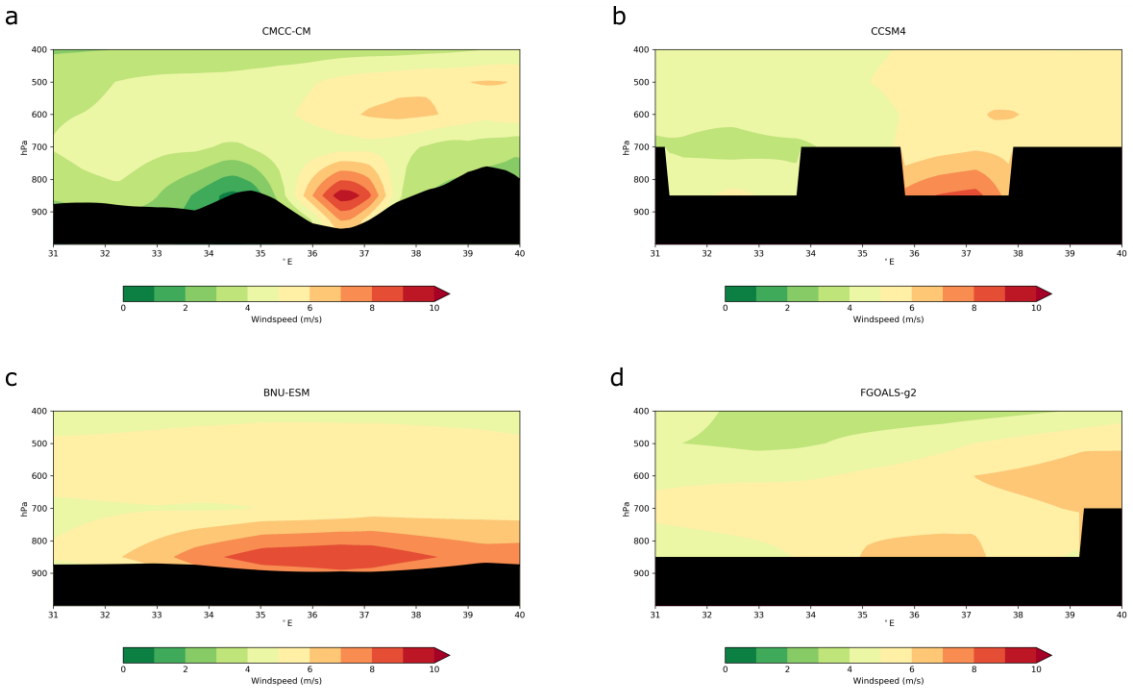


Figure 12.15 - as Figure 12.14 but for a cross-section through the Turkana Channel as per Figure 12.1.

Figure 12.15 demonstrates the role of topography representation in CMIP5 models' simulations of the Turkana LLJ. A cross-section through the wind speed field at the location of the reanalysis jet shows clear differences between models in terms of topography. The Turkana Channel is represented well in CMCC-CM and to a reasonable degree in CCSM4, where the simplified topography nevertheless features a channel of comparable magnitude to that in reality. The vertical profile of the jet in CMCC-CM compares well to that in reanalyses in terms of height and location. The jet core is less clearly defined in CCSM4. In BNU-ESM and FGOALS-g2, the

topography of the Turkana Channel is absent, and as a result the low-level jet is not simulated adequately. This both demonstrates the role of topography in forcing the jet, and the importance of considering topography as a factor in process-based climate model evaluation over East Africa.

12.4.3.4. Wind-Rainfall Covariability

We next show the association between CMIP5 model 850 hPa zonal wind at the jet core, and model rainfall across the East African domain (Figure 12.16).The results show substantial variations in models' correlations between the zonal winds in the channel and regional rainfall, which vary depending on the resolution. The higher-resolution models exhibit negative correlations between jet strength and rainfall in the area surrounding the jet, in agreement with reanalysis and theory, but also have much broader positive correlations extending across the south of the domain. By contrast, the lack of a clear within-channel negative correlation in the lower-resolution models emphasizes their lack of a clearly defined jet. South of the Turkana Channel is a sharp dividing line between 0°-10°S, which separates regions of negative and positive correlations. Compared to reanalysis, the models tend to extend the region of negative correlation much further west. The large spatial extent of the correlation fields in the lower-resolution models, and the sharp meridional dividing line between positive and negative correlations, suggests that a larger-scale feature than the Turkana Jet (potentially the Somali Jet) is controlling the wind at the location of the Turkana Channel. It is evident that lower-resolution CMIP5 models do not have adequate representation of the Turkana LLJ, which is important in light of the need to identify reasons for poor CMIP5 performance over East Africa

(Rowell et al. 2015). By contrast, higher-resolution models within in the ensemble are able to simulate the jet's structure and aspects of its correlations with rainfall.

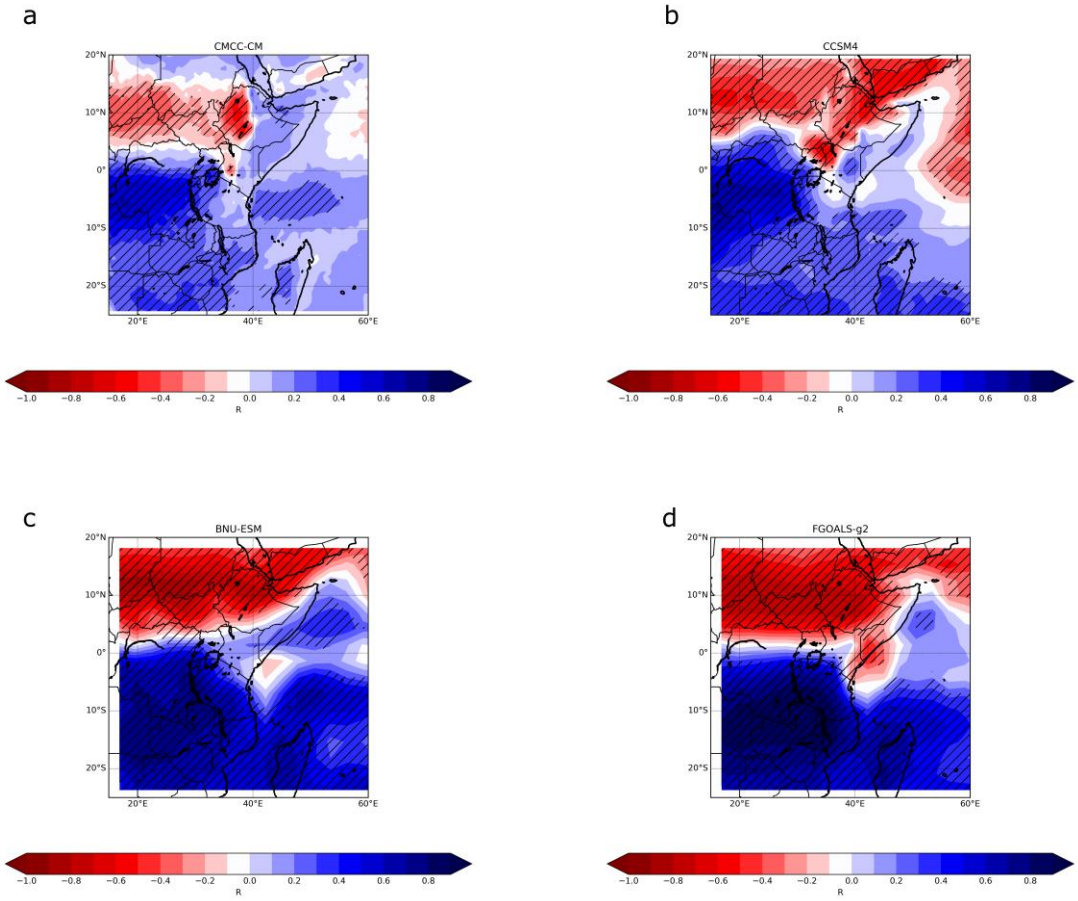


Figure 12.16 - As Figure 12.9 but for CMCC-CM (A), CCSM4 (B), BNU-ESM (C), and FGOALS-g2 (D) over 1975-2005.

12.5. Discussion

12.5.1. Climatology of the Turkana LLJ

We examined the climatology of the Turkana LLJ across three reanalysis datasets with varying resolution and underlying topography. Consistent with earlier studies (e.g. Nicholson 2016) we find that the jet is a persistent feature throughout the year.

The annual cycle of jet core zonal wind was similar in all the datasets, with jet maxima in boreal spring and autumn/winter and minima in summer. MERRA-2 consistently had faster jet speeds than ERA5 or JRA55; we concur with Vizy and Cook (2019) that the narrower topography of the channel plays a role due to Bernoulli forcing, but there is also a likely contribution from differences in surface heating and land/atmosphere coupling. The jet has significant correlations with rainfall in the region throughout the year, which are reasonably consistent between the reanalyses. A stronger jet - and attendant low-level divergence - is associated with lower rainfall in the Turkana Channel and in the jet entrance region. Positive correlations with rainfall further inland are likely to reflect some combination of the jet's impact on triggering convection (Vizy and Cook 2019), moisture transport from the Indian Ocean (Viste and Sorteberg 2013), and contribution of vorticity to the AEJ which favours the development of MCSs (Lin 2009).

12.5.2. CMIP5 Performance and Implications for Projections

Given the impacts of the Turkana LLJ on the regional climate, we briefly assessed the ability of CMIP5 models to represent it. We found that the ensemble mean performed well compared to reanalysis at representing the annual cycle of jet core zonal wind, but that this was obscuring a wide range of models, some of which had incorrect annual cycles or 100% biases in wind direction. We were able to attribute some of this variation to resolution and topography, with higher-resolution models having a much better representation of the Turkana Channel than those with lower resolutions. Model topography impacts on both the representation of the Turkana LLJ, and the extent to which the Somali LLJ moves inland (Slingo et al. 2005). We

therefore suggest that measurements of 850hPa zonal wind at the real-world location of the Turkana LLJ in some models may in fact be reflective of the simulated Somali LLJ. This latter suggestion is consistent with the interannual correlation field between jet strength and rainfall, which is continental in scale in some models. We contend that improving model topography over Africa should be a major priority in light of this and other studies (e.g. Naiman et al. 2017, Munday and Washington 2018). However, other model features, such as parameterisations of land-atmosphere interactions, should also be taken into account when identifying model improvement foci.

The deficiencies in the simulation of the Turkana LLJ, as well as the relationship between jet strength and rainfall, erode our confidence in model-derived projections of mean change and changes to rainfall variability in East Africa - and especially Kenya. This is a particular problem when using the ensemble mean model to estimate future change, which includes contributions from models with fundamental errors in the present-day representation of the jet, and its relationship with regional climate. More positively, improving the simulation of the jet - for example by increased model resolution or representation of topography, could help to reduce the uncertainty in future projections of rainfall in East Africa.

12.5.3. Long-Term Trends in the Turkana LLJ

We undertook the first analysis of the jet's behaviour on decadal timescales. A statistically significant decrease in jet core zonal wind speed was found in MERRA-2 for most of the year and for JRA55 in around half the year. The reality of the jet slowdown is tentative because the most recently developed reanalysis used, ERA5,

shows no trend for most of the year and increases in April. However, it is noteworthy that MERRA-2 performed best in an assessment of reanalysis data over tropical Africa based on quality-controlled radiosonde observations of winds in the lower troposphere (Hua et al. 2019).

We investigated dynamical fields in the reanalysis datasets to better understand what might be causing the putative decrease in the jet strength. We note that reductions in surface wind speeds have been suggested to occur worldwide (e.g. McVicar et al. 2012) as a result of the poleward expansion of the Hadley Circulation under anthropogenic climate change (Lu et al. 2007.) and the consequent decrease in surface pressure gradients between the tropics and the midlatitudes. Taking a composite approach, we found that in MERRA-2 the region around the jet exit (in the continental interior of Africa) had a change in geopotential height gradient from the entrance to the exit whereby the height increases at the exit and decreases at the entrance. This is consistent with Gebrechorkos et al. (2019) who showed that the interior of East Africa has experienced greater warming than the coastal jet entrance region over the period 1979-2012. This is a hypothesis for the jet slowdown which is thermodynamically consistent with expected spatial patterns of global warming, whereby inland areas experience faster warming than coastal areas. Variations on this pattern of regional geopotential height change are present in ERA5 and JRA55 but do not always translate into a slowing of the jet; while this slowdown is present in JRA55, it is not in ERA5 except for the month of September. It is suggested that this may reflect a weaker land-atmosphere coupling strength in the region for ERA5 and JRA55 compared to MERRA-2. We note that MERRA-2 replaces modelled precipitation with observed values before it reaches the surface in order to simulate land surface variables (Draper et al. 2018) - which ERA5 does not (Albergel et al.

2018) – which results in slight overestimations of latent heat flux (Draper et al. 2018). Differences in physical parameterisations, for example of convective mass flux over the WEIO, could also contribute to the differences.

Long-term windspeed plots (Figure 4) indicate marked differences between the reanalyses in terms of the jet's connection to prevailing winds in the region. The jet tends to enter the Turkana Channel from the north-east in ERA5, but from the south-east in MERRA-2 and JRA55. Given that the latter datasets indicate a decreasing jet strength, and the former does not, an explanation for these differences is needed. The reliance on reanalysis datasets for the study of mid-troposphere winds in this region means we cannot determine the correct direction for entry from this analysis alone. Figure 4 suggests the differences between the datasets may be related to the ways in which they simulate the connection between the Somali and Turkana Jets. The southeasterly orientation of the jet entry in MERRA-2 and JRA55 implies a closer connection to the southwesterly phase of the Somali Jet, which has shown slowing trends at 850 hPa (Rai and Dimri 2017). This may account for the slowing trends in these datasets which are not found in ERA5. However, the Turkana LLJ is present in both MERRA-2 and JRA55 when the Somali Jet is not active, or is blowing in the opposite direction as part of its seasonal reversal. Resolving the relationship between the two LLJs is an important future research direction. This is particularly important in light of evidence of decadal variability in the Mascarene High off the east coast of Madagascar, particularly since the mid-1990s (Mohapatra et al. 2020). This quasi-permanent high-pressure zone is affected by an SST dipole in the southeastern Indian Ocean (Behera and Yamagata 2001, Thompson et al. 2016). Strengthening of the Mascarene High during boreal summer is associated with the development and intensification of the Somali Jet (Feng et al. 2003), implying a role

for its variability on the Turkana LLJ if the latter is strongly controlled by the Somali Jet. Studies disagree on the response of subtropical highs to climate change (Cherchi et al. 2018); a weakening of the Somali Jet, as reported by Rai and Dimri (2017), could suggest that a weakening of the Mascarene High is underway. It is difficult to distinguish between low-frequency internal variability and externally forced trends in the climate system; however, the recently uncovered role of external forcing in controlling temperature changes on timescales >30 years has cast some doubt on the influence of internal variability modes under climate change (Haustein et al. 2019).

Following Vizy and Cook (2019), we find a significant positive correlation on climatological timescales between the jet core zonal wind speed and MSLP off the coast of Kenya, as well as significant negative correlations inland. This implies a role for pressure gradients in the jet's climatology. Linear regression analysis shows that MERRA-2 and JRA-55 exhibit increasing pressure inland of the Turkana Jet and decreasing pressure offshore. The dipole in pressure trends could relate to changes to regional overturning circulations (Hartman 2018), or to broader scale intensification to the East African Walker circulation (Mutai et al., 2012, L'Heureux et al. 2013, McGregor et al. 2014, King et al., 2020). This, again, suggests a physically plausible mechanism for the jet slowdown in these datasets that warrants further investigation. Future work should also examine why this pressure trend is not present in ERA5; the opposing sign of the MSLP gradient over continental East African in this reanalysis may go some way towards explaining the lack of a jet slowdown, but the more fundamental differences in SLP trends between the reanalysis datasets require explanation. A decreasing wind speed trend in the Turkana Channel at 850 hPa was indicated by Torralba et al. (2017) as part of a global study demonstrating agreement between reanalysis trends over the period

1980-2015. They argued that the agreement between 10m and 850hPa trends indicates that interannual variability in reanalysis wind is controlled by changes in the large-scale circulation, a view supported by our findings.

Basic meteorology suggests that the stronger surface heating in the Turkana Channel and further inland should result in decreasing surface pressure, via the formation of upslope winds within the channel, as well as an enhanced diurnal cycle, but reanalysis suggests that the surface pressure has increased over the last 40 years in several months. How should we reconcile these differing trends? We suggest that a combination of more intense small-scale overturning circulations in the channel (as discussed by Hartman (2018)) and the wider-scale Indian Ocean Walker Circulation which results in climatological descent over equatorial East Africa (Mutai et al. 2012, King et al. 2020) may be responsible for the increasing pressure within the channel and inland by acting to cap rising air driven by strong surface heating. Although our understanding of the nature of the Walker Circulation is still incomplete, it has been suggested to have been intensifying in recent decades (McGregor et al. 2014, Chung et al. 2019) and to be increasingly important as an influence in future East African climate (Giannini et al. 2018, King et al. 2020). Building on the links between the Turkana Jet and regional heating and pressure patterns found by Hartman (2018) and Vizy and Cook (2019), we therefore postulate a link between the strength of the Turkana Jet on climatological timescales and regional atmospheric dynamics including the overturning Walker Circulation in the Indian Ocean, expressed through the relationship between the large-scale zonal pressure gradient between the jet exit region and the equatorial Indian Ocean, and the strength of the jet itself. Future work will investigate this relationship in GCM projections.

The strengthening of the Pacific Walker Circulation has been linked to variability associated with the Pacific Decadal Oscillation (PDO; McGregor et al. 2014) and the Atlantic Multidecadal Oscillation (AMO; Chung et al. 2019). Pacific SST variability affects East Africa via perturbations to the Walker Circulation (e.g. Lyon and DeWitt 2012, Hoell et al. 2014, Vigaud et al. 2017). The Atlantic Walker Circulation also affects East Africa (Zhao and Cook 2021) and on decadal timescales is affected by the AMO. The AMO and PDO may therefore exert a high-order control on the Turkana LLJ through their impact on zonal pressure gradients. Investigating this hypothesis is beyond the scope of this paper, though we would encourage further research in this direction, potentially using model experiments with idealised SST. However, the AMO has recently been suggested to be externally forced (Mann et al. 2021) and the role of internal climate variability in 20th century trends is limited (Haustein et al. 2019). Therefore, its invocation as an explanation for climatic trends should be treated with caution.

The issue of trends in East African climate is important because of the uncertainty surrounding projected rainfall changes highlighted by Rowell et al. (2015). We argue that the identification of plausible trends in the Turkana LLJ strength contributes to our understanding of this uncertainty, because we demonstrate that many CMIP5 models are not able to accurately simulate the Turkana LLJ. A better understanding of the mechanisms controlling the long-term variability of the Turkana LLJ will therefore contribute towards resolving the 'East African Climate Paradox' (Rowell et al. 2015).

Further work is also needed to account for the mechanisms of the annual cycle of the Turkana LLJ. This should enable understand deeper understanding of the reliability of the slowing trend. Analysis of the hotspot in low-level inertial instability

associated with the Turkana Jet may prove useful (Cook 2015), given its development in the tropics stems from an imbalance between the Coriolis parameter (which increases along the jet axis) and the pressure gradients generated by strong temperature differences between coastal regions and continental interiors (e.g. Hagos and Cook 2007). The classic gap wind study of Overland and Walter (1981) found that winds in the Juan de Fuca Straight on the Canada/US border were approximately in in equilibrium between inertial acceleration and the along-axis pressure gradient, but this is of course a midlatitude case. Recent advances in high-resolution regional climate modelling of the African climate (Stratton et al. 2018) provide an opportunity to investigate jet drivers in additional detail.

Our understanding of the Turkana LLJ ultimately rests on observations taken using pilot balloons in the 1980s. The differences between the reanalyses reflect not only the limited observational network in the region, but also the limitations in our understanding of jet dynamics. A targeted field campaign to measure the Turkana LLJ directly using more up-to-date equipment (such as LIDAR) would be of great benefit and could help resolve outstanding questions about what drives the jet. This approach has been of value in investigating low-level winds in arid zones elsewhere in Africa (Allen and Washington 2013).

12.6. Conclusion

It is increasingly clear that the Turkana LLJ plays an important role in East African climate, but it remains under-investigated. We analyse its annual cycle and variability in three reanalysis datasets, demonstrating that the jet is present throughout the year with peak speeds between November and March in all three

datasets. The jet strength is found to have statistically significant relationships with observed rainfall, with negative correlations in the Turkana Channel and positive correlations in the East African interior. This indicates its role in the aridity of the Turkana region as well as moisture transport and convection triggering in the East African continental interior. An analysis of the interannual variability of the jet strength suggests that it may be slowing down, with consequent implications for East African hydroclimate; potentially increased rainfall in northern Kenya, but drier conditions in South Sudan and southwestern Ethiopia. There are also implications for wind power projects in the Turkana region. However, this trend is not found in the ERA5 reanalysis. We suggest that a slowing jet is a physically plausible consequence of observed patterns of climate change in East Africa, including coast-to-continent temperature gradients and/or the intensification of the Walker Circulation, but further research is needed to determine the robustness of this trend and to explain the differing behaviour of reanalysis datasets.

Given the jet's relationship with rainfall and the potential slowing trend, it is important to be able to say with confidence how it will change in future. We assessed the ability of CMIP5 models to represent the jet. We found that, while some higher-resolution models were able to simulate the jet, lower-resolution models did not resolve topography at a sufficiently high level of detail. Consequently, there is a large degree of variation within the CMIP5 ensemble in terms of jet representation and links between the jet and rainfall. We argue that models that do not simulate the jet will not be able to make reliable projections of future East African hydroclimate. Future projections should make use of high-resolution regional climate models where possible, and any assessment of the performance of CMIP6 models in East Africa should include the Turkana LLJ. Finally, there is a need for field

measurements of the jet with modern remote sensing equipment such as LIDAR. A targeted field campaign could resolve outstanding questions about the jet's diurnal and annual cycles, as well as the physical mechanisms controlling its variability. This would enable better constraints on the reanalysis datasets, and a better understanding of the impacts of climate change on East Africa.

Given the jet's relationship with rainfall and the potential slowing trend, it is important to be able to say with confidence how it will change in future. We assessed the ability of CMIP5 models to represent the jet. We found that, while some higher-resolution models were able to simulate the jet, many did not resolve topography at a sufficiently high level of detail. Consequently, there is a large degree of variation within the CMIP5 ensemble in terms of jet representation and links between the jet and rainfall. We argue that models that do not simulate the jet will not be able to make reliable projections of future East African hydroclimate. Future projections should make use of high-resolution regional climate models where possible, and any assessment of the performance of CMIP6 models in East Africa should include the Turkana LLJ. Finally, there is a need for field measurements of the jet with modern remote sensing equipment such as LIDAR. A targeted field campaign could resolve outstanding questions about the jet's diurnal and annual cycles, as well as the physical mechanisms controlling its variability. This would enable better constraints on the reanalysis datasets, and a better understanding of the impacts of climate change on East Africa.

12.7. Acknowledgements

James A. King is funded by the UK Natural Environment Research Council (NERC) through the Doctoral Training Partnership in Environmental Research (grant NE/L002621/1). This work forms part of his doctoral thesis. The CMIP5 data used in this study were downloaded from the UK Centre for Environmental Data Analysis (CEDA), (https://catalogue.ceda.ac.uk/uuid/d2d8f982d66cce55bb59fc769ca39264?jump=related-docs-anchor). CHIRPS rainfall data were downloaded from the Climate Hazards Group at the University of California, Santa Barbara. (ftp://ftp.chg.ucsb.edu/pub/org/chg/products/CHIRPS-2.0/global_monthly/netcdf/). MERRA-2 data were downloaded from the NASA Goddard Earth Sciences Data and Information Services Centre (https://disc.gsfc.nasa.gov/datasets?keywords=%22MERRA-2%22&page=1&source=Models%2FAnalyses%20MERRA-2) . ERA5 data were downloaded from Copernicus (https://cds.climate.copernicus.eu/cdsapp#!/dataset/reanalysis-era5-pressure-levels-monthly-means?tab=form). JRA55 data were downloaded from the NCAR Research Data Archive (https://rda.ucar.edu/#!lfd?nb=y&b=proj&v=JMA%20Japanese%2055-year%20Reanalysis). MIDAS data were downloaded from the CEDA archive (https://catalogue.ceda.ac.uk/uuid/220a65615218d5c9cc9e4785a3234bd0). The authors thank Dave MacLeod (University of Bristol), Edward Vizy (University of Texas at Austin), and Oscar Lino (University of Nairobi) for useful discussions. The comments of 3 anonymous reviewers, and of the editor, Chidong Zhang (NOAA Pacific Marine Environment Laboratory), helped to improve the manuscript.

Chapter 12 provided an analysis of the Turkana LLJ, demonstrating its links to rainfall. The potential slowing of the jet has important implications for East African rainfall, but the veracity of the reanalysis trends is not certain because of their differing representations of the jet and its associated regional dynamics. The potential link between the Turkana LLJ and the IOWC is important and will be recommended as a focus for future investigations in chapter 14. This link is evidence of the multi-scalar dynamics that influence East African rainfall, and the need to understand the interactions between them. The LLJ/IOWC link proposed in chapter 12 implies that a realistic simulation of the IOWC may be a prerequisite for a model also being able to accurately simulate the Turkana LLJ. It also suggests that an intensification of the IOWC may be able to account for a slowing of the Turkana LLJ.

The Turkana LLJ is not adequately represented in CMIP5 models, as a result of their simplified topography. This adds additional uncertainty to projections of East African rainfall. It has also been shown that the representation of topography affects model representation of the IOWC (Naiman et al. 2017). This suggests that topography should be a key target for model improvement and could yield major benefits in the simulation of East African climate.

Chapter 13 extends the analysis of the previous two chapters to assess how model projections of East African rainfall are affected by the representation of the IOWC. A key task is to assess if the ensemble mean projections, which include significant rainfall increases in both rainy seasons, are realistic. This includes an assessment of how the IOWC changes in future in models with strong rainfall increases compared to those without.

13. Paper 3 - Future Changes in the Indian Ocean Walker Circulation and links to Kenyan Rainfall

13.1. Abstract

East Africa is vulnerable to hydroclimatic variability and change, and therefore reliable projections of future rainfall are important for climate change adaptation planning. However, the region's climate is affected by complex multi-scalar processes and poorly represented in climate models, leading to uncertainty surrounding rainfall change. The importance of circulation features in controlling long-term rainfall variability provides an opportunity to constrain projections. We use a process-based climate model evaluation methodology to demonstrate links between Coupled Model Intercomparison Project phase 5 (CMIP5) rainfall biases over Kenya and circulation biases in the Indian Ocean Walker Circulation (IOWC). During both the long and short rains, models with wet biases in historical coupled runs continue to be wet in future. Wet future projections are associated with enhanced westerly winds over the equatorial Indian Ocean, as well as decreasing vertical velocity over Kenya and increasing vertical velocity over the Maritime Continent. We demonstrate that models with a simulated IOWC which is close to reanalysis in historical coupled runs project different changes to Kenyan rainfall than those which do not. In particular, the projected rainfall increase during the long rains is confined to a single month (April) in these 'good' models. We call for a renewed focus on the Walker Circulation as a way to constrain uncertain rainfall projections elsewhere in the tropics.

13.2. Introduction

East Africa is highly vulnerable to the impacts of climate change and variability, owing to reliance on agriculture and hydroelectricity generation (Borgomeo et al. 2018). The agricultural sector, which employs a majority of the working population in Kenya, Somalia, and Ethiopia (Salami et al. 2010), is largely rain-fed; both subsistence farming and production of crops intended for export (such as coffee) are deemed to be at risk from the impacts of climate change (Jaramillo et al. 2011). Rising temperatures may result in an expansion of the transmission range of malaria in the region (Onyango et al. 2016), while the development potential of small-scale hydroelectricity generation is also dependent on the reliability of future rainfall (Kaunda et al. 2012). Links have been drawn between droughts, migration, and conflict in the region in both modern times (Thalheimer and Webersik, 2020) and in pre-colonial history, with reconstructions of past rainfall variability coinciding with oral histories recounting political unrest and food shortages (Verschuren et al. 2000). Reliable projections of climate change, especially hydrological change, are therefore of great importance for future adaptation planning.

East Africa has experienced a series of severe droughts in the last few decades, for example in 1983-84 and 2010-2011 (Lyon 2014), and in 2015 (Philip et al. 2018). Drought conditions have prevailed in the region since around 2008 (Nicholson 2017), with a significant decline in March-April-May (MAM) rainfall observed in multiple datasets (Maidment et al. 2015, Rowell et al. 2015). Indeed, the decline in MAM rainfall is the most significant trend in the region's observational record, exceeding one standard deviation of the mean trend taken over a 35 year period between 1901-2013 (Hoell et al. 2017). This is particularly significant because the

MAM ‘long rains’ are the more important of the two rainy seasons found across much of the region; both in terms of amount of rainfall, and importance for agriculture (Nicholson 2017). Importantly, the drying trend can be attributed to a shorter long rains season, with rainfall starting later and finishing earlier from the 1980s onwards (Wainwright et al. 2019). OND (‘short rains’) rainfall trends are more spatially heterogeneous, with a weak increase in seasonal rainfall owing to strong interannual variability arising from teleconnections to the El Niño Southern Oscillation (Hoell and Funk 2014, Nicholson 2015), the Indian Ocean Dipole and associated overturning (Mutai et al. 2012, King et al. 2020), and the Madden-Julian Oscillation (Berhane and Zaitchik 2014, Zaitchik 2017).

Global climate models participating in Coupled Model Intercomparison Project Phase 5 (CMIP5; Taylor et al. 2012) have important systematic biases in East African rainfall seasonality (Yang et al. 2014, Tierney et al. 2015). Models overestimate rainfall during OND by up to 50% and underestimate it during MAM by up to and over 100%, with the short rains becoming the primary rainy season (Tierney et al. 2015). The rainfall range across the CMIP5 ensemble over East Africa (the difference between the wettest and driest models) is greater than the magnitude of the observed monthly mean rainfall in all months except April (Tierney et al. 2015).

Since the CMIP5 historical climatology exhibits large biases, projections of future East African rainfall change made using these models are uncertain. For the bimodal rainfall region, Rowell et al. (2015) found that the CMIP5 ensemble mean under the RCP8.5 scenario showed increasing rainfall during the long rains up to 2100, in direct contrast to the observed drying trend; a problem termed the ‘East African Climate Paradox’. Despite the increasingly wet long rains, the majority of the projected rainfall increases in CMIP5 models take place during the short rains, in

opposition to recent observations of little trend in this season (Tierney et al. 2015, Endris et al. 2018).

The uncertainty in future East African rainfall has been argued to be due to the unresolved nature of the relationship between dynamic and thermodynamic drivers of precipitation change; specifically, the extent to which humidity increases (following the Clausius-Clapeyron relation) are cancelled out by changes to the atmospheric circulation as a result of warming (Chadwick et al. 2013, Fereday et al. 2020). The nature of tropical precipitation changes are argued to be determined by shifts in spatial patterns of zones of convergence and divergence as a result of these circulation changes (Pfahl et al. 2017, Cook et al. 2020), and the primary contributor to uncertainty in model projections of East African rainfall in both rainy seasons is varying simulations of regional circulation dynamics (Rowell and Chadwick 2018). In this study, we focus on the dynamical changes associated with the zonal Indian Ocean Walker Circulation (IOWC) as a means of understanding projections of East African rainfall.

The zonal IOWC, and the associated zonal SST pattern known as the Indian Ocean Dipole (IOD), are important influences on the hydroclimate of East Africa (Nicholson 2017). The IOD links East Africa to wider tropical interannual variability via non-stationary teleconnections to the El Niño Southern Oscillation (ENSO; Nicholson 2015, MacLeod et al. 2020). The climatological overturning cell features ascent over the Maritime Continent and descent over East Africa from September to March (Zhao and Cook 2021), which is a contributor to the relative aridity of Kenya despite its location on the equator (Nicholson 2017, King et al. 2020). Statistical and dynamic relationships between Indian Ocean ascent and descent and rainfall over East Africa are well established during the East African rainy seasons (Black 2005,

Behera et al. 2005, Liebmann et al. 2014; 2017, Vigaud et al. 2017, King et al. 2020). The IOWC is also important for understanding intraseasonal rainfall. The vertical velocity fields over the Indian Ocean associated with the IOWC are modulated on synoptic timescales by the Madden-Julian Oscillation (MJO) (Zaitchik 2017, Vellinga and Milton 2018), which can act to suppress rainfall during the short rains by enhancing the strength of the overturning Walker Circulation (Berhane and Zaitchik 2014). Nicholson (2015) found that the zonal cell in the Indian Ocean has exerted a stronger influence on the short rains since the early 1960s. There is a strong correlation between low-level equatorial zonal winds over the Indian Ocean and East African rainfall during the short rains (Mutai et al. 2012). During the long rains, low-level zonal winds over the Congo Basin and Gulf of Guinea are also strongly correlated with East African rainfall, implying a link to the broader tropical Walker Circulation (Walker et al. 2020). The ability of CMIP5 models to simulate the Walker Circulation is therefore key to providing reliable projections of future East African rainfall (Nicholson 2017, Giannini et al. 2018), especially given that projected short rains wetting occurs in response to a weakening of the simulated IOWC (Kociuba and Power, 2015; Tierney et al., 2015; Endris et al., 2018). Climate models show a number of limitations in this area. For example, the projected tropics-wide Walker Circulation weakening is in opposition to recent observed strengthening trends (L'Heureux et al. 2013, Kociuba and Power 2015), meaning that representation of the circulation is a major source of uncertainty in model projections across the tropics (Tierney et al. 2015, Giannini et al. 2018). CMIP5 models have SST biases which predispose them to a positive IOD state (Cai and Cowan 2013), resulting in increased OND rainfall over East Africa in historical coupled mode (Black et al. 2005, Tierney et al. 2015). Hirons and Turner (2018) found that the wet biases in CMIP5 models during the short rains were connected to erroneous zonal winds over the

equatorial Indian Ocean, whereby some models simulated easterly winds rather than the observed westerlies. This resulted in enhanced moisture advection into East Africa from the central Indian Ocean, and enhanced upwelling in the eastern Indian Ocean which further enhanced the positive IOD condition (Hirons and Turner 2018). Since these zonal winds form part of the solenoidal structure of the IOWC (Nicholson 2017), this indicates an important limitation in the models' simulation of East African rainfall. King et al. (2020) demonstrated that CMIP5 models' rainfall biases over Kenya can be dynamically linked to their representation of the Walker Circulation, with dry (wet) biases linked to descending (ascending) biases over East Africa. Creese et al. (2019) found a weakening of the zonal overturning circulation over the Congo Basin in CMIP5 projections, which is projected to become a more important influence on East African rainfall in future (Giannini et al. 2018).

On smaller spatial scales, the low-level jet (LLJ) in the Turkana Channel in northwestern Kenya is also an important influence on regional rainfall. LLJ-related divergence in the channel contributes to regional aridity (Kinuthia 1992, Nicholson 2016b, Hartman 2018), but the jet is also an important moisture flux vector from the Indian Ocean into East Africa (Viste and Sorteberg 2013) and plays a role in triggering convection at its exit region (Vizy and Cook 2019). The variability of the jet is therefore an important consideration for assessing future East African rainfall projections (MacLeod 2019), but the spatial scale of the channelling topography means representation in CMIP5 models is likely to be highly dependent on the topographic accuracy of individual models. The jet's interannual variability is significantly correlated with zonal gradients in surface pressure from the Indian Ocean to continental Africa in reanalysis datasets, suggesting a link to the larger-scale dynamics of the IOWC (King et al. 2021). Future changes to the IOWC may

therefore have a second-order impact on East African rainfall through their effects on the Turkana LLJ.

Given the complex multi-scale nature of the factors affecting East African rainfall, and the uncertainty surrounding future projections, a process-based model assessment methodology is one way to assess which projections are the most plausible (Rowell et al. 2016, James et al. 2018), as well as to guide future work using regional climate modelling (RCM) studies with GCM boundary conditions (McSweeney et al. 2015). This is particularly necessary when the signal in the CMIP5 ensemble mean may not be physically plausible, as Rowell et al. (2015) suggest; this is also the case elsewhere in tropical Africa (Washington et al. 2013, Creese and Washington 2016). Progress has been made by determining the key variables and processes which may determine the plausibility of simulated East African rainfall (McSweeney et al. 2015, Creese and Washington 2016, Dyer et al. 2020, Dyer and Washington 2020). Building on recent work demonstrating a link between the IOWC and CMIP5 historical rainfall biases (King et al. 2020), we investigate the relationship between CMIP5 model projections of future East African rainfall and model dynamics linked to the IOWC. Focusing on the well-instrumented country od Kenya, we address the following research questions:

1. What are the projected changes in rainfall over Kenya in CMIP5 models up to 2100?
2. What are the projected changes in omega and zonal wind associated with the IOWC?
3. Do future projections reflect historical model biases?

The rest of the paper is organised as follows. Section 13.3 describes the datasets used in the study. Section 13.4.1 shows projected changes in East African rainfall and in dynamic fields associated with the IOWC. Section 13.4.2 uncovers the links between rainfall and IOWC projections, as well as between historical biases and future changes in the CMIP5 ensemble. Section 13.5 puts forward projections with a composite approach based on the plausibility of models' representations of East African climate. Section 13.6 discusses the findings and their implications, and section 13.7 concludes the paper.

13.3. Data

13.3.1. Observations and Reanalysis

Rainfall data were obtained from version 2 of the Climate Hazards Group Infrared Precipitation with Stations dataset (CHIRPSv2.0; Funk et al., 2015). This dataset combines gauge observations with satellite rainfall estimates derived from infrared observations of cold cloud duration, and has been extensively validated over East Africa (Kimani et al. 2017. Gebrechorkos et al. 2018). Reanalysis data from version 2 of the Modern Era Retrospective Analysis for Research and Applications (MERRA-2; Gelaro et al. 2017) were used. While we acknowledge that reanalysis products differ in their representation of climate dynamics over tropical Africa, as a result of sparse observations (Maidment et al. 2015, James et al. 2018), MERRA-2 has performed well when validated against radiosonde observations of tropospheric winds in this region (Hua et al. 2019). While we do not consider the differences in large-scale dynamics between different reanalyses to be large enough to affect our results, given

the much larger differences between CMIP5 models, we use MERRA-2 because of its strong performance in the assessment of Hua et al. (2019).

13.3.2. CMIP5 Models

An ensemble of 25 CMIP5 models was selected (Table 11.1) based on the availability of vertical velocity, zonal wind, and precipitation fields for 1975-2005 (historical coupled) and 2020-2100 (RCP8.5). We use the RCP8.5 scenario because it is the closest to observed changes in radiative forcing due to anthropogenic activity (Sanford et al. 2014), and to elicit a clear change signal in models that would reveal the dynamics involved in future rainfall projections. The first ensemble member for each model was used (R1I1P1), since for a number of model this was the only one available for key fields. Since the amount of uncertainty in climate projections due to initial model conditions is relatively small for decadal projections, we do not believe our results would change significantly if different ensemble members were used. Where composites were generated, model data were interpolated onto a common 1˚x 1˚grid using nearest-neighbour regridding.

13.4. Results

13.4.1. Projections

13.4.1.1. Projected Changes in East African Rainfall

We begin by analysing the projected changes in Kenyan rainfall up to the end of the 21st century in the RCP8.5 scenario. Following Nicholson's (2017) work which shows that the different dynamics seen in each rainy season month limit the explanatory power of analyses which aggregate the months into seasonal totals (see also Dyer and Washington 2020), we plot results for each month separately.

Table 13.1 - Slopes of the linear regression of Kenyan rainfall for each rainy season month, 2020 to 2100, under the RCP8.5 scenario. Light green (red) shading indicates significance of positive (negative) trends at p<0.1 and darker green (red) shading at p<0.05. Units are mm day^{-1} decade $^{-1}$.

Model	Mar	Apr	May	Oct	Nov	Dec
ACCESS1-3	0.193	0.258	0.091	0.110	0.348	0.312
BCC-CSM1-1-M	0.097	0.190	-0.011	0.087	0.152	0.136
BNU-ESM	0.074	0.072	0.108	0.323	0.320	0.346
CanESM2	0.282	0.196	0.124	0.234	0.172	0.109
CCSM4	0.107	0.021	0.013	0.092	0.075	0.189
CESM1-CAM5	0.108	0.064	0.064	0.024	-0.022	0.164
CMCC-CM	0.041	0.051	-0.121	-0.021	0.060	0.051
CNRM-CM5	-0.012	0.055	0.057	0.031	0.134	0.082
CSIRO-Mk3-6-0	0.189	0.219	-0.029	0.000	0.127	0.176
EC-EARTH	-0.077	0.011	0.003	0.015	0.184	0.053
FGOALS-g2	0.019	0.107	0.129	-0.038	0.051	0.065
FIO-ESM	-0.023	-0.120	-0.015	0.139	0.137	0.161
GFDL-CM3	0.038	0.032	-0.022	-0.076	0.235	0.352
GISS-E2-R	0.047	0.074	-0.038	-0.066	-0.018	-0.005
HadGEM2-AO	0.050	-0.033	0.005	-0.031	0.148	0.075
INMCM4	0.023	0.031	-0.060	0.164	0.139	0.033
IPSL-CM5A-LR	0.019	0.051	0.121	0.076	0.038	-0.038
IPSL-CM5A-MR	0.118	0.175	0.191	0.094	0.277	0.184
IPSL-CM5B-LR	0.044	0.072	-0.010	-0.063	-0.005	0.128
MIROC5	0.082	-0.060	-0.097	0.087	0.059	0.002
MIROC-ESM-CHEM	-0.021	-0.019	0.068	0.028	0.002	0.162
MPI-ESM-LR	0.056	0.051	-0.090	0.063	0.207	0.224
MPI-ESM-MR	0.041	0.036	-0.053	-0.086	0.164	0.057
MRI-CGCM3	0.047	-0.009	0.178	-0.046	0.388	0.311
NorESM1-M	0.049	0.039	-0.008	0.099	0.124	0.141
Ensemble mean	**0.064**	**0.063**	**0.024**	**0.050**	**0.140**	**0.139**
# Positive	22	21	14	18	23	24
# Negative	4	5	12	8	3	2

For the long rains months of March, April, and May, we find substantial variation between the models in the CMIP5 ensemble on both the sign and the magnitude of the rainfall trends despite the ensemble mean indicating a statistically significant increasing rainfall trend during this season over the period 2020-2100 (Table 13.1).

During the long rains, fewer than half of the models project any statistically significant changes in rainfall. In March, 10 models (40%) project statistically significant rainfall increases over Kenya, with 1 model (EC-EARTH) showing a statistically significant decrease. 7 models (28%) project significant rainfall increases in April, with significant decreases in FIO-ESM. 7 models (28%) project significant wetting in May, with significant drying in 3 models (CMCC-CM, MIROC5, and MPI-ESM-LR). The ensemble mean precipitation trends are small relative to the trends seen in individual models. The ensemble mean trends in March and April are very similar (0.063 and 0.064 mm day^{-1} $decade^{-1}$), and in May the trend is much smaller (0.023 mm day^{-1} $decade^{-1}$). The models with the strongest wetting trends in each month project rainfall trends which are an order of magnitude greater.

Table 13.1 indicates that CMIP5 rainfall slopes under RCP8.5 are in closer agreement for the long rains months of November and December compared to October, but that there is still a great degree of variation between the individual models. The ensemble mean precipitation trends are again all significant and positive; the trends in November and December are the largest of any of the rainy season months; 0.139 mm day^{-1} $decade^{-1}$ and 0.137 mm day^{-1} $decade^{-1}$ respectively, compared to 0.051 mm day^{-1} $decade^{-1}$ for October. The model biases in the rainfall annual cycle therefore continue up to 2100, with the short rains wetter than the long rains in the ensemble means, despite a few very wet models in the long rains months (notably BCC-CSM1-1-M). In October, fewer than half the models project significant rainfall trends. 10 models (40%) project significant wetting and 2 models project drying (IPSL-CM5B-LR and MPI-ESM-MR). The wetting trends are robust for October and November with a majority of models agreeing on significant rainfall increases (14 models (56%) in November, 15 models (60%) in December).

13.4.1.2. Projected Changes in Vertical Velocity (Omega)

Explaining the differences between the rainfall projections in different models requires consideration of the models' dynamics. The 400hPa vertical velocity (omega) field over the equatorial Indian Ocean indicates the key ascending and descending regions of the IOWC. Figures 13.1 and 13.2 display the projected trends in IOWC ascent and descent for the remainder of the 21st century for composites of the 5 models with the strongest wetting trends and the 5 models with the weakest wetting/strongest drying trends for each rainy season month.

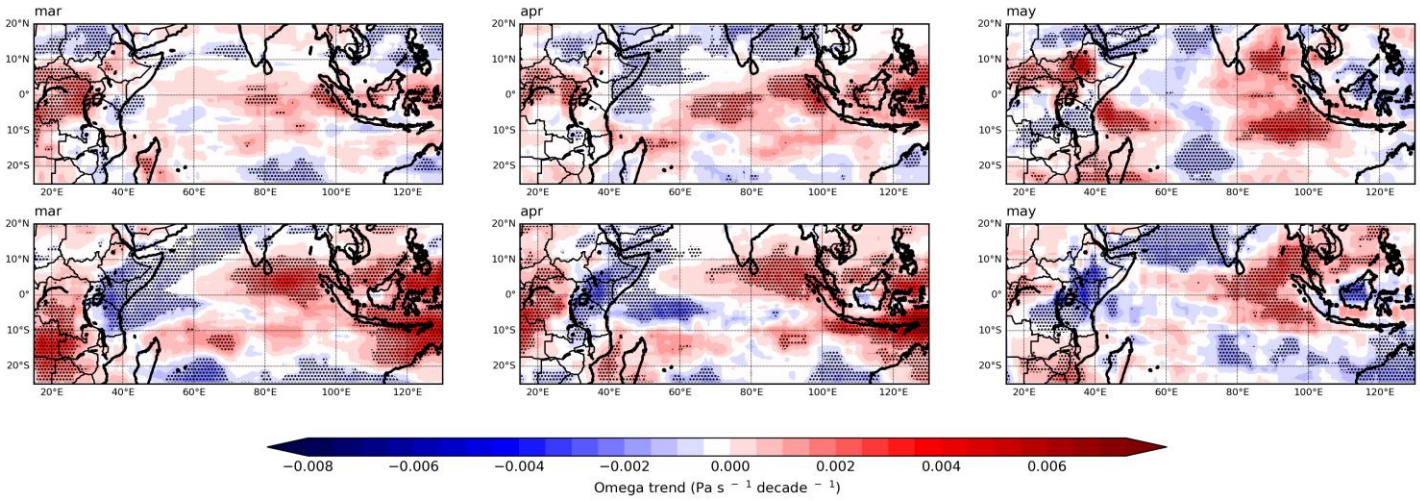


Figure 13.1 - linear regression of composite averages in 400hPa vertical velocity for March (left), April (middle), and May (right), 2020-2100, under the RCP8.5 scenario. Stippling denotes areas where the trend significance p<0.05. For each month, the top 5 models with strongest drying/weakest wetting (top row) and strongest wetting (bottom row) are averaged to form a composite.

In the long rains months (Fig. 13.1), the model composites that show drying trends or weaker wetting trends over Kenya have small (<0.002 Pa s^{-1} $decade^{-1}$) trends towards increasing descent (positive omega) over land in East Africa. Kenya lies at the margin between a region of significant omega increase inland and omega

decrease offshore in March and April. The drying/weak wetting composites also show statistically significant trends toward increasing ascent (decreasing omega) over the Maritime Continent in May, of around -0.003 Pa s^{-1} decade $^{-1}$. By contrast, models which produce wetting trends over Kenya exhibit strong and significant trends towards ascending air over Kenya and descending air over the Maritime Continent. This can be clearly seen in the composites forming the bottom row of Fig. 13.1, all of which have significant areas of increasing omega over the Maritime Continent and eastern tropical Indian Ocean of ~0.005 Pa s^{-1} $decade^{-1}$. Significant omega decreases are seen over Kenya and the Greater Horn of Africa in March, April, and May, generally between -0.004 and -0.006 Pa s^{-1} decade $^{-1}$ over Kenya. Some individual models, for example EC-EARTH and INMCM4, feature a strong ascending trend of ~0.008 Pa s^{-1} decade $^{-1}$ across the Maritime Continent region during March (not shown). INMCM4 features strong wet biases in MAM over 1975-2005 (Fig. 11.13).

Models have significant omega trends across the tropical Indian Ocean that vary in sign and spatial extent, although increasing omega in the equatorial zone is the most common pattern. Where these patterns consist of zonal bands of descending and ascending trends, this may reflect changes to the location and/or strength of the convective band associated with the Inter-Tropical Convergence Zone (ITCZ); however, the zonal asymmetry of the general pattern across the Indian Ocean Basin in Figure 13.1 implicates the zonal IOWC as a driver of these vertical velocity trends.

Figure 13.2 shows the changes to 400hPa omega projected under RCP8.5 during the short rains months. The general trend is for wetting models to have decreasing omega over Kenya which is absent from models with weak drying or no significant wetting. These omega decreases are more intense and more spatially extensive than

in MAM (≥-0.006 Pa s^{-1} decade $^{-1}$ over Kenya). In November and December, no models project significant drying over Kenya. This is reflected by weak but significant omega decreases over East Africa in the weakest wetting trend composites for these months (~-0.002 Pa s^{-1} $decade^{-1}$), and strong omega decreases in the strongest wetting models (≥-0.006 Pa s^{-1} decade $^{-1}$). Ascent over East Africa is balanced by significant increasing omega trends (~0.004 Pa s^{-1} decade $^{-1}$) over the Maritime Continent in both sets of composites. A consistent feature across the ensemble in October and November is extensive increasing omega trends with $p<0.05$ over the eastern Congo Basin region.

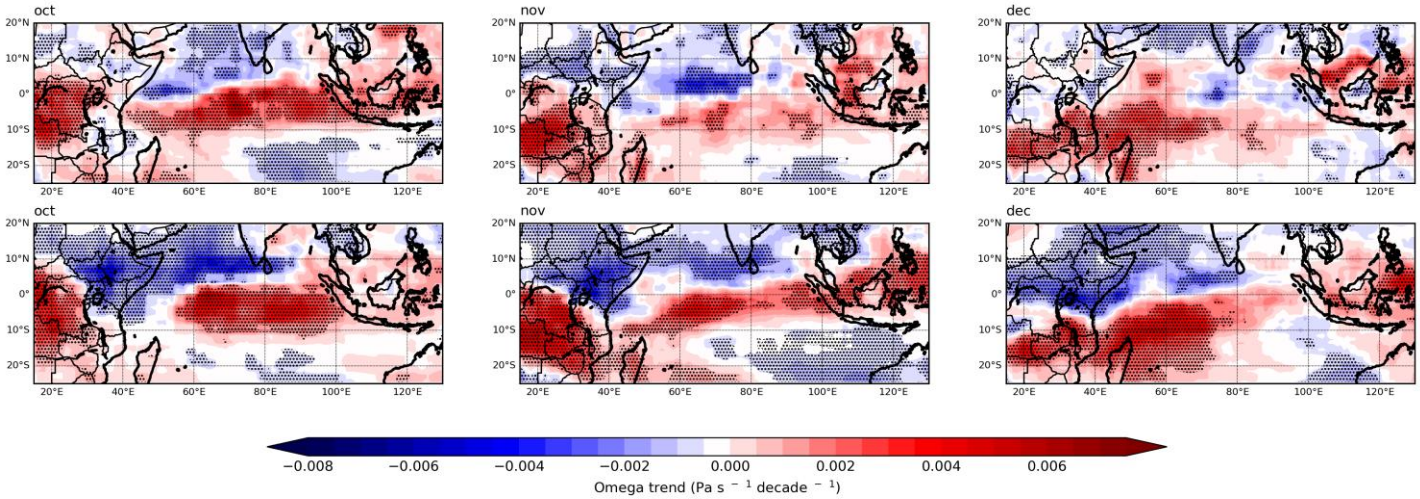


Figure 13.2 - as Figure 13.1, but for October (left), November (middle), and December (right).

Variation between models in the signs and locations of trend regions over the Indian Ocean itself suggest changes to circulation regimes in future continue to show a high contribution from model uncertainty.

13.4.1.3. Projected Changes in Zonal Winds

The role of the 850hPa zonal winds over the equatorial Indian Ocean in advecting moisture towards the continent is important in determining East African rainfall variability (Nicholson 2015). The representation of these winds is known to be a key source of CMIP5 rainfall biases during the East African short rains (Hirons and Turner 2018), and any discussion of future projections of this variable must be interpreted in the context of the known biases during the short rains. The westerly winds form the return limb of the climatological IOWC.

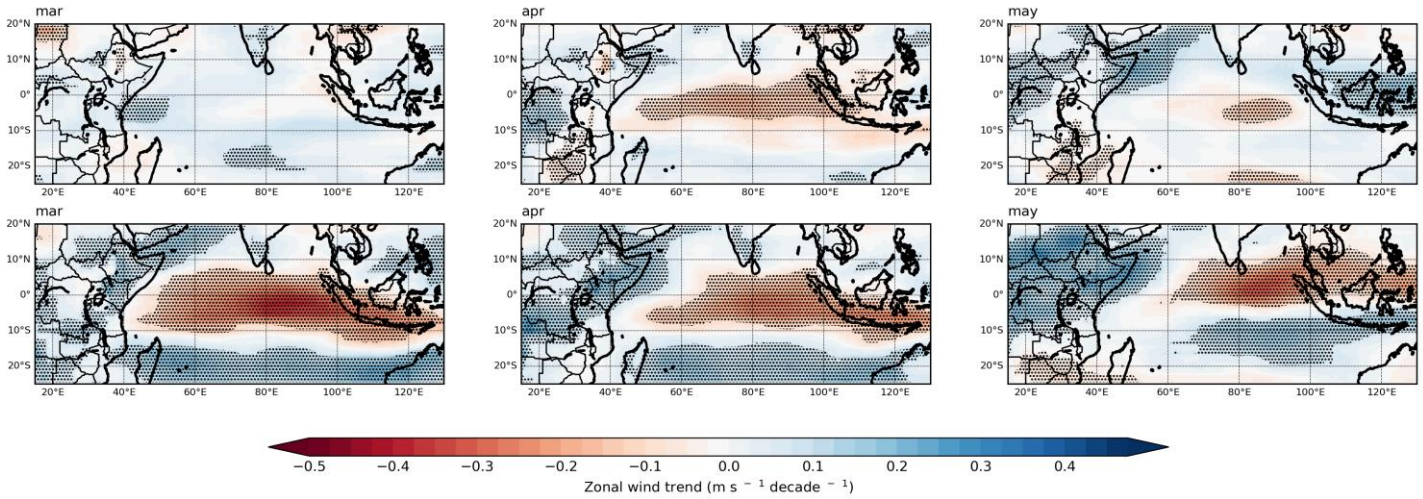


Figure 13.3 - linear regression trends in 850hPa zonal wind for March (left), April (middle), and May (right), 2020-2100, under the RCP8.5 scenario. Stippling denotes areas where p<0.05. For each month, the top 5 models with strongest drying/weakest wetting (top row) and strongest wetting (bottom row) are averaged to form a composite.

Figs. 13.3 and 13.4 show the linear trends in 850hPa zonal wind up to 2100 under the RCP8.5 scenario. Significant zonal wind trends are present during the long rains, with increasing equatorial easterlies and continental westerlies predominating (Fig.

13.3). These trends are stronger and more spatially extensive in the wetting composites, with easterly trends over the equatorial Indian Ocean reaching a magnitude of up to -0.5 ms^{-1} $decade^{-1}$. The easterly trends are absent from the drying/weak wetting composites in March, and are largely below the threshold for statistical significance in May. Similarly, there are significant westerly trends over continental East Africa in the wetting composites (0.2-0.3 ms^{-1} $decade^{-1}$) which are weaker and less significant in the drying/weak wetting composites. Given that these winds are moist, this could lead to enhanced moisture flux convergence with easterly winds from the Indian Ocean over East Africa.

For the short rains months (Fig. 13.4), the relationships between the zonal wind trends and rainfall trends are less clear in the model composites, and this is likely to reflect the idiosyncratic biases in model zonal wind direction during this season (Hirons and Turner 2018). Models which are wet biased in historical coupled runs are likely to already feature strong easterly winds over the equatorial Indian Ocean, and the trends in future wind speed may thus not be as significant an influence as the wind speed values themselves. In October, models with strong wetting trends in future feature a characteristic pattern of significantly enhanced easterlies over the equatorial Indian Ocean and significantly enhanced westerlies over continental Africa, both of similar magnitude (± 0.3 ms^{-1} $decade^{-1}$). Both easterly and westerly trends are present in the drying/weak wetting composite but are reduced in magnitude and spatial extent, with no significant trends over Kenya and easterly trends only extending to around 70˚E compared with 100˚E in the strong wetting composite. In November, the weak wetting composite shows extensive easterly wind trends over the equatorial Indian Ocean, while these trends are confined to the East African coast in the wetting composite. This may reflect the presence of wetting

across the ensemble in this month, as well as the wetting models already featuring strong easterly biases in historical coupled runs when the climatological wind is westerly. Consequently, the wetting composite indicates where the increase in easterly winds is strongest, which is off the East African coast. For example, Hirons and Turner (2018) identify MRI-CGCM3 and ACCESS1-3 as models with strong easterly wind biases in the historical coupled models, with a bias relative to reanalysis of -2.79 ms^{-1} and -1.93 ms^{-1} respectively. These models also have strong historical wet biases over East Africa as a result. We find that both models continue to be wet in future, and as such are included in the composites for Fig. 13.4. MRI-CGCM3 shows the strongest wetting trend of any model in the ensemble for November and the 4th wettest trend in December, and ACCESS1-3 has the 2nd strongest wetting trend in November and the 3rd strongest in December (Table 13.1). Conversely, models with (correct) westerly winds in historical coupled runs would appear in the composite as having strong easterly trends if the westerlies are significantly reduced in strength in future. In December, the strong wetting and weak wetting composites show similar structures, with enhanced westerlies to the north of the equator over East Africa and easterlies to the south. While both composites show significant trends here, the trends are stronger by 0.1-0.2 ms^{-1} $decade^{-1}$ in the strong wetting composite.

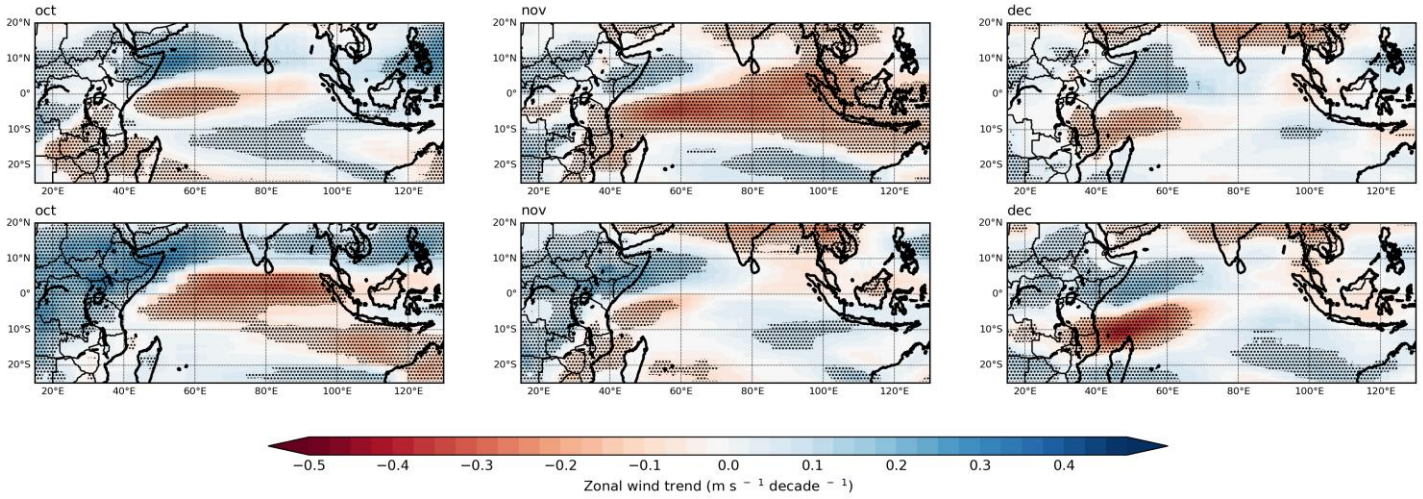


Figure 13.4 - as Figure 13.3, but for October (left), November (centre), and December (right).

13.4.1.4. Projected Circulation Changes

King et al. (2020) link the rainfall biases over East Africa in historical coupled runs of CMIP5 models to their representation of the overturning circulation over the equatorial Indian Ocean. Figs. 5 and 6 show the composite differences in the same ensemble of models between a control period representing late 20th century conditions (1975-2005, historical coupled runs) and an end of 21st century period under the RCP8.5 scenario (2070-2100). For the long rains months (Fig. 5), there are differences between the models showing drying or weak wetting trends over Kenya (top rows) and those showing strong wetting trends (bottom rows). Principally, the changes to vertical velocity over East Africa and the western Indian Ocean are quantitatively different, with weak ascent throughout the troposphere in the weak wetting/drying composites of >-0.01 Pa s^{-1}. In March, the 200hPa wind trends are easterly, implying an enhancement of the upper-level branch of the Walker Circulation. By contrast, models with strong wetting trends show stronger and more spatially extensive negative omega composite differences over East Africa (-0.02 - -

0.03 Pa s^{-1}). In these models, the changes in omega and streamlines reflect weakening of the zonal overturning, with reduced descent over East Africa and corresponding reduced ascent over the Maritime Continent, in both cases of magnitude ~±0.03 Pa s^{-1}. The streamlines indicate enhanced lower-troposphere easterlies and upper-troposphere westerlies over the equatorial Indian Ocean, as well as enhanced westerly flow into East Africa from central Africa. The zonal pattern of omega changes (ascent over East Africa and descent over the Maritime Continent) is the reverse of the climatological direction of the IOWC.

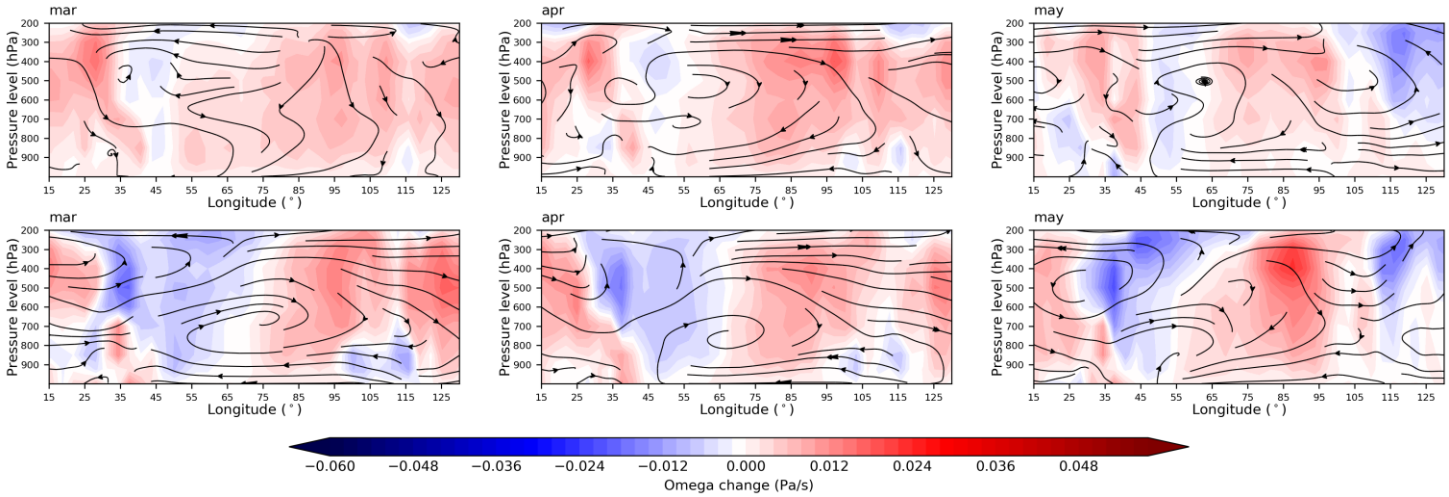


Figure 13.5 - Longitude-height plots of the circulation over the equatorial Indian Ocean, 15°E-130°E, averaged over 5°N-5°S, for March (left), April (middle), and May (right). Shading is vertical velocity (ω) (Pa s-1) with red indicating negative (upward) motion blue indicating positive (downward) motion. Streamlines are the resultant vectors of u and ω x 10^4. For each month, the means for 1975-2005 (historical coupled runs) are subtracted from the means for 2070-2100 (RCP8.5). For each month, the top 5 models with strongest drying/weakest wetting (top row) and strongest wetting (bottom row) are averaged to form a composite.

In the short rains months (Fig. 13.6), the changes to the overturning are also clearly distinct between the two sets of composites. For models with wetting trends in future, we see changes in overturning in opposition to the climatological IOWC, with streamlines indicating changes towards low-level equatorial easterly winds, and

omega changes towards rising air over East Africa throughout the troposphere, and descent over the Maritime continent. This demonstrates that the wetting trends in these models occur in conjunction with a weakening in the IOWC circulation consistent with wetter conditions over East Africa. The magnitude of the omega changes over both East African and the Maritime continent reach magnitudes of ~±0.05 Pa s^{-1}, reflecting the stronger role of zonal overturning in the tropical climate during this season. The difference between the strong wetting and weak wetting composites are greatest in October, reflecting that wetting is more consistent across the ensemble in November and December (Table 13.1). Figs. 13.5 and 13.6 show how the omega and zonal wind trends in Figs. 13.1-13.4 are dynamically linked via the changes to the zonal overturning cell, and must be considered as part of the broader IOWC. Notably, the streamlines in the wetting composite for October, and in both sets of composites in November and December, show a trend towards low-level convergence over Kenya in wetting models, as westerly wind trends from the Congo Basin and easterly wind trends over the Indian Ocean meet at between 35˚E and 45˚E. This is associated with negative omega change from 900hPa to 200hPa. There is substantial variation between the models on the magnitude and zonal extent of positive omega change over the eastern part of the domain. While this change is present in most of the models, the magnitude varies from <0.01 Pa s^{-1}, (INMCM4) to >0.05 Pa s^{-1} (CSIRO-Mk3-6-0) at the same location (95˚E, 400hPa) (not shown). This is reflected in the less strong descent in the composites relative to ascent over East Africa in Fig 13.7. This can be linked to the differing model behaviour in the 1975-2005 baseline conditions; King et al. (2020) find that the equatorial overturning associated with the IOWC is not represented during this period in November in INMCM4, for example.

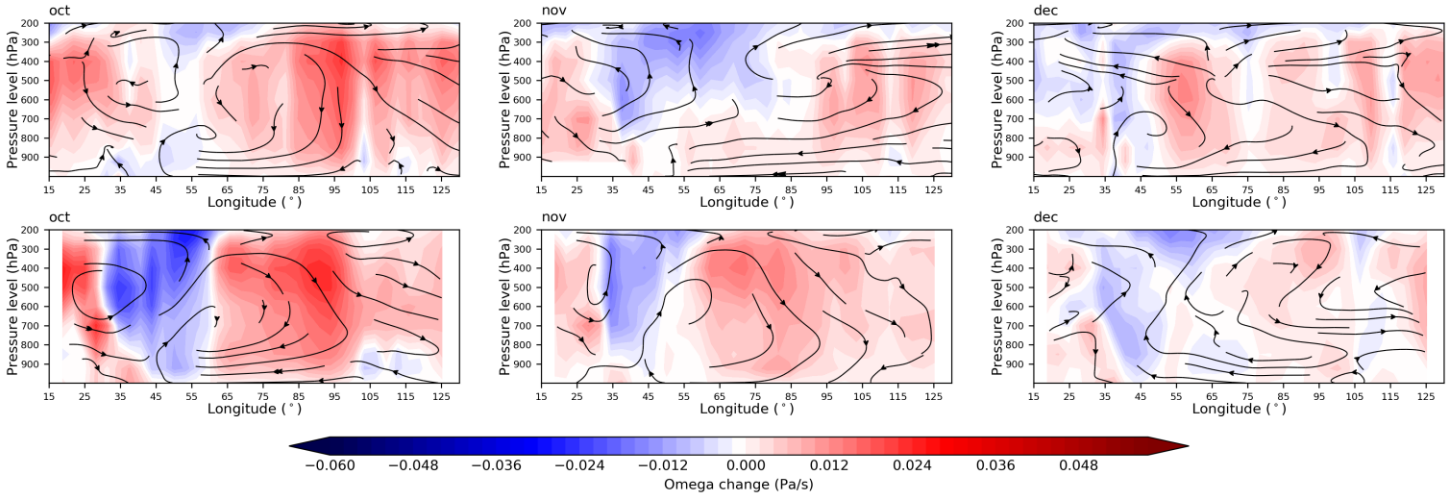


Figure 13.6 - as Figure 13.5, but for October (left), November (middle), and December (right).

13.4.2. Links Between Historical Biases and Future Projections of IOWC Variables

Section 13.4.1 has demonstrated the dynamic factors that combine to produce rainfall trends in CMIP5 model projections, which are generally towards a wetter East Africa as a result of changes to the IOWC including reduced positive omega and enhanced easterly winds. The important task that follows from this analysis is to assess the plausibility of these future projections in the context of the models' known biases in representation of the historical IOWC and associated rainfall conditions. This section addresses this by linking historical biases to future projections.

13.4.2.1. Rainfall Change

We begin by assessing the extent to which CMIP5 models' historical precipitation over Kenya correlates with their future precipitation – in other words, are models that are particularly wet or dry in historical coupled runs still particularly wet or dry

in future projections under the RCP8.5 scenario? Table 13.2 shows the results of a correlation analysis comparing precipitation averaged over Kenya during 1975-2005 and 2070-2100, for each model in our ensemble (n = 25).

Table 13.2 - Pearson product moment correlation coefficients between CMIP5 model rainfall averaged over Kenya in historical coupled (1975-2005) and RCP8.5 (2070-2100) runs of the CMIP5 models listed in Table 11.1.

Month	March	April	May	October	November	December
R	0.854	0.851	0.882	0.908	0.821	0.673
R^2	0.730	0.724	0.778	0.825	0.674	0.453
p	0.0004	7.2E-08	5.5E-09	3.5E-10	4.9E-07	0.0002

There are strong and significant correlations ($p<0.001$) for each rainy season month between historical and projected rainfall over Kenya. For each month, models with rainfall >1 standard deviation above the ensemble mean for 1975-2005 also have rainfall >1 standard deviation above the ensemble mean in 2070-2100 (with the notable exception of GISS-E2-R, a wet model which projects drying trends in all rainy season months except March). Models which fulfil this condition for multiple months include ACCESS1-3 (October and November), BCC-CSM1-M (March and April), INMCM4 (March, April, October, and November), and MRI-CGCM3 (November and December). Conversely, models with rainfall >1 standard deviation below the ensemble mean in both time slices for multiple months include GFDL-CM3 (March and April and, IPSL-CM5A-LR (October, November, and December). Since this historical rainfall is known to be biased (Tierney et al. 2015) as the result of erroneous representation of regional dynamics (Hirons and Turner 2018, King et al. 2020), the strong covariability between wet and dry models in both time slices implies similar processes may explain the spread in model rainfall projections. This

is consistent with the comparatively time-invariant evolution of the model contribution to uncertainty in regional precipitation projections (Hawkins and Sutton 2011).

13.4.2.2. Rainfall vs. Omega

Table 13.3 - Pearson product moment correlation coefficients between CMIP5 model 400 hPa omega averaged over Kenya in historical coupled (1975-2005) and RCP8.5 (2070-2100) runs of the CMIP5 models listed in Table 11.1. B. Pearson product moment correlation coefficients between model rainfall change and 400 hPa omega change over Kenya, 2070-2100 minus 1975-2005.

A.	Month	March	April	May	October	November	December
	R	0.041	0.871	0.798	0.930	0.909	0.865
	R^2	0.002	0.758	0.637	0.864	0.825	0.748
	p	0.844	1.5E-08	1.8E-08	1.9E-11	3.5E-10	2.4E-08
B.	Omega change vs rainfall change						
	R	0.227	-0.878	-0.830	-0.795	-0.902	-0.679
	R^2	0.052	0.771	0.689	0.632	0.814	0.460
	p	0.275	8.0E-09	2.9E-07	2.0E-06	7.3E-10	0.0002

Table 13.3A indicates that, apart from March, there are highly significant positive correlations during rainy season months between model vertical velocity over Kenya at 400hPa in historical coupled model runs and the RCP8.5 projections at the end of the 21st century for the same model ensemble. Correlations are more significant during the short rains months, when the IOWC is more active, especially during positive IOD events. This demonstrates that the sign and magnitude of model vertical velocity over Kenya in the historical period corresponds to that in the RCP8.5

projections. For example, models with omega values >1 standard deviation below the ensemble mean for both time slices include ACCESS1-3 (October and November), BCC-CSM1-1-M (all months except October), CNRM-CM5 (April, May, October, and November), GFDL-CM3 (November and December), and MRI-CGCM3 (October and November). Several of these models are also among the wettest for each month in both time slices, as shown above. Models with omega values >1 standard deviation above the mean include BNU-ESM (April and May), CCSM4 (April and May), FIO-ESM (May, November, and December), IPSL-CM5A-LR (October, November, and December), and IPSL-CM5A-MR (October and November). These tend to be drier models. There is also a relationship across the model ensemble between the change in Kenya rainfall (as expressed by the composite difference between 2070-2100 and 1975-2005) and the change in 400hPa vertical velocity between the same time slices (Table 4B). Apart from March, the correlations between these variables are statistically significant at $p>0.05$ and strongly negative – models with increasing (decreasing) rainfall have decreasing (increasing) vertical velocity over Kenya. This demonstrates the continued role of the large-scale descent associated with the IOWC in controlling rainfall variability in CMIP5 projections.

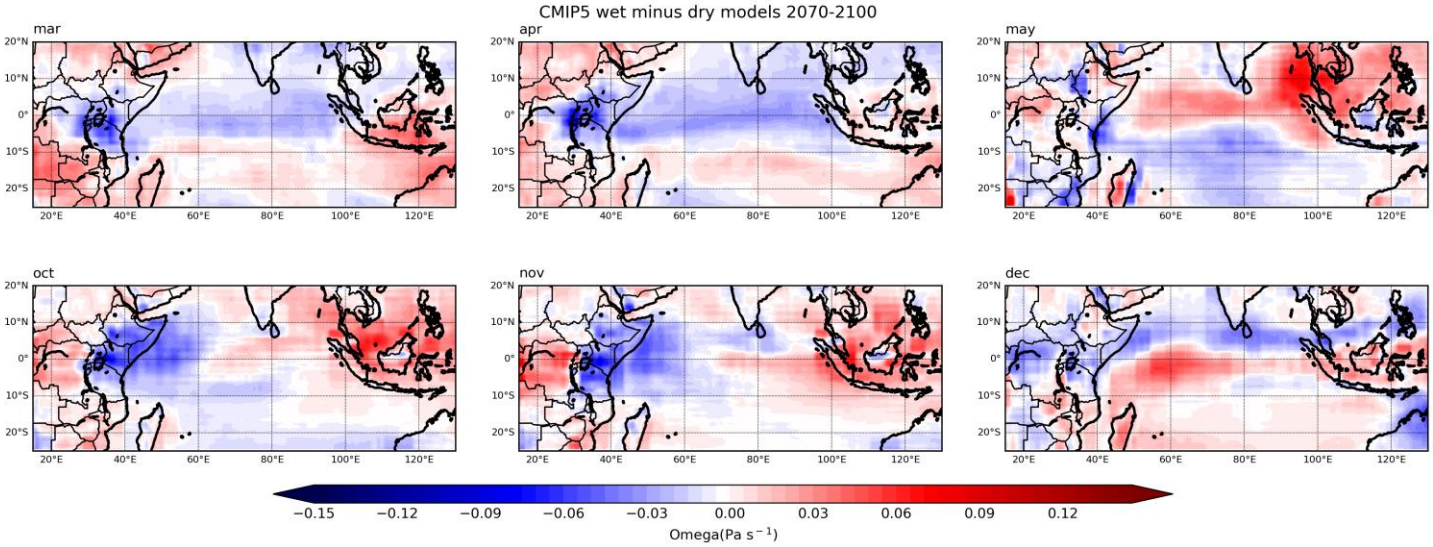


Figure 13.7 - Wet minus dry model composites of 400hPa omega, averaged over 2070-2100 under the RCP8.5 scenario.

Figure 13.7 shows the differences in 400hPa vertical velocity between the 4 wettest and 4 driest models for each rainy season month in the 2070-2100 time slice. Wet models in future are associated with negative omega (stronger ascent or weaker descent) over East Africa, with the strongest differences between wet and dry models seen over Kenya in March, April, October, and November. Conversely, wet models are also associated with positive omega (stronger descent or weaker ascent) over the Maritime continent, which is present in all rainy season months and strongest in May. The dipolar nature of the wet minus dry composites suggests a continued role for the IOWC in model projections of East African rainfall. The differing meridional gradients over the tropical Indian Ocean reflect the differing positions of the ITCZ over the Indian Ocean in each month. Wet models in March, April, and December feature increased ascent north of the equator, whereas in May there is increased ascent south of the equator. The zonal gradient between ascent and descent over the Indian Ocean is most pronounced in November and December, reflecting the increased influence of Indian Ocean SST during these months.

13.4.2.3. Rainfall vs Zonal Wind

Table 13.4 - A: Pearson product moment correlation coefficients between CMIP5 model 850 hPa zonal wind averaged over the central equatorial Indian Ocean in historical coupled (1975-2005) and RCP8.5 (2070-2100) runs of the CMIP5 models listed in Table 11.1. B. Pearson product moment correlation coefficients between model rainfall change and 850 hPa zonal wind change over the central equatorial Indian Ocean, 2070-2100 minus 1975-2005.

A.	Month	March	April	May	October	November	December
	R	0.753	0.813	0.885	0.696	0.810	0.813
	R^2	0.568	0.662	0.784	0.484	0.650	0.660
	p	1.38E-05	7.7E-07	4.2E-09	0.0001	1.2E-06	0.8E-06
B.							
	R	-0.578	-0.482	-0.411	-0.586	-0.516	-0.419
	R^2	0.334	0.232	0.169	0.343	0.267	0.176
	p	0.002	0.01	0.04	0.002	0.008	0.04

Table 13.4A shows the strong and significant positive correlation between historical and future zonal winds over the central equatorial Indian Ocean, a key contributing factor to historical model rainfall biases (Hirons and Turner 2018). The results demonstrate that models featuring erroneously easterly winds during OND in the historical coupled runs continue to simulate easterlies in future. Models that do this include ACCESS1-3 (OND), BNU-ESM (D), CMCC-CM (OND), HadGEM2-AO (OND), and MRI-CGCM3 (OND). Although the zonal winds during the Long Rains have not been investigated in detail for CMIP5 in previous studies, our results show a similar pattern whereby easterly/westerly models continue to be so in future during March and April (all models feature westerly winds during May). Models disagree on the sign of the equatorial zonal winds during March and April during both time slices. Some models change sign from westerly to easterly winds between 1975-2005 and 2070-2100: CNRM-CM5, GISS-E2-R, HadGEM2-AO, IPSL-CM5B-LR, and

MRI-CGCM3 do this in March, and BNU-ESM and MIROC-ESM-CHEM do it in April. No models change from easterly winds to westerly winds. Table 13.4B also suggests a continued role for the 850 hPa zonal winds in driving projections of East African rainfall. Correlations between model rainfall change over Kenya and model zonal wind change over the equatorial Indian Ocean are significant at $p<0.05$ and negative for all rainy season months. Because easterly wind values are negative in the zonal wind field, this implies that increasingly easterly zonal wind components in CMIP5 models are associated with increased rainfall over Kenya.

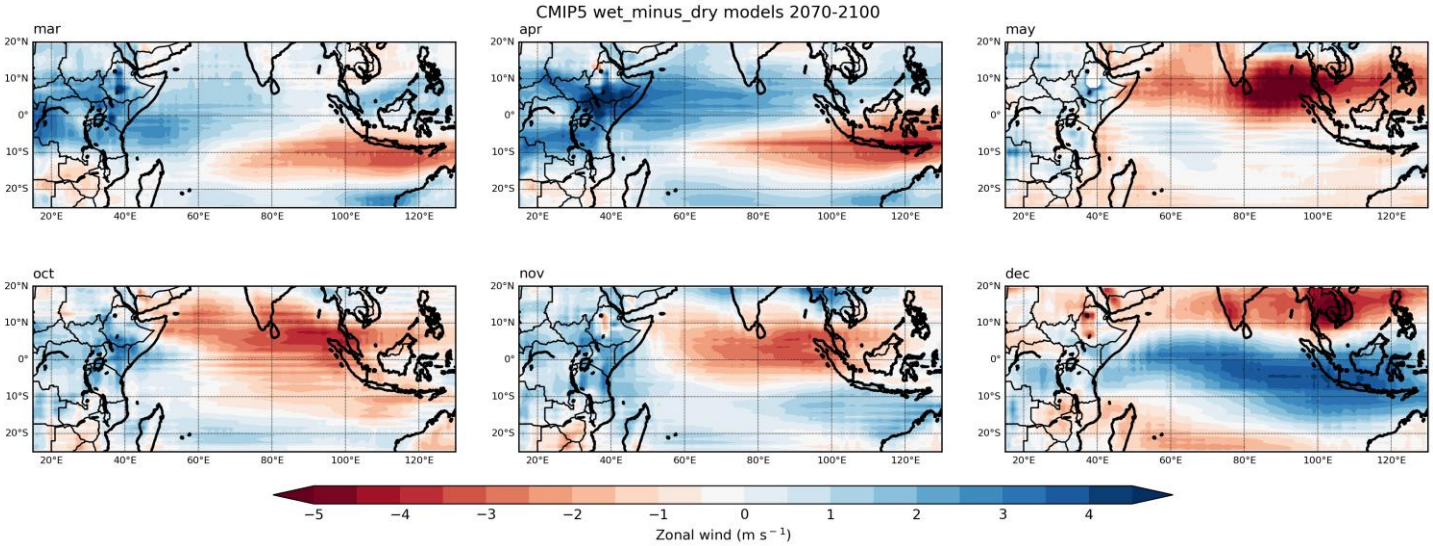


Figure 13.8 - Wet minus dry model composites of 850hPa zonal wind, averaged over 2070-2100 under the RCP8.5 scenario.

Figure 13.8 shows the differences in 850hPa zonal wind between the dry and wet models for 2070-2100. During October and November, wet models have enhanced equatorial easterly wind over the Indian Ocean, consistent with the relationship between these winds and East African rainfall in historical coupled models. In March and April, there are enhanced easterlies over the Indian Ocean at 10˚S extending from the Maritime Continent into the central Indian Ocean, and enhanced westerlies

on the equator extending to around 10˚S. In May and December, wet models are associated with enhanced easterlies at 10˚N, with strong westerlies on the equator in December. In all months, the wet minus dry composites show increasingly westerly winds over the East African landmass, particularly in March and April. Combined with patterns of enhanced easterlies over the Indian Ocean, this implies enhanced convergence of moist air masses (easterlies from the Indian Ocean and westerlies from the Congo Basin) at 850 hPa over East Africa in model projections, supporting the conclusions of Giannini et al. (2018) on the increasing importance of moisture flux from the Congo Basin in future East African rainfall. We also note that wet models show negative (westerly) signs over the Turkana Channel in northwestern Kenya, where the zonal wind field is dominated by the southeasterly Turkana LLJ. The westerly signs may reflect a slowing of low-level easterlies in wet model projections, which is consistent with some reanalysis datasets (Torralba et al. 2017)

13.4.2.4. Wet/Dry Future Composite Streamplots

Section 13.4.1.1 demonstrates that, for all rainy season months, the ensemble mean change is for increasing rainfall over Kenya, decreasing omega over Kenya, and enhanced easterly winds over the tropical Indian Ocean. Figure 13.9 reveals the structure of the overturning circulation in wet minus dry model composites, linking these findings together.

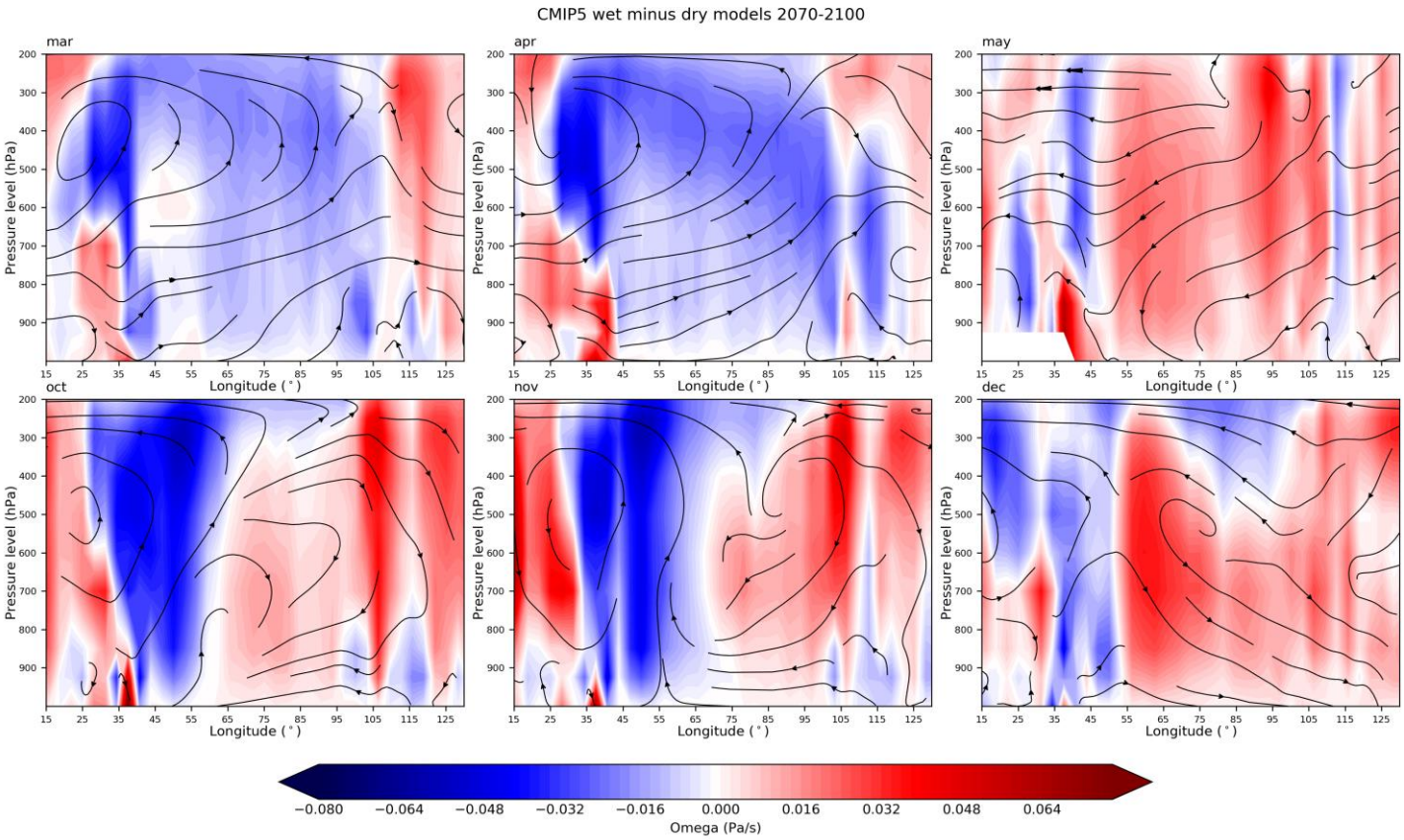


Figure 13.9 - Wet minus dry model composites of the circulation over the equatorial Indian Ocean , averaged over 2070-2100 under the RCP8.5 scenario. Shading is vertical velocity (ω) (Pa s-¹) with red indicating negative (upward) motion and blue indicating positive (downward) motion. Streamlines are the resultant vectors of u and ω x 10⁴.

The differences between wet and dry models are evident in the residual overturning circulations. For all rainy season months, the wet composites feature negative omega over East Africa extending throughout the troposphere, indicating weakened ascent/stronger descent in this limb of the IOWC. Positive omega at lower levels (e.g. below 700hPa over the East African continent between 35˚E-45˚E) may reflect divergence from enhanced low-level westerly winds (Figs. 13.3 and 13.4), while the extensive positive omega signs over the Indian Ocean in May, October, November, and December reflect the enhanced equatorial easterlies (Figs. 13.5 and 13.6). Over the Maritime Continent, in the east of the domain, positive omega indicates a weakening of the ascending limb of the IOWC at this location (Fig. 13.9), which extends throughout the troposphere and therefore suggests a reduction of deep

convection over this region. Omega differences in both ascending and descending regions are strongest in October and November, and weakest in May and December. The streamlines link the zonal wind and omega changes to demonstrate a weaker IOWC in wet CMIP5 model projections. The changes in streamlines in October and November show this clearly, with the wet minus dry residual showing overturning acting in the opposite direction to the climatological IOWC.

13.5. Composite Projections

We next demonstrate an approach using metrics related to the dynamical structure of the IOWC to constrain CMIP5 projections of rainfall over Kenya and across East Africa. For each rainy season month in each model, we calculate the root mean square error (RMSE) of rainfall averaged over Kenya during 1981-2005 compared to the CHIRPSv2.0 dataset (Funk et al. 2015). The time period chosen is a compromise between data availability for CHIRPSv2.0 and for CMIP5 historical coupled runs. We also calculate RMSE for omega averaged over Kenya at 400hPa and zonal winds averaged over the central equatorial Indian Ocean at 850hPa. For each RMSE calculation, we rank the models in order with from lowest to highest RMSE, and calculate the average rank across the three metrics. The 4 lowest and 4 highest scoring models for each month are selected to form ‘good’ and ‘bad’ composite projections respectively, representing the top and bottom 16% of the ensemble. If an otherwise ‘good’ model has a mean 850hPa central IO zonal wind value of the opposite sign to reanalysis, it is excluded from the composite and the next lowest scoring model with the correct zonal wind direction is included; however, this was only necessary for March. Table 13.5 shows the models used.

Table 13.5 - CMIP5 models used to produce 'good' and 'bad' composites of future rainfall following the procedure outlined in section 3.3.

Month	March	April	May	October	November	December
'Good'	EC-EARTH FIO-ESM INMCM4 NorESM1-M	CMCC-CM GISS-E2-R INMCM4 MIROC-ESM-CHEM	ACCESS1-3 CCSM4 IPSL-CM5A-LR MIROC-ESM-CHEM	CSIRO-Mk3-6-0 FIO-ESM IPSL-CM5A-LR MPI-ESM-MR	IPSL-CM5A-MR MIROC5 MIROC-ESM-CHEM MPI-ESM-LR	EC-EARTH IPSL-CM5A-LR IPSL-CM5A-MR MIROC-ESM-CHEM
'Bad'	BNU-ESM CanESM2 CSIRO-Mk3-6-0 IPSL-CM5B-LR	BNU-ESM IPSL-CM5B-LR MIROC5 MPI-ESM-MR	BCC-CSM1-1-M BNU-ESM FGOALS-g2 IPSL-CM5B-LR	INMCM4 CNRM-CM5 FGOALS-g2 MRI-CGCM3	ACCESS1-3 CMCC-CM GFDL-CM3 MRI-CGCM3	BCC-CSM1-1-M CESM1-CAM5 GISS-E2-R INMCM4

13.5.1. Composite Trends

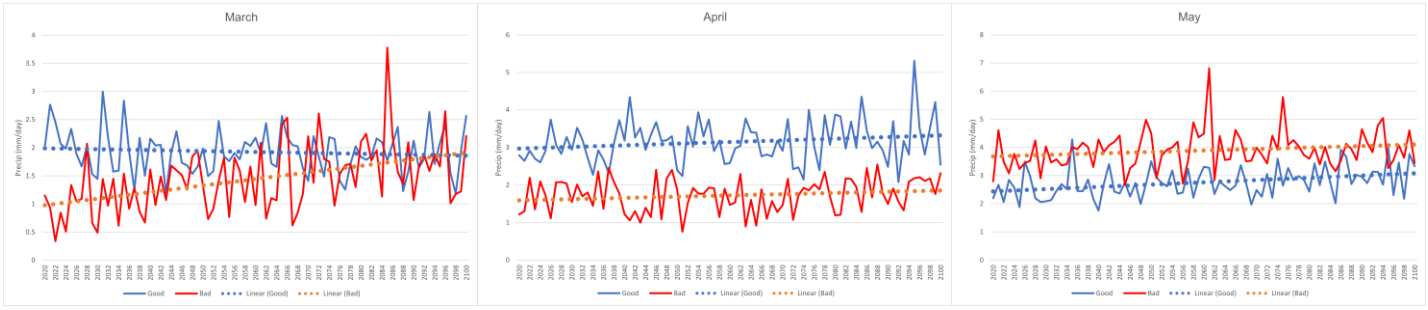


Figure 13.10 - Rainfall projections over Kenya from the 'good' (blue) and 'bad' (red) model composites shown in Table 6 for MAM, over 2020-2100 under RCP8.5. The dotted line is a linear regression model fitted to each composite time series.

Figure 13.10 shows the differences between the rainfall projections for the 'good' and 'bad' composites during the long rains months. The changes are different in each month. For March, the 'good' composite shows little change in rainfall between 2020 and 2100, with the linear regression model indicating an insignificant decrease (linear trend = -0.016 mm day^{-1} decade^{-1}, p = 0.38). By contrast, the 'bad' composite shows a significant increasing trend (0.12 mm day^{-1} decade^{-1}, p = 1.2E^{-05}), which

results in the initially dry 'bad' models approximating the rainfall totals of the 'good' models by 2100. For April, the 'good' composite is wetter than the 'bad' composite and continues to be so throughout the 21st century by around 1 mm day^{-1}. Both composites show similar wetting trends that are just over the p<0.1 criterion for statistical significance ('good' linear trend = 0.044 mm day^{-1} decade^{-1}, p = 0.11, 'bad' linear trend = 0.033 mm day^{-1} decade^{-1}, p = 0.11). In May, the 'good' composite is consistently around 1.2 mm day^{-1} drier than the 'bad' composite. Both composites have small but significant wetting trends with p<0.1, with that of the 'good' composite being stronger ('good' linear trend = 0.081 mm day^{-1} decade^{-1}, p = 0.001, 'bad' linear trend = 0.053 mm day^{-1} decade^{-1}, p = 0.094).

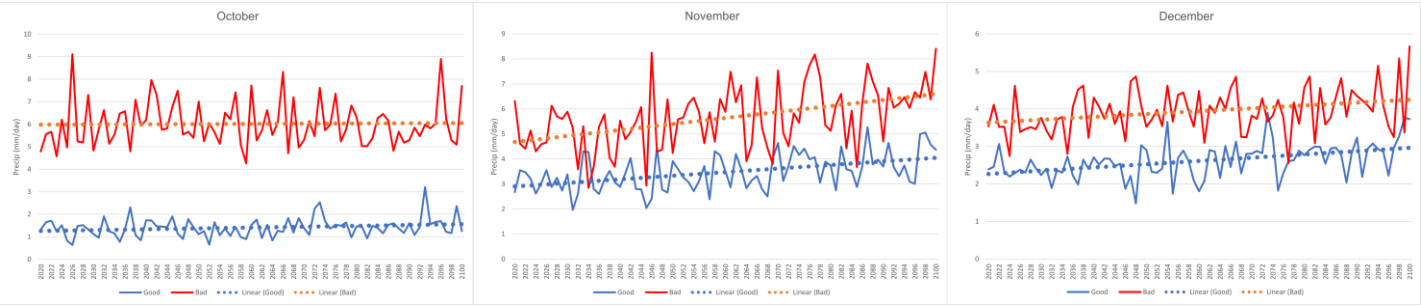


Figure 13.11 – as Figure 13.10 but for OND.

There are also key differences between the 'good' and 'bad' composites during the short rains months (Fig. 13.11). For October, the 'bad' composite is consistently around 5 times wetter than the 'good' composite. It also shows more interannual variability than the 'good' composite ('good' standard deviation = 0.42 mm day^{-1}, 'bad' standard deviation = 0.99 mm day^{-1}). The 'good' composite has a small but significant wetting trend at p<0.1 (0.038 mm day^{-1} decade^{-1}, p = 0.06), whereas there is no trend in the 'bad' composite. For November, the 'bad' composite is again consistently wetter than the 'good' composite by around 2 mm day^{-1}, with both

composites showing wetting trends which are stronger in the 'bad' composite ('good' linear trend = 0.14 mm day^{-1} decade^{-1}, p = 9.7E^{-06}, 'bad' linear trend = 0.24 mm day^{-1} decade^{-1}, p = 2.4E^{-05}). In December, the picture is similar to November. The 'bad' composite is wetter than the 'good' composite until 2100 by a consistent factor, and there are significant wetting trends in both composites ('good' linear trend = 0.09 mm day^{-1} decade^{-1}, p = 3.8E^{-05}, 'bad' linear trend = 0.08 mm day^{-1} decade^{-1}, p = 0.006).

13.5.2. Composite Trend Maps

Figures 13.12 and 13.13 show the spatial patterns of the future rainfall trends in the 'good' and 'bad' composites. Although our analysis focuses on Kenya, an accurate representation of the IOWC should result in more plausible future rainfall projections across East Africa.

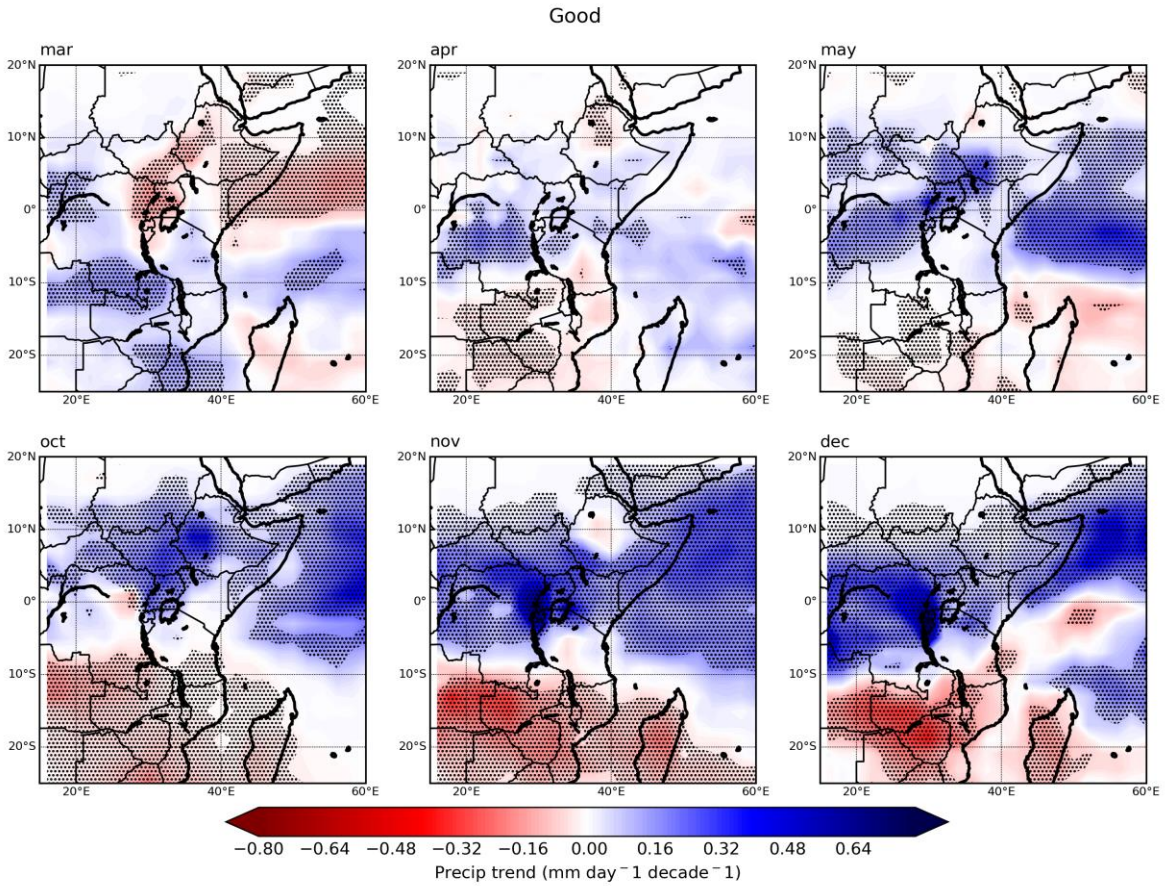


Figure 13.12 - linear regression trends of precipitation over East Africa for the 'good' composites listed in Table 13.5, 2020-2100, RCP8.5. Hatching indicates significance at p<0.1.

In March, the only significant rainfall trends over Kenya in the 'good' composite are found in the extreme east of the country, as part of an area of decreasing rainfall extending across southern Ethiopia and Somalia. Significant drying is also seen in western Ethiopia, South Sudan, and Uganda. Wetting trends are found inland in the Congo Basin area (as in all rainy season months except October), and across northern Angola, and Zambia. In April, there are fewer significant trends in the Greater Horn of Africa, with weak wetting in Kenya and southern Ethiopia. May features stronger wetting trends in northern and central Kenya, southern Ethiopia,

Uganda, and South Sudan, with a band of wetting extending from the Congo Basin and further wetting over the equatorial Indian Ocean (Fig. 13.12).

The short rains are characterised by a strong meridional gradient between wetting north of 10˚S and drying south of it. Stronger trends are found for the short rains months than the long rains. In October the strongest wetting trends are found over the Ethiopian Highlands, while in November and December they are found to the west of Lake Victoria along the DRC's borders with Uganda, Rwanda, and Tanzania. Only the northern tip of Kenya experiences a significant wetting trend in October, but wetting is evident across the whole country in November and December. The Ethiopian Highlands experience a weak drying trend in November, in contrast to the other short rains months.

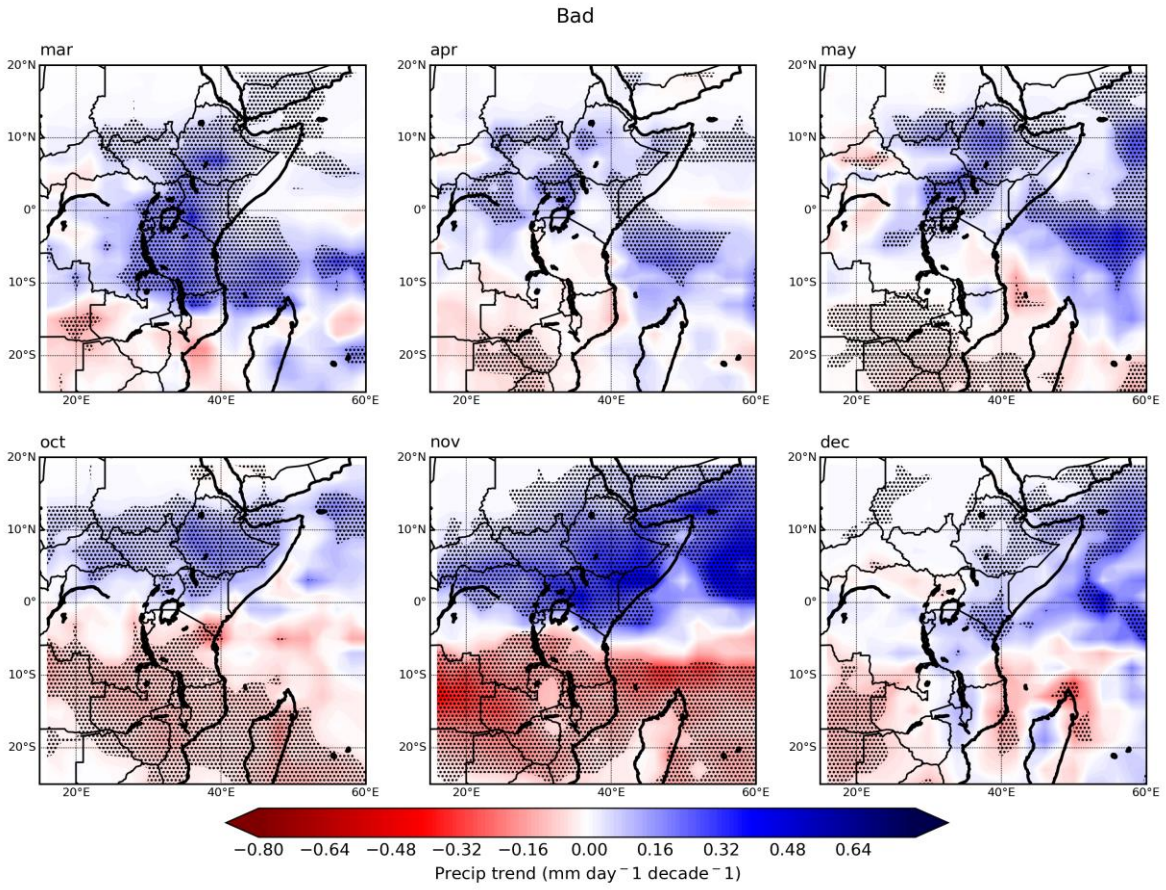


Figure 13.13 - as Figure 13.12, but for the 'bad' composites listed in Table 13.5.

Figure 13.13 shows the spatial patterns of RCP8.5 rainfall change in the 'bad' model composites. In March, there is an extensive and significant increase in rainfall across East Africa, in contrast to the drying signal seen in the 'good' composite (Fig. 13.12). The wetting covers all of Kenya, and most of Ethiopia, South Sudan, Uganda, Rwanda, and Tanzania. There is also no significant wetting over the Congo Basin, unlike in the 'good' composite. In April, wetting is seen in South Sudan and northwestern Kenya, as well as in western Ethiopia which gets drier in the 'good' composite. There are rainfall increases over the Congo Basin but these are mostly to the north of the basin, as opposed to the centre in the 'good' composites. In May, the 'bad' composite features extensive wetting over central Ethiopia but not the Congo Basin, in contrast to the 'good' composite', but the pattern of rainfall change over Kenya is similar with increases concentrated in the Turkana region.

For the short rains months, the 'bad' composite also features a meridional divide between wetting to the north and drying to the south, but the dividing latitude is further north (~5˚S). In October, there is significant wetting in northern Kenya and drying in southern Kenya. The strongest wetting is located further east over Ethiopia than in the 'good' composite, and there is much less wetting over the northwest Indian Ocean. In November, there is a stronger wetting trend across East Africa, including over areas of Ethiopia where the 'good' composite shows drying. The wetting area over the Congo Basin is shifted to the north. In December, trends are less extensive than in the 'good' composite, with increasing rainfall in southern Kenya, but no significant trends across South Sudan and the Congo Basin where strong wetting is seen in the 'good composite'.

13.6. Discussion

We demonstrate that the general wetting trends projected for East Africa in the means of large CMIP5 ensembles do not capture the spread of model projections, in particular for the long rains months where trends are equivocal. The different trends seen in different months of the rainy seasons demonstrate the limitations of taking seasonal averages (Nicholson 2017). For example, during the long rains, not all models project increasing East African rainfall – the condition leading to the 'climate paradox' (Rowell et al. 2015). Although the ensemble mean rainfall trend is statistically significant for all months, only one model in the ensemble (IPSL-CM5A-LR) has significant trends in all months; conversely, a single model, GISS-E2-R, has no significant rainfall trends during the rainy seasons in Kenya during the 21st century. 3 models have a significant rainfall decline in May until 2100. The precipitation increases projected for the short rains were robust across the ensemble (at least during ON), but models disagreed on which month had the more significant rainfall increase. We note that models which are wet (dry) over Kenya in historical coupled runs tend to be wet (dry) in RCP8.5 projections. The majority of models in our ensemble do not have significant rainfall trends during MAM. Therefore, the ensemble mean rainfall averages for both historical and future simulations of the long rains are thus dominated by a few very wet or very dry models. The wet biased models in MAM could be considered more realistic, as the ensemble mean has a dry bias during the season, but King et al. (2020) have shown that these highly biased models have unrealistic dynamics over East Africa and the tropical Indian Ocean in the historical coupled simulations.

In this case where a complex regional climate poses simulation challenges, it is necessary to constrain projections using a process-based methodology that takes into account the differing representation of key regional dynamics (McSweeney et al. 2015, Rowell et al. 2016, Dyer et al. 2020). We use an approach based on previous work linking model representation of the IOWC to historical rainfall biases. We first demonstrate that, as for rainfall, models with particularly strong (weak) IOWCs (as evidenced by vertical velocity over Kenya and zonal wind over the equatorial Indian Ocean) in historical coupled runs continue to feature these biases in RCP8.5 projections. We show the links between changes to IOWC dynamic fields (both vertical velocity and zonal wind) and changes to rainfall over Kenya. We also demonstrate that changes in these IOWC variables are strongly linked to the magnitude of model rainfall change in future. This is in line with work by others arguing that the magnitude (Chadwick et al. 2013) and spatial patterns (Pfahl et al. 2017) of future tropical rainfall change are determined by changes to regional dynamics.

The relationship between wetting and low-level continental westerlies implies that changes to the overturning circulation over the Congo Basin are important in future. The relative strength of each overturning cell, and the location of the region of maximum zonal convergence over East Africa, could therefore be an important determinant of future East African rainfall (Giannini et al. 2018, Creese et al. 2019, Zhao and Cook 2021).

Increasing omega trends over the eastern Congo Basin are consistent with the changes to local overturning in the Congo Basin found by Creese et al. (2019) across wet and dry models in that domain, although a lack of representation of the African Easterly Jet (AEJ) in CMIP5 historical coupled runs casts some doubt on model

projections in this region (Creese et al. 2019). The general pattern of omega decrease to the north of the domain and increase to the south is suggestive of a northward shift of the zone of maximum tropical convergence (Creese et al. 2019).

Fereday et al. (2020) have recently argued that tropical rainfall will also have an increasing dynamic impact on extratropical climate, meaning that an understanding of tropical rainfall dynamics is essential for both near-term predictability and longer-term climate projections on increasingly large spatial scales. We therefore consider these process-based assessments of rainfall projections to be essential for other parts of the tropics, and they must be used for the new CMIP6 model generation. Early results have suggested limited improvements between CMIP5 and CMIP6 in representation of the IOD (McKenna et al. 2020) and the atmospheric consequences of this require further investigation. The question of whether the IOD controls the IOWC or vice versa remains unresolved (Baba 2020, Yang et al. 2020).

The projections and composites indicate an important role for 850hPa zonal winds and 400hPa omega in future East African rainfall, which constitute metrics of the IOWC system. These variables are an important source of uncertainty in future projections because of their erroneous representation in historical coupled models (Hirons and Turner 2018, King et al. 2020). We show that wet minus dry composites in future feature enhanced ascent over East Africa and reduced ascent over the Maritime Continent. Wet models tend towards equatorial easterlies in ON, with stronger easterlies in the southern tropical IO in March-April and in the northern tropical IO in May and December. However, these wet composites, especially for OND, may not be plausible owing to the continuity between wet-biased models featuring erroneous zonal winds in historical coupled runs and these same models being wet in future. For example, of the 4 wettest models in 2070-2100 for ON, 3 had

mean-state easterly zonal winds in 1975-2005 where reanalysis datasets indicate westerlies. Models tend to have stronger easterlies in the region of the Turkana low-level jet (Kinuthia and Asnani 1981) in MAM rather than OND. This may contribute to the models' rainfall biases in the respective seasons, given the links between the jet and regional aridity in northern Kenya (Nicholson 2016b), and the tendency for many models to simulate easterlies at the equator in OND, which could reduce the momentum flux into the Turkana Channel (Hartman 2018). Our results also indicate that strengthening westerly winds over East Africa at 850hPa are associated with wetter conditions over East Africa in RCP8.5, with a westerly wet minus dry composite for 2070-2100 over the region. This supports findings from Dyer and Washington (2020) on the increasing importance of moisture flux from the Congo Basin into East Africa, and the link between low-level westerlies and East African rainfall found by Walker et al. (2020); however, CMIP5 model dynamics over the Congo Basin have been called into question in a number of studies (Washington et al. 2013, Creese and Washington 2016, Crowhurst et al. 2020). Combined with enhanced tropical easterlies over the Indian Ocean, these enhanced westerlies would increase moisture flux convergence over Kenya. This may also reflect a decrease in the strength of the Turkana low-level jet in future (Torralba et al. 2017). Future work on East African climate should investigate the representation of the Walker Circulation cell over the Congo Basin, including the impact of parameterised processes (Crowhurst et al. 2020, Jackson et al. 2020).

Kenya particular underlies an area of climatological descending air in the mid-troposphere, with ascending air to the west (Congo Basin) and east (Indian Ocean). The location of the margins between these zones can determine the rainfall received over East Africa in climate models. The omega trend plots show how East Africa is

also a zone of transition between areas of increasing negative omega (Congo Basin) and increasing positive omega (Indian Ocean). Representation of the topography of the East African highlands is therefore important, as the mountain ranges act as a barrier between these large-scale change regions; the Walker Circulation has been shown to be sensitive to model topography in CMIP5 models (Naiman et al. 2017). Reinforcing the argument that tropical precipitation changes will be determined by shifts in the location of convergence zones (Chadwick et al. 2013), we suggest that greater attention needs to be paid to topography in GCMs, particularly in areas of the tropics with complex relief. This is an area where high-resolution regional modelling can add value, particularly where explicit convection is available (e.g. Stratton et al 2018), and this approach is already yielding improvements (Finney et al. 2019); but care needs to be taken in the selection of the driving GCM given that zonal wind and moisture flux errors may propagate into the RCM as boundary conditions.

Finally, our results have important impacts for future East African rainfall and the issue of the 'climate paradox'. Fewer than half of the models in our ensemble projected significant rainfall increase in the long rains months. By constraining projections using metrics of the IOWC, we find that models with a good simulation of the structure of the overturning circulation over the Indian Ocean show no significant increases in rainfall over Kenya in 2/3 long rains months, and indeed widespread decreases in rainfall across East Africa in March. By contrast, models with inaccurate dynamics show strong wetting trends in March, in opposition to the 'good' models, and more spatially extensive wetting in April and May. This suggests that the 'climate paradox' may be at least partially attributable to increasing rainfall in models with unrealistic representations of the IOWC. The 'good' composite rainfall increases are concentrated in April/May, implying a shift towards a later rainy

season which aligns with projections of increased summer rainfall in CMIP5 (Yang et al. 2015) and a later onset of observed MAM rainfall (Wainwright et al. 2019). This also demonstrates that an approach based on seasonal rainfall averages is not sufficient. The increase in short rains rainfall appears robust in November and December, but 'bad' models are much wetter throughout the 21st century and also have stronger wetting trends. We therefore call into question the ensemble mean rainfall projections in the CMIP5 models, but provide a process basis for assessing the plausibility of projections from individual models that implies a reduced rainfall increase in April and May and a stronger wetting signal in November and December for the remainder of the 21st century under a high warming scenario.

13.7. Conclusions

This article addresses three main questions. Firstly, we determined the rainfall changes projected over Kenya up to 2100 by CMIP5 models under the RCP8.5 scenario for each month in the two rainy seasons. We showed that there is substantial variation between models, and that the most robust trend is towards increasing rainfall in October and November. We also showed how these rainfall changes are dynamically linked to the IOWC, with model rainfall increases associated with a weaker overturning circulation as evidenced by changes to vertical velocity over East Africa (decreasing) and the Maritime Continent (increasing), and enhanced westerly flow over the equatorial Indian Ocean. Secondly, we demonstrated relationships between historical model biases and future trends in rainfall and IOWC fields, and between the magnitude of future changes in rainfall and IOWC fields, across the rainy season months. This demonstrated that processes linked to model

biases in the past are associated with model performance in the future. Thirdly, we used simple metrics of model IOWC representation to constrain rainfall projections, demonstrating that the future of East African rainfall is quantitatively different depending on whether the models selected have realistic or unrealistic IOWC representation. Our results have important implications for East African climate, suggesting that the long rains rainfall increase projected by the ensemble mean, and the resulting 'climate paradox', may result from the disproportionate influence of models with strong wet signals resulting from unrealistic IOWC representation. Smaller rainfall increases later in the season may be a more likely outcome by 2100. Conversely, we find that increasing short rains rainfall is a feature of models with accurate IOWCs, but the spatial patterns vary. The influence of the Congo Basin as a source of moisture needs further investigation, as does the role of model topography in determining the location of future margins of ascent and descent. These results will be useful to help choose GCMs for use in downscaling experiments and impact modelling, and therefore contribute to the evidence basis for climate change impact planning in East Africa. Looking forward to CMIP6, we argue that similar process-based evaluations be carried out to determine the role of IOWC biases in future projections, including elsewhere in the tropics, and particularly the Congo Basin. Finally, given that studies of the IOWC can vary depending on the method used to define the circulation, agreement on a rigorous definition of the IOWC would improve the efficiency of these assessments.

13.8. Acknowledgements

James A. King is funded by the UK Natural Environment Research Council (NERC) through the Doctoral Training Partnership in Environmental Research (grant NE/L002621/1). This work forms part of his doctoral thesis. The CMIP5 data used in this study were downloaded from the UK Centre for Environmental Data Analysis (CEDA), (https://catalogue.ceda.ac.uk/uuid/d2d8f982d66cce55bb59fc769ca39264?jump=related-docs-anchor). MERRA-2 data were downloaded from the NASA Goddard Earth Sciences Data and Information Services Centre (https://disc.gsfc.nasa.gov/datasets?keywords=%22MERRA-2%22&page=1&source=Models%2FAnalyses%20MERRA-2) . CHIRPS data were downloaded from the Climate Hazards Group at the University of California, Santa Barbara (ftp://ftp.chg.ucsb.edu/pub/org/chg/products/CHIRPS-2.0/global_monthly/netcdf/). The authors thank Ellen Dyer and Neil Hart for useful discussions.

14. Conclusions

Our understanding of the impacts of future anthropogenic climate change is derived from climate models, which remain the sole experimental apparatuses available to investigate the effects of warming on climate processes such as rainfall. Particular importance surrounds the projections made using CMIP GCMs, which are used to inform climate policy on a global scale through the work of the IPCC and UNFCCC. Consequently, even for under-resourced and under-studied regions such as East Africa, there has been extensive scientific research into the range of future conditions projected by these models. In East Africa, it is known that CMIP5 models' ability to simulate rainfall accurately is limited, with large biases in seasonality (Yang et al. 2015, Tierney et al. 2015, Ongoma et al. 2019). It is also known that the same models vary in the future rainfall conditions that they project, with an ensemble mean that does not necessarily reflect the behaviour of individual models (Rowell and Chadwick 2018) and is difficult to reconcile with observed rainfall trends (Rowell et al. 2015). Evaluation of models against rainfall data is complicated by uncertainties in the magnitude and direction of the latter owing to limited availability of direct climate observations. East Africa is vulnerable to rainfall change (Thomas et al. 2020), but at present confidence in rainfall projections is low. This thesis takes the view that an interrogation of CMIP5 model processes can address these issues. It is argued that an approach to evaluation of model rainfall based only on comparison with observations is insufficient, and that only by understanding how models simulate key atmospheric processes related to rainfall can the plausibility of their future projections be determined. The thesis has addressed the complex multi-scalar dynamics of the East African climate system through analysing the representation of the large-scale mean state (the IOWC); determining the seasonality, drivers,

relationship to rainfall, and CMIP5 representation of a key feature of the mean state on a meso-scale (the Turkana LLJ); developing a hypothesis on the links between the two features; and examining the plausibility of CMIP5 rainfall projections in light of the dynamic links between the IOWC and East African rainfall. A detailed investigation of climate model performance of this type has not hitherto been undertaken for East Africa, but this approach has yielded important insights into the regional hydroclimate and future climate change trajectories of other African regions.

This concluding chapter summarises the results of the analyses and discusses the implications, with reference to the thesis aims discussed in section 6.2. Section 14.1 outlines the links between East African rainfall, the IOWC, and the Turkana LLJ. Section 14.2 describes how these relationships are represented in CMIP5 models. Section 14.3 evaluates model projections of East African rainfall in light of model performance relative to observations and reanalysis, and sections 14.4 and 14.5 conclude the thesis by discussing its wider implications and suggesting directions for future research.

14.1. Relationships Between Key Atmospheric Processes and East African Rainfall

The first objective of the thesis is **to understand the relationship between the IOWC and East African rainfall in the observed climate**. Analyses were performed using gridded rainfall and reanalysis datasets to address this objective.

14.1.1. The Indian Ocean Walker Circulation

The Indian Ocean Walker Circulation is a zonal overturning cell at the equator, which climatologically features ascending air over the Maritime Continent, easterly flow at 200hPa, descent over East Africa and the western Indian Ocean, and a westerly return flow with a core at 850hPa which completes the cell. It is a coupled ocean-atmosphere system associated with the IOD, ENSO, and the global Walker Circulation. Chapter 11 demonstrates a strong association between the mean state of the atmospheric component of the IOWC in individual months within the East African rainy seasons, as expressed through 400hPa vertical velocity, and the amount of precipitation in those months falling over Kenya. The stronger the descent, the drier the month (r = -0.57- -0.85, $p < 0.05$). This association has been noted by previous studies on the variability of the short rains (e.g. Mutai et al. 2012), but this thesis also finds a relationship between this descent and rainfall in the long rains. While previous studies have not indicated the presence of an IOWC during MAM, this thesis presents plots of 200hPa velocity potential and divergent wind (Fig. 11.3), and 400 hPa vertical velocity (Fig. 11.6), which demonstrate that the zonal structure

of the troposphere over the tropical Indian Ocean is similar in MAM. This suggests that the IOWC is also acting during this season. By constructing streamline plots that act as a cross-section of the troposphere over the Indian Ocean, it is shown that this mid-tropospheric descent is part of the overturning circulation of the wider IOWC (Fig. 11.4). It is important to note here that the IOWC is a mean state feature and as such cannot be invoked as an explanation for rainfall variability on timescales of days to weeks. Rather, this thesis proposes that on monthly and longer timescales, the IOWC influences East African rainfall variability via the relative strength of the descending limb over East Africa, which acts to cap deep convective development and is an explanation for why East Africa is dry compared to other parts of the tropics. This is evident from the association between high pressure anomalies and lower rainfall totals (Camberlin and Wairoto 1997, Camberlin and Okoola 2003), although the equatorial location and consequent interactions with the tropical rainbelt complicate the picture; there is not currently evidence of a clear mid-troposphere high such as that found over southern Africa in summer (Driver and Reason 2017). In particular, the location of the boundary between descending air associated with the IOWC and ascending air associated with overturning over the Congo Basin is important. A weaker IOWC may not extend the region of descent overlying the western Indian Ocean over land, thus decreasing the vertical velocity in the mid-troposphere over East Africa and enabling enhanced moisture flux from central Africa. These results are in agreement with very recently published research indicating that the IOWC strength is negatively correlated with East African rainfall during the short rains and in March, which also highlighted the importance of considering the links between the horizontal and vertical fluxes (Zhao and Cook 2021).

14.1.2. The Turkana Low-Level Jet

The thesis aims **to determine the annual cycle and interannual variability of the Turkana LLJ in reanalysis data**, and further **to investigate the multi-scalar interactions between the wider regional climate and the Turkana LLJ**. The Turkana LLJ is a feature of the East African climate which has been the subject of increased attention in the literature in recent years (Nicholson 2016b, Hartman 2018, Vizy and Cook 2019, MacLeod 2019). However, a complete picture of its mean state, variability, and links to rainfall has yet to be established. Chapter 12 addresses this knowledge gap. The annual cycle of the Turkana LLJ in 3 reanalysis datasets is determined. The LLJ is a persistent feature which is active throughout the year, with peak speeds of 7-9 ms^{-1} between November and March and minimum speeds between July and August (5-6 ms^{-1} in MERRA-2 and ERA5), although the reanalysis datasets differ in their representations of the LLJ. In JRA-55 the jet is barely present during JJA (1 -2 ms^{-1}), and MERRA-2 consistently has jet speeds 2 ms^{-1} higher than ERA5 or JRA-55 during the jet's peak months (Fig. 12.5). This is partially attributable to representation of topography, with MERRA-2 featuring a narrower channel than ERA5 (Fig 12.7; Vizy and Cook 2019), and to the behaviour of the atmosphere in the different reanalyses, with the vertical velocity gradient along the channel greatly reduced in JJA in JRA-55 relative to the other two datasets (Fig. 12.10). Although the spatial patterns vary between the reanalyses, a significant relationship (r = 0.6 over the Indian Ocean and -0.5 over the jet exit region, $p<0.1$) is found between the jet strength and the large-scale zonal pressure gradient between the East African landmass and the western Indian Ocean (Fig. 12.12).

The jet's links to rainfall have previously been examined in the literature on a theoretical basis using reanalysis data (e.g. Hartman 2018) and for August rainfall in South Sudan (Vizy and Cook 2019). An analysis is provided of the spatial correlations between the jet core zonal wind speed and observed rainfall across East Africa during the individual months of the long and short rains (Fig. 12.13). As expected because of its divergent flow (Kinuthia 1992), a strong jet is associated with reduced rainfall in the Turkana Channel itself and throughout Kenya, southern Somalia, and northern Tanzania (r =0.6-0.8, p<0.1). Negative correlations (r = -0.4 - -0.6, p<0.1) between the jet strength (which is negative in the zonal wind component) and rainfall further inland reflect the importance of the jet as a moisture flux vector (Viste and Sorteberg 2013, Munday et al. 2020); a driver of convection at its exit over South Sudan (Vizy and Cook 2019); and potentially a contributor to convective development associated with the African Easterly Jet (Lin 2009).

A preliminary analysis of the Turkana LLJ on interannual timescales suggested a decline in the jet core zonal wind speed since the 1980s. The important influence of the jet on East African rainfall necessitated detailed investigation of this potential jet slowdown, which became an additional thesis objective: **to understand the variability of the Turkana LLJ under recent climate change.** Trends were analysed for each month of the year for 3 reanalyses using linear regression and Mann-Kendall tests (Table 12.1). The trends in the jet varied depending on the reanalysis dataset used, with robust and significant decreases (-0.4 - -0.9 ms $^{-1}$ decade $^{-1}$, p<0.05) in jet strength obtained for most of the months of the year in MERRA-2 and around half the year in JRA-55, using both types of test (Table 12.1). However, no significant decreasing trends were found in the ERA5 reanalysis. There is therefore uncertainty surrounding the existence of this trend, especially given the

lack of publicly available direct observations of the jet. A hypothesis is suggested that would explain the jet decline as a physically plausible consequence of observed patterns of climate change. Enhanced surface heating in the Turkana Channel itself could increase turbulent mixing of the jet flow to the surface (or the duration of daytime turbulent mixing), reducing the jet's momentum. Additionally, strengthening of the IOWC would result in increased surface pressure at the jet exit and decreased surface pressure over the western equatorial Indian Ocean. Given that the jet is negatively correlated with MSLP at the jet exit and positively correlated with MSLP over the Indian Ocean, this would result in a slowing of the LLJ. This hypothesis suggests a dynamic link between the IOWC and the Turkana LLJ, demonstrating the complexity of multi-scalar interactions in the East African climate system, and suggesting that changes to the IOWC may have additional indirect impacts on East African rainfall.

14.2. Representation of Key Atmospheric Processes in CMIP5 Models, and Links to Simulated Rainfall Variability

The next thesis objective is **to assess the representation of the relationships between the IOWC and East African rainfall in CMIP5 historical coupled runs.** Model comparisons against observations and reanalysis are presented. Building on these results, an explanation is developed of **how the representation of the IOWC is related to the spread of CMIP5 model rainfall biases.**

14.2.1. The Indian Ocean Walker Circulation

Chapter 11 demonstrates the links between model simulation of the IOWC and rainfall biases over Kenya in CMIP5 models. Significant negative correlations are obtained (r = -0.8, p<0.05) between model rainfall over East Africa and model vertical velocity at 400hPa over the domain across the ensemble in both rainy seasons, linking the spread of model rainfall biases to the simulation of the IOWC. Figures 11.13, 11.14, and 11.15 indicate that CMIP5 models generally produce too little rainfall during the long rains and too much during the short rains, although in both seasons there are models with opposite biases to the ensemble mean (i.e. wet biases in the long rains and dry biases in the short rains). The spread in model rainfall including both positive and negative biases limits the plausibility that can be ascribed to the ensemble mean during the rainy seasons because of the degree of uncertainty associated with it, as shown in Fig. 14.1. The ensemble includes models which are wetter and models which are drier than the CHIRPSv2.0 values. For example, in March, the CMIP5 ensemble mean has a bias relative to CHIRPSv2.0 of -0.72 mm day^{-1}, but the wettest model has a wet bias of 1.19 mm day^{-1} and the driest model has a dry bias of -1.81 mm day^{-1}. Some model biases are very large compared to the CHIRPSv2.0 monthly rainfall averages. In April, the driest model only produces 16.4% of the CHIRPSv2.0 monthly rainfall and in October, the wettest model overestimates rainfall by 438%.

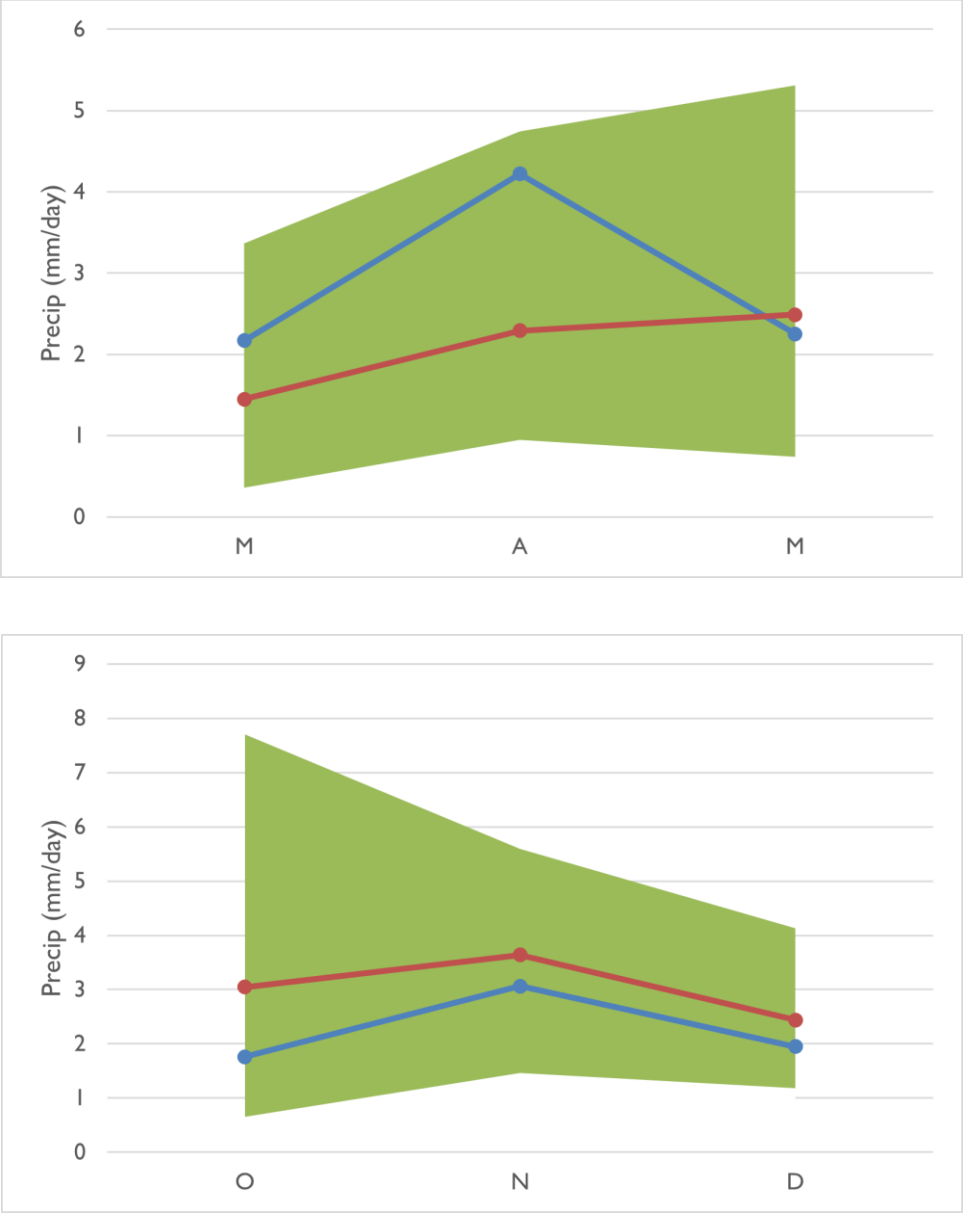


Figure 14.1 – mean 1981-2005 rainfall over Kenya across the rainy season months. Blue = CHIRPSv2.0. Red = CMIP5 ensemble mean. Green – ensemble range (wettest minus driest model).

The differences in biases between individual months also highlights the importance of sub-seasonal analysis of East African rainfall, as argued for by Nicholson (2017) and demonstrated by Dyer and Washington (2020). Composites of wet models during the short rains indicate that the overturning circulation is largely absent over

the equatorial Indian Ocean in OND, with uniform ascent across the basin reflecting a high degree of convective instability (Fig 11.18); coupled with the erroneous easterlies seen in many wet models (Fig, 11.15; Hirons and Turner 2018) which indicate the absence of the low-level westerly flow that makes up part of the IOWC, this results in wet conditions over East Africa. The differences between the wet and dry model composites (Fig. 11.18) reveal that in both rainy seasons, wet models are characterised by anomalous ascent over East Africa above around 900-800 hPa and anomalous descent over the Maritime Continent, reflecting the weaker Walker circulations in these models. The opposite is the case for dry models, where overturning is enhanced as evidenced by stronger and more longitudinally extensive descent over East Africa and enhanced upper-level easterly winds (Fig. 11.18). While the IOWC is more accurately simulated in atmosphere-only models with prescribed SSTs, the correlation between the IOWC and rainfall remains significant (r = -0.6 - -0.7, p<0.05; Fig. 11.17), highlighting that the atmospheric components of the IOWC are important drivers of coupled model rainfall biases in East Africa and that rainfall biases cannot be purely ascribed to errors in either Indian Ocean SST per se, or the zonal SST gradient in the Indian Ocean. These findings contribute to the literature by demonstrating a link between known CMIP5 model errors: the tendency for underrepresentation of long rains rainfall and overrepresentation of the short rains (Tierney et al. 2015); the tendency to overestimate the amplitude of the IOD as a result of unrealistically strong Bjerknes feedback (Cai and Cowan 2013); and the tendency to simulate 850 hPa easterlies rather than westerlies over the equatorial Indian Ocean (Hirons and Turner 2018). These biases have been identified individually, but this thesis argues that they are part of a general poor representation of the IOWC in CMIP5 models and are dynamically interconnected.

14.2.2. The Turkana Low-Level Jet

Chapter 12 extends the analysis of CMIP5 model rainfall processes to address the thesis objective: **to investigate the representation of the Turkana LLJ in CMIP5 historical coupled runs, and how this is related to representation of topography and resolution**. Having determined the spatial nature of the correlation patterns between the Turkana LLJ and rainfall in reanalysis and observations, the thesis assesses whether or not CMIP5 models can represent this. It is found that the ability of CMIP5 models to realistically represent the LLJ is dependent to the first order on their representation of the region's topography. Models which feature a Turkana Channel of sufficient depth and definition can feature realistic jet structures and annual cycles (Figs. 12. 14 and 12.15). However, models without sufficient differentiation between the East African and Ethiopian Highlands and the channel which divides them are unable to represent the jet. In general, models with higher spatial resolution (smaller grid box size) do have more accurate topography, but there are cases where models with identical grid spacing have quantitatively different topography fields, with differences in the elevation of the Turkana Channel sides above sea level of ~500m between BNU-ESM and FGOALS-g2 (Fig. 12.12).

It is evident that if CMIP5 models do not have a realistic representation of the jet, they will not be able to reproduce the spatial patterns of rainfall associated with its variability. This is demonstrated by correlating model rainfall with the zonal wind speed at the real-world location of the jet core (Fig. 12.16). There is little consistency in the spatial patterns of rainfall between the lower resolution models.. Notably, a large-scale meridional structure is evident, with stronger zonal winds at the location

of the jet core associated with opposing signs of rainfall to the north and south of the equator ($r \pm 0.6$, $p<0.1$), but whether the correlations are positive or negative in a particular hemisphere is model- and season-dependent. This structure is most evident during seasons when the Somali Jet is active. Because the Somali Jet core is at the same pressure level as the Turkana LLJ (850 hPa), the thesis hypothesises that the simplified topography in CMIP5 models results in an inland incursion of the Somali Jet core over East Africa, when in the real atmosphere it remains offshore, and that this is responsible for the rainfall correlation pattern; in essence, CMIP5 models are placing the Somali Jet at the location where the Turkana LLJ should be found. This is in agreement with sensitivity experiments demonstrating that the East African topography plays an important role in maintaining the Indian Monsoon circulation of which the Somali Jet is a key component (Slingo et al. 2005, Naiman et al. 2017).

14.3. Projections of East African Rainfall

Having determined how CMIP5 model representation of the IOWC is dynamically linked to rainfall biases in both rainy seasons, CMIP5 rainfall projections are next evaluated with respect to models' representation of key IOWC dynamic variables. This addresses the thesis objective: **to evaluate if and how future East African rainfall projections from CMIP5 models are affected by biases in their simulations of the present-day mean state**. In addition, a composite approach is used based on ranking models by their ability to simulate the IOWC to address the thesis objective: **to propose future rainfall outcomes for East Africa based on model plausibility**.

14.3.1. Links to Historical Model Biases

A process-based approach to evaluation of climate model projections is based on the assumption that simulations of future climatic conditions are less plausible when the models used have unrealistic dynamics in the present-day climate (James et al. 2018). Future projections made with such models are considered unreliable because they are derived from forcings applied to an erroneous baseline; the forced response does not reflect how the actual climate system may plausibly respond to changes in the radiative balance. This can be the case even if output statistics such as rainfall are 'correctly' simulated in historical runs, as James et al. (2015) showed for West Africa.

To improve confidence in projections of East African rainfall, this thesis has examined the model representation of the historical IOWC and the Turkana LLJ. The former is applied as a constraint on model performance; the latter, not being well represented in models generally, is presented as an example of how model development must take account of the importance of realistic topography in Africa (see also Munday and Washington 2018). The CMIP5 experiments allow for rigorous and controlled investigation of model projections because all models use the same prescribed forcing scenarios. The high RCP8.5 scenario is chosen for two reasons: firstly, as the highest available end-of-century radiative forcing increment in CMIP5, it provides the strongest potential for the identification of signals within the extremely noisy climate system; and secondly, that more severe climate change by 2100 is plausible given current socio-economic conditions and emissions trajectories. Having identified the IOWC as a key source of CMIP5 model biases in the historical coupled runs in chapter 11, chapter 13 examines how these biases condition model projections of East African rainfall.

While statistically significant ($p<0.05$) increasing linear rainfall trends are found for all months in the ensemble mean, only in October and November are more than half of the model trends significant (Table 13.1). All long rains months, as well as October, have at least one model with a significant drying trend. The uncertainty that results decreases confidence in projections, especially those using the ensemble mean.

The thesis assesses whether there is continuity between model rainfall biases in the historical coupled runs, and models' future projections. If this is the case, then it is possible that the wet biases and the future wet signal may have a common underlying dynamic cause. This has been found to be the case in central Africa, where Creese et al. (2019) identified historically wet models as still being wet in future for the same reasons that they were wet in the current climate. The thesis finds that the correlation across the ensemble between historical and future rainfall over Kenya is highly positive (r = 0.673-0.908) and statistically significant at the 95% confidence level for all months in the East African rainy seasons (Table 13.2). This indicates that wet (dry) models averaged over the 1975-2005 time slice are generally still wet (dry) at the end of the 21st century (2070-2100) when a high radiative forcing increment is applied.

It is shown that the link between historical and future rainfall across the ensemble is accompanied by a comparable link between historical and future IOWC processes. This is demonstrated by the significant ($p<0.05$) positive correlations (r = 0.798-0.909) between historical and future 400hPa omega over Kenya in all rainy season months except March (Table 13.3). The correlations between historical and future central equatorial Indian Ocean 850hPa zonal wind are significant at 95% and

positive (r = 0.696-0.885) for all rainy season months (Table 13.4). There is consequently a high degree of covariability between past and future rainfall over Kenya, and between past and future IOWC indicators.

The absolute change in rainfall over Kenya in the CMIP5 models (2070-2100 minus 1975-2005) has significant (p<0.05) negative correlations with the absolute 400 hPa omega change (r = -0.679 - -0.930) (Table 13.3, except March) and 850hPa zonal wind change (r = -0.411 - -0.586) over the same period (Table 13.4, all months). This indicates that increasing rainfall over East Africa in both rainy seasons is associated with decreasing omega and enhanced low-level easterlies. The composite differences between the wettest and driest models in 2070-2100 indicate that projections where rainfall increases significantly over East Africa are associated with anomalous ascent over East Africa, descent over the Maritime Continent, enhanced westerlies over continental East Africa, and easterlies in the tropical Indian Ocean (Figs. 13.7, 13.8, and 13.9).

Composite linear regression analysis shows that models with strong wetting trends tend to feature decreasing omega (ascent) over East Africa (-0.003 Pa s^{-1} decade $^{-1}$, p<0.05) which is absent in models with drying or weak wetting trends (Figs. 13.1 and 13.2). Although the picture for zonal winds is less clear, owing perhaps to the substantial model biases in this variable which are already present in historical coupled runs, the models with increasing rainfall exhibit patterns of enhanced continental westerlies and oceanic easterlies (±0.2-0.5 m s^{-1} decade $^{-1}$, p<0.05). Given the high moisture content of air masses originating over the Indian Ocean and the Congo Basin, this would result in enhanced moisture flux convergence and consequently increased rainfall over East Africa.

The differences in the locations of the zone of convergence, as determined by the line of zero zonal wind change dividing the areas of westerly and easterly trend change, suggest that the spatial extent of the changes to the IOWC, as well as changes to its overall strength, is important for future East African rainfall. The interaction of the IOWC with westerly winds from central Africa, particularly those associated with the Atlantic IOWC and local overturning in the Congo Basin, is suggested as an important determinant of East African rainfall change, in agreement with other recent research (Giannini et al. 2018, Walker et al. 2020, Zhao and Cook 2021).

14.3.2. Plausible and Implausible Futures

Having determined that the IOWC influences model rainfall biases in historical coupled runs and continues to impact rainfall simulation throughout the 21st century, the thesis uses metrics of the IOWC to constrain a CMIP5 model ensemble. Using the methodology described in section 13.3.3, 'good' and 'bad' composite projections of Kenyan rainfall are developed based on the RMSE of model 400 hPa and 850 hPa zonal wind relative to the MERRA-2 reanalysis, RMSE of rainfall relative to CHIRPS, and excluding models with zonal winds of the wrong sign over the equatorial Indian Ocean. The results, based on model plausibility rather than 'one model, one vote', indicate a different potential future for East African rainfall than that derived from ensemble means alone (Figs. 13.10 and 13.11). For example, there is no clear wetting trend during the long rains for 'good' models, with no significant change in March or April ($p>0.1$) and a small significant increase in May rainfall (0.081 mm day^{-1} decade $^{-1}$, $p<0.05$). By contrast, the 'bad' ensemble shows a strong rainfall increase in March (0.12 mm day $^{-1}$ decade $^{-1}$, $p<0.05$), but these

models are dry biased so this results in no overall rainfall increase compared to the baseline of the 'good' models.

The spatial maps show differences in large-scale structure between 'good' and 'bad' models. The 'good' ensemble features extensive drying over East Africa in March where there is wetting in the 'bad' ensemble, as well as more intense wetting over Uganda and Rwanda during October and November (Figs. 13.12 and 13.13.) While it is important to note the limitations of referring to the tropical rainbelt in explaining East African rainfall climatology (Nicholson 2017, 2018), the composite projections do suggest that the dynamic differences between models as defined by IOWC representations are to some extent expressed through different timing of the meridional displacement of the rainbelt, especially during the long rains (Dunning et al. 2018). The fact that the 'bad' ensemble based on IOWC metrics was drier than the 'good' ensemble in March and April, when it is known that CMIP5 models generally are predisposed to dry biases, supports the contention that the IOWC can account for model rainfall biases over East Africa during both rainy seasons.

For the short rains, precipitation increases are robust in the 'good' ensemble for November (0.14 mm day^{-1} $decade^{-1}$, $p<0.05$) and December (0.09 mm day^{-1} $decade^{-1}$, $p<0.05$), and it is these months in which the rainfall increases across all months in the study are concentrated. Neither ensemble produces a rainfall trend in October. The 'bad' models are wetter than the 'good' models in all short rains months, demonstrating how the IOWC can be linked to the wet biases of CMIP5 models in this season. The fact that the 'good' ensemble reveals plausible precipitation trends on a sub-seasonal timescale shows the importance of avoiding seasonal averaging when investigating the dynamics of East African rainy seasons, whether in models, reanalysis, or observations (Nicholson 2017). Furthermore, it is suggestive of a shift

in the timing of East African rainy seasons. During the long rains, the 'good' composite features significant wetting in April and lower rainfall totals than the 'bad' composite in May, which reflects a contraction of the long rains; during the short rains, 'good' models project significant increases in rainfall in November and December only.

These findings are in agreement with recent work on onset and cessation dates of rainy seasons over the bimodal rainfall regions of equatorial Africa (Dunning et al. 2016, Wainwright et al. 2019) which emphasise that recent decreases in the long rains are due to a shorter rainy season, but projected rainfall increases during the short rains are related to a shift towards rainfall later on in the season and the season itself ending later (Dunning et al. 2018). This lends credence to the confidence in the 'good' composite projections.

It is noteworthy that the models that are 'good' and 'bad' in each month are not the same, and that it is possible in this framework for a model to be 'good' in one month and 'bad' in another (e.g. ACCESS-1-3, which is 'good' in May but 'bad' in November); this does have the effect of ensuring that the composites are not consistently dominated by signals from one or two idiosyncratic models. Models from the same centre can be 'good' and 'bad in the same season, highlighting how small differences in model design can have substantial impacts (e.g. in May, IPSL-CM5A-LR is 'good' but IPSL-CM5B-LR is 'bad'). However, no individual model is included as both 'good' and 'bad' within the same rainy season, implying that model dynamic biases are seasonally varying and some models may be more sensitive to seasonal modes of internal variability (such as ENSO and the IOD) than others; the time-variance of internal variability teleconnections to East Africa in coupled versus atmosphere-only models requires further investigation.

Several models emerge as consistently 'good' (e.g. MIROC-ESM-CHEM) or 'bad' (e.g. BNU-ESM). It is acknowledged that there are a number of different ways of approaching the problem of how to constrain uncertain projections of East African rainfall (McSweeney et al. 2015, Rowell et al. 2016, Ongoma et al. 2019, Dyer and Washington 2020), which can result in different conclusions as a result of differing research priorities. For example, in a study encompassing multiple continents, McSweeney et al. (2015) identify CanESM2 as a poorly performing model over Africa generally, but Ongoma et al. (2019) identify it as performing well for East African rainfall specifically. McSweeney et al. (2015) also count MIROC-ESM-CHEM as a poor model on a global scale, but it performs well against reanalysis and observations over East Africa in this assessment. Our assessment suggests that configurations of IPSL-CM5 perform well with respect to IOWC indices in OND, but Rowell and Chadwick (2018) find that this model projects very large increases in rainfall during MAM as a result of anomalously strong SST warming in the southern Indian Ocean; a projection Rowell (2019) finds to be unrealistic based on observational constraints of the links between MAM rainfall and SST, leading him to argue against its inclusion in MAM projections. It is challenging to constrain a model ensemble in conditions where model performance generally is low (Sanderson and Knutti 2012), and the thesis does not argue that different subsets of models should be used for projections in different months in East Africa. Rather, attention is drawn to how the representation of the IOWC affects rainfall projections. This can add to existing work on interpreting rainfall projections (Rowell and Chadwick 2018) and on developing model metrics over East Africa (Dyer and Washington 2020).

For the purposes of submitting chapter 13 as a paper, the separation of low-error and high-error models as 'good' and 'bad' was largely done for the purposes of

convenience in the interpretation of the results and figures. However, it is acknowledged that a more sophisticated approach to model selection is required when making projections that will be used to inform policy, in light of evaluation of other aspects of model performance over East Africa (e.g. Rowell 2019, Dyer and Washington 2020). In this sense, the 'good' and 'bad' models are only 'good' or 'bad' with respect to the specific criteria applied in the thesis; that is, a 'good' model is more specifically a model with low RMSE in rainfall, zonal wind, and vertical velocity fields when compared to observed rainfall and reanalysis circulation. Therefore, when the thesis refers to a model as 'good', the inverted commas are used to remind the reader of this fact. A model that scores well in one set of process-based evaluation criteria may not score well in another, and an approach based on multiple criteria is required (James et al. 2018). This may require some compromise, but can also focus attention on selecting models based on the specific questions which their outputs will be used to answer rather than simply using all available data (Ross and Najjar 2019).

This thesis provides a process-based way forward with an explicit focus on the processes relevant to simulating the East African climate, with clear dynamic reasoning that draws attention to some important issues with CMIP5 models and highlights important directions for fundamental research on the climate of East Africa. Nevertheless, the IOWC is not the only process affecting East African rainfall, and a synthesis of multiple approaches to climate model evaluation over the region is recommended.

14.4. Suggestions for Future Research

This thesis has highlighted a number of possible future research directions on East African rainfall, both in terms of improving our understanding of real-world climate variability and change, and in further evaluating and improving climate models. This section discusses the research foci that are considered to be the most promising, in order to address the thesis objective: **to suggest future directions for research into East African rainfall and climate model evaluation**.

14.4.1. Foci for Model Development

An objective of the thesis has been **to identify foci for improving representation of East African rainfall in future generations of climate models**. This thesis has demonstrated how the IOWC is not generally well simulated by CMIP5 models and that this reduces confidence in projections of East African rainfall. However, the IOWC is a complex coupled ocean-atmosphere system; improving its representation in models necessitates attention to a number of different elements of a GCM. The tendency of coupled models to exhibit significant SST biases has been well documented (Yang et al. 2014). These biases can be of similar magnitude to anthropogenic climate change signals (~2˚C), and have persisted from CMIP3 to CMIP5. The zonal gradient in Indian Ocean SST is a particular problem for simulation of East African rainfall, because the SST biases tend toward a positive IOD state that results in excessive rainfall in OND through modification of the IOWC (Cai and Cowan 2013). A major challenge in coupled modelling is the rapid development of these biases during model spin-up owing to

the interaction between wind and SST, which has been suggested to drive the positive IOD bias because of the overestimation of Bjerknes feedback in the tropical Indian Ocean (Cai and Cowan 2013). SST biases are widely acknowledged issues with CMIP models, and efforts are ongoing to reduce their impact on tropical oceans (Zuidema et al. 2016). These efforts should improve representation of East African rainfall. A related issue is the coupling between SST and zonal wind over the equatorial Indian Ocean. These zonal winds are a major source of model rainfall biases in East Africa via unrealistically high moisture flux into the region (Hirons and Turner 2018). Erroneous winds can be driven by the positive IOD state (Cai and Cowan 2013), but the chain of causality in this coupled system is unclear. Explicit representation of moist processes is generally beyond conventional supercomputing, and advances have been made in East African rainfall simulation using high-resolution regional models with explicit convection (Finney et al. 2019, 2020). However, regional model projections require GCM input as boundary conditions. This means that the parameterisations in GCMs still exert an influence. Some of the parameterisations which are involved in GCM simulations of convection-driven circulations such as the IOWC, for example those for grid-box-scale convective mass flux, remain unsophisticated compared to other recent developments in climate model design (Rio et al. 2019, Mukhopadhyay and Roy 2020). This thesis echoes Zuidema et al. (2016) in arguing for greater attention to be drawn to the performance of model parameterisations over the Indian Ocean. Accurate representation of the IOWC and East African rainfall relies on reliable parameterisations of oceanic convection and wind stress; horizontal mass and moisture advection; coupling between horizontal and vertical mass fluxes in an overturning circulation, in particular between the lower and upper troposphere; and triggering of rainfall by small-scale turbulent processes such as those associated with the Turkana LLJ (Vizy and Cook 2019).

Detailed investigation into the configuration of relevant parameterisations over the Indian Ocean and East Africa may yield additional insights into model biases and provide a further basis for constraining projections, an approach which is beginning to be applied to other African regions with uncertain rainfall projections such as the Congo Basin (Crowhurst et al. 2020). Convection-permitting models may be preferred if computationally feasible. The application of novel approaches to evaluating climate models and identifying key sources of error in East African rainfall simulation is also to be encouraged. For example, machine learning approaches such as causal discovery networks can be used to identify how well models represent the observed relationships between circulation features, including African rainfall (Nowack et al. 2020). In the seasonal forecasting community, nonlinear statistical modelling is increasingly being used to identify the most important dynamical processes that influence rainfall, information which can then be fed back into the process of dynamical model development (Hall et al. 2019). This approach may be valuable for East Africa where, as Nicholson (2015) has shown, the IOWC-modulated teleconnection between ENSO and East African rainfall is nonlinear and has varied in strength throughout the 20th century. The application of nonlinear statistical modelling of European rainfall by Hall et al. (2019) was motivated by an analogous finding demonstrating time-dependence of teleconnections between European climate and the North Atlantic Oscillation (Weisheimer et al. 2016).

The influence of the Turkana LLJ on East African rainfall poses an additional challenge for GCMs, as the small spatial scale of the topography which drives it is not sufficiently well represented in many coarser-scale models. This is important across eastern and southern Africa because of the wider significance of low-level jets for moisture transport and convergence elsewhere, not just in the Turkana region

(Munday et al. 2020). This is a key area where downscaled RCM simulations can add value – as long as the large-scale flow is accurately simulated by the driving GCM, given the links uncovered in this thesis and by others between the Turkana LLJ and the wider synoptic (Vizy and Cook 2019) and climatological (Lin 2009 and see chapter 12) situation. This has also been identified as an issue in southern Africa, where similarly complex topography limits the ability of many CMIP5 GCMs to represent moisture flux pathways seen in reanalysis (Munday and Washington 2018). The results in section 12.4.3 suggest a minimum horizontal resolution of ~1.25° is required in a climate model to represent the Turkana Channel topography to a good enough degree for an LLJ to form within it. This means that higher-resolution GCMs could be favoured over East Africa and Kenya especially. The attention of the climate model evaluation community should be drawn to understanding why models with the same resolution have differing representations of underlying topography, and encourage more modelling groups to make transparent the process by which observationally-derived topographic data are translated into climate models.

14.4.2. Definition of the IOWC

As highlighted in chapters 7 and 11, there exists some ambiguity as to the exact definition of the Indian Ocean Walker Circulation. The complex nature of the system mean that a number of different atmospheric variables can be used to investigate its dynamic structure, measure its intensity, and perform trend analysis, with results to some extent dependent on the methodology and time period used to compute trends (see section 7.3 for a discussion). Published work using surface pressure and low to

mid tropospheric indicators such as vertical velocity has suggested a strengthening of the Walker Circulation in the Pacific (L'Heureux et al. 2013) and globally (McGregor et al. 2014), but upper-level circulation indices have suggested weakening (Tanaka et al. 2004). It is important to note that shifts in the location, rather than the magnitude, of tropical convergence and divergence have been noted to drive low latitude rainfall change in CMIP5 models (Chadwick et al. 2013), and that idealised model experiments support the contention that the Walker Circulation response to warming may be more complex than a straightforward intensification or weakening (Dhame et al. 2020). The disagreements between different studies of recent trends requires further investigation using atmosphere-only models where the circulation response cannot be controlled by model biases in the zonal SST gradient or by potentially unrealistic parameterisations related to oceanic heat flux. Additionally, the shifts in the locations of convergence/divergence maxima associated with climate change imply that approaches to the IOWC that do not rely on observations from weather stations or static area-averaging may be of value. An example would be an empirical orthogonal function (EOF) approach, which applies principal component analysis to atmospheric fields to identify areas of significant covariance. Multivariate EOF indices can be used to track trends in modes of climate variability such as ENSO using multiple salient dynamic fields, an approach which would seem to be applicable to the multiple variables that together make up the IOWC. However, caution must be taken in the interpretation of EOFs because the patterns identified do not have an *a priori* basis in atmospheric dynamics. Nevertheless, it would be advantageous to develop a rigorous definition of the IOWC, incorporating both its zonal and vertical components, as well as its three-dimensional structure (Zhao and Cook 2021). This would enable clearer answers to the questions surrounding its annual cycle and recent trends. Investigation of future projections and links to

rainfall would also be more straightforward. At least one ongoing research programme is attempting to develop an IOWC index (S. Zhao and K. Cook, personal communication) and the community is urged to make use of it when it becomes available. More detailed investigation of the mechanisms by which the IOWC controls East African rainfall is also encouraged, for example by analysing strong/weak IOWC composites of atmospheric stability profiles and moist static energy (MSE).

14.4.3. The Future of the Turkana LLJ

Chapter 12 raises important questions about the future of the Turkana LLJ and the consequent implications for future East African rainfall. Most important among these is the need to ascertain whether or not the declining trends in the jet core zonal wind speed are realistic. These trends are present in MERRA-2 and JRA-55, but not ERA5, and the analysis in chapter 12 indicates a number of differences between the reanalyses over East Africa in terms of the jet's climatology. These include variations in jet speed, the annual cycle, and the jet's covariability with surface pressure. Related to this are the different surface heating trends observed in each reanalysis. Further investigation of the mechanisms controlling the Turkana LLJ using model experiments is encouraged, as the experimental tools available have advanced significantly since the published RCM study by Indeje et al. (2001). These experiments should focus on the relationship between the jet and regional temperature and pressure changes observed over the experimental period, testing the hypotheses presented in chapter 12 that could explain a slowing jet (enhanced turbulent mixing from surface heating and/or a change in the zonal pressure

gradient from continental East Africa to the tropical Indian Ocean). Combined with constrained GCM projections as boundary conditions, RCM studies could also determine whether there are any projected future trends in jet strength and if these too are physically plausible. Insights into the future of East African rainfall may thus be gained, given the broadening evidence base demonstrating links between the LLJ and rainfall (Vizy and Cook 2019, Munday et al. 2020). A slowing jet may contribute to rainfall trends; the extent to which variability in the jet explains observed and projected rainfall variability over East Africa is another question high-resolution RCMs such as CP4Africa (Stratton et al. 2018) could answer. The increases in seasonal rainfall observed in northwestern Kenya over the period 1981-2016 (Gebrechorkos et al. 2019) could be associated with a slowing jet, for example. Sensitivity experiments where the Turkana Channel is 'filled in' by modifying model topography could also enhance our understanding of its impacts on the local and regional circulation, building on existing work showing the importance of East African topography in constraining the Indian Monsoon and the IOWC (Slingo et al. 2005, Naiman et al. 2017). The analysis of CMIP5 models presented in chapter 12 also suggests a hypothesis that the Somali Jet extends inland over Kenya to an unrealistic degree in some models, obscuring the effects of the Turkana LLJ. This too should be investigated further, potentially also with sensitivity experiments or a hierarchy of models with different spatial resolutions but the same dynamic core. This experimental setup would be possible using different configurations of the UK Met Office Unified Model (Walters et al. 2017).

In addition, the differences between the reanalyses need to be accounted for, as this has implications for the selection of datasets in East African climate research. High-resolution modelling studies can partially address this issue, but there remains a

need for the reanalyses to be directly compared to observations. Surface wind measurements exist from meteorological stations along the Turkana Jet axis, but these are of limited value in measuring winds aloft, and are not judged to be of high quality. This means that any increase in surface winds, which would be a consequence of increased thermal mixing of the jet's momentum down to the surface, cannot at present be determined. Observational constraints on the jet are currently limited to the pilot balloon measurements of Kinuthia and Asnani (1982) and Kinuthia (1992). Pilot balloons are limited in their ability to measure low-level jets, and do not provide information on jet moisture content. A recommendation for a future research project is that a campaign of targeted observations using LIDAR be undertaken in the Turkana Channel to observe the structure of the jet directly and investigate its links to the wider synoptic situation. LIDAR has been used to investigate other African low-level jets (Allen and Washington 2013) and can be used to investigate the effects of surface heating on LLJ diurnal cycles (Carroll et al. 2019) as well as real-time measurements of moisture content (e.g. Mattis et al. 2002). LIDAR is used in industry for feasibility studies of wind power (e.g. Li and Yu 2017), and there is a large wind farm located within the Turkana Channel and another under construction in the Ngong Hills in southern Kenya. The Kenyan government and energy utility companies are encouraged to consider sharing wind data from the installations and any LIDAR monitoring undertaken with the scientific community (C. Wainwright, personal communication).

14.4.4. Additional Outstanding Issues in East African Rainfall Research

For the purpose of analysing regional atmospheric dynamics, it is necessary to divide the climate system into distinct spatial domains. However defined, these are always to some extent arbitrary. Through analysis of the IOWC and Turkana LLJ, this thesis has suggested a link between the two systems which warrants further investigation. It is also the case that the circulations over the Congo Basin (Giannini et al. 2018), tropical Atlantic (Zhao and Cook 2021), and tropical Pacific (Nicholson 2015) all exert an influence on East African rainfall. A comprehensive understanding of rainfall projections therefore requires investigation of how these different systems are linked. Research should focus on how the zonal pressure gradient exerted by the IOWC affects the Turkana LLJ, and how the annual cycle and interannual variability of the IOWC interacts with zonal overturning cells elsewhere in the tropics, whether considered as individual systems or as part of the global Walker Circulation. This has important implications for seasonal forecasting of East African rainfall, particularly if modes of variability are revealed which exert a strong influence on the long rains.

This thesis has mainly focused on the present-day East African rainy seasons of March-April-May and October-November-December. However, changes in the timings of East African rainy seasons are important, as evidenced by chapter 13 and work by Dunning et al. (2016) and Wainwright et al. (2019). Increases in rainfall are projected for East Africa in seasons which are currently dry, such as June-July-August and December-January-February, particularly under high levels of global warming (James and Washington 2013). The role of the IOWC and the Turkana LLJ in these months should be determined; for example, chapter 12 shows that the Turkana LLJ is weakest during JJA, meaning that jet-related divergence would not

act to prevent an increase in moisture flux convergence over Kenya in this season as much as during the long and short rains. Finally, this thesis has focused on the CMIP5 model generation, which represented the state-of-the-art as the research was being undertaken. At the time of submission (January 2021), data from the new CMIP6 generation is beginning to be released. The methods and approaches used here are applicable to future model generations, and it is argued that any investigation into the representation of East African rainfall in CMIP6 and beyond takes into account the effects of the IOWC and the Turkana LLJ. Examination of improvements in representation of East African rainfall from CMIP5 to CMIP6 will enable further developments of constrained projections, and should reveal whether improvements in model processes have yielded results in East Africa. Early results indicate that warming is increased in CMIP6 models relative to CMIP5 and precipitation increases are projected for East Africa in high scenarios, but the range of uncertainty in rainfall projections is still greater than the magnitude of the ensemble mean rainfall change (Almazroui et al. 2020). It is argued that the model development community and the model evaluation community should build closer links in order to guide future model intercomparison projects, since changes to model design between CMIP generations do not necessarily lead to improvements in representation of key features of the climate system (Knutti et al. 2013, Bock et al. 2020).

14.5. Implications for Policy

This thesis has argued that projections of rainfall change in East Africa can be constrained by the application of process-based analysis. It has further demonstrated

the importance of the IOWC and Turkana LLJ, and shown how these may influence projections. Models with better IOWC representation project a wetter future for East Africa during OND, but potentially a shorter rainy season in MAM. Meanwhile, the Turkana LLJ may be slowing down. If these projections are reliable, there are important implications for climate change adaptation in East Africa. Increased OND rainfall could lead to more severe flooding, but maintains the potential for small-scale hydropower to improve livelihoods in rural areas (Kaunda et al. 2012). Conversely, increased rainfall combined with warming may enhance the spread of water- and mosquito- borne diseases (Onyango et al. 2016). A shorter, more intense long rains would have major impacts on agriculture given that this is the primary growing season, and would require investment in irrigation and small-scale flood control measures, as well as careful selection of crop varieties. Further refinement of rainfall projections in MAM is of paramount importance. The slowing of the Turkana LLJ may result in increased rainfall in the arid Turkana region, but could reduce rainfall in South Sudan and Ethiopia as a result of decreased moisture flux. Further inland, the impact on MCS generation could be significant over central and West Africa. A decrease in the generating capacity of the Lake Turkana wind power project could also result, with implications for regional development and decarbonisation of Kenya's energy sector. This is particularly important in light of recent work suggesting that renewable energy will have a limited role in future development of Africa's electricity infrastructure (Alova et al. 2021).

There is no dichotomy between adapting to the impacts of climate change and mitigating against its causes. However, progress on the latter has not been forthcoming, despite the efforts of international organisations. Climate science has demonstrated the need to reduce carbon emissions. It must now address the pressing

issue of climate change adaptation in areas, such as East Africa, which face an uncertain future as a result of continued inaction on emissions on the part of the countries in which most climate science research is undertaken. It is to be hoped that such work can continue in spite of the UK government's damaging and short-sighted cuts to research funded by the overseas aid budget, which were announced during the editing of this thesis. The CMIP programme is an important resource, and climate science has a moral obligation to make the most of it. This thesis has demonstrated how process-based climate model evaluation can help refine rainfall projections in East Africa, and motivate further research into the mechanisms of climate change in the region. I hope that the research presented here will make a small contribution towards the great task of climate change adaptation.

15. Bibliography

Ackerley, D., B. B. B. Booth, S. H. E. Knight, E. J. Highwood, D. J. Frame, M. R. Allen, and D. P. Rowell, 2011: Sensitivity of Twentieth-Century Sahel Rainfall to Sulfate Aerosol and CO2 Forcing. *J.Climate*, **24**, 4999-5014.

Addor, N., M. Rohrer, R. Furrer, and J. Seibert, 2016: Propagation of biases in climate models from the synoptic to the regional scale: Implications for bias adjustment. *J. Geophys. Res. Atmos.*, **121**, 2075– 2089,

Albergel, C., E. Dutra, S. Munier, J-C. Calvet, J. Munoz-Sabater, P. de Rosnay, and G. Balsamo, 2018: ERA-5 and ERA-Interim driven ISBA land surface model simulations: which one performs better? *Hydrol. Earth Syst. Sci.*, **22**, 3515–3532.

Allen, C. J. T., and R. Washington, 2013: The low-level jet dust emission mechanism in the central Sahara: Observations from Bordj-Badji Mokhtar during the June 2011 Fennec Intensive Observation Period, *J. Geophys. Res. Atmos.*, **119**, 2990– 3015.

Allen, M.R., D.J. Frame, C. Huntingford, C.D. Jones, J.A. Lowe, M. Meinshausen, and N. Meinshausen, 2009: Warming caused by cumulative carbon emissions towards the trillionth tonne. *Nature*, **458**, 1163–1166.

Alemazung, J.A., 2010: Post-Colonial Colonialism:An Analysis of International Factors and Actors Marring African Socio-Economic and Political Development. *J. Pan African Studies*, **3**, 62-84.

Almazroui, M, F. Saeed, S. Saeed, M. Nazrul Islam, M. Ismail, N. A. Browne Klutse, and M. H. Siddiqui, 2020: Projected Change in Temperature and Precipitation Over Africa from CMIP6. *Earth Systems and Environment*, **4**, 455-475.

Alova, G., P.A. Trotter, and A. Money, 2021: A machine-learning approach to predicting Africa's electricity mix based on planned power plants and their chances of success. *Nat. Energy*. doi: 10.1038/s41560-020-00755-9

Ambaum, M. H. P., 2010: Significance Tests in Climate Science. *J. Climate,* **23**, 5927-5932.

Awange, J., V. G. Ferreira, E. Forootan, Khandu, S.A. Andam-Akorful, N. O. Agutu, and X. F. He, 2016: Uncertainties in remotely sensed precipitation data over Africa. *Int. J. Climatol.*, **36**, 303-323.

Baba, Y. 2020: Roles of atmospheric variabilities in the formation of the Indian Ocean Dipole. *Ocean Dynam.* **70**, 21-39.

Balfour, N., J. Obando, and D. Gohil, 2020: Dimensions of water insecurity in pastoralist households in Kenya. *Waterlines*, **39**, 24-43.

Bari, S. H., M. Tauhid Ur Rahman, M. Azizul Hoque, and M. Manjurul Hussain, 2016: Analysis of seasonal and annual rainfall trends in the northern region of Bangladesh. *Atmos. Res.*, **176-177**, 148-158.

Baumberger, C., R. Knutti, and G. Hirsch Hadorn, 2017: Building confidence in climate model projections: an analysis of inferences from fit. *WIREs Clim. Change*, **8**, e454.

Behera, S.K. and T. Yamagata, 2001: Subtropical SST dipole events in the southern Indian Ocean. *Geophys. Res. Lett.*, **28**, 327-330.

-., J-J. Luo, S. Masson, P. Delecluse, S. Gualdi, A. Navarra, and T. Yamagata, 2005: Paramount impact of the Indian Ocean Dipole on the East African short rains: a CGCM study. *J. Climate*, **18**, 4514-4530.

Belmonte Rivas, M. and A. Stoffelen, 2019: Characterizing ERA-Interim and ERA5 surface wind biases using ASCAT. *Ocean Sci.*, **15**, 831–852.

Berhane, F. and B. Zaitchik, 2014: Modulation of daily precipitation over East Africa by the Madden-Julian Oscillation. *J. Climate*, **27**, 6016-6034.

Bhatt, U.S., 1989: Circulation Regimes of Rainfall Anomalies in the African-South Asian Monsoon Belt. *J. Climate,* **2,** 1133-1144.

Birkett, C., R. Murtugudde, and T, Allan, 1999: Indian Ocean Climate event brings floods to East Africa's lakes and the Sudd Marsh. *Geophys. Res. Lett.* **26**, 1031-1034.

Bjerknes, J. 1969: Atmospheric Teleconnections from the Equatorial Pacific. *Mon. Weather Rev.* **97**, 163-172.

Black, E., J. Slingo, and K.R. Sperber, 2003: An observational study of the relationship between excessively strong short rains in coastal East Africa and Indian Ocean SST. *Mon. Weather Rev.,* **131**, 74-94.

-, 2005: The relationship between Indian Ocean sea-surface temperature and East African rainfall. *Phil. Trans. R. Soc. A.*, **363**, 43-47.

Blunden, J. and D. S. Arndt, Eds., 2020: State of the Climate in 2019. *Bull. Amer. Meteor. Soc.*, **101**, Si–S429.

Bock, L., A. Lauer, M. Schlund, M. Barreiro, N. Bellouin, C. Jones, G. A. Meehl, V. Predoi, M. J. Roberts, and V. Eyring, 2020: Quantifying progress across different CMIP phases with the ESMValTool. *J. Geophys. Res. Atmos.* **125**, e2019JD032321.

Boos, W.R. and K.A. Emanuel, 2009: Annual intensification of the Somali jet in a quasi-equilibrium framework: Observational composites. *Q.J.R. Meteorol. Soc.*, **135**, 319-335.

Borgomeo, E., B. Vadheim, F.B. Woldeyes, T. Alamirew, S. Tamru, K.J. Charles, S. Kebede, and O. Walker, 2018: The Distributional and Multi-Sectoral Impacts of

Rainfall Shocks: Evidence from Computable General Equilibrium Modelling for the Awash Basin, Ethiopia. *Ecol. Econ.,* **146**, 621-632

Boschat, G., I. Simmonds, A. Purich, T. Cowan, and A. Bernardes Pezza, 2016: On the use of composite analyses to form physical hypotheses: An example from heat wave – SST associations. *Sci. Rep-UK*, **6**, 29599.

Brown, C., P. Alexander, A. Arneth, I. Holman, and M. Rounsevell, 2019: Achievement of Paris climate goals unlikely due to time lags in the land system

Cai, W., and T. Cowan, 2013: Why is the amplitude of the Indian Ocean Dipole overly large in CMIP3 and CMIP5 models? *Geophys. Res. Lett.*, **40**, 1200-1205.

-, G. Wang, A. Santoso, M. J. McPhaden, L. Wu, F-F. Jin, A. Timmermann, M. Collins, G. Vecchi. M. Lengaigne, M. H. England, D. Dommenget, K. Takahashi, and E. Guilyardi, 2015: Increased frequency of extreme La Niña events under greenhouse warming. *Nat. Clim Change* **5,** 132–137.

Camberlin, P. and J. Wairoto, 1997: Intraseasonal wind anomalies related to wet and dry spells during the "long" and "short" rainy seasons in Kenya. *Theor. Appl. Climatol.*, **58**, 57–69.

- and R. E. Okoola, 2003:, The onset and cessation of the "long rains" in eastern Africa and their interannual variability. *Theor. Appl. Climatol.*, **54**, 43–54.

-, V. Moron, R. Okoola, N. Philippon, and W. Gitau, 2009: Components of rainy seasons' variability in Equatorial East Africa: onset, cessation, rainfall frequency and intensity. *Theor. Appl. Climatol.*, **98**, 237-249.

Carroll, B. J., B. B. Demoz, and R. Delgado, 2019: An overview of low-level jet winds and corresponding mixed layer depths during PECAN. *J, Geophys. Res. Atmos.* **124**, 9141– 9160.

Chakravorty, S., J. S. Chowdary, and C. Gnanaseelan, 2014: Epochal changes in the seasonal evolution of tropical Indian Ocean warming associated with El Niño. *Clim. Dyn.* **42**, 805-822.

Chakravorty, S., C. Gnanaseelan, J. S. Chowdary, and J-J. Luo, 2014: Relative role of El Niño and IOD forcing on the southern tropical Indian Ocean Rossby waves, *J. Geophys. Res. Oceans*, **119**, 5105– 5122.

Chadwick, R., I. Boutle, and G. Martin, 2013: Spatial patterns of precipitation change in CMIP5: why the rich do not get richer in the tropics. *J. Climate*, **26**, 3803-3822.

Chai, T. and R. R. Draxler, 2014: Root mean square error (RMSE) or mean absolute error (MAE)?– Arguments against avoiding RMSE in the literature. *Geosci. Model. Dev.* **7**, 1247-1250.

Chambers, D. P., B. D Tapley,, and R. H. Stewart, 1999: Anomalous warming in the Indian Ocean coincident with El Niño. *J. Geophys. Res.*, **104**, 3035– 3047.

Chan, R. Y., M. Vuille, D. R. Hardy, and R. S. Bradley, 2008: Intraseasonal precipitation variability on Kilimanjaro and the East African region and its relationship to the large-scale circulation. *Theor. Appl. Climatol.* **93,** 149–165.

Cherchi, A., T. Ambrizzi, S. Behera, A.C.V. Freitas, Y. Morioka, and T. Zhou, 2018: The Response of Subtropical Highs to Climate Change. *Curr. Clim. Change Rep.* **4,** 371–382.

Chung, E-S., A. Timmermann, B.J. Soden, K-J. Ha, L. Shi, and V.O. John, 2019: Reconciling opposing Walker circulation trends in observations and model projections. *Nat. Clim. Change*, **9**, 405-412.

Collier, P., G. Conway, and T. Venables, 2008: Climate change and Africa. *Oxford Rev. Econ. Pol.*, **24**, 337-353.

Collins, C., C.J.C. Reason, and J.C. Hermes, 2012: Scatterometer and reanalysis wind products over the western tropical Indian Ocean. *J. Geophys. Res. Oceans*, **117**, C03045.

Collins, M., S. Minobe, M. Barreiro, S. Bordoni, Y. Kaspi, A. Kuwano-Yoshida, N. Keenlyside, E. Manzini, C.H. O'Reilly, R. Sutton, S-P. Xie, and O. Zolina, 2018: Challenges and opportunities for improved understanding of regional climate dynamics. *Nat. Clim. Change*, **8**, 101-108.

Cook, K.H., 2015: Role of inertial instability in the West African monsoon jump. *J. Geophys. Res. Atmos.* **120**, 3085– 3102.

-, R.G.J. Fitzpatrick, W. Liu, and E.K. Vizy 2020: Seasonal asymmetry of equatorial East African rainfall projections: understanding differences between the response of the long rains and the short rains to increased greenhouse gases. *Clim. Dyn.* DOI: doi.org/10.1007/s00382-020-05350-y.

Copland, S. 2019: Anti-politics and Global Climate Inaction: The Case of the Australian Carbon Tax. *Crit. Sociol.* **46**, 623-641.

Cormack, Z. and A. Kurewa, 2018: The changing value of land in Northern Kenya: the case of Lake Turkana Wind Power. *Critical African Studies*, **10**, 89-107.

Creese, A., and R. Washington, 2016: Using qflux to constrain modeled Congo Basin rainfall in the CMIP5 ensemble, *J. Geophys. Res. Atmos.*, **121**, 13,415–13,442.

-, 2018: A Process-Based Assessment of CMIP5 Rainfall in the Congo Basin: The September–November Rainy Season. *J. Climate*, **31**, 7417-7439.

-, R. Washington, and R. Jones, 2019: Climate change in the Congo Basin: processes related to wetting in the December–February dry season. *Clim. Dyn,* **53**, 3583-3602.

Crowhurst, D. M., S. J. Dadson, and R. Washington, 2020: Evaluation of evaporation climatology for the Congo Basin wet seasons in 11 global climate models. *J. Geophys. Res. Atmos.*, **125**, e2019JD030619.

Cundill, G., B. Currie-Alder, and M. Leone, 2019: The future is collaborative. *Nature Climate Change*, **9**, 343-349.

Dawson, A., 2016: Windspharm: A High-Level Library for Global Wind Field Computations Using Spherical Harmonics. *J. Open Research Software*, **4**, doi: 10.5334/jors.129.

Devereux, S., 2000: Famine in the twentieth century. IDS Working Paper 105, Institute of Development Studies, University of Sussex, 40 pp. Available from https://www.ids.ac.uk/publication/famine-in-the-twentieth-century, accessed 28.10.2020

Dhame, S., A. S. Taschetto, A. Santoso, and K. J. Meissner, 2020: Indian Ocean warming modulates global atmospheric circulation trends. *Clim. Dyn.* **55,** 2053–2073.

Dias, F. B., R. Fiedler, S. J. Marsland, C. M. Domingues, L. Clément, S. R. Rintoul, E. L. Mcdonagh, M. M. Mata, and A. Savita, 2020: Ocean Heat Storage in Response to Changing Ocean Circulation Processes. *J.Climate*, **33**, 9065-9082.

Dinku, T., C. Funk, P. Peterson, R. Maidment, T. Tadesse, H. Gadan, and P. Ceccato 2018: Validation of the CHIRPS satellite rainfall estimates over eastern Africa. *Q J R Meteorol Soc*, **144** (Suppl. 1), 292– 312.

Diro, G.T., D.I.F. Grimes, and E. Black, 2011: Teleconnections between Ethiopian summer rainfall and sea surface temperature: part 1 – observation and modelling. *Clim. Dyn.*, **37**, 103-119.

Draper, C.S., R.H. Reichle, and R.D. Koster, 2018: Assessment of MERRA-2 Land Surface Energy Flux Estimates. *J. Climate*, **31**, 671–691.

Driver, P. and C.J.C. Reason, 2017: Variability in the Botswana High and its relationships with rainfall and temperature characteristics over southern Africa. *Int. J. Climatol,* **37**, 570-581.

Dunning, C.M., E.C.L. Black, and R.P. Allan, 2016: The onset and cessation of seasonal rainfall over Africa. *J. Geophys. Res. Atmos.*, **121**, 11405-11424.

-, E. C. L. Black, and R. P. Allan, 2018: Later Wet Seasons with More Intense Rainfall over Africa under Future Climate Change, *J. Climate*, **31**, 9719-9738.

Dyer, E., R. Washington, and M. T. Taye, 2020: Evaluating the CMIP5 ensemble in Ethiopia: Creating a reduced ensemble for rainfall and temperature in Northwest Ethiopia and the Awash basin. *Int. J. Climatol,* **40**, 2964-2985.

-. and R. Washington, 2020: Kenyan long rains: a sub-seasonal approach to process-based diagnostics. *J. Climate,* DOI: 10.1175/JCLI-D-19-0914.1.

Easterling, K. 2014: *Extrastatecraft: The Power of Infrastructure Space*. Verso: London.

Emanuel, K. 2020: The Relevance of Theory for Contemporary Research in Atmospheres, Oceans, and Climate. *AGU Advances*, **1**, e2019AV000129.

Endris, H.S., C. Lennard, B. Hewitson, A. Dosio, G. Nikulin, and G.A. Artan, 2018: Future changes in rainfall associated with ENSO, IOD and changes in the mean state over Eastern Africa. *Clim. Dyn.*, doi: 10.1007/s00382-018-4239-7.

Fahnbulleh, M. 2007: In search of economic development in Kenya: Colonial legacies & post-independence realities. *Rev. Afr. Polit. Econ.,* **33**, 33-47.

Feng, X., J. Dabang, L. Xianmei, and W. Huijun, 2003: Influence of the Mascarene high and Australian high on the summer monsoon in East Asia: Ensemble simulation. *Adv. Atmos. Sci.*, **20,** 799–809.

Fereday, D. R., R. Chadwick, J. R. Knight, and A. A. Scaife, 2020: Tropical rainfall linked to stronger future ENSO-NAO teleconnection in CMIP5 models. *Geophys. Res. Lett.*, **47**, e2020GL088664.

Fields, S., 2005: Continental divide: Why Africa's climate change burden is greater. *Environ. Health Perspect.*, **113**, A534–A537.

Findlater, J., 1969: A major low-level air current near the Indian Ocean during the northern summer. *Q. J. R. Meteorol. Soc.*, **95**, 362-380.

Finke, T., A. Gilchrist, and S. Mouzas, 2016: Why companies fail to respond to climate change: Collective inaction as an outcome of barriers to interaction. *Ind. Market Manag.* **58**, 94-101.

Finney, D., J. Marsham, L. Jackson, E. Kendon, D. Rowell, P. Boorman, R. Keane, and C. Senior, 2019: Implications of improved representation of convection for the East Africa water budget using a convection-permitting model. *J. Climate*, **32**, 2109-2129.

-, J. H. Marsham, D. P. Rowell, E. J. Kendon, S. O. Tucker, R. A. Stratton, and L. S. Jackson, 2020: Effects of Explicit Convection on Future Projections of Mesoscale Circulations, Rainfall, and Rainfall Extremes over Eastern Africa. *J. Climate*, **33**, 2701-2718.

Flato, G., J. Marotzke, B. Abiodun, P. Braconnot, S.C. Chou, W. Collins, P. Cox, F. Driouech, S. Emori, V. Eyring, C. Forest, P. Gleckler, E. Guilyardi, C. Jakob, V. Kattsov, C. Reason and M. Rummukainen, 2013: Evaluation of Climate Models. In: Stocker, T.F., D. Qin, G.-K. Plattner, M. Tignor, S.K. Allen, J. Boschung, A. Nauels, Y. Xia, V. Bex and P.M. Midgley (eds.), 2013: *Climate Change 2013: The Physical Science Basis. Contribution of Working Group I to the Fifth Assessment Report of the Intergovernmental Panel on Climate Change*. Cambridge: Cambridge University Press.

Forster, P.M., A.C. Maycock, C.M. McKenna, and C.J. Smith, 2020: Latest climate models confirm need for urgent mitigation. *Nat. Clim. Change,* **10**, 7-10.

Funk, C., M.D. Dettinger, J.C. Michaelsen, J.P. Verdin, M.E. Brown, M. Barlow, and A. Hoell, 2008: Warming of the Indian Ocean threatens eastern and southern African food security but could be mitigated by agricultural development, *P. Natl. Acad. Sci. USA,* **105**,11081-11086.

-, P. Peterson, M. Landsfeld, D. Pedreros, J. Verdin, S. Shukla, G. Husak, J. Rowland, L. Harrison, A. Hoell, and J. Michaelsen, 2015: The climate hazards infrared precipitation with stations – a new environmental record for monitoring extremes. *Scientific Data* **2**, doi: 10.1038/sdata.2015.66

Ganguly, G., J. Setzer, and V. Heyvaert, 2018: If at First You Don't Succeed: Suing Corporations for Climate Change. *Oxford J. Legal Stud.* **38**, 841-868.

Gebrechorkos, S.H., S. Hülsmann, and C. Bernhofer, 2018: Evaluation of multiple climate data sources for managing environmental resources in East Africa. *Hydrol. Earth Syst. Sci.,* **22**, 4547-4564.

-, S. Hülsmann, and C. Bernhofer, 2019: Long-term trends in rainfall and temperature using high-resolution climate datasets in East Africa. *Sci. Rep-UK*, **9**, 11376.

Gehne, M., T. M. Hamill, G. N. Kiladis, and K. E. Trenberth, 2016: Comparison of Global Precipitation Estimates across a Range of Temporal and Spatial Scales. *J. Climate*, **29**, 7773-7795.

Gelaro, R., W. McCarty, M.J. Suárez, R. Todling, A. Molod, L. Takacs, C.A. Randles, A. Darmenov, M.G. Bosilovich, R. Reichle, K. Wargan, L. Coy, R. Cullather, C. Draper, S. Akella, V. Buchard, A. Conaty, A.M. da Silva, W. Gu, G. Kim, R. Koster, R. Lucchesi, D. Merkova, J.E. Nielsen, G. Partyka, S. Pawson, W. Putman, M. Rienecker, S.D. Schubert, M. Sienkiewicz, and B. Zhao, 2017: The Modern-Era Retrospective Analysis for Research and Applications, Version 2 (MERRA-2). *J. Climate*, **30**, 5419–5454

Gesch, D. B., K.L. Verdin, and S.K. Greenlee, 1999: New land surface digital elevation model covers the Earth, *Eos Trans. AGU*, **80**, 69– 70.

Giannini, A., B. Lyon, R. Seager, and N. Vigaud, 2018: Dynamical and thermodynamic elements of modelled climate change at the East African margin of convection. *Geophys. Res. Lett.*, **45**, 992-1000.

Giorgi, F., C. Jones, and G.R. Asrar, 2009: Addressing climate information needs at the regional level: the CORDEX framework. *WMO Bulletin*, **58**, 175-183.

Gogic, M. and Trajkovic, S., 2013: Analysis of changes in meteorological variables using Mann-Kendall and Sen's slope estimator statistical tests in Serbia. *Global Planet. Change,* **100**, 172-182.

Goswami, B.N. and D. Sengupta, 2003: A note on the deficiency of NCEP/NCAR reanalysis surface winds over the equatorial Indian Ocean. *J. Geophys. Res. Oceans*, **108**, 3124-3138.

Hagos, S.M. and K.H. Cook, 2007: Dynamics of the West African Monsoon Jump. *J. Climate*, **20**, 5264–5284.

Hall, R. J., H-L. Wei, and E. Hanna, 2019: Complex systems modelling for statistical forecasting of winter North Atlantic atmospheric variability: A new approach to North Atlantic seasonal forecasting. *Q. J. R. Meteorol. Soc.*, **145**, 2568-2585.

Ham, Y. G., J. Y. Choi, and J. S. Kug, 2017: The weakening of the ENSO–Indian Ocean Dipole (IOD) coupling strength in recent decades. *Clim. Dyn.* **49,** 249–261.

Han, F., K.H. Cook, and E. Vizy, (2019): Changes in intense rainfall events and dry periods across Africa in the twenty-first century. *Clim. Dyn.*, **53**, 2757–2777.

Harris, I., P. Jones, T. Osborn, and D. Lister, 2014: Updated high-resolution grids of monthly climatic observations – the CRU TS3.10 Dataset. *Int. J. Climatol.,* **34**, 623-642.

Hart, N.C.G., R. Washington, and R.A. Stratton, 2018: Stronger Local Overturning in Convective-Permitting Regional Climate Model Improves Simulation of the Subtropical Annual Cycle. *Geophys. Res. Lett.*, **45**, 11334-11342.

Hartman, A.T., 2018: An analysis of the effects of temperatures and circulations on the strength of the low-level jet in the Turkana Channel in East Africa. *Theor. Appl. Climatol,* **132**, 1003-1017.

Haselow, L., R. Meissner, H. Rupp, and K. Meigel, 2019: Evaluation of precipitation measurements methods under field conditions during a summer season: A comparison of the standard rain gauge with a weighable lysimeter and a piezoelectric precipitation sensor. *J. Hydrol.* **575**, 537-543.

Hastenrath, S., D. Polzin, and L. Greischar, 2002: Annual Cycle of Equatorial Zonal Circulations from the ECMWF Reanalysis. *J. Meteorol. Soc. Jpn. Ser. II*, **80**, 755-766.

-, D. Polzin, and C. Mutai, 2007: Diagnosing the 2005 Drought in Equatorial East Africa. *J. Climate,* **20**, 4628-4637.

-, D. Polzin, and C. Mutai, 2010: Diagnosing the Droughts and Floods in Equatorial East Africa during Boreal Autumn 2005–08. *J. Climate,* **23**, 813-817.

-, D. Polzin, and C. Mutai, 2011: Circulation Mechanisms of Kenya Rainfall Anomalies. *J. Climate,* **24**, 404-412.

Haustein, K., F.E.L. Otto, V. Venema, P. Jacobs, K. Cowtan, Z. Hausfather, R.G. Way, B. White, A. Subramanian, and A.P. Schurer, 2019: A Limited Role for Unforced Internal Variability in Twentieth-Century Warming. *J. Climate*, **32**, DOI: 10.1175/JCLI-D-18-0555.1

Hawkins, E. and Sutton, R, 2011: The potential to narrow uncertainty in projections of regional precipitation change. *Clim. Dyn.* **37**, 407-418.

Hersnach, H., B. Bell, P. Berrisford, S. Hirahara, A. Horányi, J. Muñoz-Sabater, J. Nicolas, C. Peubey et al., 2020: The ERA5 global reanalysis. *Q J R Meteorol Soc*, **146**, 1999-2049.

Hession, S.L. and N. Moore, 2011: A spatial regression analysis of the influence of topography on monthly rainfall in East Africa. *Int. J. Climatol*, **31**, 1440-1456.

Hewitson, B., C. Lennard, G. Nikulin, and C. Jones, 2012: CORDEX-Africa: a unique opportunity for science and capacity building. *CLIVAR Exchanges*, **60**, 6-7.

Hills, R.C. (1978): The Structure of the Inter-Tropical Convergence Zone in Equatorial Africa and Its Relationship to East African Rainfall. *T. I. Brit. Geogr,* **4**, 329-352.

Hirons, L. and A. Turner, 2018: The impact of Indian Ocean mean-state biases in climate models on the representation of the East African short rains. *J. Climate*, **31**, 6611-6631.

Hirpa, F.A., L. Alfieri, T. Lees, J. Peng, E. Dyer, and S.J. Dadson, 2019: Streamflow response to climate change in the Greater Horn of Africa. *Climatic Change*, DOI: 0.1007/s10584-019-02547-x.

Hoell, A. C. and C. Funk, 2014: Indo-Pacific sea surface temperature influences on failed consecutive rainy seasons over eastern Africa. *Clim. Dyn.* **43**, 1645-1660.

-, C. Funk, and M. Barlow, 2014: La Niña diversity and northwest Indian Ocean rim teleconnections. *Clim. Dyn*,. **43**, 2707-2724.

-, M. Hoerling, J. Eischeid, X-W. Quan, and B. Liebmann, 2017: Reconciling theories for human and natural attribution of recent East Africa drying. *J. Climate,* **30**, 1939-1956.

Hofstra, N., M. New, and C. McSweeney, 2010: The influence of interpolation and station network density on the distributions and trends of climate variables in gridded daily data. *Clim. Dyn.* **35**, 841-858.

Hogan, E., A. Shelly, and P. Xavier, 2015: The observed and modelled influence of the Madden–Julian Oscillation on East African rainfall. *Met. Apps*, **22**, 459-469.

Holbach, H. M. and M. A. Bourassa, 2014: The Effects of Gap-Wind-Induced Vorticity, the Monsoon Trough, and the ITCZ on East Pacific Tropical Cyclogenesis. *Mon. Weather Rev.*, **142**, 1312-1325.

Howard, E. and R. Washington, 2018: Characterizing the Synoptic Expression of the Angola Low. *J. Climate,* **31**, 7147-7165.

Hua, W., L. Zhou, S. E. Nicholson, H. Chen, and M. Qin, 2019: Assessing reanalysis data for understanding rainfall climatology and variability over Central Equatorial Africa. *Clim Dyn*, DOI: 10.1007/s00382-018-04604-0.

Huffman, G. J., R. F. Adler, D. T. Bolvin, and G. Gu, 2009: Improving the global precipitation record: GPCP Version 2.1. *Geophys. Res. Lett.*, **36**, L17808

Indeje, M., F. H. M. Semazzi, and L. Xie, 2001: Mechanistic model simulations of the East African climate using NCAR regional climate model: influence of large-scale orography on the Turkana low-level jet. *J. Climate*, **14**, 2710–2724.

Jackson, L. S., D. L. Finney, E. J. Kendon, J. H. Marsham, D. J. Parker, R. A. Stratton, L. Tomassini, and S. Tucker, 2020: The Effect of Explicit Convection on Couplings between Rainfall, Humidity, and Ascent over Africa under Climate Change, *J. Climate*, **33,** 8315-8337.

Jackson, R. B., P. Friedlingstein, R. M. Andrew, J. G. Canadell, C. Le Quéré, and G. P. Peters, 2019: Persistent fossil fuel growth threatens the Paris Agreement and planetary health. *Environ. Res. Lett.*, **14**, 121001.

James, R. and R. Washington, 2013: Changes in African temperature and precipitation associated with degrees of global warming. *Climatic Change*, **117**, 859–872.

-, R. Washington, and R. Jones, 2015: Process-based assessment of an ensemble of climate projections for West Africa. *J. Geophys. Res. Atmos.,* **120**, 1221-1238.

-, R. Washington, B. Abiodun, G. Kay, J. Mutemi, W. Pokam, N. Hart, G. Artan, and C. Senior, 2018: Evaluating climate models with an African lens. *Bull. Am. Meteorol. Soc.,* **99**, 313–336.

Japan Meteorological Agency, 2014: JRA-55 Product Users Handbook: Model Grid Data. Available from https://rda.ucar.edu/datasets/ds628.0/docs/JRA-55.handbook_TL319_en.pdf, accessed 28.08.2020.

Jaramillo, J., E. Muchugu, F. E. Vega, A. Davis, C. Borgemeister, and A. Chabi-Olaye, 2011: Some Like It Hot: The Influence and Implications of Climate Change on Coffee Berry Borer (*Hypothenemus hampei*) and Coffee Production in East Africa. *PLoS ONE*, **6**, e24528.

Johnson, N. C. 2013: How Many ENSO Flavors Can We Distinguish?, *J. Climate*, **26**, 4816-4827.

Jury, M. and C. Funk, 2012: Climatic trends over Ethiopia: regional signals and drivers. *Int. J. Climatol.*, **33**, 1924-1935.

Kaunda, C.S., C.Z. Kimambo, and T.K. Nielsen, 2012: Potential of small-scale hydropower for electricity generation in sub-Saharan Africa. *ISRN Renew. Energ,* 132606.

Kijazi, A.L. and C.J.C. Reason, 2009: Analysis of the 1998 to 2005 drought over the northeastern highlands of Tanzania. *Clim. Res.*, **33**, 209-223.

-, 2012: Intra-seasonal variability over the northeastern highlands of Tanzania. *Int. J. Climatol.,* **32**, 874-887.

Kim, J., D. E. Waliser, C. A. Mattmann, C. E. Goodale, A. F. Hart, P. A. Zimdars, D. J. Crichton, C. Jones, G. Nikulin, B. Hewitson, C. Jack, C. Lennard, and A. Favre, 2014: Evaluation of the CORDEX-Africa multi-RCM hindcast: systematic model errors. *Clim. Dyn.* **42,** 1189–1202.

Kimani, M.W., J.C.B Hoedjes, and Z. Su, 2017: An assessment of satellite-derived rainfall products relative to ground observations over East Africa. *Remote Sens.*, **9**, DOI: 10.3390/rs9050430.

King, J.A., R. Washington, and S. Engelstaedter, 2020: Representation of the Indian Ocean Walker Circulation in Climate Models and Links to Kenyan Rainfall. *Int. J. Climatol.,* DOI: 10.1002/joc.6714.

-, S. Engelstaedter, R. Washington, and C. Munday, 2021: Variability of the Turkana Low-Level Jet in Reanalysis and Models: Implications for Rainfall. *J. Geophys. Res. Atmos.*, DOI: 10.1029/2020JD034154.

Kinuthia. J.H., 1992: Horizontal and vertical structure of the Lake Turkana Jet. *J Appl Meteorol*, **31**, 1248–1274.

-, and G.C. Asnani, 1982: A newly found jet in North Kenya (Turkana Channel). *Mon. Weather. Rev.* **110**, 1722–1728.

Knutti, R., 2010: The end of model democracy? *Clim. Change*, **102**, 395–404.

-, D. Masson, and A. Gettelman, 2013: Climate model genealogy: Generation CMIP5 and how we got there. *Geophys. Res. Lett.*, **40**, 1194-1199.

Kripalani, R.H. and P. Kumar, 2004: Northeast monsoon rainfall variability over south peninsular India vis-à-vis the Indian Ocean dipole mode. *Int. J. Climatol.*, **24**, 1267-1282.

Krishnamurthy, V. and B.N. Goswami, 2000: Indian Monsoon–ENSO Relationship on Interdecadal Timescale. *J. Climate*, **13**, 579-595.

Kobayashi, S., Y. Ota, Y. Harada, A. Ebita, M. Moriya, H. Onoda, K. Onogi, H. Kamahori, C. Kobayashi, H. Endo, K. Miyaoka, and K. Takahashi, 2015: The JRA-55 Reanalysis: General Specifications and Basic Characteristics. *J. Met. Soc. Japan*, **93**, 5-48.

Kociuba, G. and Power, S.B., 2015: Inability of CMIP5 models to simulate recent strengthening of the Walker Circulation: implications for projections. *J. Climate*, **28**, 20-35.

Kuete, G., W. Pokam Mba, and R. Washington, 2019: African Easterly Jet South: control, maintenance mechanisms and link with Southern subtropical waves. *Clim. Dyn.,* **54**, 1539–1552.

Lanckriet, S., A. Frankl, E. Adgo, P. Termonia, and J. Nyssen, 2015: Droughts related to quasi-global oscillations: a diagnostic teleconnection analysis in North Ethiopia. *Int. J. Climatol.,* **35**, 1534-1542.

Latif, M., D, Dommenget, M. Dima, and A. Grötzner , 1999: The Role of Indian Ocean Sea Surface Temperature in Forcing East African Rainfall Anomalies during December–January 1997/98. *J.Climate*, **12**, 3497-3504.

L'Heureux, M.L., S. Lee, and B. Lyon, 2013: Recent multidecadal strengthening of the Walker Circulation across the tropical Pacific. *Nat. Clim. Change*, **3**, 571-576.

Lewandowsky, S., J. S . Risbey, and N. Oreskes, 2015: On the definition and identifiability of the alleged "hiatus" in global warming. *Sci. Rep-UK.* **5**, 16784.

Li, G. and S-P Xie, 2014: Tropical Biases in CMIP5 Multimodel Ensemble: The Excessive Equatorial Pacific Cold Tongue and Double ITCZ Problems. *J. Climate*, **27**, 1765-1780.

Li, J. and X. Yu, 2017: LiDAR technology for wind energy potential assessment: Demonstration and validation at a site around Lake Erie. *Energ. Convers. Manage.* **144**, 252-261.

Li, T., Zhang, L., and H. Murakami, 2015: Strengthening of the Walker Circulation under global warming in an aqua-planet general circulation model simulation. *Adv. Atmos. Sci*, **32**, 1473-1480.

Liebmann, B., M.P. Hoerling, C. Funk, I. Bladé, R.M. Dole, D. Allured, X. Quan, P. Pegion, and J.K Eischeid, 2014: Understanding recent Eastern Horn of Africa rainfall variability and change. *J. Climate,* **27**, 8630-8645.

-, I. Bladé, C. Funk, D. Allured, X. Quan, M. Hoerling, A. Hoell, P. Peterson, and W.M. Thiaw, 2017: Climatology and interannual variability of boreal spring wet season precipitation in the Eastern Horn of Africa and implications for its recent decline. *J. Climate*, **30**, 3867-3886.

Lin, Y-L., 2009: Formation of African Easterly Waves and Mesoscale Convective Systems over Eastern Africa and its Implication to Tropical Cyclogenesis over Eastern Atlantic Ocean. *AIP Conference Proceedings*, **1140**, 104-113.

Liu, C. and E. J. Zipser, 2005: Global distribution of convection penetrating the tropical tropopause, *J. Geophys. Res.*, **110**, D23104

Liu, W., K. H. Cook, and E. K. Vizy, 2020: Influence of Indian Ocean SST regionality on the East African short rains. *Clim. Dyn.* **54**, 4991-5011.

Lott, F. C., N. Christidis, and P. A. Stott, 2013: Can the 2011 East African drought be attributed to climate change? *Geophys. Res. Lett.*, **40**, 1177–1181.

Lu, J., G.A. Vecchi, and T. Reichler, 2007: Expansion of the Hadley cell under global warming. *Geophys. Res. Lett.*, **34**, L06805.

Luderer, G., R. C. Pietzcker, C. Bertram, E. Kriegler, M. Meinshausen, and O. Edenhofer, 2013: Economic mitigation challenges: how further delay closes the door for achieving climate targets. *Environ. Res. Lett.* **8,** 034033.

Luo, B. and P.J. Minnett (2020): Evaluation of the ERA5 Sea Surface Skin Temperature with Remotely-Sensed Shipborne Marine-Atmospheric Emitted Radiance Interferometer Data. *Remote Sens.*, **12**, 1873.

-, P.J. Minnett, M. Szczodrak, N.R. Nalli, and V.R. Morris (2020): Accuracy Assessment of MERRA-2 and ERA-Interim Sea Surface Temperature, Air Temperature, and Humidity Profiles over the Atlantic Ocean Using AEROSE Measurements. *J. Climate*, **33**, 6889-6909.

Lyon, B., 2014: Seasonal drought in the Greater Horn of Africa and its recent increase during the March-May Long Rains, *J. Climate*, **27**, 7953-7975.

-, and D.G. DeWitt, 2012: A recent and abrupt decline in the East African long rains, *Geophys. Res. Lett.*, **39**, L02702.

MacLeod, D., 2018: Seasonal predictability of onset and cessation of the East African rains. *Weather Clim. Extr.*, **21**, 27-35.

-, 2019: Seasonal forecasts of the East African long rains: insight from atmospheric relaxation experiments. *Clim. Dyn.*, doi: 10.1007/s00382-019-04800-6.

-, R. Graham, C. O'Reilly, G. Otieno, and M. Todd, 2020: Causal pathways linking different flavours of ENSO with the Greater Horn of Africa short rains. *Atmos Sci Lett.*, e1015.

Madden, R. A. and P. R. Julian, 1994: Observations of the 40–50-Day Tropical Oscillation—A Review, *Mon. Weather Rev.* **122**, 814-837.

Maidment, R., R.P. Allan, and E. Black, 2015: Recent observed and simulated changes in precipitation over Africa. *Geophys. Res. Lett.*, **42**, 8155–8164.

Mattis, I., A. Ansmann, D. Althausen, V. Jaenisch, U. Wandinger, D. Müller, Y. F. Arshinov, S. M. Bobrovnikov, and I. B. Serikov, 2002: Relative-humidity profiling in the troposphere with a Raman lidar. *Appl. Opt.* **41**, 6451-6462.

Marthews, T.R., R.G. Jones, S.J. Dadson, F.E.L. Otto, D. Mitchell, B.P. Guillod, and M.R. Allen, 2019: The impact of human-induced climate change on regional drought in the Horn of Africa. *J. Geophys. Res. Atmos.*, **124**, 4549-4566.

McGregor, S., A. Timmermann, M.F. Stuecker, M.H. England, M. Merrifield, F-F. Jin, and Y. Chikamoto, 2014: Recent Walker circulation strengthening and Pacific cooling amplified by Atlantic warming. *Nat. Clim. Change*, **4**, 888–892.

McKenna, S., A. Santoso, A. S. Gupta, A. S. Taschetto, and W. Cai, 2020: Indian Ocean Dipole in CMIP5 and CMIP6: characteristics, biases, and links to ENSO. *Sci. Rep-UK,* **10**, 11500.

McLaren, D. and N. Markusson, 2020: The co-evolution of technological promises, modelling, policies and climate change targets. *Nat. Clim. Chang.* **10,** 392–397.

McSweeney, C.F., R.G. Jones, R.W. Lee, and D.P. Rowell, 2015: Selecting CMIP5 GCMs for downscaling over multiple regions. *Clim. Dyn.* **44**, 3237-3260.

McVicar, T.R., M.L. Roderick, R.J. Donohue, L.T. Li, T.G. Van Niel, A. Thomas, J. Grieser, D. Jhajharia, Y. Himri, N.M. Mahowald, A.V. Mescherskaya, A.C. Kruger, S. Rehman, and Y. Dinpashoh, 2012: Global review and synthesis of trends in observed terrestrial near-surface wind speeds: Implications for evaporation. *J. Hydrology*, **416-417**, 182-205.

Met Office 2012: Met Office Integrated Data Archive System (MIDAS) Land and Marine Surface Stations Data (1853-current). NCAS British Atmospheric Data Centre. Available from http://catalogue.ceda.ac.uk/uuid/220a65615218d5c9cc9e4785a3234bd0, accessed 29.10.2020.

Mohapatra, S., C. Gnanaseelan, and J.S. Deepa, 2020: Multidecadal to decadal variability in the equatorial Indian Ocean subsurface temperature and the forcing mechanisms. *Clim. Dyn.*, **54**, 3475-3487.

Minasny, B., D. Fiantis, B. Mulyanto, Y. Sulaeman, and W. Widtatmanti, 2020: Global soil science research collaboration in the 21st century: Time to end helicopter research. *Geoderma*, **373**, DOI: 10.1016/j.geoderma.2020.114299.

Munday, C. and R. Washington, 2017: Circulation controls on southern African precipitation in coupled models: The role of the Angola Low. *J. Geophys. Res. Atmos.*, **122**, 861– 877.

-, and R. Washington, 2018: Systematic climate model rainfall biases over Southern Africa: links to moisture circulation and topography. *J. Climate*, **31**, 7533-7548.

-, and R. Washington, 2019: Controls on the Diversity in Climate Model Projections of Early Summer Drying over Southern Africa. *J. Climate*, **32**, 3707-3725.

-, R. Washington, and N. Hart, 2020: African Low-level jets and their importance for water vapour transport and rainfall. *Geophys. Res. Lett.,* **47**, 2020GL090999.

Mudelsee, M. 2019: Trend analysis of climate time series: A review of methods. *Earth-Sci. Rev.* **190**, 310-322.

Mukhopadhyay, P. and K. Roy, 2020: Evaluation of the convective mass flux profiles associated with cumulus parameterization schemes of CMIP5 models. *J. Earth. Syst. Sci.* **129,** 138

Mutai, C., D. Polzin, and S. Hastenrath, 2012: Diagnosing Kenya rainfall in boreal autumn: further exploration. *J. Climate*, **25**, 4323-4329.

Naiman, Z., P.J. Goodman, J.P. Krasting, S.L. Malyshev, J.L. Russell, R.J. Stouffer, and A.T. Wittenberg, 2017: Impact of mountains on tropical circulation in two Earth system models. *J. Climate*, **30**, 4149-4163.

Newman, M., M.A. Alexander, T. R. Ault, K. M. Cobb, C. Deser, E. Di Lorenzo, N. J. Mantua, A. J. Miller, S. Minobe, H. Nakamura, N. Schneider, D. J. Vimont, A. S. Phillips, J. D. Scott, and C. A. Smith, 2016: The Pacific Decadal Oscillation, Revisited. *J. Climate*, **29**, 4399-4427.

Ng, B., W. Cai, T. Cowan, and D. Bi, 2018: Influence of internal climate variability on Indian Ocean Dipole properties. *Sci-Rep UK*, **8**. 13500.

Nicholson, S.E., 2015: Long-term variability of the East African 'short rains' and its links to large-scale factors. *Int. J. Climatol,* **35**, 3979-3990.

-, 2016a: An analysis of recent rainfall conditions in eastern Africa. *Int. J. Climatol*, **36**, 526-532.

-, 2016b: The Turkana low-level jet: mean climatology and association with regional aridity. *Int. J. Climatol,* **36**, 2598-2614.

-, 2017: Climate and climatic variability of rainfall over eastern Africa. *Rev. Geophys.*, **55**, 590-635.

-, 2018: The ITCZ and the seasonal cycle over equatorial Africa. *Bull. Am. Meteorol. Soc.,* **99**, 337-348.

-, and J. Kim, 1998: The relationship of the El Niño – Southern Oscillation to African rainfall. *Int. J. Climatol.* **17**, 117-135.

Nikulin, G., C. Jones, F. Giorgi, G. Asrar, M. Büchner, R. Cerezo-Mota, O. B. Christensen, M. Déqué, J. Fernandez, A. Hänsler, E. van Meijgaard, P. Samuelsson, M. B. Sylla, and L. Sushama, 2012: Precipitation Climatology in an Ensemble of CORDEX-Africa Regional Climate Simulations, *J. Climate*, **25**, 6057-6078.

Neupane, N., 2016: The Congo basin zonal overturning circulation. *Adv. Atmos. Sci.* **33,** 767–782.

NOAA 2020: Trends in Atmospheric Carbon Dioxide. Available from https://www.esrl.noaa.gov/gmd/ccgg/trends/. Accessed 28.12.2020.

North, M.A., W. W. Hastie, and L. Hoyer, 2020: Out of Africa: The underrepresentation of African authors in high-impact geoscience literature. *Earth-Sci. Rev.*, **208**, 103262.

Nowack, P., J. Runge, V. Eyring, and J. D. Haigh, 2020: Causal networks for climate model evaluation and constrained projections. *Nat. Commun.* **11**, 1415.

Ogallo, L.J. 1988: Relationships between seasonal rainfall in East Africa and the Southern Oscillation. *Int. J. Climatol.,* **8**, 31-43.

-, 1989: The spatial and temporal patterns of the East African seasonal rainfall derived from principal component analysis. *Int. J. Climatol.,* **9**, 145-167.

Ogega, O. M., J. Koske, J. B. Kung'u, E. Scoccimaro, H. S. Endris, and M. N. Mistry, 2020: Heavy precipitation events over East Africa in a changing climate: results from CORDEX RCMs. *Clim. Dyn.* **55**, 993-1009.

Ogwang, B.O., H. Chen, X. Li, and C. Gao, 2014: The Influence of Topography on East African October to December Climate: Sensitivity Experiments with RegCM4. *Adv. Meteorol.*, DOI: 10.1155/2014/143917.

Olufadewa, I.I., M.A. Adesina, and T. Ayorinde, 2020: From Africa to the World: Reimagining Africa's research capacity and culture in the global knowledge economy. *J. Glob. Health*, **10**, DOI: 10.7189/jogh.10.010321.

Omondi, P.A., J.L. Awange, E. Forootan, L.A.Ogallo, R. Barakiza, G.B. Girmaw, I. Fesseha, V. Kululetera, C. Kilembe, M.M. Mbati, M. Kilavi, S.M. King'uyu, P.A. Omeny, A. Njogu, E.M Badr, T.A. Musa, P. Muchiri, D. Bamanya, and E. Komutunga, 2014: Changes in temperature and precipitation extremes over the Greater Horn of Africa region from 1961 to 2010. *Int. J. Climatol.*, **34**, 1262-1277.

Ongoma, V., H. Chen, and C. Gao, 2017: Projected changes in mean rainfall and temperature over East Africa based on CMIP5 models. *Int. J. Climatol.*, **38**, 1375-1392.

-, 2019: Evaluation of CMIP5 twentieth century rainfall simulation over the equatorial East Africa. *Theor. Appl. Climatol.* **135,** 893–910.

Onyango, E. A., O. Sahin, A. Awiti, C. Chu, and B. Mackey, 2016: An integrated risk and vulnerability assessment framework for climate change and malaria transmission in East Africa. *Malar. J.* **15**, 551.

Opiyo, F.E.O., O.V. Wasonga, and M.M. Nyangito, 2014: Measuring household vulnerability to climate-induced stresses in pastoral rangelands of Kenya: Implications for resilience programming. *Pastoralism*, **4**, DOI: 10.1186/s13570-014-0010-9.

Oreskes, N., K. Shrader-Frechette, and K. Belitz, 1994: Verification, Validation, and Confirmation of Numerical Models in the Earth Sciences. *Science*, **263**, 641-646.

Overland, J.E. and B.A. Walter Jr., 1981: Gap Winds in the Strait of Juan de Fuca. *Mon. Weather Rev.*, **109**, 2221-2233.

Papalexiou, S.M. and A. Montanari, 2019: Global and Regional Increase of Precipitation Extremes Under Global Warming. *Water Resour. Res.* **55**, 4901-4914.

Parker, W.S., 2016: Reanalyses and Observations: What's the Difference?. *B. Am. Meteorol. Soc.* **97**, 1565-1572.

Pfahl, S., P. O'Gorman, and E. Fischer, 2017: Understanding the regional pattern of projected future changes in extreme precipitation. *Nat. Clim. Change,* **7,** 423–427.

Philip, S., S.F. Kew, G.J. van Oldenborgh, F. Otto, S. O'Keefe, K. Haustein, A. King, A. Zegeye, Z. Eshetu, K. Hailemariam, R. Singh, E. Jjemba, C. Funk, and H. Cullen, 2018: Attribution analysis of the Ethiopian Drought of 2015. *J. Climate*, **31**, 2465–2486.

Pohl, B. and P. Camberlin, 2006: Influence of the Madden–Julian Oscillation on East African rainfall. I: Intraseasonal variability and regional dependency. *Q.J.R. Meteorol. Soc.,* **132**, 2521-2539.

Pokhrel, S., U. Dutta, H. Rahaman, H. Chaudhari, A. Hazra, S. K. Saha, and C. Veeranjaneyulu, 2020: Evaluation of different heat flux products over the tropical Indian Ocean. *Earth and Space Science*, **7**, e2019EA000988.

Power, S. B. and G. Kociuba, 2011: What Caused the Observed Twentieth-Century Weakening of the Walker Circulation? *J. Climate*, **24**, 6501-6514.

Rai, P. and A.P. Dimri, 2017: Effect of changing tropical easterly jet, low level jet and quasi-biennial oscillation phases on Indian summer monsoon. *Atmos. Sci. Lett.*, **18**, 52-59.

Ramon, J., L. Lledó, V. Torralba, A. Soret, and F.J. Doblas-Reyes, 2019: What global reanalysis best represents near-surface winds? *Q J R Meteorol Soc*, **145**, 3236-3251.

Reason, C.J.C, R.J. Allan, J.A. Lindesay, and T.J. Ansell (2000): ENSO and climatic signals across the Indian Ocean Basin in the global context: part I, interannual composite patterns. *Int. J. Climatol.*, **20**, 1285-1327.

Riahi, K., S. Rao, V. Krey, C. Cho, V. Chirkov, G. Fischer, G. Kindermann, N. Nakicenovic, and P. Rafaj, 2011: RCP 8.5—A scenario of comparatively high greenhouse gas emissions. *Climatic Change,* **109**, 33.

Rife, D.L., J.O. Pinto, A.J. Monaghan, C.A. Davis, and J.R. Hannan, 2010: Global Distribution and Characteristics of Diurnally Varying Low-Level Jets**.** *J. Climate***, 23,** 5041-5064.

Rio, C., A. D. Del Genio, and F. Hourdin, 2019: Ongoing Breakthroughs in Convective Parameterization. *Current Climate Change Reports,* **5**, 95–111.

Ripple, W. J., C. Wolf, T. M. Newsome, P. Barnard, and W. R. Moomaw, 2020: World Scientists' Warning of a Climate Emergency. *BioScience*, **70**, 8-12.

Rowell, D.P., 2013: Simulating SST Teleconnections to Africa: What is the State of the Art? *J. Climate*, **26**, 5397-5418.

-,B.B.B Booth, S.E. Nicholson, and P. Good, 2015: Reconciling past and future rainfall trends over East Africa. *J. Climate,* **28**, 9768-9788.

-, C.A. Senior, M. Vellinga, and R. J. Graham, 2016: Can climate projection uncertainty be constrained over Africa using metrics of contemporary performance? *Climatic Change*, **134**, 621-633.

-, and R. Chadwick, 2018: Causes of the Uncertainty in Projections of Tropical Terrestrial Rainfall Change: East Africa. *J. Climate,* **31**, 5977-5995.

-, 2019: An Observational Constraint on CMIP5 Projections of the East African Long Rains and Southern Indian Ocean Warming. *Geophys. Res. Lett.,* **46**, 6050-6058.

Salami, A., A. B. Kamara, and Z. Brixiova, 2010: Smallholder agriculture in East Africa: Trends, constraints, and opportunities. African Development Bank Working Papers Series No. 105, African Development Bank, Tunis, Tunisia.

Sanderson, B.M. and R. Knutti, 2012: On the interpretation of constrained climate model ensembles. *Geophys. Res. Lett.,* **39**, L16708.

Sanford, T., P.C. Frumhoff, A. Luers, and J. Gulledge, 2014: The climate policy narrative for a dangerously warming world. *Nat. Clim. Change*, **4**, 164-166.

Saji, N.H., B.N. Goswami, P.N. Vinayachandran, and T. Yamagata, 1999: A dipole mode in the tropical Indian Ocean. *Nature,* **401,** 360–363

Scannell, C., B.B. Booth, N.J. Dunstone, D.P. Rowell, D.J. Bernie, M. Kasoar, A. Voulgarakis, L.J. Wilcox, J.C. Acosta Navarro, Ø. Seland, and D.J. Paynter, 2019: The Influence of Remote Aerosol Forcing from Industrialized Economies on the Future Evolution of East and West African Rainfall. *J. Climate*, **32**, 8335–8354**.**

Schreck, C. J. and F. H. M. Semazzi, 2004: Variability of the recent climate of eastern Africa. *Int. J. Climatol.*, **24**, 681-701.

Schriener, B. and B. van Koppen, 2020: Hybrid Water Rights Systems for Pro-Poor Water Governance in Africa. *Water*, **12**, DOI:10.3390/w12010155

Schwendike, J., P. Govekar, M.J. Reeder, R. Wardle, G.J. Berry, and C. Jakob, 2014: Local partitioning of the overturning circulation in the tropics and the connection to the Hadley and Walker circulations. *J. Geophys. Res Atmos.*. **119**, 1322-1339.

Segele, Z. T., L. M. Leslie, and A. A. Tarhule, 2015: Sensitivity of Horn of Africa Rainfall to Regional Sea Surface Temperature Forcing. *Climate*, **3**, 365-390.

Shongwe, M.E., G.J. van Oldenborgh, B. van den Hurk, and M. van Aalst, 2011: Projected changes in mean and extreme precipitation in Africa under global warming. Part II: East Africa. *J. Climate*, **24**, 3718-3733.

Slingo, J., H. Spencer, B. Hoskins, P. Berrisford, and E. Black, 2005: The meteorology of the Western Indian Ocean, and the influence of the East African Highlands. *Phil. Trans. R. Soc. A.*, **363**, 25-42.

Stratton, R.A., C.A. Senior, S.B. Vosper, S.S. Folwell, I.A. Boutle, P.D. Earnshaw, E. Kendon, A.P. Lock, A. Malcolm, J. Manners, C.J. Morcrette, C. Short, A.J. Stirling, C.M. Taylor, S. Tucker, S. Webster, and J.M. Wilkinson, 2018: A Pan-African Convection-Permitting Regional Climate Simulation with the Met Office Unified Model: CP4-Africa. *J. Climate*, **31**, 3485-3508

Tanaka, H.L., N. Ishizaki, and A. Kitoh, 2004: Trend and interannual variability of Walker, monsoon and Hadley circulations defined by velocity potential in the upper troposphere. *Tellus A*, **56**, 250-269.

Tarnavsky, E., D. Grimes, R. Maidment, E. Black, R. P. Allan, M. Stringer, R. Chadwick, and F. Kayitakire, 2014: Extension of the TAMSAT Satellite-Based Rainfall Monitoring over Africa and from 1983 to Present, *J. Appl. Meteorol. Clim.*, **53**, 2805-2822.

Taylor, K.E., R.J. Stouffer, and G.A. Meehl, 2012: An overview of CMIP5 and the experiment design, 2012: *Bull. Am. Meteorol. Soc.*, **93**, 485-498.

Thalheimer, L. and C. Webersik, 2020: Climate Change, Conflicts and Migration. In: Krieger, T., D. Panke, and M. Pregering (eds.): *Environmental Conflicts, Migration and Governance*, p.59. Bristol: Bristol University Press.

Thomas, E., E. Jordan, K. Linden, B. Mogesse, T. Hailu, H. Jirma, P. Thomson, J. Koehler, and G. Collins, 2020: Reducing drought emergencies in the Horn of Africa. *Sci. Total Environ.* **727**, 138722.

Thompson, P.R., C.G. Piecuch, M.A. Merrifield, J.P. McCreary, and E. Firing, 2016: Forcing of recent decadal variability in the Equatorial and North Indian Ocean, *J. Geophys. Res. Oceans*, **121**, 6762– 6778.

Tierney, J., C.C. Ummenhofer, and P.B. deMenocal, 2015: Past and future rainfall in the Horn of Africa. *Science Advances*, **1**, e1500682.

Tompkins, A.M., 2001: On the relationship between tropical convection and sea surface temperature. *J. Climate*, **14**, 633–637.

Torralba, V., F.J. Doblas-Reyes, and N. Gonzalez-Reviriego, 2017: Uncertainty in recent near-surface wind speed trends: a global reanalysis intercomparison. *Environ. Res. Lett.*, **12**, 114019.

Uhe, P., S. Philip, S. Kew, K. Shah, J. Kimutai, E. Mwangi, G.J. van Oldenborgh, R. Singh, J. Arrighi, E. Jjemba, H. Cullen, and F. Otto, 2018: Attributing drivers of the 2016 Kenyan drought. *Int. J. Climatol.*, **38**, e554-e568.

Ummenhofer, C.C., A. Sen Gupta, M.H. England, and C.J.C. Reason (2009): Contributions of Indian Ocean Sea Surface Temperatures to Enhanced East African Rainfall. *J. Climate*, **22**, 993-1013.

Valík, A, R. Brázdil, P. Zahradníček, R. Tolasz, and R. Fiala, 2020: Precipitation measurements by manual and automatic rain gauges and their influence on homogeneity of long-term precipitation series. *Int. J. Climatol.*, DOI: 10.1002/joc.6862.

van Vuuren, D. P., J. Edmonds, M. Kainuma, K. Riahi, A. Thomson, K. Hibbard, G. C. Hurtt, T. Kram, V. Krey, J-F. Lamarque, T. Masui, M. Meinshausen, N.

Nakicenovic, S. J. Smith, and S. K. Rose, 2011: The representative concentration pathways: an overview. *Climatic Change*, **109**, 5.

-, and T. R. Carter, 2014: Climate and socio-economic scenarios for climate change research and assessment: reconciling the new with the old. *Climatic Change*, **122**, 415-429.

Vellinga, M. and Milton, S.F., 2019: Drivers of interannual variability of the East African long rains. *Q. J. R. Meteorol. Soc.*, **144**, 861-876.

Verschuren, D., K. R. Laird, and B. F. Cumming, 2000: Rainfall and drought in equatorial east Africa during the past 1,100 years. *Nature,* **403**, 410–414.

Vigaud, N., B. Lyon, and A. Giannini, 2017: Sub-seasonal teleconnections between convection over the Indian Ocean, the East African long rains and tropical Pacific surface temperatures. *Int. J. Climatol.*, **37**, 1167-1180.

Viste, E. and A Sorteberg, 2013: Moisture transport into the Ethiopian Highlands. *Int. J. Climatol*, **33**, 249-263.

Vizy, E. and K. Cook, 2019: Observed relationship between the Turkana low-level jet and boreal summer convection. *Clim. Dyn.*, DOI: 10.1175/JHM-D-16-0168.1

Wainwright, C.M., J.H. Marsham, R.J. Keane, D.P. Rowell, D.L. Finney, E. Black, and R.P. Allan, 2019: 'Eastern African Paradox' rainfall decline due to shorter not less intense Short Rains. *NPJ Clim. Atmos. Sci.,* **2**, doi: 10.1038/s41612-019-0091-7

-, D. L. Finney, M. Kilavi, E. Black, and J. H. Marsham, 2020: Extreme rainfall in East Africa, October 2019–January 2020 and context under future climate change. *Weather*. DOI: 10.1002/wea.3824

Walker, D.P., C.E. Birch, J.H. Marsham, A.A. Scaife, R.J. Graham, and Z.T. Segele, 2019: Skill of dynamical and GHACOF consensus seasonal forecasts of East African rainfall. *Clim. Dyn*, doi: 10.1007/s00382-019-04835-9

-, J.H. Marsham, C. E. Birch, A. A. Scaife, and D. L. Finney, 2020: Common Mechanism for Interannual and Decadal Variability in the East African Long Rains. *Geophys. Res. Lett.*, **47**, e2020GL089182.

Walker, G. T. and E. W. Bliss, 1932: World weather V. *Mem. R. Meteorol. Soc.* **4***,* 53–84.

Walters, D., I. Boutle, M. Brooks, T. Melvin, R. Stratton, S. Vosper, H. Wells, K. Williams, N. Wood, T. Allen, A. Bushell, D. Copsey, P. Earnshaw, J. Edwards, M. Gross, S. Hardiman, C. Harris, J. Heming, N. Klingaman, R. Levine, J. Manners, G. Martin, S. Milton, M. Mittermaier, C. Morcrette, T. Riddick, M. Roberts, C. Sanchez, P. Selwood, A. Stirling, C. Smith, D. Suri, W. Tennant, P. L. Vidale, J. Wilkinson, M. Willett, S. Woolnough, and P. Xavier, 2017: The Met Office Unified Model Global Atmosphere 6.0/6.1 and JULES Global Land 6.0/6.1 configurations. *Geosci. Model Dev.,* **10**, 1487–1520,

Wang, C. 2002: Atlantic Climate Variability and Its Associated Atmospheric Circulation Cells, *J. Climate*, **15**, 1516-1536.

-, 2019: Three-ocean interactions and climate variability: a review and perspective. *Clim. Dyn.*, **53**, DOI: 10.1007/s00382-019-04930-x.

Wang, G., W. Cai, B. Gan, L. Wu, A. Santoso, X. Lin, Z. Chen, and M. J. McPhaden, 2017: Continued increase of extreme El Niño frequency long after 1.5 °C warming stabilization. *Nat. Clim Change* **7,** 568–572.

Wang, L., Q. Bao, J. Li, D. Wang, Y. Liu, G. Wu, and X. Wu, 2019: Comparisons of the temperature and humidity profiles of reanalysis products with shipboard GPS sounding measurements obtained during the 2018 Eastern Indian Ocean Open Cruise. *Atmospheric and Oceanic Science Letters*, **12**, 177-183.

Washington, R., H. Harrison, D. Conway, E. Black, A. Challinor, D. Grimes, R. Jones, A. Morse, G, Kay, and M. Todd, 2006: African climate change: taking the shorter route. *Bull. Am. Meteorol. Soc.*, **87**, 1355-1366.

-, R. James, H. Pearce, W.M. Pokam, and W. Moufouma-Okia, 2013: Congo Basin rainfall climatology: can we believe the climate models? *Phil. Trans. R. Soc. B.,* **368**, 20120296.

Webster, P.J, 1983: The large-scale structure of the tropical atmosphere. In: Hoskins, B. and R. Pearce (eds.): *Large-Scale Dynamical Processes in the Atmosphere*, p235. London: Academic Press.

Weisheimer, A., N. Schaller, C. O'Reilly, D. A. MacLeod, and T. Palmer, 2016: Atmospheric seasonal forecasts of the twentieth century: multi-decadal variability in predictive skill of the winter North Atlantic Oscillation (NAO) and their potential value for extreme event attribution. *Q. J. R. Meteorol. Soc*, **143**, 917-926.

Wieners, C. E., H. A. Dijkstra, and W. P. M. de Ruijter, 2017: The Influence of Atmospheric Convection on the Interaction between the Indian Ocean and ENSO, *J. Climate*, **30**, 10155-10178.

Wilks, D.S., 2011: *Statistical Methods in the Atmospheric Sciences* (3rd ed.). Oxford: Academic Press.

Williams, A.P. and C. Funk, 2011: A westwards extension of the warm pool leads to a westward extension of the Walker circulation, drying eastern Africa. *Clim. Dyn.,* **37**, 2417-2435.

-, C. Funk, J. Michaelsen, S. A. Rauscher, I. Robertson, T. H. G. Wils, M. Koprowski, Z. Eshetu, and N. J. Loader, 2012: Recent summer precipitation trends in the Greater Horn of Africa and the emerging role of Indian Ocean sea surface temperature. *Clim. Dyn.* **39,** 2307-2328

Woodhams, B.J., C.E. Birch, J.H. Marsham, C.L. Bain, N.M. Roberts, and D.F.A. Boyd, 2018: What Is the Added Value of a Convection-Permitting Model for

Forecasting Extreme Rainfall over Tropical East Africa? *Mon. Weather Rev.*, **146**, 2757-2780.

Wright, J. S. and S. Fueglistaler, 2013: Large differences in reanalyses of diabatic heating in the tropical upper troposphere and lower stratosphere. *Atmos. Chem. Phys.*, **13**, 9565–9576.

Yang, K., W. Cai, G. Huang, G. Wang, B. Ng, and S. Li, 2020: Oceanic Processes in Ocean Temperature Products Key to a Realistic Presentation of Positive Indian Ocean Dipole Nonlinearity. *Geophys. Res. Lett.* **47**, e2020GL089396.

Yang, W., R. Seager, M.A. Cane, and B. Lyon, 2014: The East African Long Rains in observations and models. *J. Climate*, **27**, 7185-7202.

-, R. Seager, M.A. Cane, and B. Lyon, 2015: The annual cycle of East African precipitation. *J. Climate*, **28**, 2385-2404.

-, R. Seager, M.A. Cane, and B. Lyon, 2015: The rainfall annual cycle bias over East Africa in CMIP5 coupled climate models. *J. Climate,* **28**, 9789-9802.

Zaitchik, B, 2017: Madden-Julian Oscillation impacts on tropical African precipitation. *Atmos. Res.,* **184**, 88-102.

Zebaze, S., S. Jain, P. Salunke, S. Shafiq, and S. K. Mishra, 2020: Assessment of CMIP5 multimodel mean for the historical climate of Africa. *Atmos Sci Lett*. **20**, e926.

Zhang, Y., J. Li, S. Zhao, F. Zheng, J. Feng, Y. Li, and Y. Xu, 2020: Indian Ocean tripole mode and its associated atmospheric and oceanic processes. *Clim. Dyn*. **55**, 1367-1383.

Zhao, S. and K. H. Cook, 2021: Influence of Walker circulations on East African rainfall. *Clim. Dyn*. DOI:10.1007/s00382-020-05579-7.

Zuidema, P., P. Chang, B. Medeiros, B. P. Kirtman, R. Mechoso, E. K. Schneider, T. Toniazzo, I. Richter, R. J. Small, K. Bellomo, P. Brandt, S. de Szoeke, J. T. Farrar, E. Jung, S. Kato, M. Li, C. Patricola, Z. Wang, R. Wood, and Z. Xu (2016). Challenges and Prospects for Reducing Coupled Climate Model SST Biases in the Eastern Tropical Atlantic and Pacific Oceans: The U.S. CLIVAR Eastern Tropical Oceans Synthesis Working Group, *B. Am. Meteorol. Soc.* **97**, 2305-2328.